Dr.philos. avhandling

Harald Yndestad

The Lunar nodal cycle influence on the Barents Sea

Dr.philos. avhandling 2004:132
Fakultet for samfunnsvitenskap og teknologiledelse
Institutt for industriell økonomi og teknologiledelse
Norges teknisk-naturvitenskapelige universitet, NTNU
Trondheim

ISBN 82-471-6489-2
ISBN 82-471-6488-4 (elektronisk)

The Lunar nodal cycle influence on the Barents Sea

Harald Yndestad

Submitted to Norwegian University of Science and
Technology for the degree of
Doctor of Philosophy

Department of Industrial Ecology
and Technology Management
Norwegian University of Science and Technology

“NATURE has been defined as a 'principle of motion and change', and it is the subject of our inquiry. We must therefore see that we understand the meaning of 'motion'; for if it were unknown, the meaning of 'nature' too would be unknown. When we have determined the nature of motion, our next task will be to attack in the same way the terms, which are involved in it.”

-- Aristotle 350 BC. PHYSICS.

Preface

The research for this thesis began in 1996. The purpose was to confirm or reject the hypothesis that the life history of Northeast Arctic cod can be explained as a stationary cycle in a time series. I was rector at Aalesund University College from 1997 to 2000 and my research had to wait. In 2000 and 2001 I developed dynamic models for the most important species in the Barents Sea. The results supported the analysis from my first investigations. The next step was to look for the missing link between the 18.6-year lunar nodal cycle and the identified cycles in the Barents Sea. In 2001 I started to develop new methods to analyze climate indicators. The result was the Arctic Oscillation system theory. Wavelet analysis showed promising results and I started to analyze the biomass time series using the same analysis methods. This opened the possibility of a unified theory to explain the results from all time series.

The research on this subject has not been straightforward, partly because I did not follow the mainstream of published ideas and partly because the idea that the moon has an influence on the climate and biomass fluctuation has not been accepted by most scientists. The major problems have been to reduce complexity, to get access to data that extended over a long period of time, and to understand the complex dynamics. During this research I found that other scientists had studied the same problem earlier in the 19th century. Later, the 18.6-year cycle was estimated using a long time series, but the work failed to explain the reasons that drove this cycle length. This problem made it necessary for me to go back to the basic ideas found in early papers. I studied the early philosophy of science and general systems theory. I developed new analytical methods and new theories to explain these new results. The results were first presented at international conferences for discussion and were later published in international journals. This thesis represents a synthesis of seven papers that describe the different facets of the investigation.

Harald Yndestad

Abstract

The Barents Sea contains one of the most productive marine areas in the world. For centuries, Northeast Arctic cod and Norwegian spring spawning herring have been of vital importance for the Norwegian fish export industry and hence economic growth in Norway. It has been common knowledge that the biomass of different Barents Sea species experiences both short- and long-term fluctuations. These fluctuations have been explained by changes in herring cycles and cod cycles, or by the introduction of new fishing equipment, and more. Norwegian marine research began in earnest at the beginning of the 19th century. The main task for researchers was to discover how nature influenced cod stocks and the effects these fluctuations had on the lives of people who depended on fishing for a living. Nearly 100 years later, scientists still disagree over the causes for the biomass fluctuations in the Barents Sea. At the same time, marine research has produced long time series, which can now be analyzed using new methods. This thesis represents an investigation of a number of long time series of Arctic climate indicators and biomasses in the Barents Sea. The purpose of this analysis has been to identify a potential stationary cycle in the biomasses. A stationary cycle in the biomass allows for expanded possibilities for better long-term biomass forecasting.

The methods are based on general systems theory, analysis of systems dynamics and a wavelet analysis of time series. The wavelet analysis has identified the cycle time and the cycle phase of the dominant cycles in the time series. The phase-relation between the identified cycles contains information abort the dynamic chain of events between climate indicators and the biomasses in the Barents Sea.

The investigation has identified harmonic and sub-harmonic cycles of the 18.6-year lunar nodal cycle in all analyzed time series. The identified lunar nodal spectrum is explained by a gravity force from the 18.6-year lunar nodal cycle as the First Cause. The energy from the 18.6-year gravity force from the moon introduces a chain of oscillating events. The oscillating gravity introduces a lunar nodal spectrum in the lunar nodal tide and the polar position. A wavelet analysis of time series indicates that movement of the polar position introduces a new lunar nodal spectrum of circulating water in the Arctic Ocean. This circulation water interacts with the 18.6-year lunar nodal tide in the Atlantic Ocean and introduces an oscillation in the extent of Arctic ice, and an oscillation in the inflow of the Atlantic Ocean to the Barents Sea. The lunar nodal spectrum of Atlantic inflow introduces a lunar nodal spectrum in the Barents Sea ecology system. Analysis of the biomass in the Barents Sea shows that long-term growth, reduction and collapse are associated with the phase-relation between the biomass eigen dynamics and the lunar nodal spectrum of Atlantic inflow.

THESIS OVERVIEW

Contents

Acknowledgments

I am grateful to Professor Odd Asbjørnsen who from the beginning was an enthusiastic contact person at NTNU. Alfred Angelfoss, an assistant professor at AUC, was vital for his encouragement to start working on this thesis. Anne Stene, also an assistant professor at AUC was unstinting with her support, her enthusiasm, her comments on my papers, and the many discussions during the entire period of my work. She was a co-author on the capelin paper. Nancy Bazilchuk at NTNU, Henry Norton and Rannveig Siem at AUC all helped with my English. Professor Annik Magerholm Fet kept open my contact with NTNU after Odd Asbjørnsen sadly passed away. I would also like to thank Atle Vartdal in Ålesund, Odd Nakken at IMR in Bergen and Pål Davidsen at UiB in Bergen. They encouraged me from the beginning to keep working on this problem. Editor John Ramster at ICES Journal offered tremendous enthusiasm for my first paper. Dr. Tim Wyatt at Vigo was helpful for his enthusiasm and support on papers from the pioneers. He introduced me to the early work of Ljungman and Pettersson. Johan Blindheim at IMR in Bergen offered his enthusiasm and comments on the climate paper. Svein Sundby at Institute of IMR in Bergen also supported me with his enthusiasm for this problem in the ECOBE climate research program.

This thesis could not have been done without access to unique data time series. I thank Yu. A. Bochkov and Vladimir Ozhigin at PINRO institute in Murmansk who provided the unique Kola section time series. Ozhigin was helpful with his enthusiasm and interest in my work and the invitation to the PINRO institute. The presentation and discussion with the oceanographers and marine scientists was an inspiration to keep working on this thesis. Torgny Vinje at the Norwegian Polar Institute in Oslo provided the data series for Arctic ice extent. Gudmund Anders Dalsbø at the Norwegian Meteorological Institute in Oslo provided the Røst data series. Olav-Rune Godø at the Institute of Marine Research in Bergen willingly gave me access to early data series for Northeast Arctic cod. Reidar Toresen and Ole Johan Østvedt at the Institute of Marine Research in Bergen were extremely helpful in providing access to long time series of Norwegian spring herring and Tara Marshall at IMR in Bergen gave me access to the Barents Sea capelin time series. For their help and encouragement, I thank them all.

Motivation

Over the last 150 years, the marine industry has grown along the northwest coast of Norway. This industrial cluster consists of fishing trawlers, a fish export and fishing industry, a supply industry, a shipping industry, as well as banking, service support, education and more. This industry is dependent on a supply of fish from the Barents Sea. Fluctuations in the fish biomass therefore have major economic impacts on the entire industrial cluster. The more the cluster becomes industrialized, the more there is a need for stability. Better methods of long-term forecasting are thus of crucial importance for economic development and settlement of the Norwegian coast.

The research hypothesis

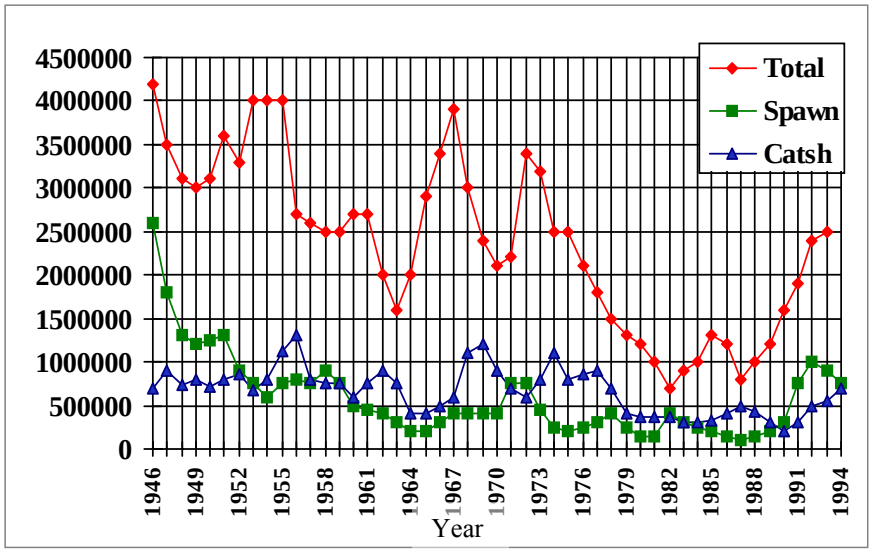

Figure 0.1 Time series of Northeast Arctic cod total biomass, spawning biomass and catch (in metric tons).

In 1995 I was involved in a life cycle analysis of a Norwegian trawler. To get an idea of the potential income from the trawler, I conducted a time series analysis of the Northeast Arctic cod biomass (Figure 0.1). A rapid falling autocorrelation indicated it was not realistic to predict future biomass for periods longer than one year. In other words, any long-term forecasting-based on historical data was essentially based on pure speculation.

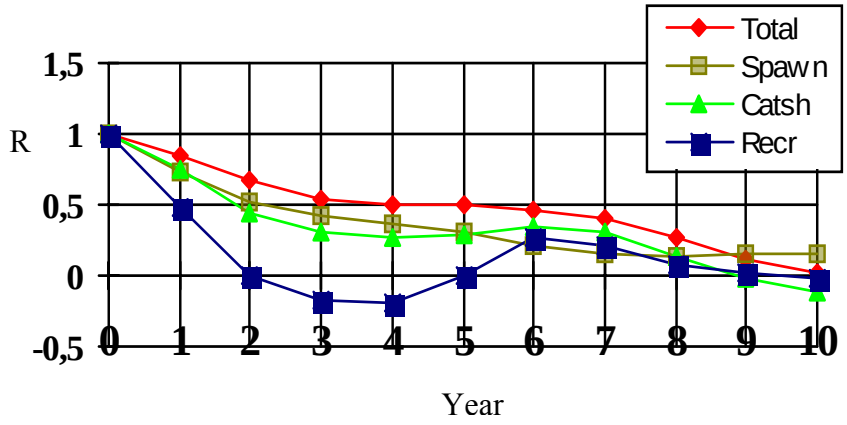

Figure 0.2 Autocorrelation of Northeast Arctic cod time series.

A closer look at the autocorrelation function indicated, however, the existence of a 6-year cycle in the time series (Figure 0.2). The absence of an expected red spectrum raised basic questions: Is there a 6-year cycle in the biomass of Northeast Arctic cod?
Additionally:

1. If this cycle exists, it could be used to predict the appropriate years to invest in the cod fishery.
2. If this is a stationary cycle, signal theory dictates that it have a stationary source.
3. If there is such a stationary source, it must come from something fundamental in nature.

Sea temperatures are one such fundamental source, so the next step was to analyze a 100-year temperature data series from the Barents Sea. The same 6-year cycle was found in this data series. The next question became: If this is the same cycle that caused a 6-year cycle in cod biomass, what is the primary cause with the power to control temperatures in the Barents Sea? Is it earth dynamics? The closest known cycle is the 18.6-year earth nutation cycle, which is caused by the moon. If the gravity from the moon is the primary cause, can the earth's nutation force temperature cycles in the Barents Sea? This thesis is written in answer to some of these questions.

Scientific approach

The major difficulty in constructing this thesis has been to reduce its complexity. Only a few early papers have been published on this problem, making it necessary to develop new methods to analyze the time series and devise new theories to explain the results.

1. The complexity: The General Systems Theory was developed as a framework to analyze the complex relations in the Barents Sea system. These relationships explain the expected dynamics in the system.
2. The cycle source: The cycle was traced according to a rule from signal theory that states "A stationary cycle must have a stationary source".
3. The time-variant problem: Time-variant cycles in time series must be separated and identified in a limited time window. This problem was solved by a wavelet transformation.
4. The cycle identification: The 18.6-year cycle in the time series has been identified by wavelet transformation and a cross-correlation to an 18.6-year reference cycle.
5. The cycle dominance: The Signal to Noise relation between the identified wavelet cycles and other unknown sources.

The General Systems Theory was chosen to reduce complexity. At the same time, this method increased the investigation complexity. To understand the cod biomass dynamics, it was necessary to understand the dynamics of the related systems. The result was an investigation of more additional species in the Barents Sea, as well as the food chain, climate indicators and earth dynamics.

The stationary dominant cycles in the time series required a different view of dynamics in nature. The Newtonian dynamic is based on the push-hypothesis, where the movement of an object is dependent on an input force. This hypothesis represents a ballistic view of dynamics in nature. The Aristotelian dynamic is a future-directed hypothesis based on a rotary motion of change. In this hypothesis the phase of the rotary movement is of most importance. Keeping track of the phase requires long-term timing measurements. The long-term estimate of time is associated with celestial movements. The rotary movement hypothesis is based on the theory that the future state is already settled by a deterministic celestial cycle. This hypothesis represents a teleological view of dynamics in nature. The research for this thesis brought with it the surprising observation that Aristotle's doctrine of dynamics in nature had the best potential for long-term biomass forecasting. Since Newtonian dynamics represent the most well-known approach in modern science, it's important to understand the difference between the Newtonian approach and the Aristotelian approach.

Related works

The idea of a relationship between biomass fluctuations and celestial observations was important in an earlier period of marine science. The pioneer Ljungman found a relation between a 111-year sunspot cycle and herring periods in Bohuslen in Sweden (Ljungman, 1879; Lindquist, 2002). Otto Pettersson investigated the same time series and found a relationship between herring periods and the 18.03-year Saros cycle and "A Great Saros" cycle of 111 years (Pettersson, 1912, 1914a, 1914b, 1915, 1930). Helland-Hansen and Nansen (1909) found a relationship between the air temperature at the Ona light and fluctuations of Northeast Arctic cod. Helland-Hansen and Nansen concluded that there is a climatic influence on biomass fluctuations.

Ottestad (1942) investigated landings in Lofoten from 1875 to 1940. Cycles were identified by a visual inspection of similarities in fluctuations. He found maximum cycles of Northeast Arctic cod at intervals of 11, 17.5, 23 and 57 years. The cycles were compared to fluctuations in tree rings from Troms and the conclusion was that biomass fluctuations must be influenced by climate fluctuations. Later he compared sunspot cycles and biomass cycles (Ottestad, 1979). Wyatt et al. (1994) investigated the time series of cod landings records from Lofoten and found a cycle of 18.6 years. The cycle was explained by the influence from the 18.6-year lunar tide.

Some related works have been published by Russian scientists. Izhevskii (1961, 1964) presented a system view of the Barents Sea. Maksimov and Smirnov (1965, 1967) identified a standing 18.6-year lunar nodal tide in the Barents Sea. Malkov (1991, 2002) has identified a statistical relationship between earth pole movements and biomass fluctuations in the Barents Sea.

This thesis is based on a general system theory and presents a more holistic approach than earlier investigations. Biomasses are analyzed using system dynamic models and a greater number of time series have been analyzed than in earlier works. The research also introduces a new wavelet analysis method to identify cycle times and cycle phases of the dominant cycles in the time series. The wavelet analysis method has opened new possibilities for the analysis of phase-relations between dominant cycles in climate indicators, biomass fluctuations and parameter fluctuations in biomass models.

Main concepts and ideas

The main concepts and ideas in this thesis are

- The First Cause: The gravity force from the 18.6-year lunar nodal cycle is the primary cause of the oscillation.
- The lunar nodal spectrum: The gravity force from the 18.6-year lunar nodal cycles is distributed as a spectrum of harmonic and sub-harmonic cycles in the tides and as polar position movements.
- The forced oscillator theory: The lunar spectrum is distributed in a set of coupled oscillators where the energy in some harmonic cycles is preserved by resonance.
- The “wine glass” theory: The Arctic Ocean behaves as a rotating on wine glass. The oscillation in polar position movements introduces a lunar nodal spectrum in the movements of water circulating in the Arctic Ocean.
- The modulation theory: The dominant 4*18.6=74.4-year cycle of circulating water in the Arctic Ocean has a multiplicative modulation with respect to the 18.6-year tide and introduces a phase-reversal in the 18.6-year cycle.
- The Barents Sea oscillation: The lunar nodal tide spectrum and the 74-year cycle in the Arctic Ocean controls the Atlantic inflow oscillation with respect to the Barents Sea.
- The biomass code of growth: The long-term growth of biomass in the Barents Sea, or its reduction or collapse, is controlled by the phase-relation between the biomass eigen-dynamic and the Atlantic lunar nodal tide inflow cycles of 6.2 and 18.6 years.
- Biomass stability: Biomasses in the Barents Sea represent a time-variant dynamic system that has no mean value and no stationary safe limit values.
- Biomass management: Sustainable biomass management must be adapted to the biomass code of growth. This may be managed by a an annual percentage of the biomass. The percentage should be related to a long-term growth period, the long-term reduction period and the special vulnerable period when the 6.2- and the 18.6-year cycle are negative at the same time.

Thesis outline

Chapter 1 Introduction

Chapter 1 is an introduction to the history of the problem. The first part of the chapter discusses the difference between the Aristotelian approach and the Newtonian approach to understanding dynamics. This section explains why the Newtonian approach has been misused in marine science. The second part is a historical review of the discovery of the 18.6-year lunar nodal cycle in time series. This section discusses results from early papers of Otto Pettersson, Izhevskii, Maksimov and Smirnov, and Currie.

Chapter 2 Analysis

Chapter 2 presents methods and a summary of each of the seven papers that comprise this work. The first part describes the analytical methods used to identify the lunar nodal cycles in time series. The next part is a summary of each paper included in this thesis, with a discussion of the paper's rationale, the methods and results, along with new concepts and ideas.

Chapter 3 Synthesis

Chapter 3 is a synthesis of all the papers presented in this thesis. The first part is a general system theory of the results from all the papers. This part describes a forced oscillator theory that unifies the research results. The next part summarizes results from climate analyses and proposes a theory for an Arctic Oscillating system. The third part summarizes the results from biomass analyses from the Barents Sea and proposes a theory for a biomass oscillating system. The last part proposes a theory for biomass oscillation management.

Chapter 4 Discussion

Chapter 4 is a short discussion of the data synthesis.

Chapter 5 Conclusions

Chapter 5 is a short summary of the conclusions related to the questions answered in this investigation. The second part is a summary of new results, theories and ideas that have resulted from this work. The third part lists the most important issues that remain for future investigation and research.

Chapter 6 Papers

Chapter 6 presents selected papers that describe different aspects of the 18.6-year lunar nodal cycle influence on the Barents Sea.

Yndestad, H: 1999. Earth nutation influence on the temperature regime of the Barents Sea. ICES Journal of Marine Science; 56: 381-387.

Yndestad, H: 1999. Earth nutation influence on system dynamics of Northeast Arctic cod. ICES Journal of Marine Science; 56: 652-657.

Yndestad, H: 2001. Earth nutation influence on Northeast Arctic management. ICES Journal of Marine Science; 58: 799-805.

Yndestad H and Stene A: 2002. Systems Dynamics of Barents Sea Capelin. ICES Journal of Marine Science; 59: 1155-1166.

Yndestad, H: 2003. The Code of Long-term Biomass cycles in the Barents Sea. ICES Journal of Marine Science.

Yndestad, H: 2004. The Cause of biomass dynamics in the Barents Sea. Journal of Marine Systems. Available online 3 October 2003.

Yndestad, H: 2004. The Lunar nodal cycle influence on the Arctic climate. Journal of Marine Science. Submitted.

Lists

Figures

Tables

Notation

A(t)	System matrix
B(t)	Binding between a set of systems
E_v	Energy sum
E[ ]	Mean value operator
F(t)	Catch rate
H(jω)	Complex frequency transfer function
I	Identity matrix
j	Complex operator
K	Scale constant
m	Number variable
n	Number variable
N	A number
N_d	Energy density constant scale
sqrt( )	Square route operator
S(t)	A system architecture
$S_{vv}(j\omega)$	Spectral density
S/N	Signal to Noise ratio
x(t)	System state
x(nT)	Sampled system state
x(jω)	State cycle
X(t)	System state vector
X(jω)	System state spectrum vector
$X_n(j\omega)$	The state spectrum at event number n
Q	The quality of a correlation
Q(k)	The quality of a correlation on cycle k
R	Cross-correlation quotient
R(k)	Cross-correlation quotient on cycle k

T	Sampling time
T_0	The lunar cycle period of 18.6 years
t	Time
$u(j\omega)$	A stationary cycle
$u_o(t)$	The 18.6-year lunar nodal cycle
$u_0(j\omega)$	The 18.6-year lunar nodal cycle
u_o	The 18.6-year lunar nodal cycle amplitude
U_0	Eccentricity amplitude
U(t)	External system state
$U(j\omega)$	A set of stationary cycles
$U(j\omega_0)$	A lunar nodal spectrum
var( )	Variance operator
v(t)	Disturbance from an unknown source
V^2	Noise variance
$V(j\omega)$	A non-correlated red spectrum
$V^*(j\omega)$	Complex conjugated spectrum
w	System model purpose
W(a,b)	A set a of wavelet cycles over the time period b
W(k,t)	A selected k-period wavelet cycle over the time t
W(t)	A sum of wavelet cycles
y(t)	Measured time series
w(t)	Measured noise

Symbols

$\angle$	Angle (rad)
φ	Angle delay (rad)
φ_0	The lunar cycle angle delay (rad)
ω	Angle frequency (rad/time)
ω_0	Lunar cycle angle frequency $\omega=2\pi/18.613$ (rad/time)
τ	Delay (time)
π	Pi or 3.14
Ψ	Wavelet operator
Δ	Difference operator
$\in$	System model purpose
$\sum$	Sum operator
$\lvert\ \rvert$	Positive value operator

Abbreviations

AUC	Aalesund University College
IT	Information technology
ICES	International Council for the Exploration of the Sea
ISDC	International System Dynamics Conference
NAO	North Atlantic Oscillation
NTNU	Norges Tekniske Naturvitenskapelige Universitet
IMR	Institute of Marine Research
PINRO	Polar Research Institute of Marine Fisheries and Oceanography. Murmansk.

Definitions

Coupled oscillators: A set of mutually related feedback systems.

Earth nutation: A small irregularity in the rotating earth axis on the equatorial plane.

Eigen-frequency cycle: The cycle time of a frequency where a feedback system has resonance.

Forced oscillator: A stationary cycle forced on a dynamic system.

Lunar nodal cycle: The time required (18.6134 years) for the line formed by intersection of the moon's orbital plane and the plane of the Earth's orbit to rotate through 360E.

Lunar nodal spectrum: A set of harmonic and sub-harmonic cycles related to the 18.6-year lunar nodal cycle.

Lunar nodal tide: A vertical and horizontal tide caused by the 5º09' inclining moon's orbital plane to the ecliptic plane in a period of 18.6 years.

Lunar node: The cross-point between the moon plane and the ecliptic plane to the sun.

NAO winter index: The mean normalized pressure difference between a station on the Azores and one on Iceland from December to March.

Oscillator: A feedback system that conserves energy by means of resonance.

Polar movement: The rotating pole on the ecliptic plane.

Polar position: The pole on the ecliptic plane.

References

Baranov, F. I. 1918. Kvoprosy obiologicheskikh osnovaniyahk rybnogo (on the question of the biological basis of fisheries). Nauchnyi Issledovatelskii Ikhtiologicheskii Institut Izvestiya /report of the Divition of Fish Management and Scientific Study of the Fish Industry), 1:81-128. (In Russian).

Borroughs, William James. 1992. Weather cycles real or imaginary? Cambridge University Press.

Bonisch, G and Schlosser, P. 1995. Deep water formation and exchange rates in the Greenland/Norwegian Seas and the Eurasian Bain of the Arctic Ocean derived from tracer balances. Prog. Oceanography. 35:29-52.

Carlson, A. Bruce. 1968. Communication systems. An Introduction to Signal and Noise in Electrical Communication. McGraw-Hill. London. ISBN 0-07-009957-X.

Currie, R. G., 1981, Evidence for 18.6 year (*sic*) signal in temperature and drought conditions in North America since A. D. 1800: Journal of Geophysical Research. 86:11,055-11,064.

Currie, R. G., 1984, Evidence for 18.6 year (*sic*) lunar nodal (*sic*) drought in western North America during the past millennium: Journal of Geophysical Research. 89:1295-1308.

Currie, R. G., 1987, Examples and implications of 18.6- and 11-yr terms in world weather records, Chap. 22, p. 378-403 *in* Rampino, M. R.; Sanders, J. E.; Newman, W. S.; and Konigsson, L.-K.; *eds*., Climate: History, periodicity, and predictability: International Symposium held at Barnard College, Columbia University, New York, New York, 21-23 May 1984 (R. W. Fairbridge Festschrift): New York, NY, Van Nostrand Reinhold Publishing Corp., 588 p.

Currie, R. W.; Wyatt, Thomas; and O'Brien, D.P, 1993. Deterministic signals in European fish catches, wine harvests, sea level, and further experiments: International Journal of Climatology. 8:255-281.

Currie, R. G. 1995. Variance Contribution of M_n and S_c Signals to Niele River Data over a 30-8 Year Bandwith. Journal of Coastal Research Special Issue No. 17: Holocene Cycles: Climate, Sea Levels and Sedimentation, pp 29-38.

Darwin, G.H. 1877. On the influence of geological changes on the Earth's axis of rotation Philosophical Transactions of the Royal Society of London. 167, 271.

Darwin, G.H. 1879. On the precession of a viscous spheroid and on the remote history of the earth. Philosophical Transactions of the Royal Society of London. 170: 447-530.

Darwin, G.H. 1880. On the secular change of the orbit of a satellite revolving about a tidally distorted planet. Philosophical Transactions of the Royal Society of London. 171: 713-891.

Daubechies I, 1992. Ten lectures of wavelet. SIAM Journal on Mathematical Analysis. Vol. 24, Nr.2, Mar 1993, pp 499-519.

Diodorus of Sicily. 1935. *Library of history*. tr. C. H. Oldfather: Cambridge, Massachusetts: Harvard University Press.

Feldman, T. S. 1988. Climate and history in the late 18th and 19th centuries. Eos. Trans. American Geophysical Union. 73: 1-4.

Godø, R. 1998. Methods for Fishery Resources Assessment. Status and Potentials of Marine Resource and Environmental monitoring. Report from a Working Group appointed by the Research Council of Norway. Olso. June, 1998.

Helland-Hansen, Bjørn and Nansen, Fritjof. 1909. The Norwegian Sea. Report on Norwegian Fishery and Marine-Investigations Vol. II. 1909. No 2. Kristiania.

Hjort Johan. 1914. Fluctuations in the great fisheries of Northern Europe. Andr. Fred. Høst & Files. Copenhagen. April 1914.

Izhevskii, G. K., 1961. Oceanological Principles as Related to the Fishery Productivity of the Seas. Moscow: Pishcepromizdat. [Translated 1966: Israel Program for Science Transactions. Jerusalem]. 95 pp.

Izhevskii, G. K., 1964. Forecasting of oceanological conditions and the reproduction of commercial fish. All Union Science Research Institute of Marine Fisheries & Oceanography. Israel Program for Science Transactions, 22 pp.

Keeling, Charles D. and T. P. Whorf. 1997. Possible forcing global temperature by oceanic tides. Proceedings, National Academy of Sciences of the United States. 94:8321-8328.

Lindquist, A. 2002. Herring periods of Bohuslan: a cross-sectorial approach. ICES Marine Science Symposia, 215: 343-351.

Ljungman, A. V. 1879. Bidrag till løsningen af frågan om de stora sillfiskenas sekulära periodisitet. Tidskrift for Fiskeri, 5: 257-268. (In Swedish).

Maksimov, I. V. and Smirnov, N. P. 1964. Long-range forecasting of secular changes of the general ice formation of the Barents Sea by the harmonic component method. Murmansk Polar Sci. Res. Inst., Sea Fisheries, 4: 75-87.

Maksimov, I. V. and Smirnov, N. P. 1965. A contribution to the study of causes of long-period variations in the activity of the Gulf Stream. Oceanology. 5:15-24.

Maksimov, I. V. and Smirnov, N. P. 1967. A long-term circumpolar tide and its significance for the circulation of ocean and atmosphere. Oceanology 7: 173-178 (English edition).

Maksimov, I. V. and Sleptsov-Shevlevich, B. A., 1970. Long-term changes in the tide-generation force of the moon and the iciness of the Arctic Seas. Proceedings of the N. M. Knipovich Polar Scientific-Research and Planning Institute of Marine Fisheries and Oceanography (PINRO). 27: 22-40.

Malkov A.S. 1991. Movement of the earth pole and population dynamics of some commercial fish species from the northern Atlantic. The 79th international ICES Annual Science Symposium. 1991/L: 77.

Malkov A.S. 2002. Movements of the Earth pole and population dynamics of Norwegian spring-spawning herring and Arctic cod. The 90th international ICES Annual Science Symposium. Copenhagen. Denmark, 1 Oct-5. CM 2002/O:09.

Matlab. 1997. Matlab. Wavelet Toolbox. Users Guide. The Math Works Inc.

Ottestad, Per. 1942. On Periodical Variations on the Yield on the Great Sea Fisheries and the Possibility of establishing Yield Prognoses. Fiskeridirektoratets Skrifter. Vol, VII. No 5. Bergen. Norway.

Ottestad, Per. 1979. The sunspots series and biospheric series regarded as results due to a common cause. Meldinger fra Norges landbrukhøgskole, 58:9, Ås. Norway.

Pettersson, Hans. 1915. Long Periodical Variations of the Tide-generating Force. Andr. Fred. Høst & Files. Copenhagen. p. 2-23.

Petterson, Otto, 1905. On the probable occurrence in the Atlantic Current of variations periodical, and otherwise, and their bearing on metrological and biological phenomena. Rapp. P.-v. R´eun. Cons. perm. int. l´Explor. Mer, 42: 221-240.

Pettersson, Otto, 1912, The connection between hydrographical and meteorological phenomena: Royal Meteorological Society Quarterly Journal. 38: 173-191.

Pettersson, Otto, 1914a, Climatic variations in historic and prehistoric time: Svenska Hydrogr. Biol. Komm., Skriften, No. 5, 26 p.

Pettersson, Otto, 1914b, On the occurrence of lunar periods in solar activity and the climate of the earth (*sic*). A study in geophysics and cosmic physics: Svenska Hydrogr. Biol. Komm., Skriften.

Pettersson, Otto, 1915, Long periodical (sic) variations of the tide-generating force: Conseil Permanente International pour l'Exploration de la Mer (Copenhagen), Pub. Circ. No. 65, p. 2-23.

Pettersson, Otto, 1930, The tidal force. A study in geophysics: Geografiska Annaler. 18: 261-322.

Pugh D T. 1993. Tides, Surges and Mean Sea-Level. John Wiley & Sons Ltd. ISBN 0471 91505.

Ricker, W.E. 1944. Furter notes on fishing mortality and effort, Copeia. 1944: 23-44.

Royer Thomas C. 1993. High-Latitude Oeanic Varibility Associated With the 18.6-Year Nodal Tide. Journal of Geophysical Research. 98: 4639-4644.

McGlade, Jacquie. 1994. Ecology, Bureaucracy and Differential Equations. Mathematics Review. April 1994. pp 8-11.

Sanders, J E. 1995. Astronomical forcing functions: From Hutton to Milankovitch and beyond: Northeastern Geology and Environmental Science.17: 306-345.

Sobel, Dava. 1999. Galileo's Daughter. A Drama of Science, Faith and Love. Fourth Estate Limited. London. ISBN I-84115-494-6.

Svansson, A. 2002. Otto Pettersson's ideas on general ocean circulation. ICES Marine Science Symposia. 215: 104-112.

Wegner, G. 1996. Herring research: remarks on a 250-year-old theory. ICES Information.. 28:8.

Wyatt, T. Currie, R.G. and Saborido-Ray, F. 1994. Deterministic signals in Norwegian cod records. ICES Marine Science Symposium. 198: 49-55.

Yndestad, H: 1996a. Systems Dynamics of North Arctic Cod. The 84th international ICES Annual Science Conference. Hydrography. Committee. Iceland. October 1996.

Yndestad, H: 1996b. Stationary Temperature Cycles in the Barents Sea. The cause of causes. The 84th international ICES Annual Science Conference. Hydrography Committee. Iceland. October 1996.

Yndestad, H: 1997. Systems Dynamics in the Fisheries of Northeast Arctic Cod. 15th International System Dynamics Conference (ISDC ´97). Istanbul. August 1997.

Yndestad, H: 1999a. Earth nutation influence on the temperature regime of the Barents Sea. ICES Journal of Marine Science. 56: 381-387.

Yndestad, H: 1999b. Earth nutation influence on system dynamics of Northeast Arctic cod. ICES Journal of Marine Science. 56: 652-657.

Yndestad, H: 2000. The predestined fate. The Earth nutation as a forced oscillator on management of Northeast Arctic cod. The 18th International Conference of The System Dynamics Society. August 6-10, 2000. Bergen, Norway.

Yndestad, H: 2001a. Earth nutation influence on Northeast Arctic cod management. ICES Journal of Marine Science. 58: 799-805.

Yndestad, H: 2001b. General Systems Theory." The Forty-Fifth Meeting of the International Society for the Systems Sciences. July 8-13.

Yndestad, H: 2001c. Tilstanden for Norsk Arktisk torsk. (The state of Northeast Arctic cod) HiÅ-Rapport 2001/06. ISBN 82-92186-10-7. Ålesund. (In Norwegian).

Yndestad H and Stene A: 2001. System Dynamics of Barents Sea Capelin. ICES Annual Science Conference. 26-29 September. 2001 Oslo.

Yndestad H and Stene A: 2002. Systems Dynamics of Barents Sea Capelin. ICES Journal of Marine Science. 59: 1155-1166.

Yndestad H: 2002. The Code of Norwegian spring spawning herring Long-term cycles. ICES Annual Science Conference. Oct 2002. Copenhagen.

Yndestad H: 2003a. A Lunar nodal spectrum in Arctic time series. ICES Annual Science Conference. Sept 2003. Tallinn. ICES CM 2003/T.

Yndestad, H: 2003b. The code of long-term Biomass cycles in the Barents Sea. ICES Journal of Marine Science. 60: 1251-1264.

Yndestad, H: 2004. The cause of biomass dynamics in the Barents Sea. Journal of Marine Systems. 44. 107-124.

Zöppritz, K. 1878. Zur Teorie der Meeresstrømungen (On the theory of ocean currents). Annalen der Hydrographie und maritimen Meteorologie, 6: 239-243. (In German):

Chapter 1

INTRODUCTION

1.1 The First Cause

> *"EVERYTHING that is in motion must be moved by something. For if it has not the source of its motion in itself it is evident that it is moved by something other than itself, for there must be something else that moves it. Since everything that is in motion must be moved by something, let us take the case in which a thing is in locomotion and is moved by something that is itself in motion, and that again is moved by something else that is in motion, and that by something else, and so on continually: then the series cannot go on to infinity, but there must be some first movement.*
>
> *--Aristotle. 350 BC. PHYSICS.*

Figure 1.1 Aristotle.

Aristotle's principle of motion in nature was based on his doctrine of The Four Causes of Motion. These are the Formal Cause, the Material Cause, the Efficient Cause, and the Final Cause. The Material Cause is constituted of the matter from which it is made, the Efficient Cause is what sets it in motion, the Formal Cause is what gives it a terminus of development and the Final Cause constitutes its end and purpose. Aristotle argued that movement in nature was a result of a chain of movements that may be traced backwards in history to a first movement. Aristotle's doctrine of dynamics reflected a dualistic thinking between the Efficient Cause and the Formal Cause and between the First Cause and the Final Cause. The Final Cause is the doctrine of Teleology (*telos* means "end" or "purpose"). Teleology is the study of ends, purposes and goals. In a history timeline with a beginning and an end, all historical events derive from their ends or purposes; that is, all events in history are directed by the future. Thus the doctrine of the Final Cause represented a deterministic view of nature.

"Since there must always be motion without intermission, there must necessarily be something, one thing or it may be a plurality, that first imparts motion, and this first movement must be unmoved. Now that these points are settled, it is clear that the first unmoved movement cannot have any magnitude. For if it has magnitude, this must be either a finite or an infinite magnitude. Now we have already proved in our course on Physics that there cannot be an infinite magnitude: and we have now proved that it is impossible for a finite magnitude to have an infinite force, and also that it is impossible for a thing to be moved by a finite magnitude during an infinite time. But the first movement causes a motion that is eternal and does cause it during an infinite time. It is clear, therefore, that the first movement is indivisible and is without parts and without magnitude."

--Aristotle. 350 BC. PHYSICS.

Aristotle believed that all causes of movements on earth may be traced backwards to the Cause of causes. This meant that the position of the sun, the moon and the stars had resulted from The First Cause of Movement. The First Cause was associated with God, and was considered to be indivisible, without parts and without magnitude.

Figure 1.2 Isaac Newton.

Isaac Newton (1642-1727) is often described as the first modern scientist. He was born in Lincolnshire and for most of his life studied ancient religion doctrines, the chronology of ancient kingdoms and ancient scientific works. He believed that an old divine knowledge was lost and some of it had been filtered down to Pythagoras, whose "music of the spheres" he regarded as a metaphor for the law of gravity. In *Principia Mathematica* Isaac Newton put the name gravity on the First Cause, the force that is indivisible, without parts and without magnitude, but still has the power to transform the universe.

Newton discovered that inertial energy is stored in the movement of a body. To prove this theory, Newton invented differential equations to describe the dynamics of objects in nature. If you know the input force, you can compute the object's dynamics using differential equations. This concept shifted the focus from a chain of rotary motions to an input-output problem. The result was a shift in focus from a holistic view of the cause of movements to the study of single objects.

Baranov (1918) introduced the constant maturity rate and fishing rate in a differential equation and thus was able to compute long-term biomass dynamics. Later this concept was adopted by Ricker (1944) and others. Ricker's differential equations allowed for new approaches to biomass management. If you can forecast future biomass, you can manage that biomass. The result was that fisheries science became increasingly dominated by Newtonian mathematics (McGlade, 1994). The increasing dominance of mathematics changed the focus from the holistic view of nature to a focus on single objects. A 2500-year holistic approach, known from Pythagoras to Pettersson, Nansen and Izevskii, has been more or less lost.

1.2 The rotary motion

> *Let us now proceed to maintain that it is possible that there should be an infinite motion that is single and continuous, and that this motion is rotary motion. The motion of everything that is in process of locomotion is either rotary or rectilinear or a compound of the two: consequently, if one of the former two is not continuous, that which is composed of them both cannot be continuous either. Moreover the progress of rotary motion is never localized within certain fixed limits, whereas that of rectilinear motion repeatedly is so. Now a motion that is always shifting its ground from moment to moment can be continuous: but a motion that is repeatedly localized within certain fixed limits cannot be so, since then the same thing would have to undergo simultaneously two opposite motions. So, too, there cannot be continuous motion in a semicircle or in any other arc of a circle, since here also the same ground must be traversed repeatedly and two contrary processes of change must occur. The reason is that in these motions the starting-point and the termination do not coincide, whereas in motion over a circle they do coincide, and so this is the only perfect motion.*
>
> --Aristotle. 350 BC. PHYSICS.

Aristotle defined nature and science by the principles of motion and change. The motive of science was the forecast doctrine. If you can forecast the future, you can control something in the future. The power of knowledge through science was related to the ability to predict movements in nature. Movements of time and changes in nature were associated with the regularities in the movements of the sun, the moon and the stars. Changes in nature were thus associated with the regular movements of the celestial bodies. Predicting star movements became the science of astronomy and predicting rhythms in nature became the sciences of astronomy and astrology. The relation between the rhythms in nature and the cycles of the stars, the sun and the moon led to the idea that the stars, the sun and the moon represented the power of nature. The power behind this rhythm was a mystery that became the foundation for cults and religions. These cults and religions communicated with people by means of legends, myths, art and symbols. Scientists who had the knowledge kept it secret to retain its power. Now, most of the ancient knowledge is lost, and only symbols, legends and myths remain.

The concept of natural cycles is an ancient doctrine that extends beyond written history. Through the centuries, people have learned to listen to the rhythms in nature. Knowledge of the rhythm of the seasons, the fluctuation of the tides, the floods of rivers and rainy seasons was a matter of survival. Our early ancestors learned the best time to sow, the time to harvest, the time to fish, the time to slaughter, and the time to follow the tides by ship. Knowledge was thus associated with rhythms in nature. If we can forecast the future, we can adapt to the future and thus make it easier to survive. Ancient science took a cyclical view of reality. A cyclic view of nature was associated with a reincarnation of nature, people and the universe. In this cyclic view, it was important to retain the timing of the cycles that were represented by the moon, the sun and the stars. Timing allowed for the prediction of the phases of natural cycles, and the ability to predict the phase opened the possibility of controlling the future. Up until the present, natural cycles continued to control agriculture, fisheries, trade, industrial production and economies.

There are two important rotary motion systems. One is controlled by the moon and one is controlled by the sun. According to an Egyptian myth, the year had 360 days, divided into 12 months comprised of 30 days, and in the beginning there was regularity in the universe. One day Ra got angry at Nut and said “I cast this spell upon Nut, so she shall not bear any children on any day or any night of any year.” The problem was solved by taking 5 days from the Moon-god Thoth, who gave five extra days

to the year so that Nut could bear her children on these five extra days. Since then, the star-time, the moon-time and the sun-time have had different cycles. For ordinary purposes, ancient Egyptians used a civil calendar with 365 days in a year. In the long run the civil calendar was compared to the Sothic year. The Sothic year was measured from one rising of the Dog Star (Sirius) to another. This star has the extraordinary property of rotating in a period of 1461 years. When the civil calendar lost a day every 4^{th} year, it took 1461/4=365.25 years to coincide with the Sothic year. This calendar made possible the long-term forecasting of a star cycle, and the Egyptians were able to forecast climate change.

In Egypt the Dog-Star was associated with the Nile water flood level. The Nile is still an indicator of meteorological conditions in Africa today. Flood levels in Upper and Lower Egypt were carved on a stone from 3150 BC to the Fifth Dynasty at about 2400 BC, with more reliable measurements from AD 622 to AD 1470. A Fourier analysis of the Nile flood time series shows dominant cycles of 18.4, 53, and 77 years (Currie, 1995; Burroughs, 1992). The same climate cycles are estimated in this thesis. The close relation between the estimated cycles of the Nile, the extent of the Arctic ice pack and the NAO index supports the theory of long-term stationary cycles.

The lunar nodal cycle

> *Abaris, a Hyperborean, came to Greece in ancient times and renewed the good-will and kinship of his people to the Delians. They say also that the moon, as viewed from this island, appears to be but a little distance from the earth and to have upon it prominences, like those of the earth, which are visible to the eye. The account is also given that the god visits the island every nineteen years, the period in which the return of the stars to the same place in the heavens is accomplished; and for this reason the nineteen-year period is called by the Greeks the 'year of Meton.'*
>
> – Diodorus of Sicily, First century BC.

In the fifth century BC, the Greek astronomer Meton discovered that the dates of a full moon repeated every 19 years. The time between two full moons described a moon rotation relative to a fixed point on the moving earth. This cycle period is called a synodic month of 29.530589 days. At the same time there are 365.25 days in a tropical year when the earth is moving around the sun. In a Julian calendar the mentonic cycle of 19 tropical years contains 365.25*19=6939.75 days. In a lunar calendar 235 synodic months contain 235*29.530589=6939.69 days. The two cycles have a resonance of 18.03 years, and the English astronomer Edmund Halley (1665-1742) called it the saros cycle. The saros cycle was used to compute eclipses and the mentonic cycle to synchronize the lunar calendar to the calendar of a tropical year.

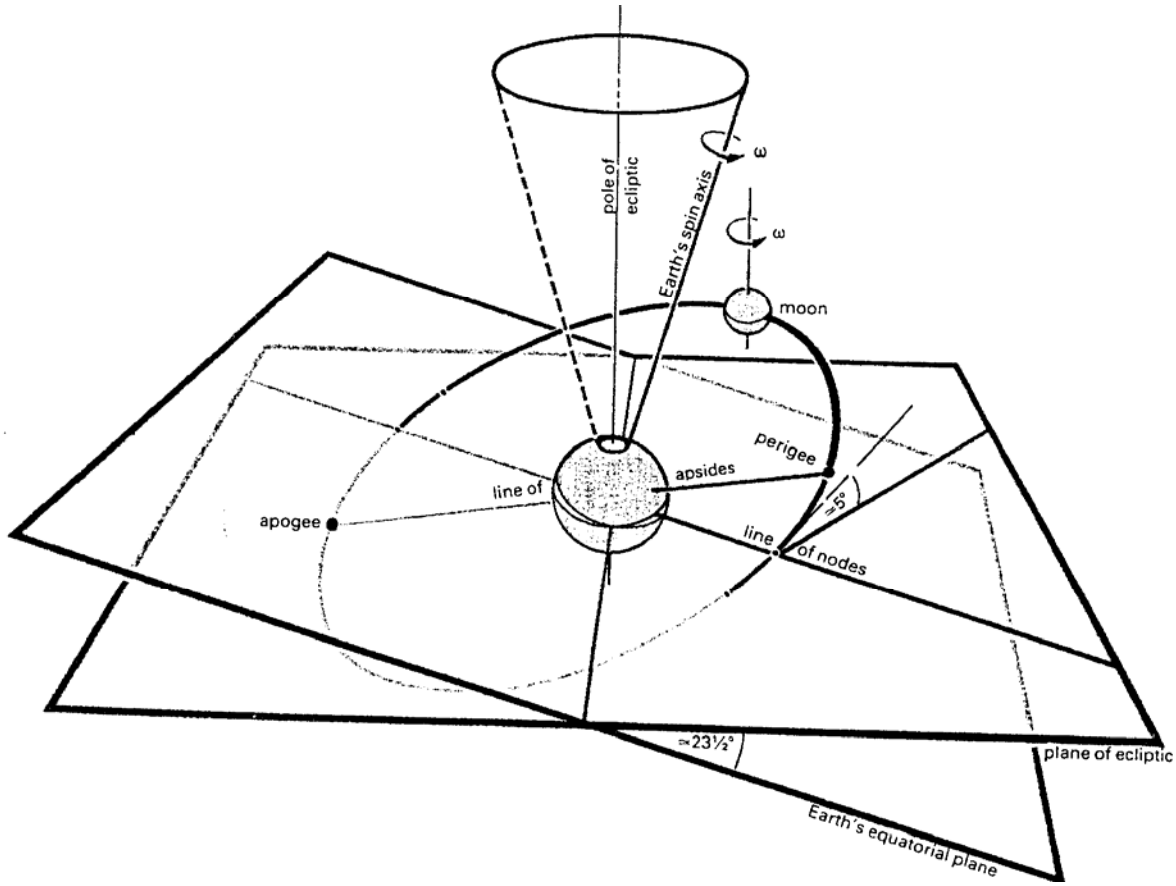

Figure 1.3 Orbital geometry of the earth-moon system (Burroughs, 1992).

The physical explanation for the lunar nodal cycle can be found in the movement of the moon's orbital plane. This plane has a +/- 5º09' degree movement in a period of 18.6134 years. The maximum angle to the equatorial is (23º27'+5º09')=28º36' and 9.3 years later the angle is (23º27'-5º09')=18º18'. The *lunar node* is the cross-point between the moon plane and the ecliptic plane to the sun. This cross-point describes a *lunar nodal cycle* of 18.6134 years.

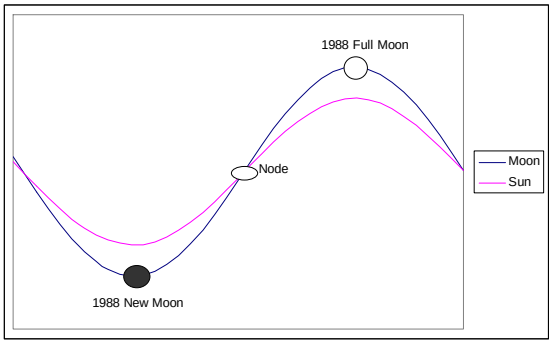

Figure 1.4 Cycles of the sun and the moon in 1988

Seen from the earth, the ecliptic plane and the moon plane form a sinus wave in the sky. When the moon plane angle is 28º36' it passes the maximum elevation of the sun and when it is 18º18' it passes under the sun's maximum elevation. The sun has an Arctic cycle that forms the southern limit of the midnight sun. In the same way, the moon has an Arctic cycle that determines the limits of the moon's visibility when it moves under the horizontal line of the earth. When the moon plane changes +/- 5º09' in a period of 18.6 years, the Arctic moon cycle is changing. In Norway this Arctic moon cycle changes between Sognefjord to Rørvik in Troms in a period of 18.6 years. The 18.6-year moon plane angle cycle of +/- 5º09' introduces a 18.6-year gravity force wave between the earth and the moon. This force influences the precession of the rotating axis and the lunar tide on the earth.

The earth's nutation cycle

James Bradley (1693-1762) discovered the earth's nutation when he sailed on the Thames. He observed how the wind vane on the mast shifted position with the varying motion of the boat, even though the wind had not changed direction. Comparing this to star observations, he concluded that the apparent stellar shift was brought about by the aberration of light, which was a result of the finite speed of light and the forward motion of the earth in its orbit.

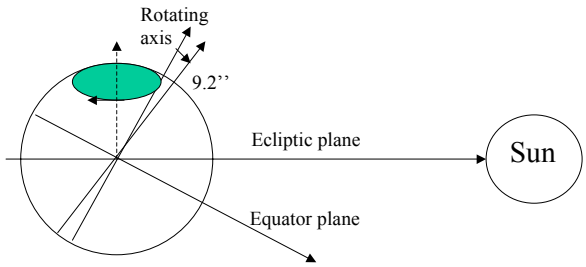

Figure 1.5 The earth's nutation

The earth's nutation (Latin *nutare*, "to nod") is a small irregularity in the rotating earth's axis on the equatorial plane. In astronomy this irregularity influences in the precession of the equinoxes. The earth axis movement has a set of cycles. Predicable precession cycles in time scale less than 300 years are called nutations. The four dominant nutation periods have cycles of 18.6 years, 9.3 years, 182.6 days (a half-year), and 13.7 days (a half-month). The most dominant of the four cycles is the nutation cycle of 18.6 years, which has an amplitude of +/- 9.2 arc seconds. The cause of the nutation lies chiefly in the fact that the plane of moon's orbit around the earth is tilted by about 5°09' from the plane of earth's ecliptic plane around the sun, and the spin of the earth's axis influences the earth's mantle and the earth's motion. Changes in the gravity angle to the moon will then influence the position of the earth axis. The 9.2'' nutation represents a change of about 6371000m*6.28*9.2/(360*60*60) = +/- 282 meters at the rotating axis on the equator plane.

The Polar position movement

The polar position movement is the rotating pole on the ecliptic plane. Leonhard Euler (1707-1783) predicted that the Earth's axis of rotation would also show a polar motion of 304 days with respect to an earth-fixed reference frame. He estimated this polar motion after analyzing the latitudes of astronomical observations over the last 50 years. The American astronomer Seth Carlo Chandler (1846-1913) predicted a polar motion period of 435 days. The pole's position changes from about 0.1 to 0.3 arc degrees, which represents a displacement of about 5 to 15 meters. It has been assumed that the pole position shows a secular drift of about 10 cm per year in the direction towards Ellesmere Island. These motions are presumed to be caused by gravitational forces from the sun and the moon as well as processes in the atmosphere, the oceans and the earth's interior. The polar motion's influence on climate seems to be poorly investigated. This thesis presents the hypothesis that this polar position controls the circulating water transport in the Arctic Ocean.

The lunar nodal tide

There are different types of tides. The first is *the diurnal and semi-diurnal tide,* caused by the rotation of the moon under the influence of the sun and the moon's gravitational field. The second type of tide is called *the parallactic tide*. This tide depends upon the varying distance of the sun and the moon and their position in relation to the earth. The third type is the *lunar nodal tide*. When moon's orbital plane inclines to the ecliptic plane by 5º09' and processes with an 18.6 year period, the oscillating angle introduces a forced 18.6-year gravitation cycle between the earth and the moon. This gravitation cycle will modulate an 18.6 year horizontal and vertical tide in the sea (Pugh, 1993).

Galileo Galilei (1564-1642) needed evidence of tides to prove his theory of the sun-centered solar system. Galileo could not account for the tides without the movement of the earth. Throughout his life he ignored the true cause of tides. He failed to see how a body so far away could exert so much power. To him the idea of lunar influence as was first described by Newton in Principia smacked of occultism

and astrology (Sobel, 1999). A mathematical framework for tides was later developed by Edmond Halley, Pierre Laplace, Lord Kelvin, and George Howard Darwin. Feldman (1988) reports that Toaldo (1784) found a correlation between climatic variations and lunar cycles. George Howard Darwin studied recorded fluctuations of the sea level at Bombay and was the first to draw attention to how the 18.6-year lunar nodal cycle introduced a long-term tide as well as geological changes (Darwin, 1877, 1879, 1880).

1.3 The lunar nodal cycle influence

> *"The end and the beginning of the lunar month are apt to be stormy"*
>
> --Aristotle and his young assistance Theophrastus of Eresus

The British astronomer Edmond Halley (1656-1742) studied the ancient knowledge of astronomy; he is best known for his studies of comets. Halley visited the physicist Isaac Newton in Cambridge and asked him about gravity's influence on bodies in motion. The result from Newton was the *Principia Mathematica.* Halley tried to solve the problem of the determination of longitude and conducted pioneering investigations in geophysics, trade winds, tides, the magnetism of the earth and the relationship between the weather and dynamic air pressure. He estimated the longitude by observing the 18.03-year lunar saros cycle, the cycle that is associated with the time between eclipses. Using this approach, he published a method that he claimed to be accurate within 69 miles at the equator. In 1699 he sailed in the Atlantic and made magnetic maps. In the paper *Atlas matitimus et commercialis* of 1728 he described the theory of a fluctuating herring stock between the Arctic Ocean and the North Sea, controlled by climate conditions (Wegner, 1993). This is probably the first paper on climate influence on biomasses in the North Sea.

In 1878, the German mathematician Karl Zöppritz (1838-1885) presented a mathematical treatment showing that wind could influence water at the greatest depths of the ocean, provided that sufficient time was allowed for what he considered a slow process (Zöppritz, 1878). The wind theory explained the circulation in the Atlantic Ocean. Later, Nansen supplemented this wind theory. He explained fluctuations of temperature and salinity in the Arctic Ocean as a product of fluctuations of wind and atmospheric conditions. This theory has been generally accepted as the main reason for ocean temperature fluctuations (Svansson, 2002).

Otto Krümmel (1854-1912**)** was a German professor of geography and considered to be the first research-oriented academic oceanographer in the modern sense. In 1887 Krümmel published the monumental *Handbuch der Ozeanographie*, which immediately attained status as the standard reference source for physical oceanographic information. The *Handbuch* contained a global chart of ocean surface circulation that depicted all the major currents in their proper locations. With this handbook Krümmel made a critical comment on long-term tides.

The Pettersson lunar-wave theory

The Swedish oceanographer Dr. Otto Pettersson (1848-1941) was skeptical about Zöppritz's wind theory. He found that variations in Swedish records occurred on a much shorter time scale than expected from the Zöppritz wind theory. Pettersson considered the temperature and salinity differences between the pole and the equator as the driving force behind ocean circulation. Differences in temperature and salinity made the cooled water sink, which in turn drove bottom water to the south. New, fresh surface water then must be transported from the equator to the Arctic Ocean. This ice-melting hypothesis is later referred to as the thermohaline theory (Svansson, 2002).

In 1909, Pettersson studied the relationship between herring catches and tides in Gullmarfjord on the west coast of Sweden. The study showed that the variation in the lunar perigee was related to fresh water movements and the arrival of schools of herring. As the ocean water presses in toward that inland sea, it dips down, allowing fresh surface water to roll out above it. At that depth, where salt and fresh water come into contact, a sharp layer of discontinuity forms, much like the surface film between water and air. This salt layer has a vertical fluctuation in long time series. Petterson found that the fluctuation correlated with the moon's phases, long-period tides and long-period herring catches. He explained these fluctuations with a long-period vertical tide that influenced the layers of different water density in the ocean. Fluctuations in these layers then influenced the sea's surface temperature, the climate and the recruitment of herring. He concluded that the long-period tide cycles of 18.09 and 111 years were the cause of herring biomass fluctuations at Bohuslen (Petterson O., 1905, 1914a, 1915, 1930; Lindquist, 2002).

Petterson argued that there were two types of tides; the *diurnal and the semi-diurnal tide* caused by the rotation of the earth under the gravitational field of the sun and the moon, and *the parallactic tide*. This tide depends upon the varying distance of the sun and the moon and their position with respect to the earth. By analyzing these distances he found oscillating periods of 9, 18, 93, 111, 222 and up to 1433 and 1850 years. The most important cycle was the 18.09-year saros cycle and the 111-year cycle that he called "The Greater Saros" (Petterson; 1914b, 1915, 1930; Hans Petterson, 1915). Ljungman had presented the theory that long-term biomass fluctuation of herring was related to a 111-year sunspot cycle (Ljungman, 1879). Now Pettersson found a 111-year cycle that matched the 111-year cycle in the herring records from Ljungman.

Petterson saw the relation between the long-term waves and extreme climate events and biomass fluctuations. He found a close relationship between the winter temperature at the Ona light house at the Norwegian west coast and the climate in Sweden (Pettersson, 1914a; Helland-Hansen and Nansen, 1909). Based on these estimates he argued that hydrographic changes affected the weather in Scandinavia. Variations in lunar-tidal effects in the Atlantic Ocean influenced climate fluctuations in the Scandinavia (Sanders, 1995).

The parallactic tide theory from Otto Pettersson and Hans Pettersson was not accepted by other scientists. The theories of tides were based on work from Laplace, which showed that the parallactic tide is too small to have any noticeable influence on the sea. Krümmel commented that: "anyone who has the slightest knowledge of the theory of tides must perceive that it cannot be a tide phenomenon". The famous meteorologist Waldemar Köppen said "this is to give our planet's satellite in space the blame for catastrophes of which she is absolutely guiltless". The leading authority in astronomy in America, Professor Charles A Young said, "The multitude of current beliefs as to the controlling influence of the moon's phases and changes over the weather and various conditions of life are mostly unfounded and in the strict sense of the word superstitious" (Pettersson, 1930). When Pettersson concluded that herring cycles were an astronomical coincidence of lunar periods, he presented his results to Krümmel. Krümmel accepted the reality of the phenomenon, but he declared that such considerable oscillations in the intermediate layer of the sea could not possibly be caused by tides (Pettersson, 1930).

Pettersson did not accept Laplace's results or the comments from other scientists. He continued to argue that Laplace's model was based on a homogenous sea. He believed his critics overlooked the fact that the sea consists of layers of different density, which can glide over each other. A long-term vertical tide could then introduce a vertical fluctuation in the layers. A vertical fluctuation in the layers could then explain fluctuations of herring recruitment in Bohuslen, fluctuations in the surface temperature, and fluctuations in climate (Pettersson; 1914b, 1915, 1930). In 1938 he predicted a new herring period from 1940. The herring period came in 1948.

The Izhevskii system approach

G K Izhevskii (1961, 1964) introduced a system approach to describe the interacting processes between the hydrosphere, the atmosphere and the biosphere. By studying the interactions of inorganic and organic processes in the ocean, he estimated dynamics of cod and herring in periods of about 20 years. The system theory was based on principles we now know from general systems theory and cybernetics: changes in relations, changes in the process dynamic (time-variant binding), processes that follow in a trend (eigen-dynamics), influences from external processes (super-systems), and the control from a constant flux of energy (forced input). This system theory represented a holistic view of processes on all levels.

Izhevskii supported Pettersson's ideas. He described ocean dynamics as the distribution of heat between the cold pole and the warm equator. The ocean heat flow and the difference between the ocean's surface and the land controlled the heat exchange in the atmosphere. Long-term tides intensified the currents to a greater or lesser degree and thus influenced heat transport in the ocean. He described long-term tides traveling around the globe where different annual periodicities and phases influenced the currents (Izhevskii, 1961, 1964).

Izhevskii analyzed the Kola section time series and described a winter theory and a temperature cycle theory. The winter theory was based on the observation that there was a close relation between the temperature in December and in October. By measuring the Kola section temperature in December, he estimated the temperature in October. The temperature cycle theory was based on the estimated temperature periods of 4-8, 8-10, 18-20 years. He explained these periods as "the complex interaction of many processes, strict periodicity, equal to the force which induced the periodicity, is upset, and variations become quasi-periodic" (Izhevskii, 1964). This means he believed that the cycles had an unknown external source.

Izhevskii explained biomasses as interacting systems. Reproduction and growth were explained by the many interactions in the food chain between plankton, phytoplankton, larvae, and young fish. The sum of regularities in the ocean influenced the fluctuations of biomasses. In the time series of cod and herring he found the same cycles as estimated in the Kola temperature series. From the estimated Kola temperature cycles, he estimated cod biomass fluctuations with a period of 20 years (Izhevskii, 1961, 1964).

The 18.6-year standing wave in the ocean

Pettersson's "lunar-wave" theory was pursued by Russian scientists. In the 1930s the concept of long-period tides and their influence on Atlantic water circulation was investigated by A L Chizhevsky, V B Shostakovich, M S Eygenson, B M Rubashev, T V Pokrovskaya and others (Maksimov and Smirnov, 1967). In the 1950s and 1960s Russian investigations were published by Lisitzin, Rossiter, Smirnov, and Maksimov (Maksimov and Smirnov, 1967). Maksimov and Smirnov (1967) and Maksimov and Sleptsov-Shevlevich (1970) identified a standing 19-year tide in the Atlantic Ocean. They found that this long-period wave influences the velocity and circulation of water masses and the sea temperature. The estimated change in temperature was about +/- 0.2 degree Celsius in the Atlantic and the Kola section. The results of the many Russian investigations were summarized by Maksimov and Smirnov (1964, 1965, 1967) with a standing wave theory and a climate theory.

1. A standing wave: There is a standing global 19-year wave in the oceans. A 19-year tidal wave that covers the Atlantic Ocean was identified in a time series from 1922 to 1960. This wave has the same cycle time in St. Andrew's Sound, Faroes-Shetland Channel, Nordøyane, Skomvær, and the Kola median.

2. A standing node: The standing wave has a maximum at the Arctic pole, a 50 percent maximum at the equator and a zero node at the 35 degree latitude.
3. A standing "astronomical" current: There is a corresponding long-term "astronomical" current that fluctuates between the Pole and the equator. The current has a maximum at the node.

The 18.6-year tidal water temperature in the North Atlantic was expressed by the equation $T_{18.6}(t)=0.24°C \sin(19.35°t+80°)$, where $T_{18.6}(t)$ has a maximum in 1950 and a minimum in 1959. The climate theory from Maksimov and Smirnov was based on the following conclusions:

1. A 19-year sea-current oscillation: Small 19-year fluctuations in Atlantic currents were sufficient to change the ocean's vertical temperature distribution and the surface temperature.
2. A 19-year atmospheric tide: Atmospheric interaction with a 19-year surface temperature fluctuation introduced a 19-year tidal fluctuation in the atmosphere.
3. A 19-year weather fluctuation: A 19-year tidal fluctuation in the atmosphere introduces a 19-year fluctuation in the weather.

Maksimov and Smirnov (1965) concluded, "The tidal phenomena in the atmosphere are not a consequence of the existence of pressure waves in the atmosphere of high latitudes, but they develop in nature solely as a result of the development in the seas and oceans (especially in high latitudes) of a long-period lunar tide which causes modifications in the transport and distribution of the heat in the hydrosphere." They commented in this same paper that: "Krümmel once commented that any idea that the moon affected weather was pure superstition. In our opinion, this judgment, which has had a great effect on science, was over hasty."

The results supported the ideas from Pettersson. At the same time these results showed that Maksimov and Smirnov identified the 18.6-year lunar nodal tide and Pettersson computed the 18.03-year Saros tide.

The 18.6-year cycles in climate indicators

Time series from nature show fluctuations in measured values. The problem is to interpret the data. Baron Jean Babtiste Joseph Fourier (1768-1830) came up with the idea of frequencies when he saw a blacksmith pulling together an anchor ring. He hypothesized that a time series might be represented by a set of stationary sinus-cycles. This means that if there is a stationary sinus-cycle in a time series, the cycle may be identified with a Fourier transform. This method makes it possible to identify dominant stationary cycles in time series.

The 1960s brought the development of better computers and better Fourier spectrum analysis algorithms. One pioneers in spectrum analysis was Robert G Currie. He analyzed a large number of time series using maximum entropy spectrum analysis. Using this method he identified the 18.6-year lunar nodal cycle in a time series of the temperatures in North America (Currie, 1981, 1984, 1987) Nile records since AD 650 (Currie et al., 1995), tree-rings in Africa and North America (Currie, 1991), fish catches, wine harvests (Currie, 1993), and many others. The collected work from Currie shows that the 18.6-year cycle has a global influence on the climate, the agriculture, the biomass in the sea and probably the economy. In 1994 Currie and Wyatt published a spectrum analysis of Lofoten records that showed 18.6-year cycle (Wyatt et al., 1994). This was probably the first time the 18.6-year cycle was identified in the time series of Northeast Arctic cod in the Barents Sea. Currie noticed the cycles had some non-linearities, but he had no explanation for these phenomena (Wyatt, pers.com). The other problem was that Currie could not explain the reason why he observed the 18.6-year cycle in the time series. This gave the impression that there was a phenomenon that was difficult to identify.

The investigations in this thesis have identified a set of harmonic and sub-harmonic cycles correlated to the 18.6-year lunar nodal cycle. This lunar nodal spectrum is identified in Arctic climate indicators and in biomass time series from the Barents Sea. The fundamental problem of the Fourier approach is that it is based on the theory of stationary cycles in time series from nature. The wavelet analysis

method introduced in this work shows that the cycle phase is related to a 74-year cycle. The source that has been identified of this important 74-year cycle is the Arctic Ocean and the polar position motion. This explains why the 18.6-year cycle has been difficult to identify in the NAO index time series and the Kola time series. The identified cycles in the Arctic climate indicators and the biomass time series are explained by the theory of coupled oscillators.

Chapter 2

ANALYSIS

"Chance " manifests itself in many forms,
Brings many matters to surprising ends;
The things we thought would happen do not happen;
The unexpected "Chance" makes possible:
And that is what is happening all the time"

--Euripides, 5th century BC, at the end of Medea.

The problem of data analysis is to identify the hidden causes behind what looks like a chance.

2.1 Analysis methods

The system architecture

The investigated system is represented by the simplified general system architecture:

$$S(t) = \{B_p(t), \{S_{sun}(t), S_{moon}(t), S_{earth}(t), S_v(t)\}\} \in \mathbf{w} \qquad (2.1)$$

where $S_{sun}(t)$ represents the sun system, $S_{moon}(t)$ the moon system, $S_{earth}(t)$ the earth geo-system, and $S_v(t)$ is a disturbance from an unknown source. In this investigation the sun system $S_{sun}(t)$ represents a constant energy flux to the earth. The relation $B_p(t)$ represents a time-variant mutual gravity force between the planetary system elements and w represents the system model purpose. Cycles in the gravity force are expected to introduce a climate disturbance in the earth system $S_{earth}(t)$. The earth system may be represented by the system elements:

$$S_{earth}(t) = \{B_{earth}(t), \{S_{man}(t), S_{oce}(t), S_{atm}(t), S_v(t)\}\} \in \mathbf{w} \qquad (2.2)$$

where $S_{man}(t)$ represents the earth mantle system, $S_{oce}(t)$ the ocean system, $S_{atm}(t)$ the atmospheric system, $S_v(t)$ is a disturbance from an unknown source, and $B_{earh}(t)$ represents the binding between the systems. In this investigation the ocean system $S_{oce}(t)$ is represented by $S_{oce}(t) = \{B_{oce}(t), \{S_{acr}(t), S_{atl}(t), S_{bar}(t), S_{gren}(t), S_v(t)\}\}$ where $S_{acr}(t)$ is the Arctic Ocean, $S_{atl}(t)$ is the Atlantic Ocean, $S_{bar}(t)$ is the Barents Sea, $S_{gren}(t)$ is the Greenland Sea, and $S_v(t)$ is an unknown source. The Barents Sea system may be represented by the system elements:

$$S_{bar}(t) = \{B_{bar}(t), \{S_{kola}(t), S_{ice}(t), S_{pla}(t), S_{bio}(t), S_v(t)\}\} \in \mathbf{w} \qquad (2.3)$$

where $S_{kola}(t)$ represents the sea temperature system, $S_{ice}(t)$ represents the ice extent system, $S_{pla}(t)$ represents the biomass plankton system, the biomass system $S_{bio}(t)$ represents the biomasses in the Barents Sea, $S_v(t)$ is a disturbance from an unknown source, and $B_{bar}(t)$ represents the binding between

the systems. In this investigation the biomass system $S_{bio}(t)$ is represented by $S_{bio}(t)=\{B_{bio}(t),\{S_{shr}(t), S_{cap}(t), S_{cod}(t), S_{her}(t), S_{had}(t), S_v(t)\}$ where $B_{bio}(t)$ is the mutual binding, $S_{shr}(t)$ is the shrimp biomass system, $S_{cap}(t)$ is the capelin biomass system, $S_{cod}(t)$ is the cod biomass system, $S_{her}(t)$ is the herring biomass system, and $S_v(t)$ is an unknown source (Yndestad, 2001b).

The system dynamics

System dynamics is the theory of how system elements change in time. In this investigation system dynamics are analyzed according to these hypotheses:

1. *The stationary cycle hypothesis:* If there is a stationary cycle in a time series, the cycle must have a stationary source.
2. *The First Cause hypothesis:* A stationary cycle may be traced backwards in a chain of events to a first stationary cycle, which is the First Cause.
3. *The Mutual Relation hypothesis:* If there is a stationary cycle in a system, it will influence all related systems.

The First Cause hypothesis

The mutual relation between the sun, the moon and the earth introduces a set of long-term cycles in the gravity force $B_p(t)$ (Equation 2.1). This investigation is limited to time series from about 50 to 160 years. The analysis is thus limited to the lunar nodal cycle, or the cross-point between the moon plane cycle and the ecliptic plan to the sun. This cross-point describes a lunar nodal cycle of 18.6134 years. The lunar nodal cycle is described by the model:

$$u_0(j\omega_0) = U_0 + u_o \sin(\omega_0 t + \varphi_0) \tag{2.4}$$

where the eccentricity U_0=23°27'. The lunar nodal cycle amplitude u_0=5º09'(deg), $\omega_0=2\pi/T_0=2\pi/18.6134$ (rad/yr) is the lunar nodal angle frequency, and t (years) is the time from t=1900. The cycle amplitude of $u_0(t)$ has a maximum in November 1987 and a minimum in March 1996 (Maksimov and Smirnov, 1965, 1967; Pugh, 1996) when the phase-angle is about $\varphi_0 = 0.9\pi$ (rad). Changes in the gravity force on the earth introduce a 18.6-year vertical and horizontal lunar nodal tide, the 18.6-year nutation of the earth's axis, and the polar position.

The stationary cycle hypothesis

The lunar nodal cycle introduces a cyclic gravity force as a forced oscillator on the earth. The gravity force has a vertical and a horizontal component. The movement energy from the force is distributed as a spectrum on the earth. This spectrum may be described as:

$$\begin{aligned} X(j\omega) &= H(j\omega)u_0(j\omega_0) \\ X(j\omega) &= \sum_{n,m} u_{n,m}(jn\omega_0/m) + V(j\omega) \\ X(j\omega) &= U(j\omega_0) + V(j\omega) \end{aligned} \tag{2.5}$$

where $H(j\omega)$ represents the frequency transfer function of a nonlinear earth system, n represents the harmonic cycles, m the sub-harmonic cycles, $u_{n,m}$ a cycle amplitude, $U(j\omega_0)$ a lunar nodal spectrum and $V(j\omega)$ a non-correlated disturbance from an unknown source.

The lunar nodal spectrum $U(j\omega_0)$ is expected to result in a set of events on the earth system. Each system element on the earth is expected to introduce a new set of events. The spectrum of the n-te event may be described by the model:

$$X_n(j\omega) = H_n(j\omega)X_{n-1}(j\omega)$$
$$X_n(j\omega) = H_n(j\omega)[U_{n-1}(j\omega_0) + V_{n-1}(j\omega)]$$
$$X_n(j\omega) = U_n(j\omega_0) + V_n(j\omega) \qquad (2.6)$$

where $H_n(j\omega)$ represents the frequency transfer function of the n-th nonlinear earth system element and $V_n(j\omega)$ a non-correlated disturbance from an unknown source.

The lunar nodal spectrum $U_{n-1}(j\omega)$ represents a set of forced oscillators on $H_n(t)$. The transfer function $H_n(j\omega)$ is expected to influence the amplitude and phase of stationary cycles $U_{n-1}(j\omega)$. According to this hypothesis the modulated stationary spectrum $U_n(j\omega_0)$ may have a harmonic spectrum related not only to the nodal spectrum $U(j\omega_0)$, but to each stationary cycle in the spectrum $U_{n-1}(j\omega_0)$. The influence of the transfer function $H_n(j\omega)$ on the non-correlated noise spectrum $V_{n-1}(j\omega)$ is expected to be a new, transformed non-correlated noise spectrum $V_n(j\omega)$.

Cycle identification

The Fourier spectrum $X(j\omega)$ of a time series x(t) may be represented by the model:

$$X(j\omega) = U(j\omega_0) + V(j\omega) \qquad (2.7)$$

where $U(j\omega_0)$ represents a lunar nodal spectrum and $V(j\omega)$ represents a non-correlated red spectrum from an unknown source.

One of the main problems encountered in this analysis is identifying a possible lunar nodal spectrum $U(j\omega_0)$ in the total spectrum $X(j\omega)$. Stationary cycles $U(j\omega_0)$ will introduce cycles of a time-variant amplitude and phase in a system element when the elements have a time-variant binding B(t). In a long time series this will introduce a time-variant amplitude and phase in the estimated cycles. This property makes it difficult to identify stationary cycles with straightforward statistical methods. A second problem is that it can be difficult to identify low frequency cycles and to separate the high frequency cycles from noise in these short time series. Wavelet transformation is an appropriate method to analyze time-variant data series. A continuous wavelet spectrum is computed by the wavelet transformation:

$$W(a,b) = \frac{1}{\sqrt{a}} \int_R x(t)\Psi\left(\frac{t-b}{a}\right)dt \qquad (2.8)$$

where x(t) is the analyzed time series, $\Psi(\ )$ is a wavelet impulse function, W(a,b) is the computed wavelet cycles, b is a translation in time and a is a time scaling parameter in the wavelet filter function. The computed wavelets W(a,b) represent a set of filtered time series from the time series x(t) and the impulse functions $\Psi(\ )$. In the following analysis, a Coiflet3 wavelet transform was chosen from many trials on tested data (Matlab, 1997; Daubechies, 1992). This wavelet transformation represents a linear phase filter that is able to separate additive cycles in a time series.

A wavelet transformation W(a,b) represents a set of cycles in the time series x(t). The time series x(t) may thus be represented by a sum of dominant wavelets that has most of the energy in the time series x(t). Then we have:

$$x(t) = \sum_k \mathrm{W(k,t)} + \mathrm{v(t)} = W(t) + v(t) \qquad (2.9)$$

where k is a cycle period, W(k,t) represents a dominant wavelet cycle where the cycle period is k a year, W(t) is the sum of wavelet cycles, and v(t) is a disturbance from an unknown source. A wavelet cycle W(k,t) represents a moving correlation to an impulse period k. A dominant cycle period thus represents the best correlation to a cycle period k.

Cycle period verification

The lunar nodal spectrum $U(j\omega_0)$ is identified in the wavelet spectrum by computing the cross-correlation quotient:

$$R(k) = E[u(j\omega_k)W(k,t)] \qquad (2.10)$$

where $u(j\omega_k)$ is the cycle k in the lunar nodal spectrum $U(j\omega_0)$ and W(k,t) is the cycle k in the computed wavelet spectrum. The wavelet cycle time k is tested by computing the correlation coefficient R(k) between the dominant wavelet cycle W(k,t) and a potential known stationary cycle $u(\omega j_k)$.

The correlation quality verification

The correlation value of quality is computed by Q(k)=R(k)*sqrt[(N-2)/(1-R(k)*R(k))] where N is the number of samples in the time series.

Cycle dominance verification

The cycle amplitude dominance is identified by the signal-to-noise ratio. The signal-to-noise ratio between the dominant wavelets and the unknown source is computed by:

$$S/N = \mathrm{var}(W(t)) / \mathrm{var}(v(t)) \qquad (2.11)$$

where v(t) = (x(t)-W(t)) represents the estimated disturbance from an unknown source in the time series.

2.2 Paper summaries

Earth nutation influence on the temperature regime of the Barents Sea

The initial research question asked if there is a stationary cycle in the biomass of cod. Signal theory tells us that a stationary cycle must have a stationary energy source. This means that if cod recruitment has a stationary 6-year cycle, the recruitment must be influenced by an unknown 6-year cycle in the Barents Sea. If there exists a stationary 6-year cycle, it must be driven by a more fundamental stationary cycle source in nature. The potential source of this 6-year cycle was the temperature in the Barents Sea where the biomass of Northeast Arctic cod is recruited.

Otto Pettersson (1930), Maksimov and Smirnov (1965) and Royer (1993) have described there has been a skeptical attitude toward a lunar cycle influence on the climate and the associated biomass fluctuation. In the 1960's Russian scientists reacted skeptically to Izhevskii's work. Research conducted by Maksimov and Smirnov (1964, 1965, 1967) represented the last research such work on the 18.6-year tide in Russia (Ozhigin, pers.comm.). During the last 40 years, almost nothing has been published on this problem. Thus it was necessary to develop new analysis methods and new theories to explain the results.

According to general systems theory, the Barents Sea system is only a sub-system in the global sea system. This means that if the Barents Sea has a stationary temperature cycle, the cycle must be influenced by a more fundamental energy source. A potential source of this energy is the change in the earth's rotation. An initial investigation showed that a 6-year cycle in the earth's rotation was unknown. But there was a 18.6-year cycle called the earth's nutation. From signal theory it is known that a stationary energy cycle in a nonlinear system will produce a set of harmonic cycles. This posed a new question: Is this 6-year cycle a third harmonic cycle of the 18.6-year earth nutation cycle? If so, the temperature in the Barents Sea may have a stationary cycle of about 6.2 years. These questions initiated an analysis of the Kola section temperature series. The results were first published at the ICES Annual Science Conference in Iceland (Yndestad, 1996a).

A rewritten paper was published in the ICES Journal of Marine Science (Yndestad, 1999a). This paper explains how the view of earth science has changed. Early science was influenced by the paradigm of the earth as a solid stable system. Modern science looks at the earth as a dynamic system influenced by planetary dynamics. It has been a common belief that temperature fluctuations in the Barents Sea are mainly driven by wind and atmospheric conditions. The paper introduces the hypothesis that the fluctuations may be driven by the harmonic spectrum from the 18.6-year earth nutation cycle. The methods are based on a general system theory. The system models are based on the concepts of state dynamics, a Wiener spectrum in the frequency distribution, the 18.6-year earth nutation cycle as the forced oscillator, a modulated spectrum from the 18.6-year cycle, and the fact that energy may be saved by resonance in feedback systems, structural instability and unstable phases.

Materials and methods

The Barents Sea temperature was represented by the annual Kola section temperature from 1900 to 1999. The data was provided by PINRO in Murmansk and IMR in Bergen. The cycle identification analysis was a challenge. The data series looked noisy and different from random noise. To learn more about this Kola data series, it was necessary to try different spectrum analysis methods to look for similarities:

- Spectrum analysis: The time series was analyzed by Fourier transforms, periodograms, Welch spectral density estimates and autocorrelation to identify dominant cycles. These methods identified the 6.2-year cycle, but there was a poor signal-to-noise ratio.
- Phase-space analysis: A phase-space analysis showed a circular pattern around a single temperature. This indicated a stationary cycle in the time series.

- Cross-correlation analysis: A cross-correlation between the time series and the lunar nodal spectrum identified the dominant cycles of 18.613, 18.613/3=6.2, and 3*18.613=55.8 years, and the method identified the cycle periods and the cycle phase.

The cross-correlation method was the most important. This method showed that the time series was highly sensitive to periods of 18.613, 18.613/3, and 3*18.613 years. It was possible to both identify the cycle phase and get an estimate of the more long-term cycles of 18.6 and 55.8 years. These long-term cycles could not have been estimated properly using ordinary spectrum estimate methods.

Results

The main results from the paper are:

- The First Cause: The 18.6-year lunar nodal cycle was identified in the Kola time series. The 18.6-year cycle from the earth's nutation was identified as the First Cause.
- A lunar nodal spectrum: Harmonic cycles of 18.6/3=6.2 years and 3*18.6=55.8 years in the Kola time series were identified in the Kola section temperature, probably for the first time.
- The cycle influence: A cross-correlation quotient R=0.5 was estimated between the Kola time series and the identified lunar nodal spectrum.
- An attractor in the phase-space: The analysis identified a stationary cycle by an attractor in the phase-space.
- The mean temperature: The 55-year cycle seems to represent a fluctuating mean temperature in the estimated time period. This indicated that the Kola section has no stationary mean temperature.

Concepts and ideas

- The forced oscillator theory: The energy from the earth's nutation may be understood as a forced oscillator that introduces a chain of events. The Kola section cycles are estimated in this chain of events.
- The modulation theory: The energy from the forced 18.6-year cycle on the earth's nonlinear systems may modulate a harmonic spectrum. In this time series a third harmonic cycle of 18.6/3=6.2 years and a third sub-harmonic cycle of 3*18.6=55.8 years are identified as a lunar nodal cycle spectrum in the Kola temperature series.
- The resonance theory: A resonance in the earth's circulating systems may conserve energy in some harmonic lunar nodal cycles.
- The structural instability theory: The circulating system that may conserve energy by resonance is fundamentally structurally unstable. This means that the identified lunar nodal spectrum may have a stationary cycle time and an unstable phase.

The concepts and ideas in this first paper have been confirmed by later investigations. The estimated cycles in the Kola time series are a reference in later analysis. In this analysis the Kola cycles were identified as a stationary stochastic process. In a later investigation a wavelet analysis identified the instabilities as phase-reversals in the lunar nodal cycles.

Earth nutation influence on the system dynamics of Northeast Arctic cod

Fluctuations in biomasses in the Barents Sea have been a main marine research subject for more than 100 years. Early marine science was influenced by the hypothesis that the fluctuations in marine biomass may be influenced by a fundamental cause in nature. Petterson. (1914a) ascribed these changes to fluctuations in long-term tides; Helland-Hansen and Nansen (1909) found a relationship between cod biomass fluctuations and the Ona air temperature; Otterstad (1942) found a relationship between the cod biomass and tree rings in Troms. In the 1960s the Russian scientists Izhevskii (1961) and Maksimov and Smirnov (1964, 1965) presented the hypothesis of a relationship between biomass fluctuations and long-term tides. Hjort (1914) introduced the hypothesis that fluctuations may be a product of a match or a mismatch between the growth of zooplankton and the food available for the

spawning recruitment of larvae. More recent research seems to have shifted focus from the fundamental causes to the more complex ecological explanations.

The Kola section temperature analysis identified dominant stationary cycles of 18.6/3=6.2 years as the potential source of the cycle that was associated with a 7-year cycle in the biomass of Northeast Arctic cod. This opened a new set of questions. How does this temperature cycle influence cod biomass? Is the biomass influenced by the estimated Kola cycles of 18.6 and 3*18.6=55.8 years? To get an answer it was necessary to correlate the identified Kola cycles with all data and parameters in a cod biomass model. A complete biomass model of Northeast Arctic cod was thus estimated to correlate biomass fluctuations with the lunar nodal spectrum. The results of the analysis were first published at the ICES Annual Science Conference in 1996 (Yndestad, 1996b). A rewritten paper "Earth nutation influence on system dynamics of Northeast Arctic cod" later was published in ICES Journal of Marine Science (Yndestad, 1999b).

Materials and methods

The biomass model of Northeast Arctic cod was estimated using the official ICES data from 1946. The investigation was based on a data analysis and a parameter analysis. The cod biomass model was implemented on a spreadsheet and on a Matlab program for data analysis. The model estimated the recruitment rate, growth rate, maturity rate, and mortality rate for each year class from 0 to 15 years. The analysis was based on the following methods:

- A lunar cycle reference: The cycle time and phase from the identified Kola cycles were the reference in all investigations.
- A spectrum analysis: A spectrum analysis first identified stationary cycles of 6.2 years in the data time series.
- A cross-correlation: A cross-correlation analysis between the estimated parameters and the Kola temperature cycles identified the relation between the temperature fluctuations and the model parameter fluctuations.
- Mean square error: The mean square error between the real biomass data from ICES identified how the Kola temperature cycles defined parameters in all year classes.

Results

The main results of the analyses are:

- Influence on recruitment: The spectrum analysis confirmed a 6-year cycle in the 3-year recruitment. Visual inspections showed that the 3-year recruitment was related to the 18.6-year Kola temperature cycle.
- A recruitment model: A deterministic recruitment model was constructed, which is exponentially related to the Kola cycles of 6.2 and 18.6 years.
- A biomass model: A dynamic biomass model of Northeast Arctic cod was presented, where the parameters were optimized to the Kola section cycles of 6.2 and 18.6 years.
- Sustainable biomass: The mean maximum catch rate in a sustainable biomass was estimated to be about 0.3 (annual catch/biomass).

Concepts and ideas

- The forced oscillator theory: The 6.2-year Kola temperature cycle acts as a forced oscillator on cod biomass dynamics.
- The biomass resonance theory: The biomass has a resonance in feedback between the spawning biomass and the biomass recruitment. This feedback is controlled by the 6.2-year Kola section temperature cycle.
- Structural instability: Fluctuations in the biomass feedback system may be influenced by disturbance from predators and catch.
- Long-term forecasting: The deterministic property of the temperature cycles opened a possibility of better long-term forecasting in periods of 6 to 18 years.

- Stationary properties: Temperature dependent recruitment showed that the biomass represents a time-variant stochastic system where there is no mean biomass.

Later investigations have confirmed that these estimates of cod biomass are a robust model.

Earth nutation influence on Northeast Arctic cod management

The biomass model of Northeast Arctic cod was enhanced to forecast biomass fluctuations during the next 20 years. This allowed for the possibility of studying the long-term influence of the 6.2- and 18.6-year Kola section temperature cycles. At the same time, it permitted the investigation of how different management strategies influenced the biomass fluctuations. The model demonstrated that the 6.2-year cycle had a major influence on new recruitment and the 18.6-year cycle controlled long-term growth. The model was tested against historical data from ICES. The new question then became, can the model forecast future biomass fluctuations? To get an answer the model has been tested on official data each year since 1996. During this period the model has identified a phase delay between estimated fluctuations and official ICES data. The forecast has shown that the climate-driven model is more optimistic than ICES forecasts when the biomass is on the increase and more pessimistic when it is declining.

Cod biomass is influenced by positive feedback between the spawning biomass, recruitment and a 6 to 7-year delay in a new spawning biomass. In this feedback system, the 6.2-year Kola cycle was associated with good recruitment cycles in periods of 6-7 years. At the same time there was a phase delay in the biomass estimates because it was based on historical data, and there was a delay in the new quota of landings. From my estimate the total delay was about 2-3 years. The result was a 180 degree phase error between the biomass fluctuations and the quota of landing. This problem was first presented at an international conference on systems dynamics in Istanbul (Yndestad, 1997). Later, the fundamental method problem of long-term forecasting was published at an international conference on systems dynamics in Bergen (Yndestad, 2000).

The phase difference between quota of landings and the observed biomass in the Barents Sea introduced a conflict between the fishing industry and marine scientists. In 1990 the Norwegian government started an investigation to find out what was wrong with existing biomass management. I was invited to IMR in Bergen in 1997 to discuss how to make better estimates of the Northeast Arctic cod biomass (Godø, 1998). In this discussion I argued that cod management was mainly a system dynamic control problem. This was the start of a paper that was published in ICES Journal of Marine Science (Yndestad, 2001a). The paper explains the fundamental problems in understanding biomass dynamics and their control. Biomass dynamics are explained by a dynamic model, by a forecast simulation and by the effect of different management strategies.

Materials and methods

The database comes from publicly available data from ICES. The model is a climate-driven model (Yndestad, 1999b). The methods are based on:

- Control theory: The study was based on fundamental principles from feedback control theory.
- Phase analysis: The influence on measurement phase delay in model simulations was evaluated.
- Case studies: The study simulated the effect of different management strategies in a period of 20 years.

Results

The main results of the analysis are:

- Biomass fluctuations: The Kola temperature cycles influence recruitment and biomass stability. This unstable situation is observed as fluctuations in biomass.
- Effects of current management: Current management introduces three types of instabilities that amplify biomass fluctuations.
- Forecasting: The biomass is expected to have a temporary increase at about the years 2003-4 as an effect of the 6.2-year Kola cycle. Biomass is expected to decline before the next growth period at about 2009.
- Phase sensitivity: The paper demonstrated the importance of phase delay in biomass assessments.
- Sustainable biomass: There is long-term growth in the biomass when the spawning biomass is about 500,000 tons.
- Optimal management: Optimal management depends on the planning range. A good long-term management strategy is to have a constant catch rate less than 0.3 (annual catch/biomass).
- Rebuilding the biomass: It will take more than 15 years to rebuild the biomass to its previous 1950 level.

Concepts and ideas

- Feedback instability: There is about a 3-year management phase delay in the biomass feedback that has a 6.2-year recruitment cycle. This delay causes feedback-driven instability.
- Reference instabilities: There is no reference in the biomass feedback control system. This means the biomass state will not converge on any level. This introduces a long-term biomass fluctuation that may cause a biomass collapse.
- Control instability: The catch rate changes each year. When the catch rate is changed faster than the biomass dynamics, there is no long-term biomass control.
- Phase delay in official ICES data: The current VPA-model in the ICES estimates (ICES, 1999) introduces a phase error in the estimate that may cause an instability in current management.

This model has been tested each year since 1996 against official ICES data (Yndestad, 2001c). In this period the model has been reliable and robust.

System Dynamics of Barents Sea Capelin

The biomass analysis of Northeast Arctic cod confirmed the hypothesis of stationary biomass fluctuations associated with the Kola temperature cycles of 6.2 and 18.6 years. This posed a next generation of questions. Is this biomass fluctuation caused by fluctuations in recruitment or in mortality? To get an answer, it was necessary to analyze the biomass dynamics of other species.

An analysis of the food chain in the Barents Sea was initiated in 2000. This work led to the development of dynamic biomass models for zooplankton, shrimp, herring, capelin, seithe, haddock and cod. The purpose of these models was to look at a relationship between the estimated Kola cycles in the food chain and other species. The results showed that all analyzed species had fluctuations where the cycle time and the cycle phase were correlated with the 6.2- and the 18.6-year Kola cycles. From this work an analysis of capelin dynamics was selected for publication. Capelin was selected because it is of special importance in the food chain, and because the dynamics are different and there is less published information on this species. The paper was first published at the 89th ICES Annual Conference in Oslo in September 2001 (Yndestad and Stene, 2001). The paper was published in ICES Journal of Marine Science the following year (Yndestad and Stene, 2002).

Materials and methods

The database comes from publicly available information from ICES. The methods are based on:

- A cross-correlation analysis: A cross-correlation analysis was conducted to compare data and parameters in the capelin biomass model and the identified Kola temperature cycles.
- Model identification: The mean square error between the capelin biomass model and official data from ICES was identified.
- Frequency response: The biomass frequency transfer function was identified.

Results

The main results from the paper are:

- Dominant cycles: Dominant cycles of 18.6/3=6.2 and 18.6/2=9.3 were identified in the time series of recruitment and biomass growth.
- Resonance: A biomass eigen-frequency cycle (resonance) was identified with a cycle time of about 6.2/2=3.1 years.
- The cycle phase: Biomass growth, reduction and collapse are related to the phase-relation between the biomass eigen-frequency cycle and the Kola section cycles of 6.2 and 18.6 years.
- Biomass collapse: The collapse in the biomass was related to a combination of a climate cause and overfishing.
- Max catch rate: The biomass seems to have long-term growth when the catch rate is less than 0.5 (annual catch/biomass).

Concepts and ideas

- Long-term growth: It was concluded that large biomass fluctuations are necessary for long-term growth.
- The importance of eigen-dynamics: The biomass has an eigen-dynamics adapted to an optimal long-term dynamics.
- Kola cycle relations: The capelin biomass eigen-dynamics is adapted to the identified 6.2 and 18.6-year Kola cycles.
- The importance of phase: The biomass growth is dependent on the phase-relation between the Kola temperature cycles of 6.2 and 18.6 years, and the biomass eigen-dynamics of 6.2/3=3.1 years.
- Ecological dynamics: The biomass analysis indicated that the dominant fluctuations are caused by the plankton biomass fluctuations in the recruitment period.

The Code of Long-term Biomass Cycles in the Barents Sea

The analysis of the time series and the dynamics biomass models explained why the recruitment of cod, shrimp, haddock, capelin and herring are influenced by the 6.2-year cycle and why the 18.6-year cycle influenced growth in life cycles. All analyzed species had a growth where the cycle time and the cycle phase are correlated with the Kola section temperature cycles. This indicated a relationship between the Kola temperature cycles, food for recruited biomass and biomass growth. But there remained unanswered questions. Why are there long-term fluctuations of about 50 to 80 years in the biomasses of Northeast Arctic cod and Norwegian spring-spawning herring? Is this cycle caused by the 55.8-year Kola temperature cycle? If so, are long-term biomass fluctuations caused by the mean Barents Sea temperature, which is close to the 55.8-year cycle? What caused the biomass collapse of cod, herring and capelin? Were these biomass collapses caused by nature or by overfishing?

The third harmonic cycle was another mystery from the beginning. Why are there third harmonic and third sub-harmonic cycles in the cod biomass, capelin biomass, the Kola temperature and the climate cycles? The problem was solved by mathematics. Interactions between the Kola cycle influence on the recruitment rate and the biomass feedback introduced a frequency modulation. A paper on this subject was first presented at the ICES Annual Science conference in Oslo (Yndestad, 2002) and later published in ICES Journal of Marine Science (Yndestad, 2003b).

Materials and methods

Most of the information comes from publicly available data from ICES. The methods are based on:

- Cycle separation: A wavelet analysis of the time series was used to separate the dominant cycles from the time series and the phase relation to the Kola temperature cycles.
- The cycle source: A cross-correlation between lunar nodal reference cycles and the dominant wavelet cycles was used to identify the relation to the lunar nodal spectrum.
- Correlation quality: The computed cross-correlation was analyzed for quality.
- Dominance analysis: The influence from the lunar nodal spectrum in the time series was estimated using the signal-to-noise ratio.

Results

The main results from the paper are:

- The eigen-frequency: Capelin, herring and cod have an eigen-frequency cycle which is related to the 6.2-year Kola cycle.
- Long-term growth: There is long-term biomass growth when the 6.2 and the 18.6-year Kola cycles are positive at the same time.
- Long-term reduction: There is a long-term biomass reduction when the 6.2 and the 18.6-year Kola cycles are not positive at the same time.
- The biomass collapse: There is a minimum biomass when the 6.2 and the 18.6-year Kola cycles are negative at the same time.

Concepts and ideas

- The growth code: Long-term growth or reduction of biomass is not associated with the absolute Kola temperatures, but the phase-relation between the biomass eigen-frequency cycle and the Kola cycles.
- The code of biomass collapse: Biomass collapse is associated with the worst-case phase-relation between the biomass eigen-frequency cycle and the Kola cycles.
- The climate clock: The Kola cycles may be represented by a set of vectors or a “climate clock” with cycles of 6.2, 18.6 and 55.8 years.

The Cause of biomass dynamics in the Barents Sea

The parameter analysis of capelin, cod and herring showed that the parameters in all biomass models were influenced by the 6.2- and the 18.6-year Kola temperature cycles. This means that the biomasses may be described as a time-variant stochastic system controlled by something connected to the Kola temperature cycles. A time-variant stochastic biomass represents good news and bad news at the same time. The bad news is that there is no stationary mean biomass, no stationary safe limit, and that previous data will have limited predictive value. This property introduces a fundamental stability problem in current biomass management (Yndestad, 2001a). The good news is that the stationary cycles are a deterministic process controlled by the stable lunar nodal cycle. This allows us to revisit the first research question. If we are able to forecast biomass dynamics, then it is possible to control future dynamics.

The wavelet analysis of climate time series and biomass time series represented a paradigm shift in time series analysis and supported the discussion from the “Predestined Fate paper” (Yndestad, 2000). This paper has evaluated the consequences of a paradigm shift from Newtonian dynamics and introduced a “phase-clock” to represent dominant wavelet cycles (Yndestad, 2004).

Materials and methods

The database comes from publicly available data from ICES. The methods are based on:

- Cycle separation: A wavelet transformation of the time series was used to separate the dominant cycles from the time series and the phase relation to the Kola temperature cycles.

- The cycle source: A cross-correlation between lunar nodal reference cycles and the dominant wavelet cycles was used to identify the relation to the lunar nodal spectrum.
- Correlation quality: The quality of the computed cross-correlation was analyzed.
- Dominance analysis: The influence from the lunar nodal spectrum in the time series was estimated by the signal-to-noise ratio.

Results

The main results from the paper are:

- The eigen-frequency cycle adoption: The biomass of shrimp, capelin, herring, cod and haddock have an eigen-frequency cycle time where the cycle time and phase are correlated to the 6.2-year Kola cycle.
- Lunar nodal spectrum in biomass fluctuations: A wavelet analysis shows that the dominant biomass fluctuations of shrimp, capelin, herring, cod and haddock are correlated to the 6.2-, 18.6- and 55.8-year Kola cycles.
- Data reduction to a "phase-clock": The dominant cycles of 6.2, 18.6 and 55.8 years in the Kola temperature may be represented as vectors or a "phase-clock" that shows the current state and the expected state in the future.

Concepts and ideas

- The phase-clock: The time series and forecasting may be represented by three rotating vectors, which may be visualized as a phase-clock. The clock shows the cycle history, the cycle state and expected cycle fluctuations.
- The paradigm shift in forecasting: The phase-clock concept represents a paradigm shift in biomass forecasting. If we know the cycle phase, we may forecast future biomass fluctuations.
- A paradigm shift in dynamics: The transformation of the phase-clock represents a paradigm shift from the Newtonian approach of dynamics to the Aristotelian approach of rotary movements.

The Lunar nodal cycle influence on Arctic Climate

Analysis of shrimp, capelin, herring, cod and haddock biomass all showed that biomass was adapted to the identified lunar nodal spectrum in the Kola time series. This was a strong indication of a long-term influence on the biomass. But where is the missing link? What are the potential links between the 18.6-year lunar nodal cycle and estimated biomass cycles in the Barents Sea? Is the Barents Sea influenced by the 18.6-year Atlantic Ocean tide? Or is the Barents Sea influenced by Arctic Ocean circulation, which is controlled by the earth's nutation? Is there a relation between the earth's nutation and polar motion? Is there any relation to the NAO winter index or the air temperature at Røst where cod are spawning? These questions initiated a new time series analysis of Arctic climate indicators.

The search for the missing link between the 18.6-year lunar nodal cycle and the 18.6-year cycle in the Kola section started early in 2001. The Kola section temperature papers from 1996 and 1999 reported a dominant 18.6-year nodal cycle in the data series, but the link between the Kola section temperature and the 18.6-year lunar nodal cycle was still unclear. One possible hypothesis was the 18.6-year lunar nodal tide in the Atlantic Ocean. The second possibility was pressure from circulating water in the Arctic Ocean, which is controlled by the earth's 18.6-year nutation. There was, however, no access to a long earth nutation time series, but there was a long polar position time series. A short paper on this subject was presented at the ICES Annual Science conference in Tallinn (Yndestad, 2003a). A full unpublished paper is presented in this thesis.

Materials and methods

The study relied on data describing the polar position, the Kola temperature, the extent of ice in the Barents Sea, the annual sea level at Hammerfest, the ice extent in the Greenland Sea, air temperatures at Røst, and the NAO winter index. The methods are based on:

- Cycle separation: A wavelet transformation of the time series was used to separate the dominant cycles from the time series.
- The cycle source: A cross-correlation between lunar nodal reference cycles and the dominant wavelet cycles was used to identify the lunar nodal spectrum.
- Correlation quality: The quality of the computed cross-correlation was analyzed.
- Dominance analysis: The influence from the lunar nodal spectrum in the time series was estimated by the signal-to-noise ratio.

Results

The main results from the paper are

- The polar position oscillation: The polar position time series has dominant cycles of about 18.6*4=74.4, 18.6, 18.6/3=6.2, and 18.6/15=1.2 years.
- The Chandler wave: The 1.2-year Chandler wave in the polar position is identified as a possible fifth harmonic of the 6.2-year cycle envelope. When the 6.2-year cycle is zero the 1.2-year cycle has a delay which causes a total period of about 6.5 years.
- The Barents Sea ice oscillation: The Barents Sea ice extent time series has dominant cycles of about 18.6*4=74.4, 18.6, and 18.6/3=6.2 years.
- The Kola temperature oscillation: The Kola temperature time series has dominant cycles of about 18.6*4=74.4, 18.6*3=55.8, 18.6, and 18.6/3=6.2 years.
- The lunar nodal tide oscillation: The Hammerfest annual sea level time series has dominant cycles of about 18.6 and 18.6/3=6.2 years.
- The Greenland ice oscillation: The Greenland ice extent time series has dominant cycles of about 18.6*4=74.4 and 18.6*4/3=25.5 years.
- The Røst winter temperature oscillation: The mean winter temperature at Røst has dominant cycles of about 18.6*4=74.4 and 18.6*4/3=25.5 years.
- The NAO index oscillation: The NAO winter index time series has dominant cycles of about 18.6*4=74.4, 18.6, and 18.6/3=6.2 years.
- The 74-year NAO index cycle: The 74-year cycle in the NAO winter index is related to the mean value of Barents Sea ice extent and the Greenland ice extent.
- The NAO index cycle phase-reversal: The 18-year cycle has a phase-reversal that is controlled by the 74-year cycle.

Concepts and ideas

- The First Cause: The First Cause is a 18.6-year gravity force cycle from the moon.
- The lunar nodal spectrum: The gravity force from the 18.6-year lunar nodal cycle is distributed as a spectrum of harmonic and sub-harmonic cycles in polar position movements.
- Phase-reversal: There may be a multiplicative modulation between the cycles in the lunar nodal spectrum. When a less frequent cycle has limitations in the negative direction, it will introduce a 180 degree phase-reversal in the more frequent cycles.
- The wine glass theory: The Arctic Ocean behaves like a rotating wine glass. A 74-year rotating polar motion introduces a 74-year cycle of water movement in the Arctic Ocean as a result of resonance. Harmonic circulating cycles of movement are distributed at different water densities and at different water layers.
- The Arctic oscillating system theory: The polar movement and the lunar nodal tide are the driving forces behind an Arctic oscillating system. There is a mutual relation between the Arctic Ocean, the Atlantic Ocean, the Barents Sea, the extent of ice coverage, the reflection of light from ice and northern atmospheric conditions.

- The Barents Sea push-pull theory: The inflow of Atlantic water to the Barents Sea is a result of a push-pull effect between polar position movements of water in the Arctic Ocean and the lunar nodal tide spectrum in the Atlantic Ocean.
- The Kola cycle oscillation: The Kola cycle oscillation is an indicator of the inflow of Atlantic water and plankton to the Barents Sea.
- The climate theory: The lunar nodal spectrum in the NAO winter index is influenced by a lunar nodal spectrum of the Arctic ice extent. The oscillation of Arctic ice is controlled by the Atlantic inflow to the Arctic Ocean and the movement of the polar position.

Chapter 3

SYNTHESIS

Philosophy is written in the grand book the universe,
Which stands continually open to our graze,
But the book cannot be understood,
unless one first learns the alphabet in which it is composed.
It is written in the language of mathematics,
without which it is humanly impossible to understand a single word of it.
Without mathematics, one wanders about in a dark labyrinth.

--Galileo Gallilei (1564-1642).

3.1 General Systems Theory

In this thesis the syntheses of all investigations are described according to systems theory. *Systems theory* is the doctrine of abstract organizations working together toward a common purpose. The system approach is characterized by the study of organizations and their relationships.

The system model

System Architecture is a set of mutually related sub-systems. A system S(t) may be represented by the model:

$$S(t) = \{B(t), \{S_1(t), S_2(t),,,S_n(t)\}\} \in w \qquad (3.1)$$

where $S_n(t)$ represents the nth sub-system, B(t) represents the mutual binding between the sub-systems and w is the model purpose. A system element $S_i(t)$ may represent an organization from nature, a man-made system, a substance, or any type of abstract organization. The chosen system elements in the system S(t) are dependent on the system model purpose w. The binding B(t) may represent a force, a flux, and any type of relationship that influences related system elements. A time-variant binding B(t) will introduce a time-variant and structurally unstable system. Equation (3.1) indicates that *science is dealing with concepts*. This means that the results are dependent on the number of sub-systems or the selected holistic view.

A *sub-system* $S_i(t)$ may be modeled by a new set of sub-systems represented by the simplified architecture:

$$S_i(t) = \{B_i(t), \{S_{i1}(t), S_{i2}(t),,,, S_{im}(t)\}\} \in w \qquad (3.2)$$

where $S_{im}(t)$ represents the m-th sub-system and $B_i(t)$ represents the mutual binding between the sub-systems. The sub-system $S_{im}(t)$ may be modeled by a new set of sub-systems. A system model is thus dependent on the abstraction level. This means that explanations of dynamics in nature are dependent on the integration of events at a system level. Equation (3.2) indicates that a scientific *concept is dependent on the abstraction level*. The chosen abstraction level will influence sampling of data. Sampling of data represents integration of information in the time. This means that the results of the time series analysis are based on a chosen sampling time.

System dynamics

A system $S_i(t)$ has a state dynamics that may be represented by the differential equation:

$$\dot{X}(t) = A(t)X(t) + B(t)U(t) + V(t) \qquad (3.3)$$

where X(t) represents a [m x 1] state vector, A(t) is a [m x n] system growth matrix, U(t) represents the states in [m x 1] vector on a known source $S_u(t)$, B(t) represents a [m x n] binding matrix from the U(t) vectors, V(t) represents a [m x 1] disturbance vector from an unknown source $S_v(t)$. This is a Newtonian approach to dynamics.

Energy distribution

The energy of an unknown source $S_v(t)$ is distributed in a time series and in the frequency spectrum. From Parseval's theorem we have:

$$E_v = \int_{-\infty}^{+\infty} |v(t)|^2 dt = \frac{1}{2\pi} \int_{-\infty}^{+\infty} \left| V^*(j\omega) \right|^2 d\omega \qquad (3.4)$$

If the spectrum V(jω) is white noise, the spectral density is:

$$S_{vv}(j\omega) = |V^*(j\omega)|^2 = V^2 \qquad (3.5)$$

where V^2 is the noise variance. In this case the integrated energy will be infinite. Since this is impossible, the energy disturbance must have a red spectrum. A first-order red spectrum has the property:

$$V(j\omega) = \frac{N_d}{j\omega - A} \qquad (3.6)$$

This means that a time-variant time series v(t) is expected to introduce a non-correlated red spectrum where the energy density is falling by N_d/ω, or 20 dB/decade or more. The longer the cycle, the more the energy is related to the cycle. This non-correlated red spectrum is what we may expect when analyzing time series from nature. In this thesis it is shown that long period cycles in the spectrum are not random noise. The sources of the long period cycles are identified as sub-harmonic cycles of the 18.6-year lunar cycle. The energy from these cycles influences the phase of shorter period cycles.

The Forced Oscillator theory

The First Cause

The lunar node is the cross-point between the moon plane cycle and the ecliptic plane to the sun. This cross-point describes a lunar nodal cycle of 18.6134 years. The corresponding cycle of changing inclination of the moon's orbit to the earth's equatorial plane is described by the model:

$$u_0(t) = 23^\circ 27' + 5^\circ 09' \sin(\omega_0 t + 0.90\pi) \qquad (3.7)$$

where $\omega_0=2\pi/T_0=2\pi/18.6134$ (rad/year) is the lunar nodal angle frequency and t (year) is the time. The cycle amplitude has a maximum in November 1987 and a minimum in March 1996. The gravity energy from the moon introduces a 18.6-year lunar nodal vertical and horizontal tide in the ocean and movements of the earth's axis. The lunar nodal cycle is the First Cause in a chain of movements.

Eigen-frequencies in systems

A mutual relation between a system $S(t)=\{B(t),\{S_1(t), S_2(t)\}\}$ may represent a feedback system. This feedback may have a time delay τ between the system elements and a loss factor K. The feedback circulation between the system elements may then be modeled by:

$$x(t) = Kx(t-\tau) + u(t) \qquad (3.8)$$

where u(t) is forced input, x(t) is the state at a system element $S_1(t)$ and $x(t-\tau)$ is the delayed state between a system $S_1(t)$ and $S_2(t)$. K represents the loss in the circulating systems. A Fourier transformation of Equation (3.8) has the frequency transfer function:

$$H(j\omega) = \frac{x(j\omega)}{u(j\omega)} = \frac{1}{1 - Ke^{-j\omega\tau}} = \sum_n K_n e^{-jn\omega\tau} \qquad (3.9)$$

This function system is asymptotically stable when $K < 1$. Equation (3.9) has a singularity for when $K=1$, $\omega\tau=2\pi n$, and $n=0,1,2,3\ldots N$. A singularity at an angle frequency cycle ω_0 means that the state x(t) will have a frequency cycle $x(j\omega)$ where the amplitude is amplified to infinity. A singularity in the frequency function will introduce stochastic resonance. In this thesis a resonance frequency is called an *eigen-frequency*. This feedback system thus has a set of eigen-frequencies for $\omega=2\pi n/\tau$, where $n=0,1,2\ldots N$.

When the input force u(t) is a stationary cycle $u(j\omega)=u\exp(j\omega_0 t)$, the output from Equation (3.9) has a maximum response when $\omega_0=2\pi n/\tau$, where $n=0,1,2\ldots N$. This means that a stationary cycle u(t) may be amplified by resonance in a feedback system $H(j\omega)$. The feedback system may have resonance at the singularities of $(n\omega\tau+\omega_0 t)=2\pi n$ where $n=0,1,2,3\ldots N$. This will introduce an *even harmonic spectrum*. When $K=K\exp(j\omega_0 t)$ the transfer function has singularities for $K=1$ and $(\omega\tau+\omega_0 t)=2\pi n$. This transfer function has singularities at $\tau=0$, $\omega 3\tau=\omega_0 t$, and $\omega\tau=\omega_0 3t$. When $\omega_0=2\pi/T_0$, there will be singularities in cycles of T_0, $T_0/3$, and $3T_0$ years. An interaction between the feedback loop and the loss function K(t) is then expected to introduce a third harmonic and a third sub-harmonic cycle in the biomass time series. This system may have resonance at the eigen-values mT_0, T_0/m, where $m=2n+1$ and $n=0,1,2,3\ldots N$. The result will introduce an *uneven harmonic spectrum*.

Modulation in nonlinear systems

The energy from a forced stationary cycle $u_0(t)$ on a nonlinear system $S_o(t)$ will be distributed as a spectrum of harmonic and sub-harmonic cycles. This spectrum is a sum of harmonic cycles:

$$U(j\omega_0) = \sum_{n,m} u_{n,m} \sin(n\omega_0 t / m + \varphi_{n,m}) \tag{3.10}$$

where $U(j\omega_0)$ is the lunar nodal spectrum, $u_{n,m}$ is a cycle amplitude, angle frequency $\omega_0=2\pi/T_0=2\pi/18.6134$ (rad/year) and $\varphi_{n,m}$ is the phase delay.

Frequency transfer function

A frequency function represents a shift from the time domain to a frequency view of system dynamic properties. The frequency properties are computed from the Fourier transformation of the state dynamic model (Equation 4.3) to:

$$\begin{aligned} X(j\omega) &= (j\omega I - A)^{-1} BU(j\omega_0) + (j\omega I - A)^{-1} V(j\omega) \\ X(j\omega) &= H(j\omega)U(j\omega_0) + H(j\omega)V(j\omega) \end{aligned} \tag{3.11}$$

where I is an identity matrix, j is a complex operator, ω represents the angle frequency, A is the mean of the growth system matrix A(t), B is the mean of the binding matrix B(t), X(jω) is the state spectrum vector and $U(j\omega_0)$ the state spectrum vector from the known lunar nodal cycle. The transfer function H(jω) describes in the frequency domain how the system responds to stationary cycles from the known lunar nodal spectrum $U(j\omega_0)$ and the unknown source V(jω).

Frequency response

A stationary cycle $u_0(t)$ in a feedback system $S(t)=\{B(t),\{S_1(t),S_2(t),S_o(t)\}\}$ will have the frequency response:

$$U(j\omega_0) = H(j\omega)u_0(j\omega_0) = \sum_{n,m} u_{n,m}(jn\omega / m) \tag{3.12}$$

where H(jω) represents the frequency transfer function, U(jω) represents the modulated spectrum, and $u_{n,m}$ is a cycle amplitude.

Chain of coupled forced oscillators

The frequency response $X_i(j\omega)$ from the stationary cycle spectrum $U_{i-1}(j\omega_0)$ and a non-stationary red spectrum $V_{i-1}(j\omega)$ is expected to be:

$$\begin{aligned} X_i(j\omega_0) &= H_i(j\omega)X_{i-1}(j\omega_0) = H_i(j\omega)[U_{i-1}(j\omega_0) + V_{i-1}(j\omega)] \\ X_i(j\omega_0) &= U_i(j\omega_0) + V_i(j\omega) \end{aligned} \tag{3.13}$$

where $H_i(j\omega)$ represents the frequency transfer function of the n-th nonlinear earth system element and $V_i(j\omega)$ is a non-correlated red spectrum. According to this theory the modulated stationary spectrum $U_i(j\omega_0)$ may have a harmonic spectrum related to each stationary cycle in the spectrum $U_{i-1}(j\omega)$. The transfer function $H_i(j\omega)$ is expected to influence the amplitude and phase of the stationary cycles $U_{i-1}(j\omega_0)$. The influence of the transfer function $H_i(j\omega)$ on the non-correlated noise spectrum $V_{i-1}(j\omega)$ is expected to be a new non-correlated noise spectrum $V_i(j\omega)$. This means there may be a chain of coupled oscillators where each step may modify the amplitude and phase of harmonic cycles.

Phase-reversal

A stationary lunar nodal cycle $u_0(t)=\sin(\omega_0 t)$ may interact with a sub-harmonic cycle $u(k,t)=\sin(\omega_0 t/k)$ and thus introduce an amplitude modulated wave where u(k,t) represents the envelope of the carrier wave $u_0(t)$ (Carlson, 1968). A multiplicative amplitude modulation process may be described by:

$$U_0(t) = K[1 + m\sin(\omega_0 t / k)]\sin(\omega_0 t) \tag{3.15}$$

In an amplitude modulated spectrum $U_0(t)$ the carrier $u_0(t)=\sin(\omega_0 t)$ will have a phase-reversal of π (rad) if $m>1$. In an ocean system this may be the case when the temperature cycle u(k,t) has limits below zero. This phase-reversal will introduce a time-variant phase in the stationary cycle $u_0(t)$.

3.2 The Arctic Oscillating System

The Arctic lunar nodal spectrum

Climate Indicator	***Nodal spectrum*** ω_0 **(rad/yr)**	***Cycle phase*** φ **(rad)**	***Phase delay to Polar*** $\Delta\varphi$ **(rad)**	***Nodal cycle correlation*** **R**	***Signal to noise ratio*** **S/N**
Lunar nodal cycle	ω_0	0.90π	0.00π		
Polar position	$\omega_0/4$ ω_0 $3\omega_0$ $15\omega_0$	1.29π $1.00/0.00\pi$ -1.09π -1.09π		0.86 0.70 0.44 0.96	2.6
Arctic Ocean	$\omega_0/4$ $3\omega_0/4$ $9\omega_0/4$				
Barents ice ext.	$\omega_0/4$ $\omega_0/$ $3\omega_0$	0.25π $1.50/0.50\pi$ $-1.09/-0.09\pi$	1.04π 0.50π 1.00π	0.73 0.74 0.64	2.0
Kola section temp.	$\omega_0/4$ $\omega_0/3$ ω_0 $3\omega_0$	0.29π 0.90π $1.55/0.55\pi$ $-1.09/-0.09\pi$	1.00π 0.45π 0.00π	0.95 0.89 0.90 0.37	3.2
Hammerfest sea level.	ω_0 $3\omega_0/$	0.55π $-1.09/-0.09\pi$	0.45π 1.0π	0.73 0.37	1.6
Greenland ice ext.	$\omega_0/4$ $3\omega_0/4$ $9\omega_0/4$	1.78π $0.70/1.70\pi$ $1.38/0.38\pi$	-0.49π	0.50 0.77 0.54	3.2
Røst winter temp.	$\omega_0/4$ $3\omega_0/4$ $9\omega_0/4$	1.51π $-1.70/-0.70\pi$ $-1.38/-0.38\pi$	0.78π	0.92 0.88 0.37	1.8
NAO winter index	$\omega_0/4$ ω_0 $3\omega_0$	1.01π $1.48/0.48\pi$ $-1.29/-0.29\pi$	0.28π -0.48π -0.2π	0.90 0.48 0.2	3.0

Table 3.1 Identified lunar nodal cycles in Arctic climate indicators.

Table 3.1 shows the lunar nodal spectrum is identified in all analyzed Arctic climate indicators. In this table the angle frequency $\omega_0=2\pi/T_0=2\pi/18.6134$ (rad/yr). The results in Table 3.1 show that there is a stationary Arctic oscillating system controlled by the deterministic 18.6-year lunar nodal cycle.

The lunar nodal spectrum was identified in all analyzed time series. The time series of the polar position, the Barents Sea ice extent, the Kola section temperature, the Hammerfest sea level and the NAO winter index all have a harmonic spectrum from the T_0=18.6-year cycle. The Greenland ice

extent and the Røst winter air temperatures have a harmonic spectrum from the sub-harmonic cycle of $4T_0$=4*18.6=74.4 years.

Table 3.1 shows that the identified cycles have a good correlation to nodal reference cycles and a good signal-to-noise ratio between the identified cycles and influences from other sources. These estimates show that the cycles from the lunar nodal spectrum have a major influence on the dominant fluctuations in the time series. The close relationship between the cycle phase in the different time series demonstrates that the wavelet analysis method is of good quality.

Lunar nodal cycle phase-reversal
The lunar nodal spectrum has a stationary cycle time but its amplitude and phase are not stationary. In most time series the amplitude of the $4T_0$=74.4-year cycle introduces a 1.0π (rad) phase-reversal in the harmonic cycles of T_0=18.6, $T_0/3$=6.2, $4T_0/3$=24.8 and $4T_09/$=8.3 years. The phase-reversal property introduces a new type of uncertainty in forecasting. The lunar nodal cycles may still be deterministic, but to make long-term forecasts we must know more about the timing of the next phase-reversal.

The physical process behind this phase-reversal is still unclear. This thesis presents the theory that there is a multiplicative modulation between the 74-year cycle and the others. When the 74-year cycle meets a physical limitation in the negative direction, it will lead to a phase-reversal of the modulated carrier cycle (Equation 3.15).

The Arctic system

The Arctic system has an input influence from the sun-earth-moon system:

$$S(t) = \{B_{gra}(t),\{S_{sun}(t), S_{earth}(t), S_{moon}(t), S_v(t)\}\} \in w \qquad (3.16)$$

where the sun system $S_{sun}(t)$ represents a constant flux radiation, $S_{earth}(t)$ represents the earth system, $S_{moon}(t)$ represents the moon system, $S_v(t)$ represents disturbance from an unknown source and $B_{gra}(t)$ represents a mutual binding between the system elements. The mutual binding $B_{gra}(t)$ represents the gravity force and radiation flux in the planetary system. The earth system architecture may be modeled by the simplified system architecture model:

$$B_{gra}(t),S_{earth}(t)=B_{gra}(t),\{B_{earth}(t),\{S_{pol}(t),S_{arc}(t),S_{atl}(t),S_{gren}(t),S_{bar}(t),S_{atm}(t),S_v(t)\}\}\in w \qquad (3.17)$$

where $S_{pol}(t)$ represents the polar position system, $S_{arc}(t)$ represents the Arctic Ocean system, $S_{atl}(t)$ is the Atlantic Ocean system, $S_{gren}(t)$ represents the Greenland Sea system, $S_{bar}(t)$ represents the Barents Sea system, $S_{atm}(t)$ represents the northern earth atmospheric system, $S_v(t)$ represents a disturbance from an unknown source and $B_{earth}(t)$ represents a mutual binding between the system elements. The mutual binding $B_{earth}(t)$ between the system elements implies that an influence on one system will affect the others. The oscillating binding $B_{gra}(t)$ and the eigen-dynamics in each system element will influence the total system (Equation 3.17).

A system element $S_i(t)$ may amplify cycles from $B_{gra}(t)$ by resonance. A total oscillating system then is based on the idea that the Arctic oscillation system has a set of resonators where the energy source comes from the gravity force $B_{gra}(t)$ as the first cause of oscillation.

The First Cause

The time-variant gravity binding $B_{gra}(t)$ has a set of long-period and short-period cycles that will introduce a force in all earth systems of $S_{earth}(t)$. In this thesis, the lunar nodal cycle is investigated.

The time-variant gravity binding $B_{gra}(t)$ changes the intersection between the moon's orbital plane and the earth's orbital plane around the sun (ecliptic plane) in a cycle of 18.6134 years. The oscillating angle between the ecliptic plane to the sun and the plane to the moon orbit is described by Equation 3.7 The oscillating moon orbital plane introduces a 18.6134 year oscillation gravity vector between the moon and the earth. In this thesis the oscillation is associated with *The First Cause,* which introduces a horizontal and a vertical disturbance on all system elements in Equation (3.17). The energy of this earth dynamic cycle is distributed as a *lunar nodal spectrum* in periods of 6 to 74 years or more. These cycles are associated with an Arctic oscillation system.

The lunar nodal tide

The gravity force from the lunar nodal cycle in $B_{gra}(t)$ will introduce a vertical and a horizontal lunar nodal tide in the Atlantic Ocean system $S_{atl}(t)$. The vertical lunar nodal tide represents the sea level. In the Barents Sea this tide has a phase delay of about $\varphi_T=0.55\pi$ (rad) (Maksomov and Smirnov, 1967). The same phase delay is identified in the dominant 18-year cycle of the Hammerfest sea level.

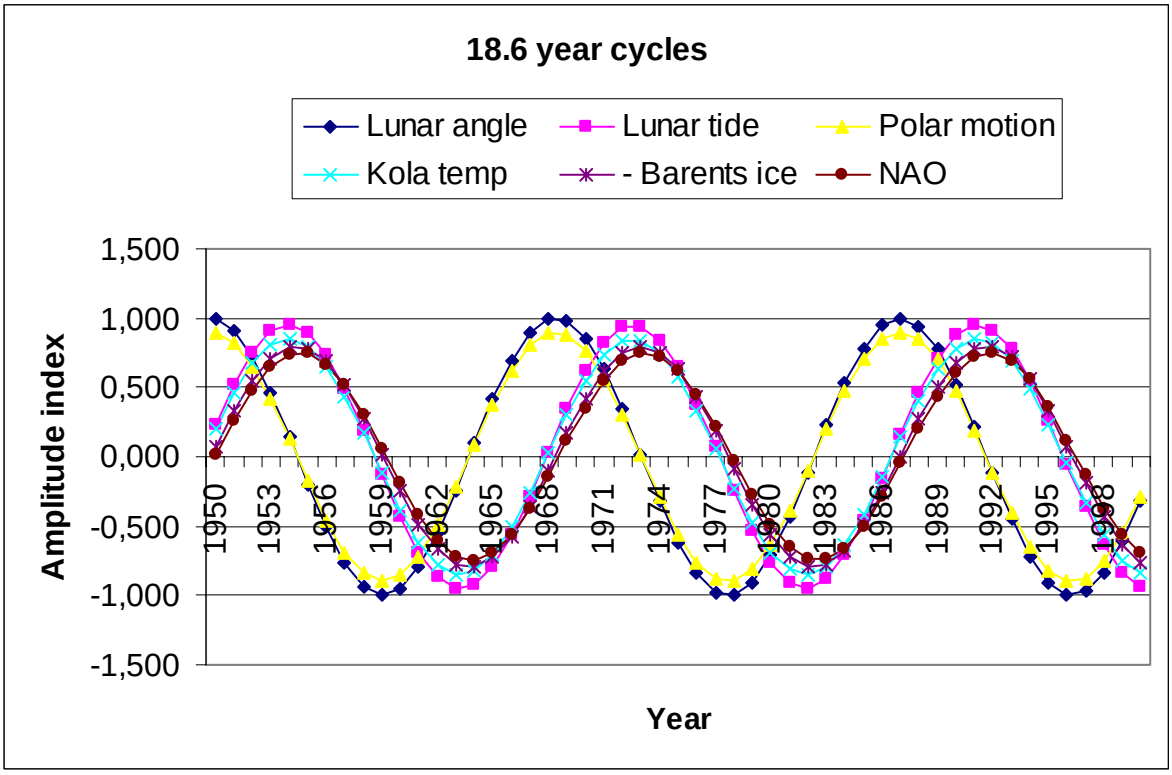

Figure 4.1 Identified 18.6-year cycles in the Arctic Oscillating system.

Figure 4.1 shows the identified 18-year cycles periods from 1950 to 2000 in the Arctic Oscillating system. The 18-year cycle of Barents Sea ice extent is shifted 1.0π (rad) to show the similar warm period. The figure shows that the cycles from the lunar angle and the polar position has the same phase. The lunar nodal tide has a delay of about 0.45π (rad) or about 4 years. There is new delay of 0.10 π (rad) or about 1 year to the 18-year Kola cycle and a new delay of less than a year to the warm 18-year Barents Sea ice cycle and to the 18-year NAO winter index cycle. The phase delays shows that the 18.6-year lunar nodal tide controls the inflow of Atlantic water and the 18-year Kola section water temperature cycle, 18-year cycle of Barents Sea ice extent and the 18-year cycle in the NAO winter index.

The second identified dominant cycle in the Hammerfest sea level is the harmonic cycle of about 18.6/3=6.2 years. This important cycle controls the 6-year Kola temperature cycle and the cycles of biomass recruitment in the Barents Sea. The cause of this cycle is not fully understood. Keeling and Worf (1997) have estimated strong 18-year tidal waves in 1974 and 1987 from lunar cycle events. From these estimates a 93-year tide and a group of 9-year and 6-year tide events were calculated. This group of events had their maximums in 1965, 1974 and 1983. The same maximum periods are identified in the Hammerfest sea level time series. This means that the long-term tide shows a lunar-nodal spectrum. The group event between a 9-year cycle and a 6-year cycle has been identified as a phase-reversal of the 6-year cycle in this wavelet cycle analysis.

The polar position oscillation

The earth's nutation represents small fluctuations of the rotating earth axis on the equatorial plane. The polar position $S_{pol}(t)$ represents the position of the rotation of the pole in the ecliptic plane. Small fluctuations in the earth axis rotation then influence the polar position.

The time series analysis of the polar position has identified dominant cycles of $4T_0$=4*18.6=74.4, T_0=18.6, T_0/3=18.6/3=6.2 and $T_0$15=18.6/15=1.2 years. The identified cycles are stable in the time series period and the 18.6-year cycle has the same phase as the lunar nodal cycle and the lunar nodal tide. This indicates that the polar position and the tide are influenced in parallel by the same source. We may then present a mantle tide theory to explain the identified cycles of polar motion. The cause movement of the polar position is caused by forces that are not explored in the investigations presented in this thesis. The oscillation may, however, be caused by a the shape of the earth, a mutual interaction to with the sea and a mantel nodal tide in the mantle.

The mantle nodal tide hypothesis

The identified nodal spectrum may be explained by a *mantle nodal tide* in the liquid core of the earth. This hypothesis has the following elements:

1. The movement force: A 18.6-year oscillating lunar nodal cycle introduces an oscillating vertical and horizontal gravity force between the earth and the moon.
2. The mantle nodal tide: The energy from the 18.6-year vertical and the horizontal oscillating gravity force on the liquid mantle is distributed as a lunar nodal spectrum in the movement of the liquid mantle. In this movement some cycles are temporarily amplified by resonance. The spectrum of the liquid core movements is reflected in the polar position movement.
3. The 74-year step movements: The 74-year cycle is estimated in a step-by-step movement in the y-direction. This indicates that there exists a more low-frequency cycle in polar position movement, or that the offset of the polar position is slowly increasing in the y-direction.
4. The Chandler wave: The 1.2-year Chandler wave is identified as a fifth harmonic cycle of the 18.6/3=6.2-year lunar nodal cycle envelope. The 1.2-year cycle has a short friction delay when the 6.2-year cycle is zero. The delay introduces results in a total time of about 6.5 years. This indicates that the potential energy source of the Chandler wave may be the gravity force from the moon.

The Arctic Ocean oscillation

The Arctic Ocean system $S_{Arc}(t)$ is a cold energy pool that is connected to the other system elements. Cooled Arctic water accumulates and circulates as the Arctic Surface Water, the Atlantic Water, the Deep Water and the Bottom Water, which have different densities and circulation patterns. The circulating pattern in the Arctic Ocean is most likely influenced by the circulating polar position movement. Deep Water down to 2600 m from the Norwegian Sea is exchanged between the Greenland Sea and the Eurasian Basin (Nansen Basin and Amundsen Basin). The residence time of

Atlantic Water and Deep Water in the Eurasian Basin is estimated to be about 25 and 75 years (Bonisch and Schlosser, 1995). A 75-year residence time is the same cycle period as the identified cycle period in the polar position motion, and the extent of ice in both the Barents Sea and the Greenland Sea. In the Amundsen Basin, the Bottom Water (depth > 2600 m) is estimated to have a residence time of approximately 290-year +/- 30-year (Bonisch and Schlosser, 1995). This shows that the Arctic Ocean has layers of water circulation that follow the lunar nodal spectrum of about $4T_0$=4*18.6=74.4, $4T_0/3$=74.4/3=24.4 and $4*4T_0$=4*74.4=297.6 years. The lunar nodal spectrum in the movement of circulating water may be explained by a "wine glass" theory.

The wine glass theory
The wine glass theory is based on the idea that the rotating Arctic Ocean behaves like liquid in a rotating wine glass. According to this theory, the Deep Water oscillation has a resonance of about 74 years. This resonance is related to water volume and density. A forced polar position movement cycle of about 74.5 years will then control the phase of a 74-year water Deep Water oscillation in the Arctic Ocean. Energy from the forced 74.5-year Deep Water oscillation is distributed as a harmonic spectrum. In this spectrum there is a 4*74.5≈290-year resonance in the Bottom Water where the water has the most density, with a 74.5/3=25-year resonance in the Atlantic Water where there is less dense water. The estimated lunar tide in the Barents Sea (Malenkov and Smirnov, 1967) indicates that the circulation is synchronized with the 18.6-year lunar nodal tide.

The Barents Sea oscillating system

The Barents Sea has been analyzed using a time series for ice extent and the Kola section temperature. Both time series are dominated by the lunar nodal spectrum. The Barents Sea ice extent is dominated by cycles of about $4T_0$=4*18.6=74.4, T_0=18.6, $T_0/3$=18.6/3=6.2 years. The Kola temperature data series is dominated by the cycles of $4T_0$=4*18.6=74.4, $3T_0$=3*18.6=55.8, T_0=18.6, $T_0/3$=18.6/3=6.2 years. This indicates that the Barents Sea is an oscillating system controlled by energy from the lunar nodal spectrum. The 74-year cycle introduces a phase-reversal of π (rad) in the 18.6- and 6.2-year cycles.

The Push-Pull theory
The North Atlantic and the Arctic Ocean have deep water systems. The Barents Sea oscillation may be explained as a surface water link between the Atlantic Ocean oscillation system and the Arctic Ocean oscillation. The identified 18.6/3=6.2 and the 18.6-year Kola cycles have the same cycle time and phase as the identified cycles in the Barents Sea ice extent and in the polar motion. This indicates a push-pull effect between the Atlantic tidal inflow and the oscillating pole position.

The 74-year cycle seems to be of most importance. The 74-year cycle phase-relation between the polar position and the Barents Sea ice extent is about 1.0π (rad). This indicates that the 74-year cycle of polar position movement controls water circulation in the Arctic Ocean and the flow of cooled water between the Arctic Ocean and the Barents Sea. The 74-year cycle in the Kola section temperature has about the same phase-angle. This surprising estimate means more ice when there is more Atlantic inflow. The result may be explained by deep sea circulation from the Arctic Ocean to the Greenland Sea to the North Atlantic Ocean and then to the Barents Sea. This circulation may have a phase delay of about 74.5/2 years or 1.0π (rad).

The source of the estimated 55-year cycles in the Kola section temperature is unknown. A possible explanation of this cycle is an additive mean envelope of the 6.2-year and the 18.6-year cycle.

The 18.6-year cycle is identified in the time series of the polar position, the Barents Sea ice extent, the Kola section temperature and the lunar nodal tide. The main source of this cycle seems to be the 18.6-year vertical Atlantic inflow tide. An interaction between the 18.6-year Atlantic inflow tide and the

cold Arctic 74-year cycle may introduce a multiplicative modulation between the cycles. In the modulation process, negative limitations in the 74-year cycle may have the power to introduce a phase-reversal in the 18.6-year tidal inflow to the Barents Sea.

The 6.2-year cycle is identified in the time series of the polar position, the Barents Sea ice extent, the Kola section temperature and in the lunar nodal tide. The main source of this cycle is most likely a parallel force of the stable 6.2-year polar position movement and the harmonic 18.6/3=6.2-year Atlantic tide. The 6.2-year cycle in the Barents Sea ice extent, the Kola section temperature and the lunar nodal tide all have the same phase-reversal effect as identified in the 18.6-year cycle.

The Greenland Sea oscillating system

The Greenland Sea ice extent system $S_{barIce}(t)$ has dominant fluctuations related to the lunar nodal spectrum. The estimated lunar nodal spectrum in the time series of the Greenland ice extent is estimated to be $4T_0$=4*18.6=74.4, $4T_0/3$=74.4/3=24.5, $4T_0/9$=24.5/3=8.2 years. This time series shows a phase-reversal at both 24.5 years and 8.2 years when the 74.5-year cycle changes between a positive and a negative state. The residence time of circulation water in the Arctic Ocean has the same cycle time as the identified in Greenland ice extent.

The identified cycles indicate that the fluctuations of Greenland ice extent are controlled by cycles in the outflow of the circulating Arctic Ocean water to the Greenland Sea.

The climate oscillation

The Røst oscillating winter air temperature has dominant fluctuations related to the lunar nodal spectrum. The estimated lunar nodal spectrum in the time series of Greenland ice extent is estimated to be $4T_0$=4*18.6=74.4, $4T_0/3$=24.5, $4T_0/9$=24.5/3=8.2 years. Time series shows a phase-reversal at both 24.5 and the 8.2 years when the 74.5-year cycle changes between a positive and a negative state. The fluctuation of the annual mean winter air temperature at Røst has the same cycle time as the identified cycles of Greenland ice extent.

A phase delay of 1.0π (rad) shows that there is a close correlation between more ice in the Greenland Sea and colder winter temperature at Røst. From these estimates we may conclude that the dominant 74-year and the 24-year cycles at Røst have their source in the extent of ice in the Greenland Sea. This analysis shows that the Røst oscillating winter temperature is forced by cold winds from the ice mass in the Greenland Sea.

The NAO winter index

The NAO winter index is an important climate indicator for the earth's northern hemisphere. A wavelet analysis of the NAO winter index time series has identified the dominant time series of $4T_0$=4*18.6=74.4, T_0=18.6, $T_0/3$=18.6/3=6.2 years.

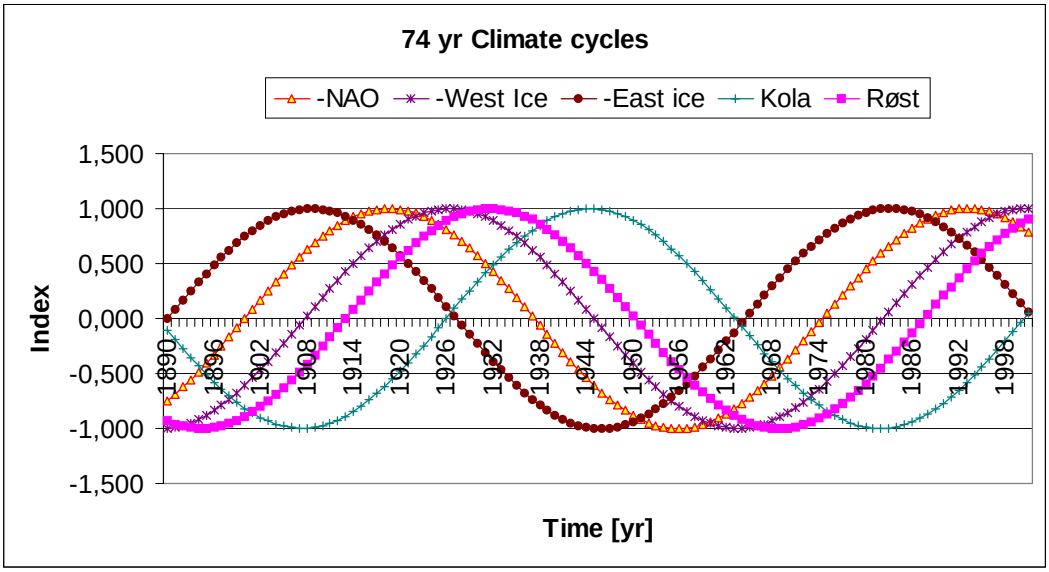

Figure 4.2 Identified 74-year cycles of warm periods in the Arctic Oscillating system.

Figure 4.2 shows the identified 74-year cycles of warm periods in the Arctic oscillating system, represented by the inverted NAO cycle, the inverted Greenland ice, the inverted Barents Sea ice, the Kola temperature and the Røst winter temperature. The figure illustrates that the identified 74-year NAO winter index cycle has a phase delay at the mean phase between Barents Sea ice extent and Greenland Sea ice extent. This indicates that the identified 74-year cycle in the NAO winter index is controlled by the mean ice extent in the Arctic Ocean.

In 1865 the mean Barents Sea ice extent was about 1,250,000 km^2 and the fluctuations were about 500,000 km^2. In 1997 the mean level had decreased to about 750,000 km^2 but the fluctuations had remained at about 500,000 km^2. This shows that the fluctuating segment of the Arctic ice extent has increased by 27 percent, from about 40 percent to 67 percent. In the same period, the fluctuation in the NAO winter index increased from about 2 to 2.5. This represents an increased fluctuation of about 25 percent. Relatively more fluctuation in the extent of Arctic ice may introduce relatively more disturbance in the NAO winter index. This observation explains a possible cause of the increased NAO winter index amplitude fluctuation in the last 50 years. This means that if the Arctic ice extent continues to be reduced, the amplitude of the NAO index can be expected to increase, resulting in an increase in extreme climate fluctuations.

Otto Pettersson (1915, 1930) and Maximov and Smirnov (1967) have reported a 18-year cycle in the atmosphere that is caused by interaction with the sea. In this investigation the same cycle has been identified in the NAO winter index time series. The 18.6-year cycle in the NAO winter index has the same phase as the horizontal 18.6-year lunar nodal tide, the 18.6-year cycle in the Kola, and the Barents Sea ice extent. This indicates that the 18.6-year cycle may by caused by the 18.6-year nodal tide and by the fluctuations in the Barents Sea ice extent.

The climate oscillation theory

The identified nodal spectrum in the NAO winter index may be explained by a *climate oscillation theory*. This theory has the following elements:

1. The long-term mean level: The long-term mean level of the NAO winter index is related to the long-term mean surface temperature of the northern land and sea, and the Arctic ice.
2. Disturbance in the NAO winter index: Fluctuations in the cold Arctic ice extent will introduce a negative disturbance in the air temperature, which is reflected in the NAO winter index.

3. The lunar nodal spectrum: When fluctuations in the Arctic ice extent have a lunar nodal spectrum, the lunar nodal spectrum will be reflected in the NAO winter index.
4. The oscillating amplitude: When the mean Arctic ice extent is decreasing, the amplitude fluctuation of the NAO winter index is increasing. A constant fluctuation of ice extent will then increase the disturbance and the amplitude of the NAO winter index oscillation.

Wavelet analysis of the movement of the polar position indicates there is a relationship between the polar position and long-term decreases in Arctic ice extent. This relationship may lead to the following possible long-term causes.

1. The polar position: When the polar position increases in the y-direction, there is an increased inflow of Atlantic water to the Arctic Ocean.
2. The Atlantic inflow: Increased Atlantic inflow increases the temperature in the Arctic Ocean.
3. The reduced Arctic ice extent: The increased temperature in the Arctic Ocean reduces the Arctic ice extent. The process is amplified by an increase in air temperature and by a reduction of light reflection from the ice.
4. Longer cycles: The polar position may have cycles which are longer than 74 years or a drift in the offset position. This may lead to longer cycles of Arctic ice reduction and more climate fluctuations.

From this analysis it can be concluded that the large fluctuations in the climate time series have a set of stationary cycles which are controlled by a deterministic 18.6-year gravity cycle from the moon.

3.3 The Ecosystem Theory

Species	Eigen frequency ω_e	Dominant Cycle ω_0	Cycle phase φ	Kola cycle phase delay $\Delta\varphi$	Signal-to-noise ratio S/N	Nodal cycle correlation R
Zooplankton		ω_0 $3\omega_0$	0.55π $-1.09/-0.09\pi$			0.43
Capelin	$6\omega_0$	$\omega_0/2$ ω_0 $3\omega_0$	 0.55π $-1.09/-0.09\pi$		1.8	0.73 0.73
Shrimp	$3\omega_0$	ω_0 $3\omega_0$	1.55π $-0.09/-1.09\pi$	1.0π	3.5	0.85
Herring	$3\omega_0$	$\omega_0/3$ ω_0 $3\omega_0$	0.90π 1.05π $-1.09/-0.09\pi$	0.0π -0.5π 0.0π	3.0	0.92
Cod	$3\omega_0$	$\omega_0/3$ ω_0 $3\omega_0$	0.72π 0.22π $-1.09/-0.09\pi$	0.18π -0.33π 0.0π	3.8	0.85
Haddock	$3\omega_0$	ω_0 $3\omega_0$	0.22π $-1.09/-1.09\pi$	-0.33π 0.0π	6.5	0.80

Table 3.2 The identified lunar nodal spectrum in the Barents Sea biomasses.

Table 3.2 shows the identified lunar nodal spectrum in all analyzed time series of biomasses in the Barents Sea. The angle frequency $\omega_0=2\pi/T_0=2\pi/18.6134$ (rad/yr). The results in the table show there is a set of stationary cycles from the lunar nodal spectrum in all analyzed biomasses from the Barents Sea. The cycle phase of the dominant cycles is close related to the Kola temperature cycles and the lunar nodal tide. The identified cycles have a good correlation to the nodal reference cycles and a good signal-to-noise ratio between the identified lunar cycles and disturbance from unknown sources. This shows that the cycles from the lunar nodal spectrum have a major influence on the biomass fluctuations. The close relationship between the cycle phase in the different time series demonstrates that the wavelet analysis method is of good quality.

The identified lunar nodal spectrum shows that the biomass eigen-dynamics are related to the lunar-nodal harmonic cycle of 18.6/3=6.2 years. The biomasses behave as a set of resonators where the cycle phase and amplitude are controlled by cycles in the lunar nodal spectrum.

The Barents Sea ecosystem

The Barents Sea system $S_{bar}(t)$ may be modeled by the simplified architecture:

$$S_{bar}(t) = \{B_{bar}(t), \{S_{oce}(t), S_{pla}(t), S_{bio}(t), S_v(t)\}\} \qquad (3.29)$$

where $S_{oce}(t)$ is the Barents Sea ocean system, here represented by the lunar nodal tide, the Kola temperature, and the ice extent. $S_{pla}(t)$ represents the phytoplankton and zooplankton in the Barents Sea. $S_{bio}(t)$ represents the investigated biomasses of shrimp, capelin, herring, cod and haddock in the Barents Sea. $S_v(t)$ represents disturbance from an unknown source and $B_{bar}(t)$ represents a mutual

binding between the system elements. According to this general systems theory, the dynamics of the Barents Sea system $S_{bar}(t)$ is influenced by the mutual binding $B_{bar}(t)$ and the eigen-dynamics in each element. If there is one dominant energy source, or if a source has a correlated set of dynamic movements, it will influence the other system elements.

The forced oscillator theory

The forced oscillator in this model is the Barents Sea ocean system $S_{oce}(t)$. Atlantic inflow to the Barents Sea will influence the Barents Sea temperature, transport of zooplankton into the sea, reduce its ice extent, and increase the amount of open sea surface. When the Atlantic inflow is controlled by the lunar nodal spectrum, the spectrum will be reflected in the Kola time series and in the time series of ice extent. The Barents Sea system $S_{oce}(t)$ is then a forced oscillator on the plankton system $S_{pla}(t)$ and the biomass systems $S_{bio}(t)$ in the Barents Sea.

There is a fundamental difference between the response from a set of stationary cycles and random cycles. A set of stationary and random cycles may be represented as a Fourier spectrum:

$$X_{oce}(j\omega) = U_{oce}(j\omega_0) + V_{oce}(j\omega) \tag{3.30}$$

where $U_{oce}(j\omega_0)$ represents the lunar nodal spectrum of Atlantic inflow, $V_{oce}(j\omega)$ represents the non-correlated disturbance spectrum from an unknown source, and $X_{oce}(j\omega)$ represents the total spectrum. These cycles may be explained as a forced oscillator on the Barents Sea plankton system:

$$X_{pla}(j\omega) = H_{pla}(j\omega)X_{oce}(j\omega) = U_{pla}(j\omega_0) + V_{pla}(j\omega) \tag{3.31}$$

where $H_{pla}(j\omega)$ represents the frequency transfer function of the food chain system between the ocean dynamics and plankton dynamics, $U_{pla}(j\omega_0)$ represents the lunar nodal spectrum in the food chain system, and $V_{pla}(j\omega)$ represents the non-correlated spectrum from an unknown source. The spectrum from the $X_{pla}(j\omega)$ represents a new set of stationary and random cycles. This new set of food chain cycles, extending from plankton up to and including fish recruitment, is explained as a forced oscillator in the Barents Sea biomass system.

$$X_{bio}(j\omega) = H_{bio}(j\omega)X_{pla}(j\omega) = U_{bio}(j\omega_0) + V_{bio}(j\omega) \tag{3.32}$$

where $H_{bio}(j\omega)$ represents the frequency transfer function of the biomass system eigen-dynamics from plankton dynamics to recruitment and growth. $U_{bio}(j\omega_0)$ represents the lunar nodal spectrum in the biomass system, $V_{bio}(j\omega)$ represents the non-correlated spectrum from an unknown source, and $X_{bio}(j\omega)$ represents the new set of stationary and random cycles of biomasses. In this model the frequency transfer function $H_{bio}(j\omega)$ is dependent on the eigen-frequencies of each species (Equation 3.11) and the mutual relation $B_{bio}(t)$ between the biomass systems in the Barents Sea. This forced oscillator theory explains why a stationary forced cycle will influence a chain of events in the Barents Sea ocean system.

The Plankton system oscillation

In this investigation, the Barents Sea plankton analysis has been limited to a zooplankton time series from 1987 to 2000. The time series has limitations in the first year of the period (Yndestad and Stene, 2002). Lunar nodal cycles of T_0=18.6 and $T_0/3$=18.6/3=6.2 years have been estimated from this relatively short time series. Both cycles have the same phase-angle as the identified Kola temperature

cycles. This indicates that plankton are influenced by Atlantic inflow from the lunar nodal tide. The Barents Sea plankton system $S_{plank}(t)$ is expected to have a major influence on the recruitment and growth of biomass in the Barents Sea. The zooplankton time series is, however, short compared to the Kola section time series. Since there is a good correlation between Atlantic inflow, the Kola section temperature and the mean zooplankton growth, the Kola temperature data series is used as a reference indicator for biomass growth and recruitment.

The Plankton system oscillation theory

$S_{pla}(t)$ represents the phytoplankton and zooplankton in the Barents Sea. The theory of a plankton system oscillation is based on the following elements:

1. The plankton potential difference: The warm Atlantic Ocean has a higher density of plankton than the cold Barents Sea.
2. The plankton inflow: The 6.2- and the 18.6-year horizontal nodal tides causes cycles of plankton inflow to the Barents Sea.
3. More growth: Increased Atlantic inflow increases the plankton density in the Barents Sea and an increased Barents Sea temperature and increases the plankton biomass growth.
4. The matching theory: The oscillation of plankton growth leads to more food for fish larvae in the Barents Sea. Thus more of the fish larvae in the Barents Sea biomass system $S_{bio}(t)$ will survive when the plankton oscillation and the biomass oscillation have the same phase.

This theory explains why the biomass fluctuations are related to the fluctuations in the Kola section temperature. The Kola section temperature is an indicator of inflow of Atlantic water and plankton to the Barents Sea. In this investigation we have a short plankton time series and a long Kola section temperature series. Since both time series are influenced by the lunar nodal tides, the Kola section time series are used as a reference time series to analyze biomass dynamics.

The Barents Sea capelin oscillation

The Barents Sea capelin biomass system $S_{cap}(t)$ has a mutual binding $B_{bar}(t)$ to the Barents Sea ocean system $S_{bar}(t)$, the total plankton system $S_{pla}(t)$, the total biomass system $S_{bio}(t)$, and an unknown source $S_v(t)$.

The cycle code

The fluctuations in Barents Sea capelin are controlled by the phase-relation between the 3.1-year biomass eigen-dynamics and the Kola temperature cycles of 6.2 and 18.6 years. The capelin biomass has long-term growth and dominant cycles of about 18.6/3=6.2 years when the 6.2- and the 18.6-year Kola cycle is positive at the same time. The biomass has fluctuations of about 3*3.1=9.3 years when the 18.6-year Kola cycle is negative. The capelin biomass is strongly reduced when the 6.2- and the 18.6-year Kola cycles are negative at the same time.

The Barents Sea shrimp oscillation

The shrimp biomass system $S_{shr}(t)$ has a mutual binding $B_{bar}(t)$ to the Barents Sea ocean system $S_{bar}(t)$, the total plankton system $S_{pla}(t)$, the total biomass system $S_{bio}(t)$, and an unknown source $S_v(t)$.

The cycle code

The shrimp biomass has long-term growth and dominant cycles of about 18.6/3=6.2 years when the 18.6-year Kola cycle is negative at the same time. The shrimp biomass is expected to have a strong reduction when the 6.2- and the 18.6-year Kola cycles are positive at the same time. The biomass has a short cycle of about 6 years when the 6.2-year Kola cycle is negative and the 18.6-year Kola cycle is positive.

The Norwegian spring spawning herring oscillation

The biomass system $S_{her}(t)$ of Norwegian spring spawning herring has a mutual binding $B_{bar}(t)$ to the Barents Sea ocean system $S_{bar}(t)$, the total plankton system $S_{pla}(t)$, the total biomass system $S_{bio}(t)$, and an unknown source $S_v(t)$. The biomass of Norwegian spring spawning herring has an eigen frequency of about 18.6/3=6.2 years.

The cycle code

The biomass growth is dependent on the phase-relation between the biomass eigen-dynamics of about 6.2 years and the Kola cycles of 6.2 and 18.6 years. The herring biomass has long-term growth and dominant cycles of about 18.6/3=6.2 and 18.6 years in periods when the 6.2-year and the 18.6-year Kola cycles are positive at the same time. The biomass has a long-term reduction and a short cycle of about 6 years in periods when the 6.2-year Kola cycle is positive and the 18.6-year Kola cycle is negative. The herring biomass is expected to experience a ”worst case” situation for recruitment and a strong reduction when the 6.2- and the 18.6-year Kola cycles are negative at the same time. When the 6.2- and the 18.6-year cycles are positive in 3 periods, the biomass will experience long-term growth in a period of about 20 years. This will lead to a large long-term biomass fluctuation in a period of about 50 to 80 years.

The Northeast Arctic cod oscillation

The biomass system $S_{cod}(t)$ of Northeast Arctic cod has a mutual binding $B_{bar}(t)$ to the Barents Sea ocean system $S_{bar}(t)$, the total plankton system $S_{pla}(t)$, the total biomass system $S_{bio}(t)$, and an unknown source $S_v(t)$. The biomass of Northeast Arctic cod has an eigen-frequency of about 18.6/3=6.2 years.

The cycle code

The Northeast Arctic cod biomass growth is dependent on the phase-relation between the biomass eigen-dynamics of about 6.2 years and the Kola cycles of 6.2 and 18.6 years. The biomass has long-term growth and dominant cycles of about 18.6/3=6.2 and 18.6 years when the 6.2-year and the 18.6-year Kola cycles are positive at the same time. The biomass has a long-term reduction and a short cycle of about 6 years when the 6.2-year Kola cycle is positive and the 18.6-year Kola cycle is negative. The biomass is expected to have the worst possible recruitment and to be strongly reduced when the 6.2- and the 18.6-year Kola cycles are negative at the same time. When the 6.2- and the 18.6-year cycles are positive in 3 periods, the biomass will have a long-term growth in a period of about 20 years. This will lead to a large long-term biomass fluctuation in a period of about 50 to 80 years.

The capelin biomass is an important food source for Northeast Arctic cod biomass in the age group from about 3 to 7 years. In a period when the 6.2-year and the 18.6-year Kola cycles are negative, the capelin biomass is reduced to a minimum. At the same time there is a strong 6-year class from the last 6.2-year Kola cycle. In this situation the cod biomass may survive by cannibalism on the younger cod biomass. This situation will increase the cod biomass reduction.

Biomass collapse is associated with periods when the 6.2-year and the 18.6-year cycles are negative and the catch rate at the same time is too high.

The Northeast Arctic haddock biomass oscillation

The biomass system $S_{had}(t)$ of Northeast Arctic haddock has a mutual binding $B_{had}(t)$ to the Barents Sea ocean system $S_{had}(t)$, the total plankton system $S_{had}(t)$, the total biomass system $S_{had}(t)$, and an unknown source $S_v(t)$. The biomass of Northeast Arctic haddock has an eigen-frequency of about 18.6/3=6.2 years.

The cycle code

The Northeast Arctic haddock biomass growth is dependent on the phase-relation between the biomass eigen-dynamics of about 6.2 years and the Kola cycles of 6.2 and 18.6 years. The biomass has a long-term growth and dominant cycles of about 18.6/3=6.2 and 18.6 years when the 6.2-year and the 18.6-year Kola cycles are positive. The biomass has a long-term biomass reduction and a short cycle of about 6 years when the 6.2-year Kola cycle is positive and the 18.6-year Kola cycle is negative. The biomass is expected to have a strong reduction when the 6.2-year and the 18.6-year Kola cycles are negative at the same time.

The Barents Sea ecological theory

The identified nodal spectrum in all Barents Sea biomasses may be summarized by a common Barents Sea ecological theory. This theory has the following elements:

1. The Atlantic inflow oscillation: The Atlantic inflow to the Barents Sea is controlled by the lunar nodal tides of 6.2 and 18.6 years. The tides represent a time variant process where a 74-year tide from the Arctic Ocean seems to have the power to introduce a phase reversal of π (rad) on the 18.6-year tide and the 18.6-year tide seems to have the same influence on the 6.2-year tide.
2. The Kola temperature oscillation: The Kola temperature oscillation is an indicator of the Atlantic inflow oscillation.
3. The plankton oscillation: The plankton oscillation is influenced by the Atlantic inflow oscillation.
4. The biomass eigen-frequency: The biomasses in the Barents Sea exhibit an eigen-frequency that is tuned to the 6.2-year Atlantic inflow oscillation.
5. Optimal recruitment: Optimal recruitment is associated with an optimal phase-relation between the biomass eigen-frequency cycle and the plankton oscillation.
6. Long-term growth: Long-term biomass growth is associated with long periods when the 6.2- and the 18.6-year Kola cycles are positive at the same time.
7. Biomass collapse: The worst-case situation of water and plankton inflow to the Barents Sea occurs during the periods when the 6.2- and the 18.6-year Kola cycles are in a negative state. New recruitment suffers from the worst-case food availability for larvae. Over a long period the biomass will be strongly reduced to a minimum level. During this period the biomass is vulnerable. Overfishing in this period may lead to a biomass collapse.
8. Parallel growth: All analyzed species have a parallel growth that follows the Atlantic inflow and the Kola temperature oscillation. The exception is the shrimp biomass. This biomass exhibits inverse cycle dynamics.

From this analysis it is concluded that the large biomass fluctuations in the Barents Sea are controlled by deterministic cycles where the 18.6-year lunar nodal gravity cycle is the First Cause.

3.4 The Management Theory

The Newtonian concept of dynamics is based on the simple differential equation dx/dt=Ax(t). From this equation the future state x(t) may be computed when the parameter A and the initial condition x(0) are known. In biomass modeling, x(t) represents the biomass state vector and the system matrix A represents parameters of recruitment rates, maturing rates, growth rates and mortality rates. From this equation we may predict the future biomass state x(t) when the initial biomass state x(0) is known. The ability to predict future biomasses allows for the possibility of controlling the future biomass. When we introduces a quota vector u(t), we have a biomass management model:

$$\dot{x}(t) = Ax(t) + u(t) \tag{3.33}$$

A biomass is managed by the control law:

$$u(t) = (R(t) - x(t))K(t) \tag{3.34}$$

where K(t) is the control strategy and R(t) is the reference level. Using this simple dynamic model, we may predict how a quota u(t) may influence the biomass state x(t) in the future. If the growth matrix A is based on a stationary stochastic process, the management model allows for the possibility of computing an optimum quota u(t), a sustainable biomass x(t), and biological reference points related to a catch rate F(t).

The control problem

In this investigation it has been shown that the biomasses in the Barents Sea are governed by a time-variant stochastic process. All parameters in the growth matrix A are influenced by the lunar nodal spectrum. The growth matrix then has the property:

$$A(t) = f(3\omega_0, \omega_0, \omega_0/3, t) \tag{3.35}$$

where the angle frequency is $\omega_0=2\pi/T_0=2\pi/18.6134$ (rad/yr). Stationary cycles in the growth matrix imply this is not a stochastic stationary process. This means there are:

1. No mean biomass in the Barents Sea.
2. No stationary optimum quota u(t).
3. No stationary sustainable biomass x(t).
4. No stationary biological reference points.

When the biomass state x(t) is estimated over a time period, it will introduce a phase-delay in an estimated time series. This phase-delay in the x(t) estimate will make a phase-delay in the control law. From control theory it is well known that a phase-delay in a feedback loop will introduce a dynamic instability that may lead to a collapse in the biomass.

The stability problem

This investigation has identified three sources that will cause management-driven instability in the biomass of Northeast Arctic cod.

1. Feedback-driven instability: The biomass shows a fluctuation of about 6 years. At the same time there is a phase delay of about 3 years between the biomass state estimate and the catch of new quota of cod. Real and measured biomass fluctuation will then be roughly in reversed phases. Then we have a positive feedback or an instable system.
2. Reference instability: Biomass control has no stationary reference level R(t) (Equation 3.34). This will lead to a long-term instability caused by the 18.6-year growth cycle (Equation 3.35).

3. Control instability: Changes in the control strategy K(t) each year mean that it may not be possible to forecast the biomass state (Equation. 3.33).

These stability problems will sooner or later lead to a biomass collapse.

Management of stationary biomass cycles

This analysis of the biomass in the Barents Sea has identified large biomass fluctuation in cycles of 6.2, 18.6 and 50 to 80 years. This means optimal biomass management depends on a planning range from 1 to about 75 years. The investigation has identified a code of biomass long-term growth, long-term reduction and biomass collapse, which is related to the lunar nodal cycles in the Kola time series. This code demonstrates the importance of the timing in allowing for large biomass growth over the long run. At the same time it demonstrates that the biomass is extremely vulnerable in the periods when the 6.2-year and 18.6-year Kola section temperature cycles are in a negative state. The consequence of code of biomass growth is that:

1. The biomass must have fluctuations in order to grow over the long run.
2. The biomass can not provide constant production for the fishery industry.

This leads to the conclusion that short- and a long-term biomass management should be based on the taking of an annual percentage of the biomass. This percentage should be related to the long-term growth period, the long-term reduction period and the special vulnerable period when the 6.2- and the 18.6-year cycle are negative at the same time.

Chapter 4

DISCUSSION

Otto Petterson (1905, 1912, 1914a, 1914b, 1915, 1930) argued that long-term gravity cycles from the moon influenced both the climate and fluctuations of herring populations. Later Maksimov and Smirnov (1965, 1967) reported a 18.6-year standing wave in the Atlantic Ocean. They believed that a 18.6-year fluctuation in the surface water introduced a 18.6-year cycle in the weather. In more recently investigations Currie identified the 18.6-year cycle in many climate indicators.

In this investigation a standing lunar nodal spectrum has been identified from the 18.6-year cycle. This spectrum has been identified in the polar position, the extent of Arctic ice coverage, the tide, the Kola section sea temperature and the NAO winter index. The investigation has analyzed the fluctuation in biomasses and model parameters for plankton, shrimp, capelin, cod, herring and haddock in the Barents Sea. The results show that the 18.6-year lunar nodal spectrum has a dominant influence on the biomass fluctuations in recruitment, growth, maturity and biomass eigen-dynamics in all investigated species. These results raise the question as to why this lunar nodal spectrum has not been identified in earlier analysis?

Time series are usually analyzed by spectrum estimate methods. These methods are based on the assumption that the spectrum represents a stochastic stationary process in the time series. A closer analysis of the time series showed that the cycle spectrum had a time-variant phase. To overcome this problem an analysis method was developed based on the Coiflet wavelet transform. Using this method it was possible to identify single dominant cycles and the phase-relation between dominant cycles in climate indicators, biomass fluctuations and parameters fluctuations in biomass models. This shift from a spectrum analysis to a wavelet cycle analysis explains why other researchers have had difficulty identifying the lunar nodal spectrum.

The wavelet analysis method is a new means of analysis. The newness of this approach raises the question of its reliability. The analysis method has been developed from many trials of test data. It is, however, the coherence between the identified cycle phase in the many time series from nature that has demonstrated the robust nature of this wavelet analysis.

What about other causes of biomass fluctuation? This thesis has investigated stationary cycles in the climate indicators and biomasses in the Barents Sea. The lunar nodal spectrum is identified by a cross-correlation quotient and a signal-to-noise ratio. The cross-correlation quotient represents a match to a perfect lunar nodal spectrum. The signal-to-noise ratio represents the dominance of the lunar nodal spectrum compared to influences from other causes. In this investigation other causes and errors in time series are represented by a disturbance that is the summation of unidentified sources.

Chapter 5

CONCLUSIONS

5.1 Conclusion

This investigation was initiated to answer the research question: Is there a stationary cycle in the biomass time series of Northeast Arctic cod? The results from this thesis confirm that the biomasses in the Barents Sea are subject to a set of dominant stationary cycles, which are related to the 18.6-year lunar nodal cycle. The identified cycles have a stationary cycle time, but not a stationary phase. The set of stationary cycles represents a lunar nodal spectrum. This dominant lunar nodal spectrum is explained by an earth oscillation, an Arctic oscillation system, an ecological oscillation system and a management oscillation.

The earth oscillation

The 18.6-year lunar nodal cycle introduces an oscillating gravity force on the earth. This oscillating gravity force introduces:

- A lunar nodal tide: This is comprised of a vertical and horizontal 18.6-year lunar tide spectrum in the Atlantic Ocean.
- A core mantle tide: This is comprised of a possible vertical and horizontal 18.6-year lunar tide spectrum in the liquid core of the earth.
- A core mantle movement spectrum: This entails a possible 18.6-year spectrum in the liquid core movement, which is identified as the 18.6-year lunar nodal spectrum in the movement of the polar position.

The Arctic oscillation system

The earth oscillation represents a forced oscillator on the Arctic oscillation system. The Arctic oscillation system is represented by the mutual relation between the lunar nodal spectrum in the Arctic Ocean circulation, the Atlantic water, the Barents Sea water, the Arctic ice extent, the reflection of Arctic light and interaction with the atmosphere. The Arctic oscillation system introduces a lunar nodal spectrum in:

- The Arctic Ocean water circulation.
- The inflow of Atlantic water to the Arctic Ocean.
- The inflow of Atlantic and Arctic water to the Barents Sea.
- The Barents Sea temperature.
- The Arctic ice extent.
- The NAO winter index.

The Ecological oscillation system

The lunar nodal spectrum in the Arctic System oscillation system represents a forced oscillator on the ecological system in the Barents Sea. The ecological oscillation system introduces:

- A 18.6-year spectrum in the inflow of plankton from the Atlantic Ocean to the Barents Sea.

- Optimal biomass recruitment in cycles of about 6.2 years when the 6.2-year nodal tide carries plankton from the Atlantic Ocean to the Barents Sea.
- Biomass eigen-frequency cycles of about 6 years, which are adapted to the optimal recruitment cycle of about 6.2 years.
- Biomass fluctuations in the Barents Sea, which are caused by fluctuations in recruitment and growth.
- A long-term biomass growth when the 18.6-year and the 6.2-year cycles of Atlantic inflow are positive at the same time.
- A strong biomass reduction when the 18.6-year and the 6.2-year cycles of Atlantic inflow are negative at the same time.

The management oscillation
The ecological oscillation system represents a forced oscillator on the management of biomass in the Barents Sea. The ecological oscillation system introduces:

- Instabilities in biomass quota management.
- A potential risk of a biomass collapse when the 6.2- and the 18.6-year Kola cycles are negative at the same time.
- Constraints on fisheries investments, which are dependent on the phase-relation to the 18.6-year Kola temperature cycle.

5.2 Summary of contributions

The thesis presents the results from seven papers. The main contributions from these papers are:

- A wavelet analysis method: This method was devised to identify the cycle-time and the cycle phase in time-variant time series.
- The forced oscillator theory: A stationary cycle force from the moon will produce a set of movement cycles on the earth. These cycles will produce a new set of cycles. In this chain of movement some cycles may be amplified by resonance.
- The nodal spectrum: A spectrum of harmonic and sub-harmonic cycles has been identified from the 18.6-year lunar cycle with respect to polar motion, Arctic climate indicators, and biomasses in the Barents Sea. The lunar nodal spectrum is explained by a stationary energy distribution in feedback systems.
- The phase-reversal phenomenon on: A 180 degree phase-reversal has been identified in the 18.6-year climate indicators, which is controlled by the 74-year cycle from the lunar nodal spectrum. The phase-reversal phenomenon is explained by a multiplicative modulation between two cycles.
- The climate oscillation theory: There is a correlation between the lunar nodal spectrum of the polar position movement, water circulation in the Arctic Ocean, the extent of the Arctic ice cover and the NAO winter index. This indicates that the identified climate fluctuations in the NAO winter index are controlled by the pull of gravity from the moon.
- The biomass growth code: Long-term biomass growth, reduction and collapse are associated with the phase-relation between the biomass eigen-dynamic of about 6 years and the Kola temperature cycles of 6.2 and 18.6 years.
- The phase-clock approach: A method has been presented to transform the Newtonian ballistic approach to rotating vectors that visualizes the stationary cycles in the biomass and climate indicators.
- Management instability: The identification of three types of instabilities in current biomass management.

5.3 Future Research

This investigation represents a broad analysis of time series and system dynamics, which is reflected in Arctic climate indicators and biomasses in the Barents Sea. The discovery of the 18.6-year lunar

nodal spectrum in all time series represents a first step into a new research area. This new research area should have a focus on a systems approach toward the lunar nodal spectrum and how it is distributed. Some important topics for research are:

- The wine glass theory: The movement energy from the 74-year cycle of polar position movement seems to be distributed as movement of water in harmonic cycles at different levels in the Arctic Ocean. This theory may be confirmed or rejected by a computer simulation. In this simulation it may be necessary to simulate the connections between water circulation in the Arctic Ocean, the Atlantic Ocean, the Greenland Sea and the Barents Sea.
- The 6.2-year cycle: The 6.2-year cycle has been identified in all time series. There is a need for more research to look for this cycle in other time series from the Atlantic Ocean. This investigation may identify the polar motion or the tide as the most important driving force behind this cycle.
- The 55.8 year cycle: The 55.8-year cycle has only been identified in the Kola temperature cycle. It has to be confirmed or rejected. The hypothesis that this is the sum of the 6.2 and the 18.6-year cycle must be confirmed or rejected. There is a need for more research and computer simulation models of the oscillating water transport in the Arctic Ocean and water oscillation in interaction with the Arctic Ocean and the Barents Sea.
- The phase-reversal problem: More research is needed to understand the physical processes behind the identified phase-reversal of the 6.2- and the 18.6-year cycles in the Arctic climate indicators.
- The biomass oscillation: More research is needed to understand how biomass management and predators influence the identified code of biomass fluctuations in periods of 6, 18 and 50 to 80 years.
- The biomass management: More research is needed to understand how the biomass cycles of 6 and 18 years influences the marine and maritime industrial cluster.

PAPERS

Chapter 4

Paper I. Earth nutation influence on the temperature regime of the Barents Sea

Paper II. Earth nutation influence on system dynamics of Northeast Arctic cod

Paper III. Earth nutation influence on Northeast Arctic management

Paper IV. Systems Dynamics of Barents Sea Capelin

Paper V. The code of long-term biomass cycles in the Barents Sea

Paper VI. Cause of biomass dynamics in the Barents Sea

Paper VII. The Lunar nodal cycle influence on Arctic climate

Paper I

ICES Journal of Marine Science, 56: 381–387. 1999
Article No. jmsc.1999.0469, available online at http://www.idealibrary.com on IDEAL®

Earth nutation influence on the temperature regime of the Barents Sea

H. Yndestad

Yndestad, H. 1999. Earth nutation influence on the temperature regime of the Barents Sea. – ICES Journal of Marine Science, 56: 381–387.

A General System theory of the influence of the Earth's nutation on the temperature of the Barents Sea is presented. According to this theory, the Earth's axis behaves dynamically as a forced oscillator on a non-linear sea system that modulates a set of harmonic and subharmonic low-frequency temperature cycles.

A spectrum analysis of the Kola meridian sea temperature time series indicates a correlation between it and the Earth nutation cycles of 18.6 yr, 18.6/3=6.2 yr, and 18.6 × 3=55.8 yr. The 55.8 yr cycle seems to follow a moving average in the temperature series.

If the theory is confirmed by the analysis of other data sets it will open new perspectives in the forecasting of future temperature, ecological, and biological changes not only in the Barents Sea but also worldwide.

Key words: system theory, Earth nutation, temperature cycles, Barents Sea.

Received 20 March 1998; revised 28 September 1998; accepted 18 February 1999.

Harald Yndestad: Aalesund College, Box N-5104 Larsgaarden, 6021 Aalesund, Norway. Tel: +47 70 16 12 00; fax: +47 70 16 13 00; e-mail: harald.yndestad@hials.no

Introduction

Aristotle explained the dynamics of objects in nature by the four causes, namely the efficient cause, the material cause, the structure cause, and predestined fate. The latter was decided by the "cause of causes"; the positions of the Sun, the Moon, and the stars. Does this doctrine have any relevance today?

In 1543 Copernicus associated the change of star positions with a changing direction of the rotational axis of the Earth. Isaac Newton explained in "Principia" (Chandrasekhar, 1995) that the Earth is a spinning object where the axis describes a circle about the North Pole. This motion is called "precession" and proceeds, in about 25 800 yr, along a cone with a half-apex angle of 23.439 degrees and moves along the elliptic by 50.291 arc s yr^{-1}. In 1754 Kant predicted that friction with tidal forces on the Earth would cause a deceleration of the Earth's rotation. Euler predicted in 1758 that the rotation of the Earth's axis would show the Earth's motion with respect to an Earth-fixed reference frame (polar motion). Some years later in 1776 Laplace made theoretical tidal modelling involving periodic hydrodynamics on a rotating sphere. In the eighteenth century the English astronomer Bradley discovered that the Earth's rotational axis wobbled around the precession cone. This change was called the "nutation". Better instrumentation slowly modified the view of the movement of the Earth as a stable, dynamic process.

Earth axis dynamics are now described by the four components precession, nutation, celestial pole offset, and polar motion. The nutation has an amplitude of 9.2 arc s and a 18.6 yr cycle caused by the Moon. By new high-precision measurements more than 100 frequency components in the nutation have been discovered. The four dominant cycles of the nutation are 18.6 yr (precession period of the lunar orbit), 9.3 yr (rotation period of the Moon's perigee), 182.6 d (half a year), and 13.7 d (half a month). New geodetic techniques now make it possible to detect Earth displacement influenced by the tide, the Earth core and mantle, and from atmospheric disturbance. These cycles seem to influence global ecological changes. A worldwide correlation between the 18.6 yr Earth nutation and rainfall, tree-rings, air temperatures, and dates of wine harvests has been reported (Currie, 1991; Wyatt *et al.*, 1992). In historical records of cod landings in Norway a correlation has been reported between cod landings and the 18.6 yr Earth nutation (Wyatt *et al.*, 1994). A correlation has also

1054–3139/99/030381+07 $30.00/0

been reported between historical records of cod and nutation harmonics 18.6/3 yr, 18.6 yr, and 3 × 18.6 yr (Yndestad, 1996b).

In the Barents Sea the inflow of warm North Atlantic water meets a stream of cold Arctic water from the north and cool, mixed water circulates back to East Greenland. These currents may vary in intensity and slightly in position and cause biological changes in the Barents Sea. Since the first analysis by Helland-Hansen and Nansen (1906), changes in their patterns have been explained by variability in average wind and climatic conditions (Loeng *et al.*, 1992; Dyke, 1996). There is, however, no clear understanding of how meteorological and oceanographic conditions influence each other (Loeng *et al.*, 1992).

Russian scientists at the PINRO institute in Murmansk have provided monthly temperature values from the upper 200 m in the Kola section along the 33°30′E meridian from 70°30′N to 72°30′N in the Barents Sea (Bockov, 1982). The data series has quarterly values from the period 1906–1920 and monthly values from 1921, partly measured and partly interpolated. Loeng, *et al.* (1992) have studied this time series and found dominant coefficients at 3.3, 7.2, 8.8, 11.7–13.6, and 17.5 yr cycles in the Fourier spectrum. Latterly a more complete monthly data series from 1900 to 1994 has been compiled (Tereshchenko, 1996).

In 1994 a modelled projection of the lifetime earning capacity of a Norwegian trawler was carried out as an item of contractual research (Yndestad *et al.*, 1994). By chance, one of the findings was that the time series of North Atlantic cod catches has a dominant 6–7 yr cycle in the Fourier amplitude spectrum. The same dominant cycle was found in cod recruitment. After more research the same cycle, as an harmonic relation to the Earth's nutation, was found in the Kola series (Yndestad, 1996a). This paper presents a more detailed spectrum analysis of the Kola meridian temperature time series. The analysis detects harmonic and subharmonic periodic cycles related to the Earth's nutation of 18.6 and the 1 yr seasonal variation. The cycles have been analysed according to a General System theory and the concept of forced oscillators. According to this theory the Moon represents the "cause of causes" behind the low-frequency temperature cycles in the Barents Sea. Gravity from planetary forces causes changes of the Earth's rotation axis. In the long run this generates a set of harmonic and subharmonic energy cycles that modulate the current amplitudes. Some cycles may be amplified by resonance and some of them are depressed by energy loss. According to the General System theory, the cycles are phase sensitive. High-frequency cycle changes will be recorded as noise and influenced by local conditions. Low-frequency cycles will be recorded as climatic change.

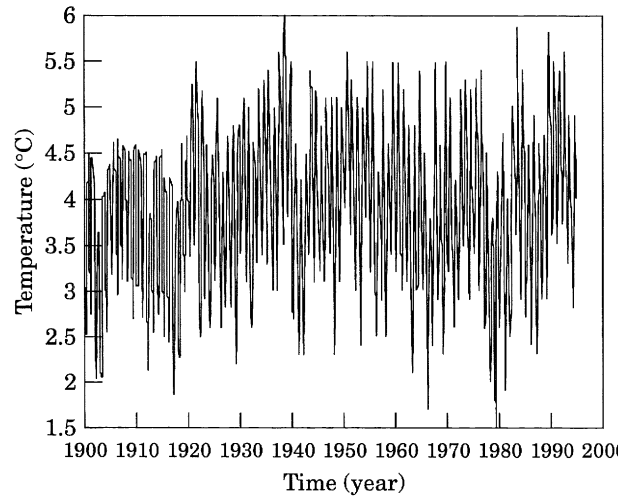

Figure 1. A yearly average temperature in the Barents Sea from the year 1900.

Materials and methods

Materials

Figure 1 shows the temperature series taken from the Kola section (Y. A. Bockov, pers. comm.). The data are measured along 33°30′E from 70°30′N to 72°30′N and have a sampling time "T" of 1 month from 1900 to 1994. According to the Shannon sampling theorem (Phillips and Harbor 1989) we may investigate planetary forced cycles up to about 50 yr. The figure shows that the temperature oscillates rapidly about 1°C from a mean value of about 3.7°C. To understand the more fundamental aspects of this temperature series we will relate the data series to a General System theory.

General System theory

"General System theory" is a means of understanding abstract organizations independent of time and space. A system is a set of subsystems cooperating to a common purpose. This may be expressed as:

$$S(t)=\{B(t), S_N(t)\} = \{B(t), \{S_1(t), S_2,(t) \ldots, S_n(t)\}\} \varepsilon w, \quad (1)$$

where S(t) is the system, $S_N(t)$ is a set of subsystems, $S_1(t)$ is a subsystem, B(t) is a dynamic binding between the subsystems, and w is the common system purpose. According to the general theory, systems are time varying, structurally unstable, and mutually state dependent.

In this case we have the planetary system: $S(t)=\{B_p(t), \{S_e(t), S_m(t), S_s(t)\}\}$ where $S_e(t)$ represents the Earth system, $S_m(t)$ the Moon system, $S_s(t)$ the Sun system, and $B_p(t)$ is the mutual dynamic binding. In this case the planetary system represents a stable periodic system.

The Earth system has the subsystems $S_e(t)=\{B_e(t), \{S_b(t), S_g(t), S_w(t), S_c(t), S_v(t)\}\}$ where $S_b(t)$ is the Barents Sea system, $S_g(t)$ the Earth axis system, $S_w(t)$ a warm Atlantic flow system, $S_c(t)$ a cold-water stream system, $S_v(t)$ an unknown disturbance system, and $B_e(t)$ the dynamic binding between the systems. Since all subsystems are dynamic mutually dependent we have to understand some fundamental dynamic properties of each system.

System state dynamics

The temperature state dynamics in the Barents Sea system $S_b(t)$, may then be modelled by the state space equation:

$$\ddot{x}(t)=A(t)\cdot x(t)+B(t)\cdot u(t)+C(t)\cdot v(t);$$
$$y(t)=x(t)+w(t), \tag{2}$$

where x(t) represents a temperature state vector, A(t) represents a time varying internal binding, and u(t) represents a state vector from planetary system as a forced oscillator. B(t) represents the dynamic binding from the planetary objects to the Barents Sea, $S_w(t)$ is the warm-water system, $S_c(t)$ the cold-water system, v(t) is a disturbance vector, C(t) the dynamic binding from disturbance, D(t) is the measure matrix, y(t) is the measured temperature, and w(t) is noise in measurement.

Wiener spectrum

The energy E_v from an unknown system state v(t), may be estimated by Parseval's theorem:

$$E_v=\int_{-\infty}^{+\infty}|v(t)|^2=\frac{1}{2\pi}\int_{-\infty}^{+\infty}|V^*(j\omega)|^2 d\omega. \tag{3}$$

If the spectrum $V(j\omega)$ is white noise, the spectral density is:

$$S_{vv}(j\omega)=|V^*(j\omega)|^2=V^2{}_0, \tag{4}$$

where $V^2{}_0$ is the noise variance. In this case the integrated energy will be infinite. Since this is impossible, the temperature spectrum must be coloured. Such process may be modulated by the first order process:

$$\dot{v}(t)=-a\cdot v(t)+n(t), \tag{5}$$

where n(t) is non-correlated white noise. The autocorrelation of this process (5) is:

$$R_{vv}(\tau)=E[v(t)\cdot v(t+\tau)-E[v(t)]^2]=\frac{V_0^2}{2a}\cdot e^{-a|\tau|} \tag{6}$$

where τ is a time displacement. This indicates that the autocorrelation function of the time series v(t) is expected to fall exponentially. The frequency transform of the first order process (5) is a Wiener spectrum:

$$V(j\omega)=\frac{N_0}{a+j\omega}. \tag{7}$$

This indicates that spectrum of the measured time series is expected to fall by N_0/ω, or 20 dB/decade, when $\omega>a$.

Periodic properties

The planetary system S(t) is a stable system generating periodic states u(t). These states can be represented by the Fourier series:

$$u(t)=\sum_{n=0}^{\infty} u_n\cdot e^{jn\omega_i t}, \tag{8}$$

where u_n represents amplitude series and the angle frequency $\omega_i=2\pi/T_i$. In this case the most important cycles are the Earth's seasonal frequency $\omega_s=2\pi/1$ (rad yr^{-1}), the Earth's nutation $\omega_n=2\pi/18.6$ (rad yr^{-1}) and the precession $\omega_p=2\pi/26\,800$ (rad yr^{-1}). The autocorrelation of the periodic u(t) has the property:

$$R_{uu}(\tau)=E[u(t)\cdot u(t+\tau)-E[u(t)]^2]=\frac{u_0^2}{2}\cos(\omega_i\tau), \tag{9}$$

where τ is the time displacement. This means that if the measured time series y(t) has a periodic property, it will be reflected in the autocorrelation function.

Forced oscillators on non-linear systems

In this case the Earth's axis dynamics is a forced oscillator on a non-linear sea system. Such a system may be modelled by the Duffing equation:

$$\ddot{x}(t)+A\cdot\ddot{x}(t)\times F[x(t)]=B\cdot\cos(\omega t), \tag{10}$$

where F[x(t)] is the non-linear system. It is well known that such a system has chaotic behaviour and generates a set of harmonic and subharmonic frequencies (Moon, 1987).

The warm Atlantic inflow and the cold Arctic water in the Barents Sea are parts of a complex global hydrodynamical system. Each of them may be modulated as a forced oscillator u(t) on the feedback systems. The warm-water stream system may be modulated as $S_w(t)=\{B_w(t), \{S_f(t), S_b(t)\}\}$ where the feed forward system $S_f(t)=\{B_f(t), \{p_{f1}(t), p_{f2}(t) \ldots p_{fn}(t)\}\}$ and a feedback system $S_b(t)=\{B_b(t), \{p_{b1}(t), p_{b2}(t) \ldots p_{bm}(t)\}\}$. Each subpartner $p_i(t)$ may have a local circular stream of water and each subsystem p(t) will have an energy loss h(t) that has the frequency transfer function $H(j\omega)$. From the theory of feedback dynamic systems,

the frequency transfer function of a circular system of water flow is:

$$\frac{V_{fb}(j\omega)}{U(j\omega)} = \frac{H_{f1}(j\omega)\ldots H_{fn}(j\omega)\cdot e^{j[\tau_{f1}(t)+\tau_{fn}(t)]\omega t}}{1+[H_{f1}(j\omega)\ldots H_{fn}(j\omega)][H_{b1}(j\omega)\ldots H_{bm}(j\omega)]}, \quad (11)$$

$$e^{j(\tau_{f1}(t)+\tau_{fn}(t))\omega t} e^{j(\tau_{b1}(t)+\tau_{bm}(t))\omega t}$$

where $H_i(j\omega)$ represents an energy transfer function, $\tau_i(t)$ represents a time-dependent transport delay, $U(j\omega)$ the input energy to the sea, and $V_{fb}(j\omega)$ the output energy to the Barents Sea. From the theory of feedback system dynamics this type of system has some fundamental properties:

(1) The forced oscillator u(t) will modulate a set of harmonic and subharmonic temperature cycles into the Barents Sea;
(2) The feedback property will introduce a set of harmonic cycles related to the total transport delay. Changes in this transport delay will influence the phase dependent cycles;
(3) The feedback system (11) may have resonance, and thus be able to absorb energy. This explains why a small movement of the Earth's nutation can be amplified and cause a significant force oscillator to the Barents Sea;
(4) The system is structurally unstable. Changes in binding B(t) between subpartners may force changes in the cycle phase and thus introduce a disturbance and major state changes in the system;
(5) The temperature in the Barents Sea will be disturbed by the sum of the warm-water feedback system and the cold-water feedback system.

The state dynamics of the forced oscillator system then will have the property:

$$y(t)=F^{-1}\{V_{fb}(j\omega)\}+v(t)+w(t)=y_u(t)+v(t)+w(t);$$

$$y_u(t)=\sum_{(n,m)=0}^{\infty} A_{(n,m)}\cdot\sin\left[\frac{n}{m}\cdot\omega_i t+\varphi_{(n,m)}(t)\right] \quad (12)$$

where ω_i is the periodic cycle, A_i the cycle amplitude, n the harmonic number, m the subharmonic number, $\varphi_i(t)$ the phase delay, v(t) a disturbance from an unknown source, and w(t) is measured noise.

According to this theory, there may be harmonic and subharmonic cycles from the precession, nutation, and from the polar motion.

Results

Figure 2 shows the power density spectrum periodogram of the Kola section temperature–time series y(t). This

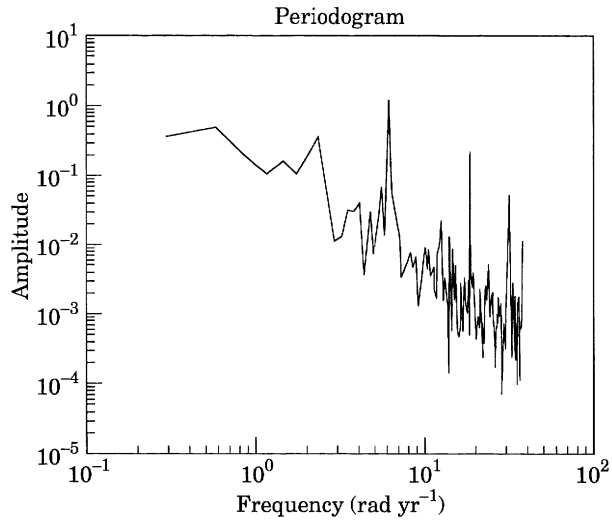

Figure 2. Power density spectrum of the temperature series y(t).

figure confirms some fundamental properties from the general system theory:

(1) The power density spectrum of y(t) is falling by k/ω^2. This confirms the theory of energy distributions (7);
(2) Most power density is concentrated at the 1 yr seasonal angle frequency $\omega_e=6.28$ (rad yr^{-1}) forced from the Sun;
(3) The seasonal 1 yr cycle from the Sun generates the harmonics $2\omega_e$ and $3\omega_e$ and there is a trace of the subharmonics $\omega_e/2$ and $\omega_e/4$. This is according to the modulation theory (10) and (11);
(4) At the lower end of the spectrum there are some indications of the nutation harmonics frequency $\omega_e/2=0.6$ (rad yr^{-1}) or 9.3 yr, $\omega_e/3=1.1$ (rad yr^{-1}) or 6.2 yr, and at $\omega_e/4=1.3$ (rad yr^{-1}) or at 4.6 yr. This confirms the modulation theory (10) and (11).

The time series y(t) is dominated by the 1 yr seasonal cycle. The next step is to look more closely for cycles related to the Earth's nutation.

Filtered time series

Figure 3 shows a low pass filtered temperature series. In this case the 1 yr cycle is suppressed by the linear phase, moving average filter:

$$y_{lp}(nT)=\frac{1}{2M+1}\sum_{m=-M}^{m=M} y(nT+mT), \quad (13)$$

where M is 12 months. The filtered time series now seems to be dominated by state changes. The fundamental properties of this time series have been analysed more closely by looking at the phase-space, the

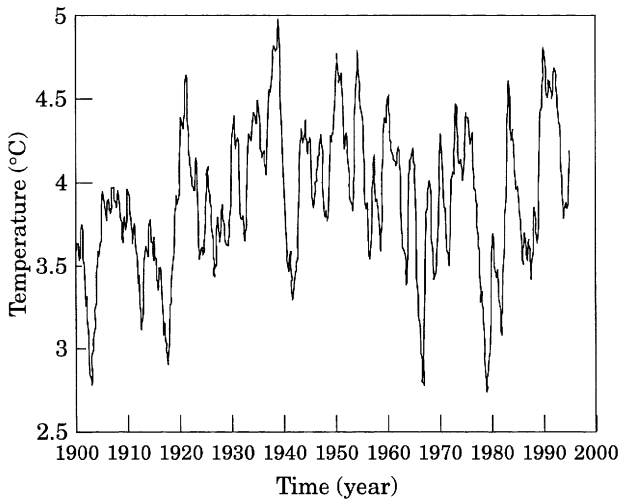

Figure 3. The Kola section temperature–time series.

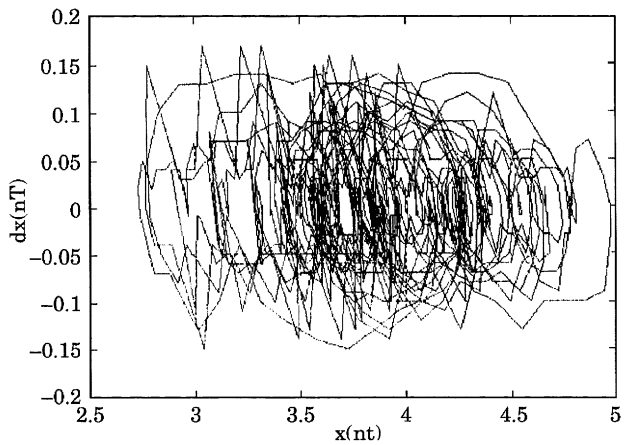

Figure 4. Phase-space analysis of dx(nT) and x(nT) (°C).

autocorrelation, and a number of spectrum estimation methods.

Phase space analysis

Figure 4 shows a phase-space analyses of the time series. The x-axis shows the time series y(nT) and on the y-axis and we have the velocity:

$$dx(nT) \approx \frac{x(nT) - x(nT - T)}{T}. \tag{10}$$

Figure 4 indicates a chaos attractor in the phase-space at the temperature x=3.73°C. This attractor in the phase-space supports the theory that there are deterministic periodic cycles in the 100 yr temperature–time series.

Correlation analysis

Figure 5 shows the computed normalized autocorrelation function $R_{yy}(\tau)$ of the filtered time series $y_{lp}(nT)$.

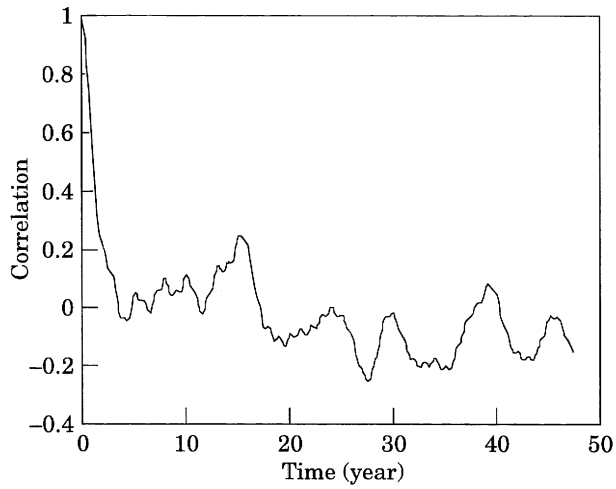

Figure 5. Autocorrelation function.

The rapidly falling autocorrelation indicates there is a significant amount of noise v(t) from an unknown source in the time series $y_{lp}(t)$ (6). The periodic variations in the autocorrelation indicate periodic cycles in the temperature series (9). The next step is to estimate the cycle parameters of $y_u(t)$ (12).

In this case the data series is corrupted with noise v(t) and w(t). To suppress the noise a closer spectrum analysis has been done by analysing the power density spectrum of the time series. The time series is short compared to the nutation cycle and the power density spectrum loses the phase information. The phase is estimated by a cross-correlation between the time series $y_{lp}(nT)$ and harmonic nutation cycles. The estimated harmonic nutation related cycles were the third harmonic cycle $y_{m,3}(nT)$ of 6.2 yr, the nutation test cycles $y_{1,1}(nT)$ of 18.6 yr, and the subharmonic cycle $y_{3,m}(nT)$ of 55.8 yr.

$$\begin{aligned} y_{m,3}(nT) &= 3.9 + 0.4 \cdot \sin\left(\frac{3 \cdot 2 \cdot \pi}{18.6} \cdot nT + 12T\right); \\ y_{1,1}(nT) &= 3.9 + 0.6 \cdot \sin\left(\frac{2 \cdot \pi}{18.6} \cdot nT + 9.6T\right); \\ y_{3,n}(nT) &= 3.9 + 0.4 \cdot \sin\left(\frac{2 \cdot \pi}{3 \cdot 18.6} \cdot nT + 336T\right), \end{aligned} \tag{14}$$

where n=0, 1, 2, months from the year 1900, T is the sampling time of 1 month, and $\varphi_i = 12T$ is a phase displacement.

The power density spectrum analysis has identified a peak at about 18.6/2 or 10 yr and a significant peak at about 4 yr. The 4 yr peak seems to be the 4. harmonic of the seasonal 1 yr cycle. These cycles were not estimated.

Figure 6 shows the filtered time series $y_{lp}(t)$ and the estimated third subharmonic temperature cycle $y_{3,m}(nT)$ of 55.8 yr. The cycle has a maximum at about 1945 and

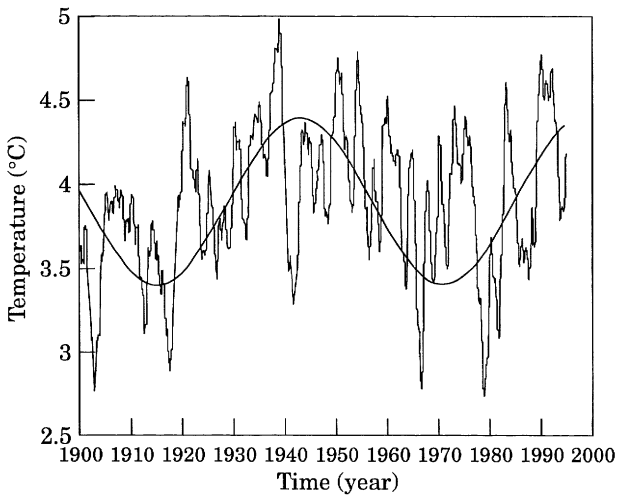

Figure 6. Temperature series $y_{lp}(t)$ and a 55.8 yr cycle $y_{3,n}(nT)$ (°C).

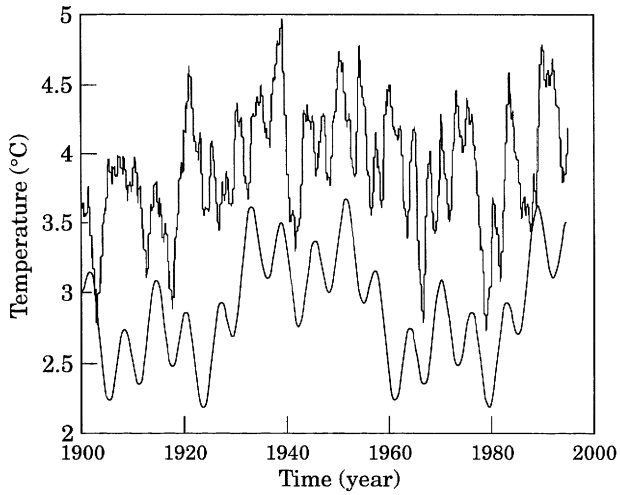

Figure 7. Temperature–time series $y_{lp}(t)$ and estimated cycles $y_u(t) - 1$ (°C).

will reach a new maximum around the year 2000. The figure shows that the temperature seems to follow this 3. subharmonic cycle as a moving mean temperature. This indicates that the Barents Sea has no stationary mean temperature.

Figure 7 shows the low pass filtered time series $y_{lp}(t)$ and sum of harmonic cycles $y_n(t)=y_{m,3}(t)+y_{1,1}(t)+y_{3,m}(t)$ (displaced 1 degree down). The estimated cycles now have the same pattern. Some years, however, the 6.2 yr cycle seems to have a phase shift.

The correlation between the time series, $y_{lp}(t)$ and the three estimated cycles $y_n(t)$ is 0.5. The correlation is sensitive when changing cycle frequency or phase. This is a strong indication that the source of the basic cycle is Earth nutation. The non-linear sea system modulates a set of harmonic and subharmonic cycles in the Barents Sea.

Discussion

The Kola meridian temperature–time series has been analysed. The power density spectrum of this is falling by k/ω^2 as expected according to the General System theory. The important property of the estimated spectrum is that major low-frequency cycles are correlated with the harmonics and subharmonics of the Earth's nutation of 18.6 yr. Since these are known and simple deterministic cycles it opens a new perspective in the prediction of fundamental long-term changes in sea temperature, and associated environmental and ecological changes, not only in the Barents Sea but also worldwide. The analysis has estimated cycles of 18.6/3=6.2 yr, 18.6 yr, and $18/6 \times 3 = 55.8$ yr. However there may be more subharmonic temperature cycles in the data from the Barents Sea.

The estimated harmonic cycles are explained by a General System theory and the theory of forced oscillators. According to this theory the dynamics of the Earth's axis behave as a forced oscillator that transfers low-frequency energy to the non-linear sea system. Limits of predictions may be more low-frequency cycles and non-stability in the cycle phase. This introduces an uncertainty in the prediction of future temperatures.

To confirm this theory by oceanographic measurements existing data sets should be examined for matches to the harmonics of the Earth's nutation.

Acknowledgements

The author is grateful to Mr Yu. A. Bochkov at PINRO, Murmansk, for his assistance in providing access to the Kola meridian temperature–time series.

References

Bochkov, Y. A. 1982. Water temperature in the 0–200 m layer in the Kola-Meridian in the Barents Sea, 1900–1981. Sb. Nauchn. Trud. PINRO, Murmansk, 46: 113–122 (in Russian).

Chandrasekhar, S. 1995. Newton's: Principia for the Common Readers. Oxford University Press Inc, New York.

Currie, R. G. 1991. Deterministic signals in three-rings from Tasmania, New Zealand and South Africa. Annals of Geophysics, 9: 71–81.

Dyke, P. 1996. Modelling marine processes. Prentice Hall, London.

Helland-Hansen, B., and Nansen, F. 1909. The Norwegian Sea. Fiskeridirektoratets skrifter. Havundersøkelser, 2: 1–360.

Loeng, O. 1994. Statistical Modelling of Temperature Variability in the Barents Sea. ICES CM 1994.

Loeng, H., Blindheim, J., Ådlandsvik, B., and Ottersen, G. 1992. Climatic variability in the Norwegian Barents Sea. ICES Marine Science Symposium, 195: 52–61.

Moon, F. C. 1987. Chaotic Vibrations. John Wiley & Sons, New York.

Phillips, C. L., and Harbor, R. D. 1989. Feedback Control Systems. Prentice-Hall International (UK) Limited, London.

Tereschenco, V. V. 1996. Seasonal and year-to-year variations of temperature and salinity along the Kola meridian transect. The 84th international ICES Annual Science Conference. Hydrography Committee, Iceland.

Wyatt, T., Currie, R. G., and Larraneta, M. G. 1992. Codstock recruitment problems, the nodal tide and sunspot cycles. ICES CM 192/L:17.

Wyatt, T., Currie, R. G., and Saborido-Ray, F. 1994. Deterministic signals in Norwegian cod records. ICES Marine Science Symposium, 198: 49–55.

Yndestad, H., Helgesen, Ø., and Walde, P. 1994. Livssyklus-analyse av tråler. Høgskolen i Ålesund. Ålesund (In Norwegian).

Yndestad, H. 1996a. Stationary temperature cycles in the Barents Sea. The cause of causes. The 84th international ICES Annual Science Conference. Hydrography Committee, Iceland.

Yndestad, H. 1996b. Systems dynamics of North Arctic Cod. The 84th international ICES Annual Science Conference. Hydrography Committee, Iceland.

Paper II

ICES Journal of Marine Science, 56: 652–657. 1999
Article No. jmsc.1999.0491, available online at http://www.idealibrary.com on IDEAL®

Earth nutation influence on system dynamics of Northeast Arctic cod

H. Yndestad

Yndestad, H. 1999. Earth nutation influence on system dynamics of Northeast Arctic cod. – ICES Journal of Marine Science, 56: 652-657.

This paper reports a correlation between the time series of Northeast Arctic cod population estimates and the Earth's nutation of 18.6 years. In the Barents Sea harmonic temperature cycles of 3*18.6=55.8 years, 18.6 years, and 18.6/3=6.2 years are correlated to the growth rate of cod and will cause long-term biomass fluctuations. Harmonic temperature cycles of 18.6/3=6.2 years cycle are correlated exponentially to time series of the recruitment cycles of cod. The influence of the Earth's nutation is explained by a General Systems theory where temperature cycles are a forced oscillator on the biological system in the Barents Sea. The system dynamics of the cod biomass are synchronized to the temperature cycle and amplified by a biological stochastic resonance to the supply of food.

Key words: Northeast Arctic cod, the Earth's nutation, stationary cycles, forecasting cod.

Received 8 February 1999; accepted 21 May 1999.

Harald Yndestad: Aalesund College, Box N-5104 Larsgaarden, 6021 Aalesund, Norway. Tel: +47 70 11 12 00; fax: +47 70 11 13 00; e-mail: harald.yndestad@hials.no

Introduction

The Northeast Arctic cod is the largest stock of true cod in the world. Over the centuries it has been of vital importance for settlement and economic growth in the western part of Norway. In some years cod is abundant but in others there may not be enough to meet the demand. People dependent on fishing have always known that the stock has short- and long-term fluctuations. These have been explained to date by the onset of "herring periods" as opposed to "cod periods", the introduction of new fishing equipment, etc. When Norwegian marine research started at the beginning of this century its main aim was to discover how nature influenced the stock of cod and, if possible, to lessen the impact of the fluctuations on those who depended on fishing for their livelihood (Rollefsen, 1949). Better forecasting over the time span of 5–10 years, has always been crucial to better planning of the economical and sustainable utilization of the cod biomass.

Early scientific explanations of fluctuations of the stock were changes in food availability, mortality, hydrographic conditions in general, sea temperature fluctuations in particular, and positive feedback in recruitment (Rollefsen, 1949). More recently the fluctuations of the Northeast Arctic cod stock have been described in more detail (Jørgensen, 1992; Nakken, 1994), but the fundamental explanations are much the same: firstly the relation between the sea temperature and cod recruitment (Sætersdal and Loeng 1987; Nakken and Raknes, 1987; Eilertsen *et al.*, 1989; Nakken, 1994; Ottersen *et al.*, 1996), secondly the impact of predators like birds, marine animals, and cannibalism (Haug *et al.*, 1991; Gabrielsen and Ryg, 1992), and finally the amount of food *per se* (Ajiad *et al.*, 1992).

There may, however, exist a more fundamental cause of these fluctuations. In 1938 Petterson explained the fluctuations of herring by a tidal cycle of 112 years period and those of North Arctic cod by a 20–25 year cycle (Rollefsen, 1949). In historical records of cod landings in Norway, Ottestad (1942) reported 11, 17.5, 23, and 57 year cycles of cod. Later, Wyatt *et al.* (1992, 1994) found a correlation between cod landings and the 18.6 year cycle of the Earth's nutation. Yndestad *et al.* (1994) and Yndestad (1996b) has reported a correlation between historical records of Northeast Arctic cod and harmonic cycles of the 18.6 year Earth nutation.

This paper suggests the fundamental cause of fluctuations in the biomass of Northeast Arctic cod is an

1054–3139/99/050652+06 $30.00/0

exponential relation between a stationary temperature cycle of 18.6/3=6.2 years and new recruitment of the Northeast Arctic cod population. The cycles of 18.6 years and 3*18.6=55.8 years, seem to influence the growth rate and the maximum level of cod biomass. The cycles are explained by a General Systems theory where the temperature is a forced oscillator to the biomass and the systems elements in the Barents Sea have a stochastic resonance close to the temperature cycles.

Materials and methods

All the time series on Northeast Arctic Cod that are used here appear in reports that are in the public domain (ICES, 1995; NIMR 1995).

Systems theory

Systems theory is a means of understanding abstract organizations independent of time and space. A system is a set of subsystems working together to give an effect. This may be expressed as:

$$S(t)=\{B(t),\ S_N(t)\}=\in w, \tag{1}$$

where S(t) is the system, $S_N(t)$ is a set of subsystems, B(t) is a dynamic binding between the subsystems, and w is the common system purpose. According to the General Systems Theory, systems are time varying, structurally unstable, and mutually state dependent. In this case the Barents Sea may have the General System architecture

$$S_B(t)=[B_B(t),\ \{S_T(t),\ S_D(t),\ S_P(t),\ S_S(t)\}]\in w, \tag{2}$$

where $S_T(t)$ is the temperature system, $S_D(t)$ is a detritus system, $S_P(t)$ is a plankton system (phyto, microzoo, mezozoo, macrozoo, predatoryzoo), $S_P(t)$ is a predator system (seabirds, cod, seal, and whale) $S_F(t)$ is the food system (cod, capelin, herring, redfish, shrimp), and $B_B(t)$ is an interaction or the binding between the Barents Sea systems.

System dynamics

The system dynamics of a Barents Sea element $S_e(t)$, may be modelled by the state space equation:

$$\dot{x}_e(t)=A_e(t)\cdot x_e(t)+B_e(t)\cdot u(t)+C_e(t)\cdot v_e(t)$$

$$y_e(t)=D_e(t)\cdot x_e(t)+w_e(t), \tag{3}$$

where $x_e(t)$ represents system element state vector, $A_e(t)$ a time varying growth rate binding matrix on the autonomous system, u(t) a state vector on an external system, $B_e(t)$ the dynamic binding matrix to the external system. $V_e(t)$ a disturbance vector from an unknown source, $C_e(t)$ the dynamic binding matrix to the unknown source, $D_e(t)$ the measure matrix, $y_e(t)$ the measured state vector, and $w_e(t)$ the measurement noise vector.

Forced oscillator on the biomass

In this case the temperature system $S_T(t)$ is expected to be a stationary cyclic process related to the Earth's nutation (Yndestad, 1996a, 1999). Since most energy is related to the cyclic temperature system $S_T(t)$, the Barents Sea system may be modulated as a forced oscillator non-linear ecological sea system. This forced oscillator temperature system has the property (Yndestad, 1999):

$$x_e(t)=\sum_{k=1/M}^{1}\sum_{k=1}^{M} a_k\cdot\sin[k\omega_n t+\varphi_k(t)]+v_e(t), \tag{4}$$

where a_k represents a cycle amplitude, M is the number of cycles, $\omega_n=2\pi/18.6$ (rad yr^{-1}) is the Earth's nutation angle frequency and $v_e(t)$ is a disturbance from an unknown source. The total temperature dependent system is a sum of the elements

$$x_{tot}(t)=\sum_{e=1}^{N} x_e(t_1)=\sum_{e=1}^{N}[x_e(t)+v_e(t)], \tag{5}$$

where $x_e(t)$ is the stationary cycle dependent element, N is the number of elements, and $v_e(t)$ is the non-correlated stochastic process. Each stationary cycle dependent element $x_e(t)$ is correlated to the Earth's nutation cycles and will be accumulated in the total biomass. The disturbance element $v_e(t)$ is not correlated and will not be accumulated. The cyclic temperature cycle is then expected to influence the biomass maximum potential.

Biomass resonance between bio systems

The biomass has a mutual relation $S_B(t)=\{B_B(t),\ [S_P(t),\ S_F(t)]\}$ where $S_P(t)$ is the predator system, $S_F(t)$ is the food system, and $B_B(t)$ is a mutual binding between the systems. A mutual relation between systems is a feedback system. Such a system may have the frequency transfer function:

$$M_B(j\omega)=\frac{H_F(j\omega)\cdot e^{j\tau_S(t)\omega t}}{1+[H_F(j\omega)H_P(j\omega)]e^{j[\tau_F(t)+\tau_P(t)]\omega t}}, \tag{6}$$

where $H_F(j\omega)$ represents an energy transfer function of the food system, the $H_P(j\omega)$ transfer function of the predator system, $\tau_F(t)$ the phase delay in the food system, and $\tau_P(t)$ the phase delay in the predator system.

Such a dynamic will have the following important results:

(1) A forced temperature oscillator will synchronize a cycle response and introduce a set of sub-harmonic cycles in the biomass (*Forced oscillator*).
(2) The frequency transfer function (6) has a resonance property. This means there may be a biological stochastic resonance between the food system and the predator system. Such a resonance, will be tuned to the temperature cycle and this will amplify the fluctuation property. In this case we have a biological resonance when maximum biomass density is matching maximum recruit rate of 6–7 years (*Biological resonance*).
(3) The frequency transfer function (6) has a time-dependent phase property. This means the biological resonance is structurally unstable. Such a system may be chaotic and deterministic, but the same dynamic interactions between the food system and the predator system will never be repeated (*Structural stability*).

System dynamics of Northeast Arctic cod

The system dynamics of Northeast Arctic cod may be modelled by the discrete difference equation:

$$x_c(nT+T)=A_c(nT)\cdot x_c(nT)+u_c(nT)+v_c(nT)$$

$$y_c(nT)=D_c(T)\cdot x_c(nT)+w_c(nT), \quad (7)$$

where $x_c(nT)$ represents a year-class vector at the year n, T sample the time of one year, $A_c(nT)$ represents a time varying growth rate binding matrix on the autonomous system, $u_c(nT)$ represents the quota vector, $v_c(nT)$ represents a disturbance vector from an unknown source, $D_c(nT)$ is the measure matrix, $y_c(nT)$ is the measured state vector, and w(nT) is the measurement noise vector. A growth rate element $a_{ci}(nT)$ in the growth matrix $A_c(nT)$ at age index i is:

$$a_{ci}(nT)=x_{ci}(nT+T)/x_{ci}(nT), \quad (8)$$

The estimated number of cod at age 3 is $yn_{c3}(nT)$, the estimated biomass $y_{c3+}(nT)$ is the vector sum from age 3, and the spawn biomass $y_{c8+}(nT)$ is the vector sum from age 8.

According to this theory, the Earth's nutation of 18.6 years is introducing a set of harmonic temperature cycles in the Barents Sea (Yndestad, 1999), the temperature cycles are a forced oscillator that introduces biomass cycles and biological stochastic resonance in the Barents Sea. These cycles are expected to be reflected in the growth matrix $A_c(t)$ of Northeast Arctic cod.

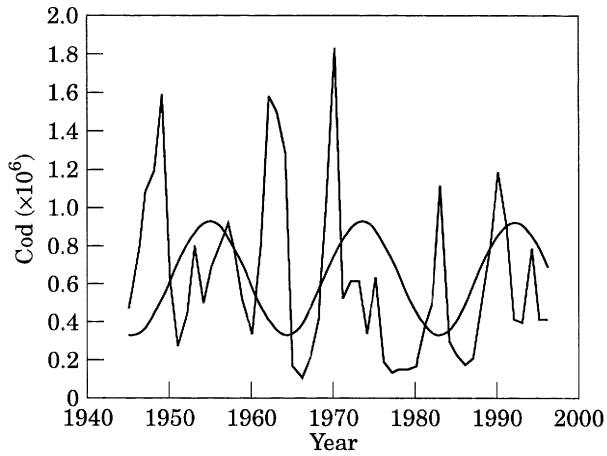

Figure 1. Time series of 3-year cod recruitment and the 18.6-year temperature cycle.

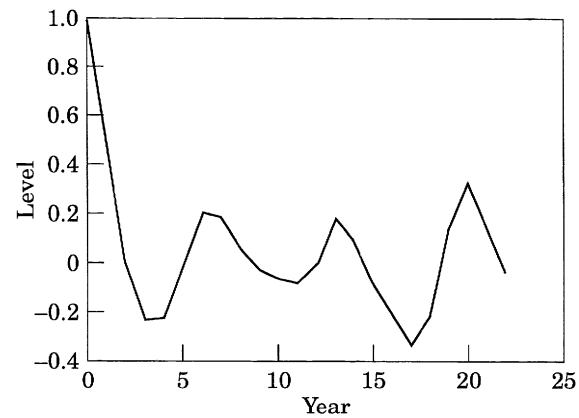

Figure 2. Autocorrelation of 3-year cod recruitment time series from 1945 to 1995.

Results

Identification of the Earth's nutation cycle

Figure 1 shows the time series $yn_{c3}(nT)$ of the number of 3-year Northeast Arctic cod since 1946 and the estimated 18.6 year temperature cycle in the Barents Sea (Yndestad, 1999). A visual inspection of Figure 1 indicates that the recruitment of 3-year cod has a low frequent component correlated in frequency and phase to the lower frequency temperature cycle of 18.6 years. This means that the growth matrix has a relation $A_c(t)=f(\omega_n)$ where $\omega_n=2\pi/18.6$ (rad yr^{-1}).

Figure 2 shows the autocorrelation function $R_{y3y3}(mT)$ of the recruitment $yn_{c3}(nT)$. The peaks in interval of about 6 years indicate a stationary cycle at about 6 years in the time series.

The cyclic properties may also be estimated by computing the auto power density spectrum. This

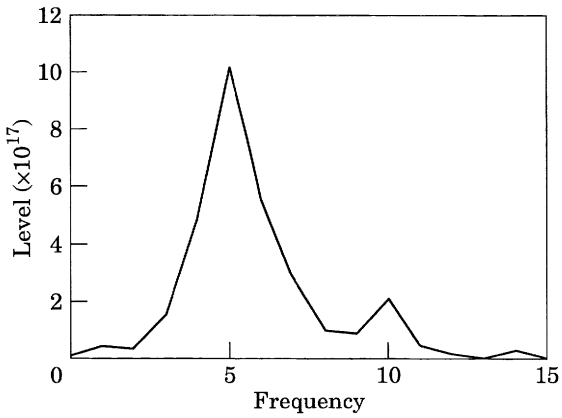

Figure 3. Power density spectrum of 3-year cod recruitment time series from 1946 to 1995.

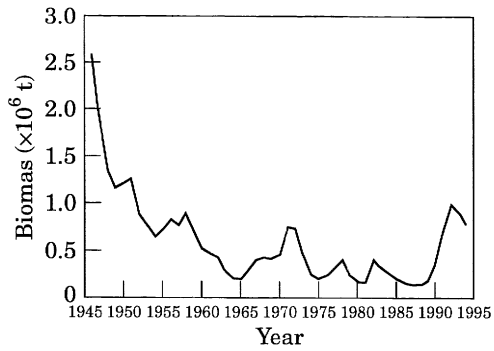

Figure 4. Spawning stock cod from 1946 to 1995.

spectrum is computed by the Fourier transform of the autocorrelation:

$$S_{y3y3}(k)=\sum_{n=0}^{N-1} R_{y3y3}(mT)\cdot e^{-jkmT/N}, \quad (9)$$

Figure 3 shows the power density spectrum windowed by 32 samples. Here there is a peak at the cycle $32/5\approx 6$ years. This is close to the temperature cycle of 6.2 years. This analysis indicates that there is a close correlation between the recruitment of Northeast Arctic cod and the temperature cycles of 6.2 years and 18.6 years. The growth matrix then has a property $A_c(t)=f(\omega_n, 3\omega_n)$.

Ottestad (1942) has investigated landings in Lofoten from 1875 to 1940. He found maximum cycles of Northeast Arctic cod in intervals of 11, 17.5, 23, and 57 years but did not find any explanations. These cycles may be explained by the harmonic growth cycles of 18.6/3=6.2, 18.6, and 3*18.6=55.8 years. The 57 year cycle is close to the 55.8 year cycle and the 17.5 year cycle from Otterstad is approximately the same as the 18.6 year cycle. Otterstad found cycles of 11 and 23 years which are both about 6 years from the 17.5 year cycle. The 11 and 23 year cycles are counted because the nutation harmonic cycles are additive by nature. The growth rate is then expected to be influenced by the sum of three stationary temperature cycles. This indicates that the growth matrix has the property $A_c(t)=f(3\omega_n, \omega_n, \omega_n/3)$. The growth rate of each elements in the growth matrix $A_c(t)$ is then expected to be influenced by the sum of three stationary temperature cycles plus a random disturbance from an unknown source. The total growth rate $a_{ci}(nT)$ at age index i may be expressed as:

$$a_{ci}(nT)=a_{cia}(nT)+a_{cin/3}(nT)+a_{cin}(nT)+a_{ci3n}(nT)+a_{civ}(nT), \quad (10)$$

where $a_{cia}(nT)$ is the average growth rate, $a_{cin/3}(nT)$ is the growth rate influenced by the 6.2 year cycle, $a_{cin}(nT)$ is the growth rate from the 18.6 year cycle, $a_{ci3n}(nT)$ is the growth rate from the 55.8 year cycle and $a_{civ}(nT)$ is a growth rate from an unknown source. The next step is to estimate some of these parameters.

Parameter identification

From known data (ICES, 1995) the growth rate $a_{cia}(nT)$ for each year class i=1.8 is estimated (3.33, 2.10, 1.95, 1.61, 1.55, 1.47, 1.35, 1.26.). The temperature dependent growth from the 6.2 year cycle $a_{cin/3}(nT)$ is estimated (4.00, 2.25, 2.33, 1.71, 1.56, 1.43, 1.35, 1.26). The parameters of $a_{cin}(nT)$ and $a_{ci3n}(nT)$ have not been estimated since there is a lack of data.

Figure 4 is the time series of the spawning stock biomass $y_{c8+}(nT)$ of cod from 1946 (ICES, 1995). The linear production rate $p_{ci}(nT)$ of cod may be defined as the relation between the number of first year cod and the spawning stock of cod biomass. This rate may be computed by:

$$p_{ci}(nT)=\frac{yn_{c1}(nT)}{y_{c8+}(nT)}, \quad (11)$$

where $y_{c8+}(nT)$ is the known spawning-stock biomass of cod. $yn_{c1}(nT)$ is the backward estimated recruited number of 1-year-old cod when $yn_{c3}(nT)$ and the mortality is known. In this case the discrete mortality rate M=0.2.

The result is shown in Figure 5. A constant production rate indicates a linear biomass-dependent recruitment. In this case there is a strong periodic fluctuation in the production rate. The fluctuation is correlated in frequency and phase to the 6.2 year temperature cycle. This supports the theory of the influence of the Earth's nutation and introduces a 6.2 year temperature cycle in the recruitment of North Arctic cod.

The system element $S_e(t)$ is a temperature dependent food chain. In the Barents Sea the system elements in the food chain are temperature dependent. Since there is an additive correlation (5), we may expect there is an

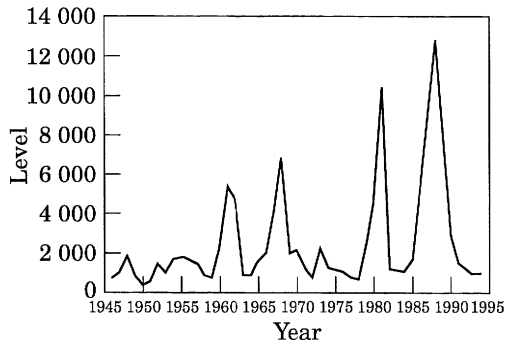

Figure 5. Linear production rate from 1946 to 1995.

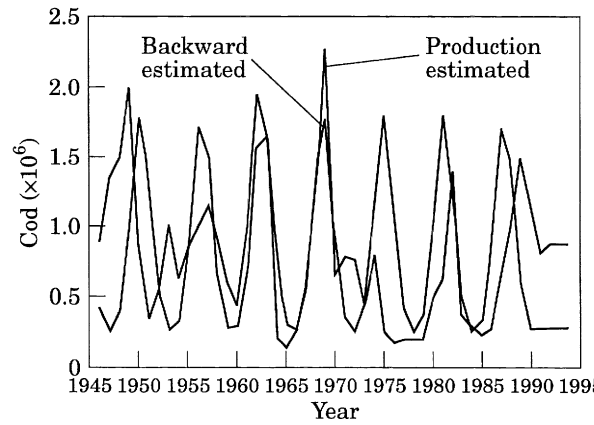

Figure 6. Backward estimated 1 year recruitment and forward estimated 1 year recruitment.

exponentially temperature-dependent recruitment in the biomass. Such a relation is expressed by the model

$$p(nT)=\bar{p}\cdot\exp[T_B(nT)], \tag{12}$$

where $T_B(nT)$ is an exponential relation to the nutation cycles of 6.2, 18.6, and 55.8 years and $\bar{p}$ is the mean production rate. The production rate is than estimated to the 6.2 year cycle. In this case:

$$\bar{p}=E[p(nT)]=1600 \text{ fry/ton spawn cod}, \tag{13}$$

and the relation to the 6.2 year temperature cycle is estimated to be:

$$T_{Bn/3}(nT)=-0.38+1.0\cdot\sin\left(\frac{3\cdot 2\cdot\pi}{18.6}nT+T\right), \tag{14}$$

where T is the sample time of 1 year and n is a number of years from the reference year 1900. Forward estimated recruitment of 1-year cod is estimated from known spawn biomass $y_{c8+}(nT)$ and known production rate. From (10) to (13) the forward estimated recruitment is:

$$yn_{c1f}(nT)=y_{c8+}(nT)\cdot\bar{p}\cdot\exp[T_{Bn/3}(nT)], \tag{15}$$

In this case only the 6.2-year cycle is used in the temperature binding $T_{Bn/3}(nT)$.

Figure 6 shows backward estimated, 1-year recruitment $yn_{c1}(nT)$ and forward estimated, 1 year recruitment $yn_{c1f}(nT)$. It shows a close correlation between the two estimates. If we introduce the temperature cycle of 18.6 years in the model the amplitude error will be further reduced. These estimates indicate that the recruitment is exponentially dependent on the temperature cycle and linearly dependent on the biomass.

Discussion

This paper shows that there is a correlation between the Earth's nutation and the time series of estimated annual stock recruitment of the Northeast Arctic cod. It supports the theory that the Earth's nutation of 18.6 years is introducing a set of harmonic and sub harmonic temperature cycles in the Barents Sea (Yndestad, 1999). The estimated temperature cycle of 18.6/3=6.2 years is correlated exponentially to the recruitment pattern. The temperature cycles of 3*18.6=55.8 years, 18.6 years, and 18.6/3=6.2 years are correlated to the growth rate. These estimates explain the time series of cod landing cycles in Lofoten from 1880 to 1940 (Otterstad, 1942). The 122 year cycle of herring (Rollefsen, 1949) may be explained by a sub-harmonic biomass cycle of 4*18.6=111.6 years periodicity. This theory will open a new perspective into forecasting short-time fluctuations of 6–7 years and long-time fluctuations of 50 years or more.

The cycles of biomass are explained by a General Systems theory, temperature cycles as a forced oscillator on the ecological system, and a biological stochastic resonance that will amplify the cod biomass fluctuations. According to this theory the temperature cycles first influence the food system of the Northeast Arctic cod. The food system will then influence exponentially the recruitment rate and the mortality fluctuates exponentially since recruitment and mortality are dual aspects of the same process. The growth rate is estimated to be linearly dependent on the temperature cycle. The biomass of cod has a maximum recruitment rate and a maximum density at 6–8 years of age. This means the biomass has a biological stochastic resonance close to the temperature cycle.

References

Ajiad, A. M., Mehl, S., Korsbrekke, K., Dolgov, A. V., Korzhev, V. A., Tretyak, V. L., and Yragina, N. A. 1992. Tropic relationships and feeding-dependent growth in the Northeast Arctic cod. Proceedings of the Fifth PINRO-IMR Symposium, Murmansk, August 1991. Institute of Marine Research, Bergen.

Currie, R. G. 1991. Deterministic signals in tree-rings from Tasmania, New Zealand and South Africa. Annual Geophysics, 9: 71–81.

Eilertsen, B., Fossum, P., and Sundby, S. 1989. Relation between temperatures and survival of eggs and first-feeding larvae of Northeast Arctic Cod (*Gadus morhua* L). Rapports et Procès-Verbaux des Réunions du Council International pour l'Exploration de la Mer, 191: 209–219.

Gabrielsen, G. W., and Rygg, M. 1992. Sjøfugl og sjøpattedyr. *In* Økosystem Barentshavet, pp. 203–229. Ed. by E. Sakshaug. Mesne Trykk, Lillehammer, Norway (in Norwegian).

Haug, T., Krøyer, A. B., Nilssen, K. T., Ugland, K. T. I., and Aspholm, P. E. 1991. Harp seal (*Phoca groenlandica*) invasions in Norwegian costal waters, composition and feeding habits. ICES Journal of Marine Science, 48: 363–371.

ICES 1995. Report of the arctic fisheries working group. ICES Headquarters. Copenhagen. Denmark.

Jørgensen, T. 1992. Long-term changes in growth of Northeast Arctic cod (*Gadus morua*) and some environmental influences. ICES Journal of Marine Science, 49: 263–277.

Nakken, O., and Raknes, A. 1987. The distribution and growth of Northeast Arctic cod in relation to bottom temperatures in the Barents Sea in the period 1977–1984. ICES CM 1984/G:20.

Nakken, O. 1994. Causes of trends and fluctuations in the Arcto-Norwegian cod stock. ICES Marine Science Symposium, 198: 212–228.

NIMR 1995. Norwegian Institute of Marine Research. Ressursoversikt. Bergen. Norway.

Ottestad, P. 1942. On periodical variations on the yield on the great sea fisheries and the possibility of establishing yield prognoses. Fiskeridirektoratets Skrifter. Vol, VII. No 5. Bergen. Norway.

Ottersen, G., Michalsen, K., and Nakken, O. 1996. Ambient temperature and distibution of Northeast Arctic cod. ICES, Annual Science Conference. Reykjavik, Iceland, 27 September–4 October 1996.

Rollefsen, G., and Strøm, J. 1949. Norsk Fiskeri og Fangst Handbook. Bind 1. Alb. Cammermeyers Forlag. Oslo.

Sætersdal, K., and Loeng, H. 1987. Ecological adaption of reproduction in Northeast Arctic cod. Fisheries Research, 5: 253–270.

Wyatt, T., Currie, R. G., and Larraneta, M. G. 1992. Codstock recruitment problems, the nodal tide and sunspot cycles. ICES CM 192/L:17.

Wyatt, T., Currie, R. G., and Saborido-Ray, F. 1994. Deterministic signals in Norwegian cod records. ICES Marine Science Symposium, 198: 49–55.

Yndestad, H. 1996a. Stationary Temperature Cycles in the Barents Sea. The cause of causes. The 84'th international ICES Annual Science Conference. Hydrography Committee. Reykjavik, Iceland, 27 September–4 October 1996.

Yndestad, H. 1996b. Systems Dynamics of North Arctic Cod. The 84th international ICES Annual Science Conference. Hydrography Committee. Reykjavik, Iceland, 27 September–4 October 1996.

Yndestad, H. 1999. Earth Nutation Influence on the Temperature in the Barents Sea. ICES Journal of Marine Science, 56: 381–387.

Paper III

ICES Journal of Marine Science, 58: 799–805. 2001
doi:10.1006/jmsc.2000.1070, available online at http://www.idealibrary.com on IDEAL®

Earth nutation influence on Northeast Arctic cod management

H. Yndestad

Yndestad, H. 2001. Earth nutation influence on Northeast Arctic cod management. – ICES Journal of Marine Science, 58: 799–805.

Northeast Arctic cod in the Barents Sea is the largest stock of *Gadus morhua* cod in the world. The cod biomass seems to have stationary cycles related to the Earth's nutation. The present paper suggests that current management strategy has three aspects that may introduce an instability in the biomass. The first is the 6–7 year positive feedback of recruitment in combination with a phase-delay in estimating data and getting the next quota of landings. The second is that the biomass has no stationary biomass reference in the control strategy and the third is the change in the rate of landings each year. Simulations demonstrate that the biomass needs a 15–20 year planning perspective and it is suggested that the spawning-stock biomass level is managed by a feedback control and the fluctuations of landings by a feed-forward control.

Keywords: Northeast Arctic cod, management, biomass stability, forecasting.

Received 17 May 1999; accepted 28 December 2000; published electronically on 11 June 2001.

Harald Yndestad: Aalesund University College, Box N-5104 Larsgaarden, 6021 Aalesund, Norway. Tel: +47 70 16 12 00; fax: +47 70 16 13 00; e-mail: harald.yndestad@hials.no

Introduction

Northeast Arctic cod is the largest stock of *Gadus morhua* cod in the world. The fishery of this stock is located along the northern coast of Norway and in the Barents Sea. For centuries it has been the most important economic biomass for Norwegian fishermen and of vital importance for settlement and economic growth in the western part of Norway. The biomass of Northeast Arctic cod has always fluctuated and there have been several theories on the causes of these fluctuations. One is the relationship between the sea temperature and cod recruitment (Sætersdal and Loeng, 1987; Nakken and Raknes, 1987; Eilertsen *et al.*, 1989; Nakken, 1994; Ottersen *et al.*, 1996; Yndestad, 1996). Another is the impact of predators like birds, marine animals and cannibalism (Haug *et al.*, 1991; Gabrielsen and Rygg, 1992) and a third is the amount of food available in a given year (Ajiad *et al.*, 1992). Other explanations can be found in Jacobsen *et al.* (1994), and Pennington (1999).

Figure 1 shows the time-series of the total biomass, spawning-stock biomass and landings of Northeast Arctic cod from 1950–1998. In the 25 year period from 1950–1975 the total biomass decreased from about 310 000 tons to about 250 000 tons and the biomass fluctuated about 1 000 000 tons and the landings were about 800 000 tons in 1974. Over the next ten years there was a collapse with the biomass decreasing to about 66 000 tons and the landings to 27 000 tons in 1984. To save the biomass the Norwegian government started quota regulation in 1984–1985 based on scientific advice from ICES. In the period from 1983 there was growth of the biomass and, as a result, a new trawler fleet was built in Norway and the quota increased to 520 000 tons in 1987. However the increase in biomass and quota was temporary and in 1990 the quota was down to 210 000 tons. In the period 1990–1993 the biomass again grew to about 2 300 000 tons and the landings to about 770 000 tons in 1994. A quota of 770 000 tons was too much and in 1998 there were indications of a serious reduction of the biomass. Again the quota of landing was reduced to 480 000 tons and as a first step of further quota reductions.

This paper focuses on how current management policies influence the Northeast Arctic cod resource. The Earth's nutation is introducing a stationary temperature cycle in the Barents Sea (Yndestad, 1999a) causing cycles of varying recruitment and growth of Northeast Arctic cod (Wyatt *et al.*, 1994; Yndestad, 1996; Yndestad, 1999b). The current management method does not take account of these fluctuations and introduces an instability in the biomass dynamics. It is suggested that the spawning-stock biomass should be stabilised by a feedback control and the landings dynamics by a feed-forward control.

1054–3139/01/040799+07 $35.00/0

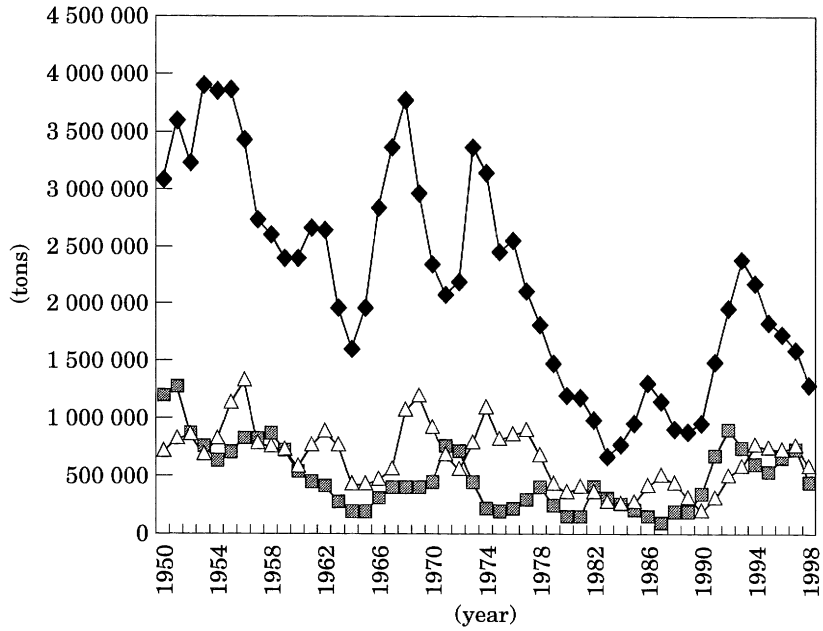

Figure 1. History (1950–1998) of total biomass stock, spawning stock biomass and the official "quota" of landings. —◆—, total stock; —□—, spawning stock; —△—, official quota.

Materials and methods

All history time-series on Northeast Arctic Cod are based on the ICES Report of Arctic Fisheries (ICES, 1999). The biomass time-series from 1999–2020 are forecast by the author and based on a temperature-dependent growth and recruitment model (Yndestad, 1999b).

Systems theory

The biomass of Northeast Arctic cod is related to a complex food chain system. Systems theory is a theory of understanding complex organisations independent of time and space (Lin, 1999). In this case the Barents Sea may have the general system architecture:

$$S_B(t)=\{B_B(t),\ \{S_T(t),\ S_C(t),\ S_L(t),\ S_F(t)\}\}w \qquad (1)$$

where $S_T(t)$ is the temperature system, $S_C(t)$ is a cod biomass system, $S_L(t)$ is a landings system, $S_F(t)$ is a food system, $B_B(t)$ is the interaction or the binding between the Barents Sea systems and w is the common purpose. According to Equation (1) general systems are time varying, structurally unstable and mutually state dependent. Management of Northeast Arctic cod must be based on a fundamental understanding of the system dynamic of the biomass system $S_C(t)$ and the influence of bindings to other systems.

A dynamic biomass system is described by a set of first order differential equations:

$$\dot{x}(t)=f(x(t),u(t),v(t),t)$$

$$y(t)=g(x(t),w(t),t) \qquad (2)$$

where x(t) represents the biomass-age vector, u(t) a landing-state age vector, v(t) a disturbance-age vector from an unknown source and the w(t) is the error-measurement-age vector. A linear time variant dynamic system of the biomass $S_C(t)$ and landings $S_L(t)$ of Northeast Arctic cod may be modelled by the state space equation:

$$\dot{x}(t)=A(t)\cdot x(t)+v(t)$$

$$y(t)=D\cdot x(t-\tau)+w(t) \qquad (3)$$

where D is the measurement matrix and τ is the estimate delay. Comparing statements from people fishing in the Barents Sea and published biomass data (ICES, 1999), it is estimated that the phase delay τ is about 2–3 yr. The disturbance v(t) and the estimate error w(t) are unknown (ICES, 1999). Comparing data from a growth model (Yndestad, 1999b) and published data (ICES, 1999) the author has estimated v(t)+w(t) to be more than $\pm$ 30% of the published biomass data y(t). The autonomous system growth matrix $A(t)=A_r(t)+A_g(t)+A_m(t)$ where $A_r(t)$ represents the recruitment matrix, $A_g(t)$ the growth matrix and $A_m(t)$ the mortality matrix.

The system matrix A(t) has a temperature-dependent, stationary disturbance related to the Earth's nutation (Yndestad, 1999a, 1999b) or $A(t)=f(3\omega_n,\ 3\omega_n,\ \omega_n/3)$

where $\omega_n = 2\pi/18.6$ (rad/yr) is the Earth nutation angle frequency. The angle frequency of $3\omega_n$ will introduce a biomass fluctuation of 6.2 yr, ω_n will introduce a fluctuation of 18.6 yr and $\omega_n/3$ will introduce a fluctuation of 55.8 yr. The biomass x(t) then is a time-variant, stochastic process that has no stationary state, no stationary mean value, no stationary limit values, no stationary sustainability reference level, no stationary maximum or minimum reference level and no stationary optimum management level. This dynamic property will influence how the biomass has to be managed. The main task of a proper management is to optimize quota of landings and at the same time keep a sustainable biomass. Such a policy depends on having good biomass estimates and a fundamental understanding of the biomass dynamics.

Current management

Current management of Northeast Arctic cod is based on the control strategy:

$$u(t) = -F(t) \cdot y(t) \tag{4}$$

where u(t) is the quota of landings vector and F(t) is the continuous landings' rate. This control strategy changes the landings' rate F(t) each year. Future estimate of the biomass is than only predictable from one year to the next. The biomass shift from one year to the next is computed from equation (3):

$$x(t_1) = e^{A(t_0)T}x(t_0) + \int_{t_0}^{t_1} e^{A(t_0)(t_1-\tau)} \cdot u(t_0)d\tau$$
$$\approx [I + A(t_0)]Tx(t_0) + Tu(t_0) \tag{5}$$

where $v(t) = 0$, a one year time interval $T = t_1 - t_0$ and I is an identity matrix. Equation (5) describes how this control strategy influences the biomass dynamics. The control of the biomass is based on choosing a proper quota of landing $u(t_0)$ that moves the biomass to the wanted state $x(t_1)$. There are some fundamental problems related to this control strategy viz.:

(1) The growth matrix A(t) has time-variant, stationary cycles of 6.2 yr, 18.6 yr and 55.8 yr because of the Earth's nutation influence on the Barents Sea temperature. Estimates of the growth matrix will than change each year and biomass dynamics will introduce errors in the estimated data.
(2) The estimate delay τ of 2–3 yr will introduce a phase error in the estimate. A combination of the phase error τ and the stationary cycle of about 6 yr in the growth matrix A(t) will introduce an instability in the biomass.
(3) The quota of landings is changed each year. When the landings rate F(t) is changed faster than the growth rate dynamics of A(t), the future state of the biomass is not predictable.
(4) The control strategy has no long-term strategy that moves the biomass x(t) to a desired level and the biomass will have a low frequency instability.

This means that the current control strategy will introduce three different types of instabilities that sooner or later may lead to a collapse of the biomass.

The same properties may be studied from the system frequency transfer function. A Laplace transform of (3) and (4) gives us:

$$x(t) = [sI - A(t_0)]^{-1} \cdot [u(s) + v(s)] \tag{6}$$

$$y(s) = D \cdot e^{-\tau s} \cdot x(s) + w(s)$$

$$u(s) = -F(t_0) \cdot y(s) \tag{7}$$

where $s = j\omega$ (rad/yr). Equation (6) may be reduced to (7)

$$x(s) = H(s)^{-1}\,[v(s) - F(t_0)w(s)] \tag{8}$$

where

$$H(s) = [sI - A(t_0) + F(t_0)\,De^{-\tau s}]$$

Equation (8) shows that the estimated biomass dynamic y(s) is only driven by the disturbance v(s) and the error estimate w(s) and the biomass will not be stabilised at any level. In other words there is no long-term reference control and the biomass may collapse. A second observation of Equation (8) is that the biomass may be unstable when $|H(s)| = I$ and the phase delay $\angle H(s) = -\pi$.

Constant landings rate

The high frequent instability may be reduced when selecting a stationary landings' rate $F(t) = F(t_0)$. In this case Equations (3) and (5) is reduced to:

$$\dot{x}(t) = [A(t_0) - F(t_0) \cdot D]x(t) \tag{9}$$

when $v(t) = 0$. Equation (9) has the general solution:

$$x(t) = e^{[A(t_0) - F(t_0) \cdot D](t - t_0)}x(t_0) \tag{10}$$

and describes how a stationary landings' rate influences the biomass dynamics. In this case the control strategy is based on choosing a proper landings' rate F(t) that in the long run optimises the landings' quota and, at the same time, maintains a sustainable biomass. This control strategy still has some problems. The first is that the

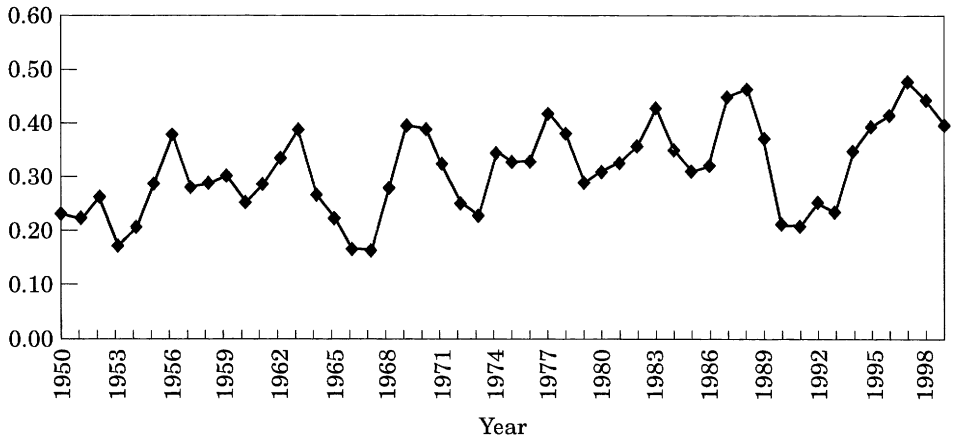

Figure 2. History of the current landings' rate from 1950–1998.

landings' rate $F(t_0)$ influences the total biomass growth rate and the sustainable level. Hence it may take many years to estimate the influence of the landings' rate. A second problem is that the growth rate $A(t_0)$ has a stationary low frequency cycle of 18.6 yr. This will influence the growth rate, the sustainable reference level and the optimum management level. The landings' rate $F(t_0)$ will than have to be modified after some years. When the landings' rate $F(t_0)$ is modified to optimise the landings' quota, it is easy to introduce a low frequency instability in the biomass.

Feedback control

The spawning-stock biomass may be controlled by a feedback control strategy:

$$\dot{x}(t)=A\cdot x(t)+u(t)+v(t)$$

$$y(t)=D\cdot x(t)+w(t) \qquad (11)$$

$$u(t)=H_R[r(t)-y_s(t)]$$

where r(t) is the required spawning-stock biomass level, $y_s(t)$ the estimated spawning stock and H_R is a control parameter and u(t) is the quota of landings. According to this control strategy, the biomass is controlled by the difference between the reference level r(t) and the estimated spawning-stock biomass $y_s(t)$. The Laplace transformation of a dynamic system has information on the frequency property when $s=j\omega$ (rad/yr). In this case the Laplace transform of Equation (11) is:

$$x(s)=[sI-A(t_0)]^{-1}u(s)+[sI-A(t_0)]^{-1}v(s)$$

$$y(s)=D\cdot x(s)+w(s) \qquad (12)$$

$$u(s)=H_R[r(s)-y_s(s)]$$

from (12) we have the frequency response:

$$y_s(s)=(sI+DH(s)H_R)^{-1}\,DH(s)H_R r(s)$$

$$+(sI+DH(s)H_R)^{-1}\,DH(s)v(s)$$
$$+(sI+DH(s)H_R)^{-1}\,w(s) \qquad (13)$$

that may be reduced to

$$y_s(s)\approx r(s)+(I+DH(s)H_R)^{-1}$$
$$DH(s)v(s)+(I+DH(s)H_R)^{-1}\,w(s) \qquad (14)$$

According to Equation (14) the estimated state $y_s(s)$ will converge to the reference level r(s) and the influence from the disturbance spectrum v(s) and measurement spectrum w(s) is reduced.

Results

During the past 50 years the biomass has varied between 1×10^6 and 4×10^6 tons. In this biomass interval the growth rate is changing between 1.5 and 1.2 and the mean discrete growth rate is estimated to be about 1.3. This means that the sustainable level of the biomass is dependent on the present biomass level but in the long run the biomass has been sustainable when the discrete landing rate $F(nT)<0.3$.

Figure 2 shows the history of the current landings rate,

$$F(nT)=\frac{u(nT)}{y_{3+}(nT)} \qquad (15)$$

from 1950–1998 where u(nT) is the quota of landings at the year n and $y_{3+}(nT)$ is the ICES estimated total biomass at the year n. In this time series the discrete landings' rate F(nT) has the range from 0.18–0.49 and the mean landings rate $E[F(nT)]=0.3$. The F(nT) time-series demonstrates the low frequency and high instability of the biomass dynamics. The landings' rate has been

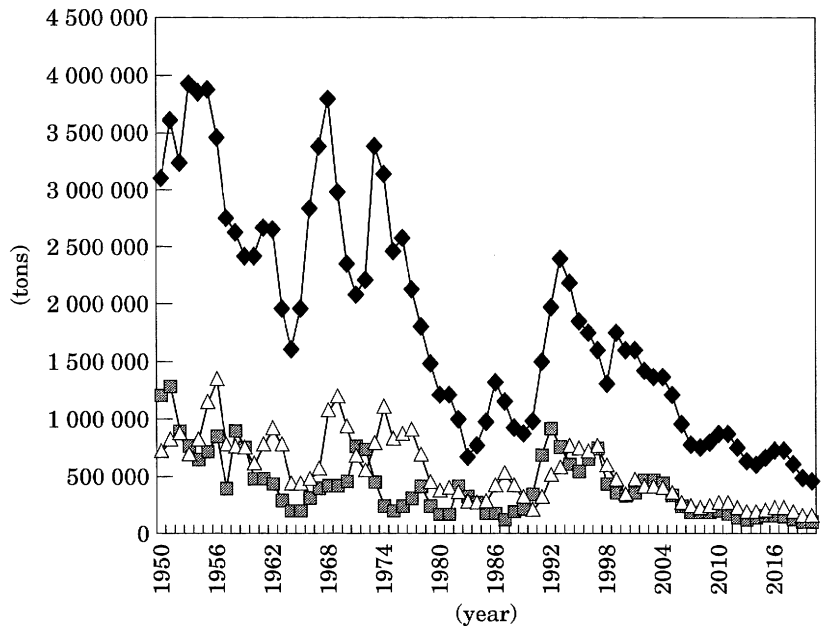

Figure 3. History (1950–1998) and forecast (1999–2020) total biomass stock, spawning-stock biomass and landings when landings' rate constant F(nT)=0.25. —◆—, total stock biomass; —□—, spawning stock biomass; —△—, official quota.

growing over a period of 40 years. Most of this time the landing quotas were too high to maintain a sustainable biomass and in 1987 and in 1996 the landing rate was about 0.5 and caused a collapse in the biomass. A spectrum analysis of the time-series shows that the landings rate F(nT) has a cycle of about 6 yr. This indicates both a low and a high frequency instability in the biomass dynamics.

Constant landings' rate

Figure 3 shows the time-series of historical records of total biomass, spawning-stock biomass and landings in millions of tons over the period 1950–1998. The time-series from 1999–2020 is a modelled forecast based on a constant landings' rate F(nT)=0.25, a discrete mortality rate M(nT)=0.22 and a temperature-dependent, discrete growth rate A(nT). The temperature-dependent recruitment $x_1(t)$ is estimated by the recruitment model (Yndestad, 1999b).

$$x_1(nT)=p_m+p\cdot y_{8+}(nT)\cdot\exp\{k_0+k_1\sin(6.28n/6.2+\varphi_1)+k_2\sin(6.28n/18.6+\varphi_2)\} \quad (16)$$

where the year number n=1950–2020, the minimum recruitment p_m=20 000 cod, the mean linear recruitment rate p=4000 number of cod/spawn biomass, the nutation amplitude relations $k_0=-0.7$, $k_1=0.60$, $k_2=0.3$, the nutation phase relation $\varphi_1=-3.5$, $\varphi_1=1.0$ (Yndestad, 1999b). The spawning-stock biomass is estimated by the proportion mature vector [0,00 0,00 0,00 0,02 0,07 0,23 0,48 0,92 0,98 1,00 1,00 1,00 1,00 1,00] (ICES, 1999).

Figure 3 shows that the biomass is reduced exponentially as expected by Equation (10). In a period of about 20 years the total biomass will converge at about 500 000 tons, the spawning stock biomass at about 100 000 tons and the landings at about 90 000 tons. In this case the 6.2 yr cycle in the growth and recruitment will introduce some small fluctuations in the total biomass. If the landings' rate F(nT) is changed each year forecasting cannot be made on a realistic basis. If the landings' rate F(nT)=0.25 the biomass will grow exponentially to about 1 500 000 tons, the spawning-stock biomass to 400 000 tons and the landings to 400 000 tons.

Feedback control

An FAO white paper (FAO, 1993) suggests that the minimum spawning-stock biomass should be more than 500 000 tons. Figure 4 shows the time-series of historical records of total biomass, spawning biomass and landings over the period 1950–1998. The time-series from 1999–2020 is forecast from the model. The forecast biomass is estimated assuming feedback control strategy, the control parameter $H_R=1$ and the spawning stock biomass reference level r(nT)= 600 000 tons. In this forecast the biomass will converge to about 2 700 000 tons and the spawning biomass to about 600 000 tons as expected.

The fundamental approach on the feedback control strategy is that the spawning stock biomass has a fixed reference level r(nT) and landings quota u(nT) is the difference between the reference level and the estimated spawning stock biomass of the measured spawning stock biomass $y_{8+}(nT)$.

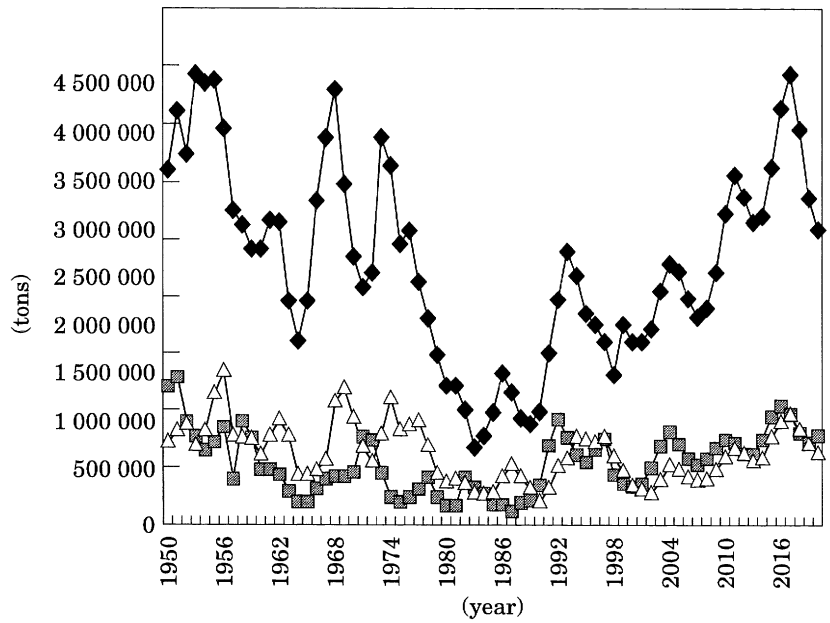

Figure 4. History (1950–1998) and forecast (1999–2020) total biomass, spawning-stock biomass and landings by feedback control. —◆—, total stock biomass; —□—, spawning stock biomass; —△—, official quota.

The forecast illustrates the sensitivity of the biomass to the quota strategy. The control strategy will force the spawning stock biomass to remain at a level of about 600 000 tons and the total biomass will grow to about 3 000 000 tons over the next 20 years. The biomass has a disturbance cycle of 18.6 yr and the time to reach a maximum level is about 20 years. This means that the total planning time of the total biomass should be about 15–20 years. The stochastic resonance at 6–7 yr will still introduce fluctuations in the biomass. This fluctuation is balanced by fluctuations in quota of landings. In this forecast the landings will converge to about 500 000 tons and fluctuate ± 100 000 tons at a cycle of 6.2 yr.

People dependent on fishing for their living need stability and predictability. There are methods to reduce the fluctuations of landings. One method is to introduce an integration $H_R(s)=k/(s+a)$ in the control law of Equation (12). This introduces a phase delay between fluctuations in the biomass and fluctuation in the landings. A second method is to introduce feed-forward control (Phillips *et al.*, 1989). This method will not introduce phase errors. On the other hand, it requires a good future estimate of the biomass. A third method is to optimise landings and the biomass by the object function:

$$J=\int_0^t (x(t)Px(t)+u(t)Qu(t)+\dot{u}(t)R\dot{u}(t)dt \qquad (17)$$

where P, Q and R are chosen cost indexes. By this method the biomass is managed by a chosen compromise between biomass size, the landings' quota and changes in that quota.

Discussion

The fluctuations of Northeast Arctic cod seem to be influenced by a more fundamental source than temperature, predators, cannibalism, quota estimates and assessment methods. The biomass fluctuation is correlated to stationary fluctuations of 6–7 yr, 18.6 yr and 55.8 yr. This fluctuation is a deterministic and time varying dynamic process that changes the stochastic biomass properties each year. The fluctuations of the biomass have influenced the landing's quota and during the last 50 years the landings have varied between 20% and 50% of the biomass.

Current management strategy has three aspects that may introduce instability in the biomass. The first is the 6–7 yr positive feedback of recruitment in combination with a phase delay in estimating data and getting the next landings' quota. This will introduce a high frequency instability of about 6–7 yr. The second is the biomass which has no stationary reference in the control strategy. This will introduce a low frequency instability in the biomass. The third source of instability is the change of landings' rate each year. This will lead to unpredictability of the biomass dynamics.

To control the biomass dynamics, a long-term strategy for mananging the spawning-stock biomass is needed. In this paper the forecasted biomass indicates that management of the total biomass needs to take into account a period of 15–20 years. Dynamic systems are controlled by the feedback concept. Such a concept will stabilise the spawning-stock biomass, reduce the long-term, temperature-dependent fluctuations and reduce

uncertainty in expensive stock assessment exercises. This paper demonstrates that the feedback concept can maintain the spawning-stock biomass level at 600 000 tons. The feedback control is too slow to control the more higher frequency 6.2 yr cycle. This cycle is then reflected in the landing's quota and may be suppressed by introducing a feed-forward control from the forecasted biomass.

References

Ajiad, A. M., Mehl, S., Korsbrekke, K., Dolgov, A. V., Korzhev, V. A., Tretyak, V. L., and Yragina, N. A. 1992. Tropic relationships and feeding-dependent growth in the Northeast Arctic cod. Proceedings Fifth PINRO-IMR Symposium, Murmansk, August 1991. Institute of Marine Research, Bergen.

Eilertsen, B., Fossum, P., Solemdal, P., and Sundby, S. 1989. Relation between temperature and survival of eggs and first feedind larvae of Northeast Arctic cod (Gadus morhua L.). Rapports et Procès-Verbaux des Réunions du Conseil International pour l'Exploration de la mer, 191: 209–219.

FAO 1993. Reference points for fishery management. Their potential application to straddling and highly migratory resources. FAO Fisheries Circular No. 864, Firm/ C864, Rome.

Gabrielsen, G. W., and Rygg, M. 1992. Sjøfugl og sjøpattedyr. *In* Økosystem Barentshavet, pp. 203–229. Ed. by E. Sakshaug. Mesne Trykk, Lillehammer, Norway. (in Norwegian).

Haug, T., Krøyer, A. B., Nilssen, K. T., Ugland, K, T. I., and Aspholm, P. E. 1991. Harp seal (Phoca groenlandica) invasions in Norwegian coastal waters: composition and feeding habits. ICES Journal of Marine Science, 48: 363–371.

ICES 1999. Report of the Arctic fisheries. ICES CM 2000/ACF M3. 23 August–1 September 1999. ICES Headquarters. Copenhagen, Denmark.

Jacobsen, T., Sunnanå, K., and Bogstad, B. 1994. Forvaltning av Norsk-Arktisk torsk. Havforskningsnytt. nr 19 (in Norvegian).

Lin, Yi. 1999. General Systems Theory. A Mathematical Approach. IFSR International Series on Systems Science and Engineering. Volume 12. Plenumm Publishers, New York.

Nakken, O. 1994. Causes of trends and fluctuations in the Arto-Norwegian cod stock. ICES Marine Science Symposium, 198: 212–228.

Nakken, O., and Raknes, A. 1987. The distribution and growth of Northeast Arctic cod in relation to bottom temperatures in the Barents Sea in the period 1977–1984. ICES: CM 1984/G. 20.

Ottersen, G., Michalsen, K., and Nakken, O. 1996. Ambient temperature and distibution of northeast Arctic cod. ICES, Annual Science Conference. Reykjavik, Iceland, 27 Sep–4 Oct 1996.

Pennington, M. 1999. Report of the workshop on comparision of stof assessment model strategies, with application to Northeast Arctic cod. IMR. Bergen. Norway.

Phillips, C. L., and Harbor, R. D. 1989. Feedback Control Systems. Prentice-Hall International (UK) Limited, London.

Sætersdal, K., and Loeng, H. 1987. Ecological adaption of reproduction in Northeast Arctic cod. Fisheries Resesarch, 5: 253–270.

Wyatt, T., Currie, R. G., and Saborido-Ray, F. 1994. Deterministic signals in Norwegian cod records. ICES Marine Science Symposium, 198: 49–55.

Yndestad, H. 1996. Systems Dynamics of North Arctic Cod. The 84th international ICES Annual Science Conference. Hydrography Committee. Reykjavik, Iceland, 27 Sep–4 Oct 1996.

Yndestad, H. 1999a. Earth Nutation Influence on the Temperature in the Barents Sea. ICES Journal of Marine Science, 56: 381–387.

Yndestad, H. 1999b. Earth Nutation Influence on System dynamics of Northeast Arctic cod. ICES Journal of Marine Science, 56: 652–657.

Paper IV

ICES Journal of Marine Science, 59: 1155–1166. 2002
doi:10.1006/jmsc.2002.1285, available online at http://www.idealibrary.com on IDEAL®

System dynamics of the Barents Sea capelin

Harald Yndestad and Anne Stene

Yndestad, H., and Stene, A. 2002. System dynamics of the Barents Sea capelin. – ICES Journal of Marine Science, 59: 1155–1166.

The capelin (*Mallotus villosus*) in the Barents Sea plays a key role in the Arctic food web. The large fluctuations in the biomass of the Barents Sea capelin have been poorly understood and collapses in the biomass have occurred. A system analysis of the capelin stock has identified a state differential equation model and a frequency transfer function model of the stock properties. The results of this research show that the capelin stock dynamics is adapted to the 18.6 year and the 18.6/3=6.2 year lunar nodal tide that influences the temperature in the Barents Sea. An analysis of the capelin time series has identified a 6.2 yr cycle of recruitment, maturity and fish stock growth. An estimated frequency response of a stock-number, life-cycle model has identified a stochastic resonance of about half of the 6.2 yr cycle. The stochastic resonance shows that fluctuation of the stock number is a natural adaptation to the environment and a strategy for optimal growth and survival in the long run. In this stochastic resonance timing between the stock number fluctuation and the 6.2 yr cycle is most important.

Keywords: capelin ecology, capelin model, capelin management, stochastic resonance, 18.6 yr lunar nodal tide.

Received 30 August 2001; accepted 15 May 2002.

H. Yndestad: Aalesund University College, N-6025 Aalesund, Norway; tel: +47 70 16 12 00; fax: +47 70 16 13 00; e-mail: Harald.Yndestad@hials.no

Introduction

The capelin (*Mallotus villosus*) has a northerly circumpolar distribution. In the Atlantic the capelin is located in the Barents Sea (ICES areas I and IIa), Iceland, Greenland, Labrador and Newfoundland. The capelin stock in the Barents Sea is the largest in the world and has maintained a fishery with annual catches of up to 3 million tons.

The capelin stock is of vital importance in the Arctic food web. It is the main plankton feeder in the area and serves as an important forage fish for other fish stocks, seals, whales and sea birds. The capelin is therefore influenced by its abiotic environment and by the abundance of food, predators, and fisheries.

Because of high spawning-mortality, the capelin stock consists of only a few year classes. With only 5 cohorts and a fishery that influences most of the age groups, reliable estimates of year class strength are indispensable. The abundance of capelin in the Barents Sea is monitored annually by a larval survey, a 0-group survey and an acoustic survey on individuals older than 1 year. The Barents Sea capelin stock has had large fluctuations, with collapses in the biomass around 1985 and 1993 (Figure 1). A question to be answered is whether these collapses are due to natural dynamics in the stock and the environment or due to a "fishery management" problem, or both.

Variations in the biomass of any fish stock are dependent first on the environmental temperature and second on the thermal regulation of the individuals. Fluctuations in temperature will affect the stock characteristics directly through effects on growth and recruitment, or indirectly through the variability of food and predators.

The environmental conditions in the Barents Sea are influenced by three water masses: Coastal Water in the south, North Atlantic Water extending over the western and central parts and the Arctic Water flowing in from northeast. The temperature is therefore partly determined by the flux and the temperature of the different water masses in the area.

Climate variations may have a predictable fluctuation caused by the 18.6 yr and the 6.2 yr lunar nodal tide (Pugh, 1996; Keeling and Whorf, 1997). The oceanic response to this nodal tide is documented by Maksimov and Smirnov (1965); Royer (1989, 1993). A correlation between the 18.6 yr lunar nodal tide and the temperature

1054–3139/02/061155+12 $35.00/0

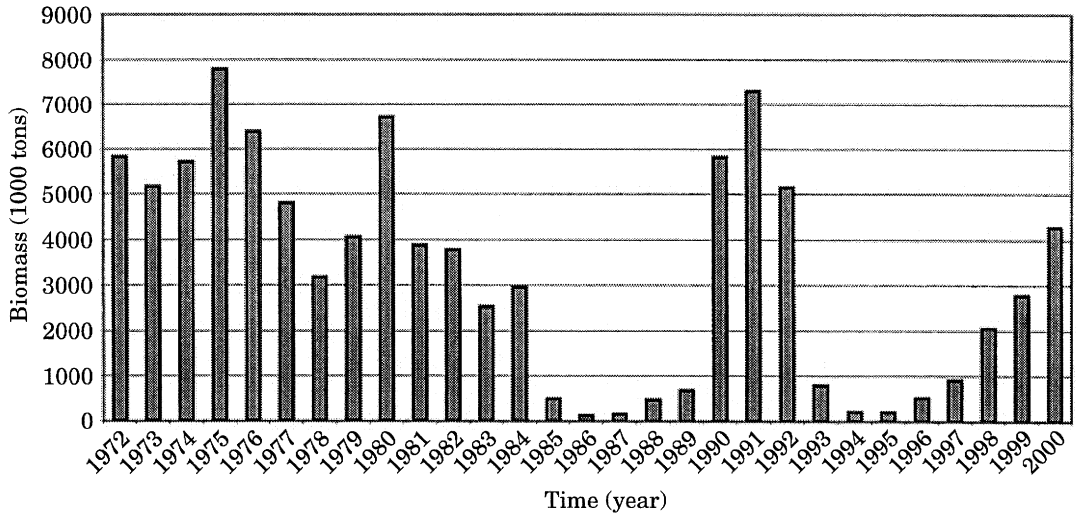

Figure 1. Time series of Barents Sea capelin biomass 1972–2000 (ICES, 2001b).

in the Barents Sea is also reported (Yndestad, 1999a). In addition, the fluctuations in North Atlantic fish species have been related to the 18.6 yr lunar nodal tide (Wyatt, 1984; Wyatt *et al.* 1994; Yndestad, 1996, 1999b).

The aim of this study is to identify some basic system dynamic properties of the capelin stock related to growth, maturity, recruitment, and the response to environmental condition. The importance of temperature fluctuations, in particular, has been considered when the time series of the capelin stock is analysed. The results show that stock dynamics i.e. recruitment, maturity and growth, are adapted to the 6.2 yr temperature cycle, influencing the temperature and the food chain in the Barents Sea. This cycle has a stationary frequency since it is driven by the lunar nodal tide.

Materials and methods

Materials

Official monitoring of the Barents Sea capelin started in 1972 by ICES. Biomass, number, growth, maturity and recruitment are used as parameters in this capelin model for identification of the stock dynamics. Registration of growth and recruitment dates back to 1972 while registrations of maturity started in 1988. ICES has capelin-stock time series from surveys in January, April, August and October (ICES, 2001a). In this investigation the October time series is used.

Zooplankton abundance was used as a parameter to find a possible connection between the capelin stock and the Barents Sea food system. The ICES data set of zooplankton in the Barents Sea started in 1987. The Barents Sea zooplankton is measured from "multi-species" region 2 to 8. The biomass of this plankton is the sum of the following size fractions: 180–1000 μm, 1000–2000 μm, and >2000 μm. The samples covers the total water column from bottom to surface (ICES, 2001a). There are no registrations from region 2, 3, 4, 6 and 8 in 1988 and from region 6 in 1989.

Reliable time series on stock characteristics are obtainable for commercial fish species. Since young Northeast Arctic cod (*Gadus morhua*) prey heavily on the mature capelin and the young Norwegian spring-spawning herring (*Clupea harengus*) are believed to prey on the early capelin stages, these species were chosen as predators in this model to find possible links between the capelin and the Barents Sea predator system. The time series of herring and cod stock are based on ICES reports (2001a, b).

Russian scientists at the PINRO institute in Murmansk have provided monthly temperature values from the upper 200 m in the Kola section along the 33°30′E medial from 70°30′N to 72°30′N in the Barents Sea (Bochkov, 1982). The data series has quarterly values from the period 1906–1920 and monthly values from 1921, partly measured and partly interpolated.

The uncertainties in the data series of zooplankton, capelin herring and cod are not reported in the ICES reports (2001a, b). Norwegian scientists believe, however, the uncertainty in the capelin biomass time series is about 30% (Tjelmeland, personal comm.).

Systems theory

The Barents Sea system $S_B(t)$ may be represented by a simplified system architecture

$$S_B(t) = \{B(t), \{S_{ca}(t), S_c(t), S_f(t), S_p(t), S_o(t), S_v(t)\}\} \quad (1)$$

where B(t) is a time-varying mutual link between all the subsystems of $S_B(t)$. Then the dynamics of a subsystem $S_i(t)$ is dependent on its autonomous dynamics, the

mutual linking to the other subsystems and the autonomous dynamic of each system. To understand the dynamics of a capelin system we need to understand the fundamental properties all systems and their dynamic mutual relations to it. In this simplified system-architecture, $S_{ca}(t)$ is the autonomous capelin system, $S_c(t)$ is the system of capelin catch to landings, $S_f(t)$ is the plankton food system, $S_p(t)$ is the predator systems which are mainly herring and cod, $S_o(t)$ is the oceanographic system has 18.6 yr lunar tide that introduces a 18.6 yr and a 6.2 yr temperature cycle in the Barents Sea, $S_v(t)$ represents a disturbance from an unknown source.

The Barents Sea system consists of a set of different abiotic and biotic factors. In this case the oceanographic system $S_o(t)$ represents a cyclic process that influences all the others. The theory of this investigation is based on the 18.6 yr lunar tide, causing fluctuations in the water temperature in this area. These fluctuations will, directly or indirectly, lead to fluctuations in the capelin stocks.

Capelin biomass dynamics

The capelin system $S_{ca}(t)$ has stock numbers of age where the dynamics are represented by the state differential equation

$$\dot{X}(t)=A(t)X(t)+B(t)U(t)+V(t) \tag{2}$$

where X(t) represents a [m × 1] state vector of the capelin year class numbers, A(t) is a [m × n] system growth matrix, U(t) represents all known states in [m × 1] vector, B(t) represents a [m × n] binding matrix from the U(t) vectors, V(t) is a [m × 1] disturbance vector from an unknown source $S_v(t)$, m and n are the maximum age numbers in the biomass. In the system growth matrix A(t) of Equation (2)

$$A(t)=\begin{bmatrix} R(t)Ma(t) \\ I-M(t) \end{bmatrix} \tag{3}$$

where R(t) is the recruitment rate function, Ma(t) a [1 × n] maturing vector, I is an [m − 1 × n − 1] identity matrix and M(t) a [m − 1 × n] mortality matrix. The system matrix A(t) is a time varying process modelled by

$$A(t)=A+B_A(t)\cdot U_A(t)+V_A(t) \tag{4}$$

where A is the mean growth system matrix, $U_A(t)$ a known external sources that influences the system matrix A(t), $B_A(t)$ is the link from $U_A(t)$ to the system matrix A(t) and $V_A(t)$ is a disturbance from an unknown source.

Weight

The system dynamics of the individual weight growth is modelled by the differential equation

$$\dot{X}_w(t)=A_w(t)\cdot X_w(t) \tag{5}$$

where $X_w(t)$ is the individual vector of weight-at-age and $A_w(t)$ is the individual growth rate matrix. The elements of the biomass vector $X_b(t)$ are computed by

$$x_{bi}(t)=x_{wi}(t)\cdot x_i(t) \tag{6}$$

where $x_{bi}(t)$ is the i-th element in the biomass vector $X_b(t)$, $x_{wi}(t)$ is the i-th element in the individual weight vector $X_w(t)$ and $x_i(t)$ is the i-th element in the stock number vector X(t). The elements of the spawning number vector $X_s(t)$ are computed by

$$x_{si}(t)=Ma_i(t)\cdot x_i(t) \tag{7}$$

where $x_{si}(t)$ is the i-th element in the spawn biomass vector $X_s(t)$ and $Ma_i(t)$ is the i-th element in the mature vector Ma(t).

Stability

The eigenvalues of a mean system matrix A=E[A(t)] provide information on the fundamental stability and oscillating properties of the capelin stock. The eigenvalues of the mean system matrix A are computed by

$$\det[\lambda I-A]=0 \tag{8}$$

where I is an identity matrix and the eigenvalues are a diagonal matrix $\lambda I=\Lambda$. The dynamic system is asymptotically stable if, and only if, $Re[\lambda]<0$ for all eigenvalues λ in Λ. The system has an oscillating property when eigenvalues of Λ has complex values (Lunze, 1992).

Frequency properties

Frequency functions represent a shift from the time domain to a frequency view of system dynamic properties. The frequency properties are computed from the Fourier transformation of the state dynamic model [Equation (2)] to

$$X(j\omega)=(j\omega I-A)^{-1}BU(j\omega)+(j\omega I-A)^{-1}V(j\omega) \tag{9}$$

where I is an identity matrix, j is a complex operator, ω represents the angle frequency, A is the mean of the growth system matrix A(t), B is the mean of the binding matrix B(t), $X(j\omega)$ the state spectrum vector and $U(j\omega)$ the state spectrum vector from a known source. The stationary frequency transfer function $H(j\omega)$ from a known source $U(j\omega)$ to the state $X(j\omega)$ is from Equation (9)

$$H(j\omega)=\frac{X(j\omega)}{U(j\omega)}=(j\omega I-A)^{-1}B \tag{10}$$

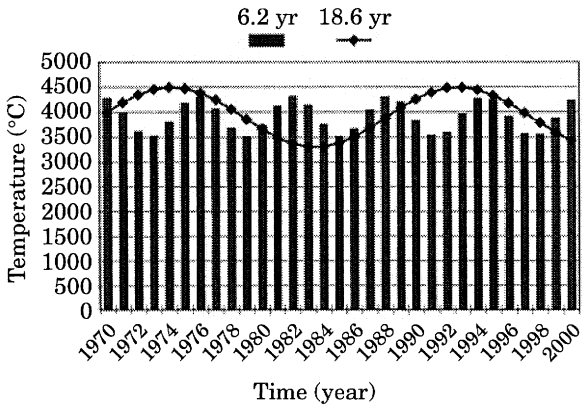

Figure 2. Stationary temperature reference cycles 1970–2000.

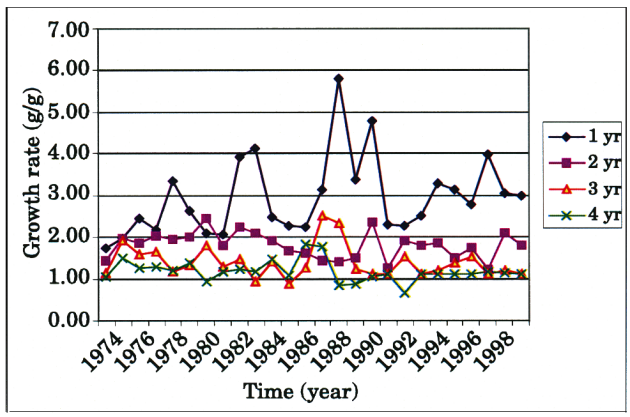

Figure 3. Growth rate in weight of different age groups 1973–2000.

where H(jω) is a complex function. The transfer function H(jω), describes in the frequency domain how the capelin biomass responds to stationary cycles from the known source U(jω).

Stochastic resonance

The stochastic resonance is a symmetric bi-stable stochastic process between recruitment and the spawning biomass where the process is driven by an external random processes. The resonance frequency is dependent on the eigenvalues of the A system matrix. In a time variant system the resonance frequency will be adjusted by the time variant system growth matrix A(t).

Linking to the 18.6 yr nodal tide

The Barents Sea oceanographic system has complex dynamics from currents, temperature, salinity, ice extension and the inflow of Atlantic water. A frequency analysis of the Kola section temperature series (Bochov, 1982) from the Barents Sea, has identified stationary temperature cycles of 18.6 yr and 6.2 yr (Yndestad, 1999a) which are correlated to the lunar nodal tide (Pugh, 1996; Keeling and Worf, 1997).

Figure 2 shows the estimated stationary temperature reference cycles of 18.6 yrs, the 3. sub-harmonic 18.6/3=6.2 yr cycle in the Kola section time series (Yndestad, 1999a).

The time series is based on the estimated model

$$x_t(nT)=3.9+0.4\sin(3\omega_n nT-0.29)+0.6\sin(\omega_n nT+1.52) \quad (11)$$

where the sample time T=1 yr, n=1930 . . . 2000 and the angle frequency $\omega_n=2\pi/18.6$ (rad/yr) (Yndestad, 1999a). The correlation coefficient between a 18 yr wavelet cycle and the stationary model $x_t(nT)$ is estimated to 0.9 in the period 1930 to 2000. In the period 1900 to 1930 the phase is shifted 180 degrees. This means the temperature cycle has a stable frequency, but the phase may shift because of more dominant low frequent cycles. These temperature cycles are used as a reference in this paper.

Results

Capelin model identification

Important subjects to be analysed in this study of stock dynamics are the direct and indirect effect of temperature on growth, recruitment and mortality.

Growth

Different fish species, and year classes within the same species, have a general temperature preference for optimum growth. Growth is however also dependent upon food and activity. The ambient temperature of the capelin may therefore vary with non-thermal components like zooplankton abundance and stock size. Growth rate in grams-per-year is used as a parameter to analyse growth in relation to temperature, stock densities, and food.

The different age groups do not grow synchronously (Figure 3). As expected, the capelin growth rate is highest early in life. The growth rate will decrease when body size is increasing and during sexual maturity when energy is diverted into reproductive activities. There are also large fluctuations in growth rates from year to year because of differences in growth conditions with time.

In this short time series the time variant growth rate (kg/kg) is given by the stationary model

$$A_{ws}(nT)=1.8+0.5\sin(\omega_o nT/3-0.29) \quad (12)$$

where sample time T=1 yr, n=1973 . . . 2000 and the lunar nodal cycle angle frequency $\omega_0=2\pi/18.6$ (rad/yr). The mean growth rate of weight A_{ws} is estimated to $E[A_{ws}(t)]=1.8$ and the mean influence from the 6.2 yr cycle is estimated by $sdv[A_{ws}(t)]=0.5$. The cross correlation coefficient R between the measured mean growth

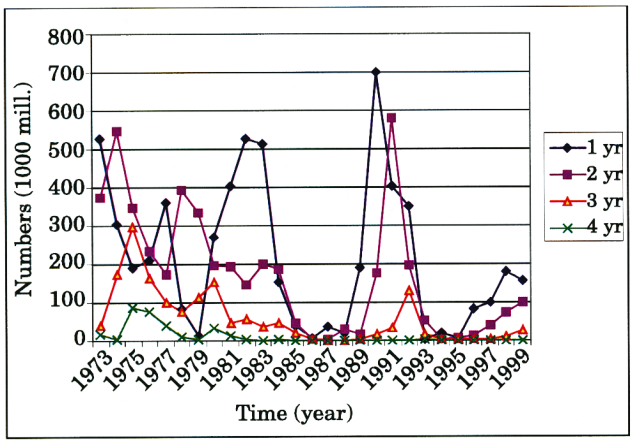

Figure 4. Variations in number of individual age groups 1973–2000 (ICES, 2001b).

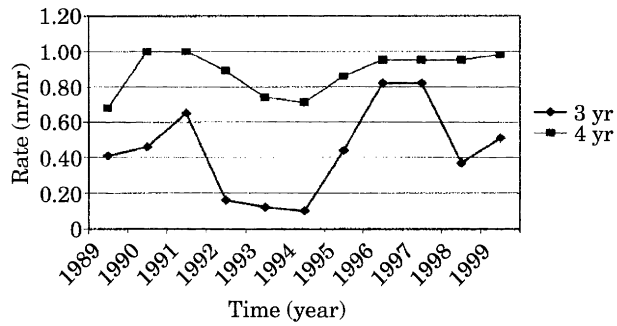

Figure 5. Maturity rate of three- and four-year-old capelin 1988–2000 (ICES, 2001b).

rate $A_{wm}(nT)$ [Equation (5)] and the stationary cycle model [Equation (12)] is estimated to 0.42.

The growth rate of the one-year-old had a maximum around 1977, 1982, 1988 and 1996, close to the maximum of the 6.2-yr climate cycle. The growth rate maximum of this age group is in accordance with the maximum zooplankton abundance illustrated in Figure 8. The growth rate of the three-year-old have their maximum around 1973, 1979, 1986, 1991 and 1997, close to the minima of the 6.2 yr cycle. The growth rate of the two-year-old does not fluctuate to the same extent as the one- and three-year-olds. Different relationships to the climate cycle may be due to differences in the abundance of preferred food but may also be related to the stock size and size of the year class.

Stock density

Intraspecific competition is generally believed to have a major influence on growth if other environmental conditions are stable. The time series of the numbers in the different age groups of capelin are shown in Figure 4.

Density-dependent effects may be identified by comparing the variations in the number of individuals with the variation in growth-rate. When the number of individuals in each year class are low then the increase in growth rate is high. One exception is the maximum growth rate and the number of the one-year-old capelin around 1982. Most prominent is the growth rate maximum of all age groups in the late 1980s and mid-1990s after the collapses in the stock. The increased growth rate in this period is followed by an increase in number. An increase in numbers of individual is related to an increase in recruitment rate as shown in Figure 6.

Recruitment

The growth potential in a fish stock is mainly a function of recruitment and mortality. Yearly recruitment is dependent on the size and condition of the spawning biomass related to, the environmental conditions for growth and survival. This will influence age-at-first-reproduction and the number of spawning individuals. Figure 5 shows the age-at-first-reproduction expressed as maturity rate of the three- and four-year-old capelin from 1988 to 2000.

The maturity rate has a maximum in 1991 and 1997. This short time series indicates that the maturity rate increases when the temperature of the 6.2 year cycle is decreasing. The fluctuations in the maturity rate are caused mainly by the varying maturing rate of the three-year-old capelin. ICES-data shows that the weight of this age group was at its maximum in 1991 and 1997, indicating weight-dependent maturity.

A model of the mean maturity rate by year [Equation (4)] of the three-year-old year class is, in this short time series, estimated to be:

$$Ma_{3s}(nT) = 0.5 - 0.3\sin(\omega_o nT/3 - 0.29) \quad (13)$$

where sample time T=1 yr, n=1989 ... 2000 and the 18.6 year lunar nodal cycle angle frequency $\omega_0 = 2\pi/18.6$ (rad/yr). The stationary model shows that the maturity is inverse related to the 6.2 year temperature cycle. In this case the cross correlation coefficient R between the three years of age maturity $Ma_3(nT)$ and the stationary model cycle $Ma_{3s}(nT)$ [Equation (13)] is estimated to 0.62.

The recruitment rate is an estimate of the reproductive success of the individuals in the spawning stock. Figure 6 shows the scaled temperature cycles [Equation (14)] and the computed 1-year recruitment rate $Rr_1(nT) = x_1(nT - T)/x_{3+}(nT)$ where $x_{3+}(nT)$ is the spawning stock numbers and $x_1(nT)$ is the 1-year recruitment.

The recruitment rate and the growth rate of the one-year-old capelin had a maximum in 1976, 1981/82, 1990, 1995 and 1997. These years are close to the maximum of the 6.2 yr temperature cycle and the maximum in zooplankton abundance (Figure 8) in the Barents Sea registered by ICES. High recruitment rate seems associated with periods of good conditions for growth and survival for one-year-old capelin.

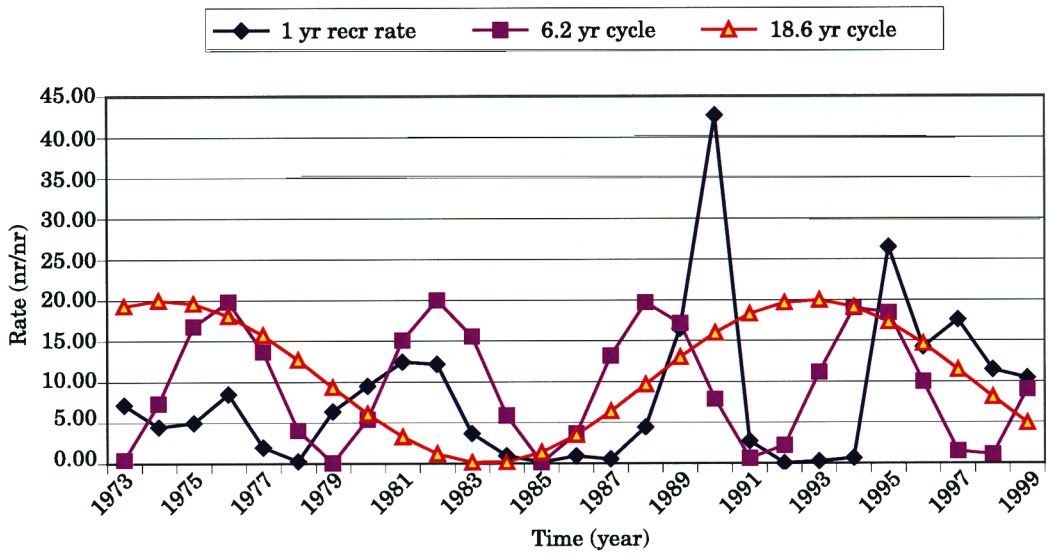

Figure 6. The number of one-year-old capelin produced per spawning individual 1973–1999 and the scaled temperature cycles of 6.2 and 18.6 years.

To demonstrate the close relationship between the one-year-old computed recruitment rate $Rr_1(nT)$ and the estimated stationary Kola section temperature cycles [Equation (11)], the recruitment rate $Rr_1(nT)$ and the scaled temperature cycles

$$Rrs_{6.2}(nT) = 10 + 10\sin(3\omega_0 nT - 0.29)$$

$$Rrs_{18.6}(nT) = 10 + 10\sin(\omega_0 nT + 1.52) \qquad (14)$$

are shown on Figure 6. The cross correlation coefficient between one-year-old recruitment rate $Rr_1(nT)$ and the stationary cycles $[Rrs_{6.6}(nT) + Rrs_{18.6}(nT)]$ is estimated as 0.2. This low correlation is influenced by the biomass collapse in 1982–1987 and 1991–1994.

Stability

The eigenvalues are computed from the estimated mean system matrix A [Equation (3) and (8)] where all parameters are estimated from the capelin data series. The computed eigenvalues in the Λ matrix are $\lambda_1 = -0.46 + j2.48$, $\lambda_2 = -0.46 - j2.48$, $\lambda_3 = -0.09 + j1.68$, $\lambda_4 = -0.09 - j1.68$ and $\lambda_5 = 0.18$. The complex conjugated eigenvalues (λ_1, λ_2) and (λ_1, λ_2) indicate a highly oscillating system of stock numbers. The real positive eigenvalue λ_5 shows that the system is asymptotically unstable and that the mean stock numbers will grow in the long run.

The frequency response

A frequency response function is a frequency view of how the biomass system responds to environmental conditions as a set of frequencies. Figure 7 shows the computed mean frequency response function $H(j\omega)$ from Equation (10).

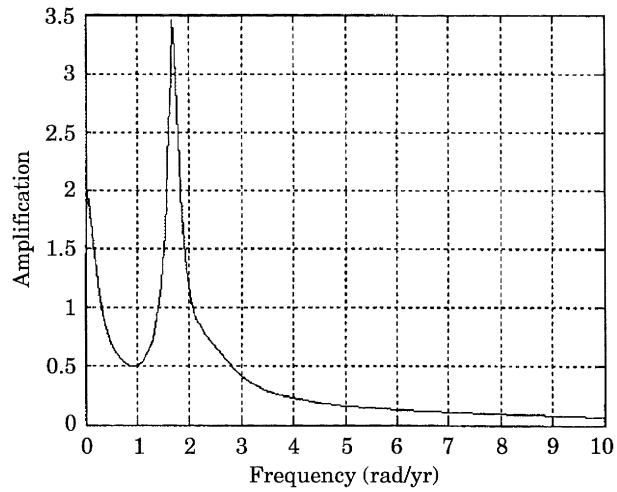

Figure 7. The computed frequency response function of the capelin stock.

The transfer function shows the total capelin stock has a stochastic resonance at the angle frequency $\omega_R = 1.8$ (rad/yr) or at the cycle time $T_R = 2\pi/1.8 = 3.4$ yr which is close to half of the temperature cycle of $18.6/3 = 6.2$ yr. This means that the capelin system has adapted a stochastic resonance adapted to the 6.2 yr temperature cycle in periods of about 6 years. According to these dynamics the biomass will have an optimal recruitment when a resonance cycle 3.4 yr and a positive temperature cycle of 6.2 yr are positive the same time.

In these dynamics it is important for the year-class strength that there is a synchronization between new recruitment and the 6.2 yr cycle. These large fluctuations are an important strategy for long-term growth.

The mean long-term growth of the capelin stock exists when the angle frequency $\omega = 0$. The computed long-term

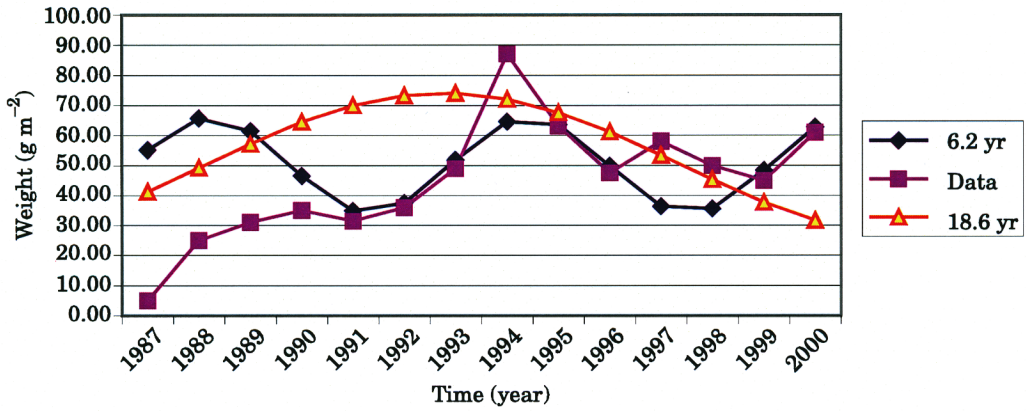

Figure 8. Zooplankton abundance data in the Barents Sea and the estimated deterministic 18.6 yr and 6.2 yr temperature cycles 1987–2000.

amplification is $|H(j\omega=0)|=2$ (Figure 7). This indicates that the mean capelin recruitment is twice its need for population growth in the long run. The stock numbers will grow when the catch rate is less than F=0.5 (catch numbers/stock numbers).

The mean frequency response function $H(j\omega)$ is computed from the mean system growth matrix A. This growth matrix is estimated from stock numbers [Equation (2)], mortality, and recruitment [Equation (3)]. The standard deviation error of the parameters in the A-matrix is estimated to be 30%. Long-term parameter fluctuations in the system matrix A(t) will influence the spectrum of the frequency response function $H(j\omega)$. If these parameter fluctuations are white noise the amplitude of the total spectrum will be influenced. When the temperature influences the maturity parameters in the system matrix A(t), a delayed maturity will introduce a slower resonance cycle.

Linking to the food system

Capelin is the main plankton feeder in the Barents Sea. The abundance of zooplankton varies between years and areas and its biomass in the Barents Sea has been surveyed throughout the period 1987–2000. The variations found may induce fluctuations in the capelin stock.

A possible relationship between a deterministic 18.6 yr and a 6.2 yr temperature cycle and the zooplankton density in the actual distribution areas of the capelin is illustrated in Figure 8. The estimated zooplankton model is based on the deterministic linking to the 18.6 yr lunar cycle by the model

$$x_z(nT)=50+40\sin(3\omega_n nT-0.29)+40\sin(\omega_n nT+1.52) \quad (15)$$

where sample time T=1 yr, n=1987 ... 2000 and the 18.6 yr lunar angle frequency $\omega_n=2\pi/18.6$ (rad/yr). In this model the estimated zooplankton biomass cycles has the same phase as the 18.6 yr and 6.2 yr temperature cycle [Equation (2)]. The cross correlation coefficient between the data series and the stationary model is estimated to 0.43. The correlation is weak during the warm period around 1988. This may be due to the lack of data from region 2, 3, 4, 6 and 8 in this period.

Linking to predator system

Young Northeast Arctic cod prey heavily on the mature capelin and the young Norwegian spring spawning herring is believed to prey on the early capelin stages. The development in the biomass of cod (3–7 yr) vs. the biomass of 3+ capelin is illustrated in Figure 9, while the biomass of herring (0–4 yr) and one-year-old capelin is illustrated in Figure 10.

The results indicate an inverse relationship between the predator and its prey. Before 1978 juvenile herring was at a low level, the cod stock was decreasing and the capelin stock was at its highest level. From 1983–1987 and from 1990–1994 the juvenile herring and young cod were increasing while the capelin stock decreased to almost zero.

The predator biomass had a maximum level in 1987 and 1994. These periods are related to the warm periods of the 6.2 yr temperature cycle, indicating an increased food demand and increased consumption of capelin. By adding the fishing activity to predation, it seems obvious that mortality has contributed to the two collapses observed in the period.

Linking to catch

Fishing activity is expressed as a catch rate. The catch rate $F_b(nT)$ (biomass catch/biomass) is computed from the biomass in October and the catch in the spring and the autumn, since stock numbers in January are unknown. This may introduce an unexpectedly high

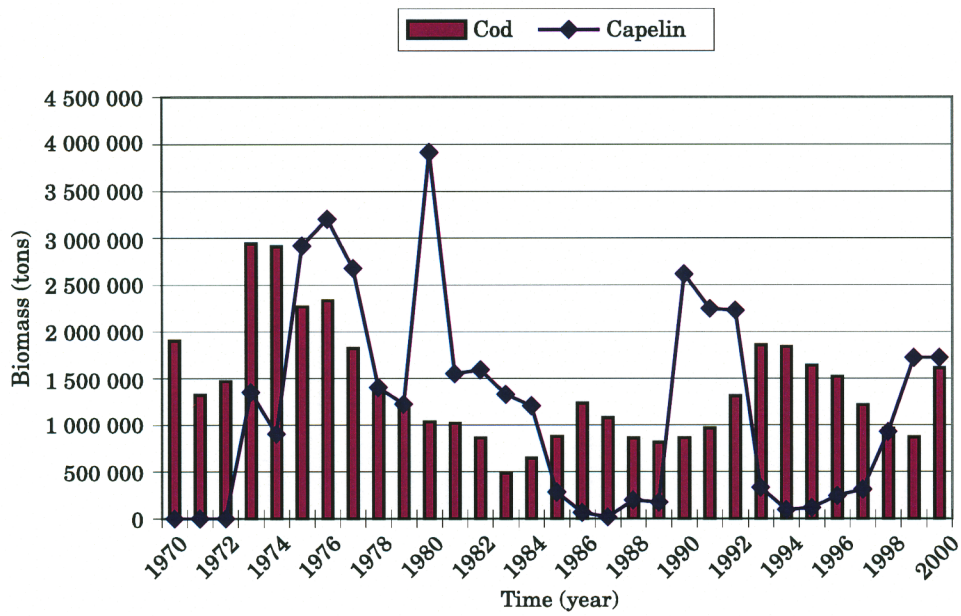

Figure 9. Development of the biomass of the Northeast Arctic cod (3–7 years) and 3+ year capelin 1970–2000.

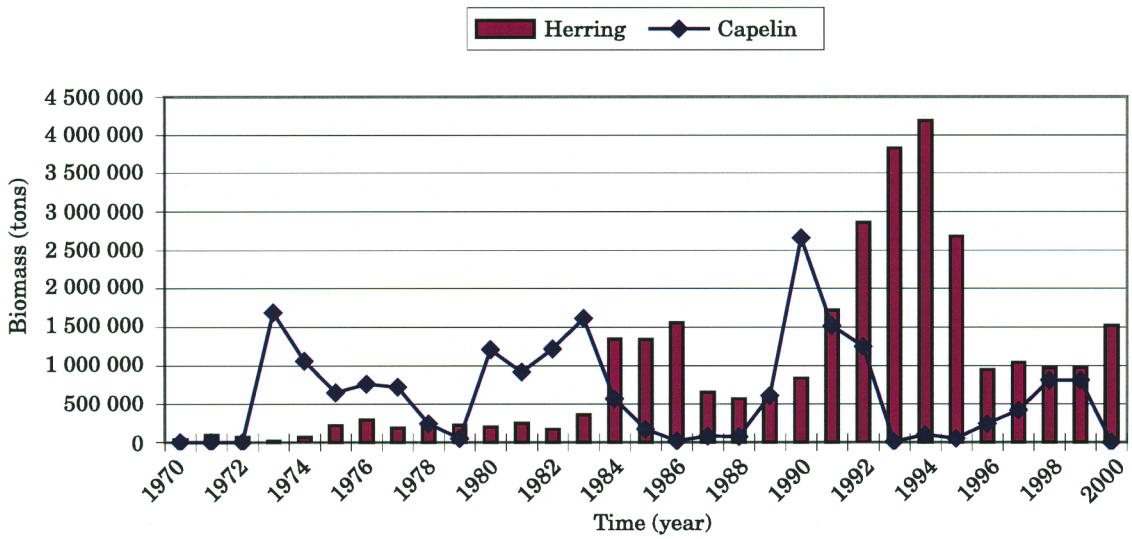

Figure 10. Development of the biomass of Norwegian spring-spawning herring (0–3 years) and one-year-old capelin.

catch rate when there is a high mortality in the spring. $F_b(nT)$ is not exactly the same as in the earlier described F(nT) (catch numbers/biomass numbers).

$$F_b(nT) = \frac{\|x_c(nT)\|}{\|x_b(nT)\|} \tag{16}$$

where $\|x_c(nT)\|$ is catch (in tons) to landings (spring plus autumn) at the time nT and $\|x_b(nT)\|$ is the total biomass (in tons). The history of the computed catch rate is illustrated in Figure 11.

The estimated frequency response has indicated that the stock numbers are expected to grow in the long run with the catch rate F(nT)<0.5 (catch numbers/stock numbers). The results show an increase in that rate in 1977, 1985 and 1993. Until 1977 it was about 0.3–0.4. In the early 1980s it passed the 0.5 limit to about 0.6 and increased to 1.78 in 1985. The combination of a cool Barents Sea (Figure 2), reduced growth and survival of the youngest age-groups [Equation (4)], and an increased catch rate of the maturing stock (Figure 11) caused a collapse of the biomass in 1985.

By comparing the development of the capelin stock biomass with the development in catch rate, there seem to be increased landings when the stock biomass is decreasing. Maximum catch rate also coincides with the maximum level of predators. From 1983 until the first collapse in 1985 it increased from 0.45 to 1.78 and in

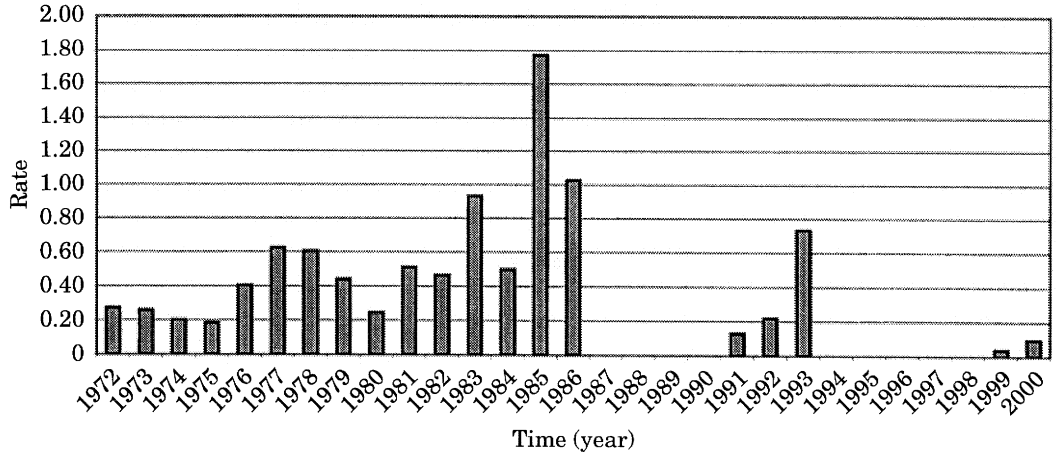

Figure 11. The catch rate of capelin 1973–1999.

1993 again increased to 0.75 while the stock was rebuilding. The capelin stock needed more years to recover from the second collapse. In this period cod and herring were at their maximum level preying on all age groups of the capelin stock when the spawning stock was producing little and few recruits in the period 1985–1988 (Figure 4 and Figure 6).

Discussion

In this paper a model of the Barents Sea capelin has been established to analyse the dynamic properties of the stock. The results show that the variations are due to dynamics in growth, recruitment, mortality and suggest that their frequency is related to the 6.2 yr temperature cycle. This cycle has a stationary frequency since it is driven by the lunar nodal tide. A closer analysis of the Kola section time series has shown a stable phase during the years being considered.

All parameters in the model have been estimated from official ICES data. The uncertainty in the ICES data series of capelin and zooplankton respectively are not known and so the estimated time-variant parameters is influenced by some unknown noise. The mean system matrix has an estimated error deviation of about 30% of the estimated mean parameters. Some of this deviation is related to noise. There are, however, some indicators of reasonably good estimates. The maximum catch rate of long-term growth is estimated to be 0.5. This is the same level as estimated by Icelandic scientists. Most of all, though, there is a good coherence between the results. The estimated long-term growth, the estimated resonance frequency, and the parameter fluctuations all are related to the 18.6 years lunar nodal cycle.

Zooplankton

The zooplankton abundance in the Barents Sea increased during periods of an estimated increase in water temperature, showing a correlation to the 6.2 yr temperature cycle. The time series of zooplankton abundance are short, and therefore just an indication of a probable relationship.

The spring bloom in Arctic waters starts earlier in cold years and culminates a month or more earlier than in warm years. In cold years the zooplankton spawns later and copepodite stages do not reach a size which allow them to fully utilize the early phytoplankton bloom (Melle and Skjoldal, 1998). This may explain the high zooplankton abundance in warm phases of the temperature cycles.

Gjøsæter (1997) reported the mean annual individual growth in weight of Barents Sea capelin to be positively correlated to the average zooplankton density. The strongest relationships were found between one-year-old capelin and the smallest zooplankton and between three-year-old capelin and the largest size fraction. The one-year-old capelin prefer the size fraction of food and the temperature related to the Atlantic water. Total zooplankton density, dominated by the copepod (*Calanus finmarchicus)* is almost three times higher in the Atlantic water than in melt water (Hassel *et al.*, 1991; Melle and Skjoldal, 1998). This probably explains the high growth rate of one-year-old capelin found during warm periods. The density of plankton in the largest size fraction is significantly higher in the colder Arctic water in the eastern areas of the Barents Sea (Melle and Skjoldal, 1998). The three-year-old capelin prefers the size fraction and the temperature related to the Arctic water. This may explain the high growth rate of this age group in periods of estimated low temperatures.

Recruitment

The growth rate in numbers of any population is influenced by age at maturity which is often sex and size dependent. Differences in age at maturity of the capelin are registered only for 10 years, giving a short time series

for system dynamic analyses. The results indicate, however, an inverse relationship to the temperature cycle with a decreasing age at sexual maturity when the temperature in the 6.2 yr temperature cycle is increasing. Since sexual maturity is size dependent the increased growth of 3+ capelin during cold periods will result in a related decrease in age at maturity.

The number of one-year-old capelin produced per spawning individual had its maximum around 1982, 1990 and 1995. These years coincide with the maximum of the 6.2 yr climate cycle. The growth rate maximum of the one-year-old capelin and the maximum in zooplankton abundance also indicates that warm periods give good conditions for the growth and survival of juvenile capelin.

Stochastic resonance

Stochastic resonance is an important source of understanding stock-number fluctuations. The frequency transfer function shows the stock-number dynamics has a dominant 3.4 yr resonance cycle, which is close to a half of the 6.2 yr temperature cycle. By this stochastic resonance the stock numbers will have optimal conditions for recruitment in periods of 3, 6 or 9 years dependent on a match or a mismatch between the 3 yr biomass resonance cycle and the 6.2 yr temperature cycle. When there is such a match the recruitment rate may change from about 0 to 40. The timing between stock-number fluctuation and the 6.2 yr temperature cycle is of the greatest importance in this context. A forced phase delay of fluctuation from predation or catch may cause a collapse of the capelin biomass.

Growth

The growth maximum of the one-year-old capelin corresponds to the maximum of the 6.2 yr climate cycle. The growth rate of the three-year-olds is negatively correlated to the same cycle however. The large fluctuations in growth rate between years and age groups observed in this study seems to stem from differences in temperature and food as discussed above. The growth-rate maximum of the one-year-olds found in this study is in accordance with the growth maximum of the total Barents Sea capelin stock found in other investigations (Gjøsæter, 1997). The correlation between the growth rate of the one-year olds and the total population must stem from the fast growth rate of the youngest age groups dominating the growth rate mean.

The growth of stock numbers is directly related to changes in the recruitment rate and the spawning stock numbers. Most prominent is the growth rate maximum of all age groups in the late 1980s and mid-1990s. This may be a response to the collapse in the stock inducing good conditions for growth and survival. Optimal growth conditions result in a later increase in numbers as illustrated by the recruitment rate. Natural populations that suffer a major, rapid decline in abundance usually display a subsequent increase in growth rate (Ross and Almeida, 1986).

Mortality

The collapses in the capelin stock may be caused by fishing activity but also are a result of factors like climate, food abundance, and predation as suggested here. Indeed Norwegian and Russian investigations indicate collapses in this stock in the 1950s and early 1960s, before the commercial fishery of capelin started (Olsen, 1968; Ozihigin *et al.*, 1996).

Recruitment failures have also been associated with presence of young herring in the nursery area of capelin (Hamre, 1994). There are however few observations of capelin larvae in herring stomachs (Huse and Toresen, 2000). The presence of 0-group herring has little effect on capelin recruitment compared to significant amounts of one-year-old and older herring in the Barents Sea (Gjøsæter and Bogstad, 1998). The results in this investigation show an inverse relationship between the biomass of one-year-old capelin and young herring 0-4 year, also indicating a negative interaction between these two species.

Cod interacts with the capelin through heavy predation on the spawning stock on its way south to the spawning grounds. Large year classes of cod (3 to 7 yr) are believed to have important effects on the biomass of the maturing capelin stock (Hamre, 2000). Analysis of the consumption by cod (ICES, 2000a) shows that relative consumption was at its highest level in 1985–1987 and from 1993–1995 when the biomass collapsed. The fisheries also exploited the maturing part of the stock. The results in this investigation indicate that increased landings appear simultaneously with increased predator abundance. If mortality exceeds recruitment over time then severe reduction in stock biomass is the result.

It was suggested earlier that the growth in stock numbers is related to the estimated 6.2 yr temperature cycle and that the stock number will grow when the landing rate is below 0.5. From this analysis, three different phases of stock collapses have been identified:

- First, there was a negative climate shift from two climate cycles. The 18.6 yr temperature cycle shifted from a maximum value in 1974 to a minimum in 1983 and the 6.2 yr temperature cycle from a maximum in 1982 to a minimum in 1985. This resulted in less growth in the biomass.
- Second, there was an increase in the catch rate from about 0.2 in 1974 to a level far above the sustainable level 0.5 in the period 1983–1986. The biomass

declined from about 600 thousand tons in 1974 to about 300 thousand tons in 1984 and collapsed in 1985.

- Third, there was an increase in the biomass of interacting age groups of cod and herring from the mid-80s. The consumption of capelin by cod (ICES, 2001a) shows that the relative importance of cod increased in the late third phase, i.e. when the biomass was collapsing from 1984–1986.

In the period 1985–1989, a time of low stock levels, there was a cold climate and new recruitment was at a minimum. In the years 1989 and 1990 there were optimal climatac conditions. A new positive 18.6 yr and a 6.2 yr cycle increased the zooplankton biomass and the capelin stock numbers to a level last found in the 1970s. When the biomass matured in 1993, the 6.2 yr climate cycle was at a minimum giving poor conditions for new recruits. No new recruited year classes were observed in the Barents Sea in the period 1985–1989. The catch rate increased from 0.2 in 1991 to 0.75 in 1993 and again predation from herring and cod increased, causing a second collapse in 1993. Recovering started in 1998 because of high recruitment rates in 1995 and 1997 and a positive period of the 6.2 yr climate cycle.

Conclusion

In this paper a dynamic model of the Barents Sea capelin stock has been established. Fluctuations in stock numbers, growth in weight, age at maturity and recruitment have a close relation to a stationary 6.2 yr temperature cycle in the Barents Sea. The dynamic analysis also shows a correlation between zooplankton abundance and the 6.2 yr temperature cycle.

It would seem, in consequence, that the 6.2 yr temperature cycle, directly or indirectly, is influencing both the food chain and the dynamic properties of the populations in the area and, thereby, the fluctuations in the capelin stock. This approach permits a better understanding of capelin stock dynamics and better long-term forecasting of the biomass and these, in turn, could give improved long-term forecasting and management of the stock. If it is possible to indicate when the stock has optimal conditions for growth and survival then long-term prognoses can make future management more reliable.

A frequency analysis of the stock estimation model shows a stochastic resonance at about half the 6.2 yr climate cycle. This suggests that the fluctuation of the stock number is a natural adaptation to the environment and a strategy for optimal growth and survival in the long run.

The aim of fisheries management is to try to control stock dynamics. In the management of the capelin stock it would seem to follow that, at any given time, the catch rate should be adjusted according to the nature of the link between the phase of the climate cycles and the stochastic resonance.

References

Bochkov, Yu. A. 1982. Water temperature in the 0–200 m layer in the Kola-Meridian in the Barents Sea, 1900–1981. Sb. Nauchn. Trud. PINRO, Murmansk, 46: 113–122 (in Russian).

Gjøsæter, H. 1997. Studies of the Barents Sea capelin, with emphasis on Growth. Dr scient thesis, Department of Fisheries and Marine Biology, University og Bergen, Norway, Paper III, IV and V.

Gjøsæter, H., and Bogstad, B. 1998. Effects of the presence of herring (*Clupea harengus*) on the stock-recruitment relation of the Barent Sea capelin (*Mallotus villosus*). Fisheries Research, 38: 57–71.

Hamre, J. 1994. Biodiversity and exploitation of the main fish stocks in the Norwegian Sea-Barents Sea ecosystem. Biodiversity and Conservations, 3: 273–929.

Hamre, J. 2000. Capelin and Herring as key species for the yield of north-east Arctic cod. Results from multispecies model runs. SAP symposium 4–6 December 2000. Bergen. Norway.

Hassel, A., Skjoldal, H. R., Gjøsæter, H., and Omli, L. 1991. Impact of grazing from capelin (*Mallotus villosus*) on zooplankton: a case study in the northern Barents Sea in August 1985. Polar Res., 10(2): 371–388.

Huse, G., and Toresen, R. 2000. Juvenile herring prey on Barets Sea capelin larvae. Sarsia, 85: 385–391.

ICES. 2001a. Report of the Arctic Fisheries Working group. ICES CM 2001/ACFM:19. 24 April–3 Mai. Bergen. Norway.

ICES. 2001b. ICES Northern Pelagic and Blue Whitning Fisheries Working Group. ICES CM 2001/ACFM: 18 April 27. Reykjavik, Iceland.

Keeling, C. D., and Whorf, Timothy P. 1997. Possible forcing global temperature by oceanic tides. Proceedings National Academy of Science of the United States, 94: 8321–8328.

Lunze, J. 1992. Feedback Control of Large-Scale Systems. Prentice Hall, New York.

Maksimov, I. V., and Smirnov, N. P. 1965. A contribution to the study of causes of long-period variations in the activity of the Gulf Stream. Oceanology, 5: 15–24.

Melle, W., and Skjoldal, H. R. 1998. Distribution, life cycle and reproduction of *Calanus finmarchicus, C, hyperboreus* and *C. Glacialis* in the Barents Sea. Dr scient thesis, Department of Fisheries and Marine Biology, University og Bergen, Norway, Paper III, 33 pp.

Olsen, S. 1968. Some results of the Norwegian capelin investigations 1960–1965. Rapports et Proces-Verbaux des reunions du Conceil International pour l' Exploration de la Mer, 158: 18–23.

Ozihigin, V. K., Yaragina, N. A., Tret'yak, V. L., and Ivshin, V. A. 1996. Growth of the arcto Norwegian cod. Izdatel'stovop PIRNO. ISBN 5-86349-033-0. p. 60.

Pugh, D. T. 1996. Tides, Surges and Mean Sea-Level. John Wiley & Sons, New York.

Ross, M. R., and Almeida, F. P. 1986. Density-dependent growth of silver hakes. Transaction of the American Fisheries Society, 115: 584–554.

Royer, T. C. 1989. Upper ocean temperature variability in the northeast Pacific: Is it an indicator of global warming? Journal of Geophysical Research, 94: 18175–18183.

Royer, Thomas C. 1993. High-Latitude Oeanic Varibility Associated With the 18.6-Year Nodal Tide. Journal of Geophysical Research, 98(No. C3): 4639–4644.

Wyatt, T. 1984. Periodic fluctuations in marine fish populations. Envir. Educ. Inform., 3: 137–162.

Wyatt, T., Currie, R. G., and Saborido-Ray, F. 1994. Deterministic signals in Norwegian cod records. ICES Marine Science Symposium, 198: 49–55.

Yndestad, H. 1996. Systems Dynamics of North Arctic Cod. The 84'th international ICES Annual Science Conference. Hydrography Committee. Reykjavik, Iceland, 27 Sep.–4 Oct. 1996.

Yndestad, H. 1999a. Earth Nutation Influence on the Temperature in the Barents Sea. ICES Journal of Marine Science, 56: 381–387.

Yndestad, H. 1999b. Earth Nutation Influence on System dynamics of Northeast Arctic cod. ICES Journal of Marine Science, 56: 652–657.

Paper V

ICES Journal of Marine Science, 60: 1251–1264. 2003
doi:10.1016/S1054–3139(03)00152-8

The code of the long-term biomass cycles in the Barents Sea

Harald Yndestad

Yndestad, H. 2003. The code of the long-term biomass cycles in the Barents Sea. – ICES Journal of Marine Science, 60: 1251–1264.

Barents Sea capelin (*Mallotus villosus*), Norwegian spring-spawning herring (*Cluea harengus*), and Northeast Arctic cod (*Gadus morhua*) have been associated with large fluctuations of biomass growth. The cause of these large fluctuations has been poorly understood and led to problems in biomass management. The identification of a deterministic cause would provide the possibility of forecasting future biomass fluctuations. In this investigation, the Kola Section sea temperature and the biomasses of capelin, herring, and cod have been analyzed by a wavelet transform to identify the source of the long-term cycles. The wavelet analysis shows that the Kola Section temperature has dominant cycles at the lunar-nodal tide cycles of $3 \times 18.6 = 55.8$, 18.5 and $18.6/3 = 6.2$ years. The recruitment of Barents Sea capelin, Norwegian spring-spawning herring, and Northeast Arctic cod has adopted an optimal recruitment cycle close to the stationary 6.2 years Kola temperature cycle. Long-term biomass growth is correlated to the phase relation between the biomass eigen-frequency cycle and the Kola temperature cycles. The biomasses of capelin, herring and cod have long-term growth when the 6.2 and 18.6 years Kola temperature cycles are positive at the same time. There is a long-term biomass reduction when the temperature cycles are not positive at the same time, and a biomass collapse when the temperature cycles are negative at the same time. The deterministic property of the 18.6 years lunar-nodal tide provides a new way of long-term biomass forecasting over periods of 50–80 years or more.

Keywords: biomass eigen-frequency, long-term biomass cycles, wavelet analysis, 18.6-years lunar cycle.

Received 26 June 2002; accepted 28 March 2003.

H. Yndestad: Aalesund University College, Aalesund N-6025, Norway; tel: +47 70 16 12 00; fax: +47 70 16 13 00; e-mail: harald.yndestad@hials.no.

Introduction

Norwegian records document good herring periods from 1500 to 1570, 1600 to 1650, 1690 to 1774, and from 1808 to 1874 (Vollan, 1971). Since the herring biomass had a fluctuation of about 50–80 years, early marine scientists looked for its fundamental cause. Helland-Hansen and Nansen (1909) analyzed time-series from 1875 to 1905 and found close relationships between variations in the number of sunspots, the quality of cod roe, the quality of cod liver and the anomaly of the mean air temperature at Ona in Norway. These were explained by the periodicity in sunspot occurrence, or rather in the energy received from the Sun, which caused variations in the ocean currents through processes in the atmosphere. They concluded that the sea temperature is only an indicator of the variations from another primary cause.

The Swedish oceanographer Dr. Otto Pettersson [1848–1941] postulated that the orbits of the Moon and the Earth have an influence on long-period tides, climate cycles and fluctuations of marine biomasses. Pettersson (1905, 1914, 1915, 1930) explained the fluctuation of herring by a tidal 112-year cycle. Later Maksimov and Smirnov (1964, 1965, 1967), Maksimov and Sleptsov-Shevlevich (1970), Loder and Garret (1978), and Royer (1993), identified the 18.6-year lunar-nodal tide in the Atlantic Ocean while Yndestad (1996a, 1999a) found the spectrum of the lunar-nodal tide in the Barents Sea. Ottestad (1942) discovered 11-, 17.5-, 23-, and 57-year cycles in historical records of cod landings in Norway. He compared the estimated cycles with the annual growth-zones of Norwegian pine at Sørfold close to the Lofoten area and concluded that the recruitment of cod is influenced by climate cycles. Hjort (1914) analyzed the length distribution of Northeast Arctic cod. He explained fluctuations in the biomass by a match between the spawning time, on the one hand, and food available to the larvae on the other.

Izhevskii (1961, 1964) reconditioned a system-view of the interacting processes between the hydrosphere, the atmosphere and the biosphere. He argued that the heat in

1054–3139/03/121251+14$30.00

the ocean is a non-homogeneous system flowing from a warm equator to the cold pole. In this flow of heat, influenced by tidal forces, the ocean influences the atmospheric processes. Izhevskii analyzed the Kola Section temperature data series and estimated cycles of 4−6, 8−10, and 18−20 years. Russian records of the Northeast Arctic cod stock suggested cycles of 8−10 and 18−20 years. In an analysis of Norwegian spring-spawning herring he concluded that cod and herring do not represent substantially different ecological types in terms of their patterns of reproduction. Wyatt *et al.* (1994) analyzed landing records of Northeast Arctic cod from 1885 to 1951 and found a correlation with the 18.6-year nodal tide. Yndestad (1996b, 1999b) reported lunar-nodal cycles of $18.6/3 = 6.2$, 18.6, and $18.6 \times 3 = 55.8$ years in growth and recruitment of Northeast Arctic cod. The same cycles of 6.2 and 18.6 years have been identified in recruitment of the Barents Sea capelin and Norwegian spring-spawning herring (Yndestad and Stene, 2001; Yndestad, 2002).

The Barents Sea capelin, Norwegian spring-spawning herring and Northeast Arctic cod are well described by Gjøsæter (1997), Hamre (2000), Toresen and Østvedt (2000), Nakken (1994), and many others. In this paper the long time-series of the sea temperature in the Barents Sea and the separate biomasses of these three species are analyzed to find a common cause for the long-term biomass fluctuations. The investigation is based on a wavelet analysis that identifies the cycle time and phase in dominant biomass fluctuations. The result shows that the long-term fluctuation in the biomass of capelin, herring and cod is caused by a match or mismatch between a biomass eigen-frequency cycle and dominant stationary Kola Section temperature cycles.

Materials and methods

Russian scientists at the PINRO institute in Murmansk have provided monthly temperature values from the upper 200 m of the Kola Section along the 33°30′E medial from 70°30′N to 72°30′N in the Barents Sea (Bochkov, 1982). The data series from 1900 to 2000 has quarterly values over the period 1906−1920 and monthly values from 1921, partly measured and partly interpolated. In this presentation the annual mean temperature is analyzed.

The time-series of Norwegian spring-spawning herring (*Cluea harengus*) data covers the period 1907−2000. That from 1907 to 1945 are given in Toresen and Østvedt (2000), whilst the information covering 1945−2000 was provided by ICES (2001a).

The time-series for Northeast Arctic cod (*Gadus morhua*) covers the period from 1900 to 2000. That from 1900 to 1945 is based on published estimates from Hylen (2002) and the period from 1946 to 2000 was provided by ICES (2001b). The time-series of Lofoten catch numbers from 1866 to 1957 is given in Godø (2000). From 1958 until 1979 the Lofoten time-series is catch in tons. The data are interpolated to catch numbers by a scaling of 3.5 (tons/1000 numbers).

The time-series of Barents Sea capelin (*Mallotus villosus*) covers the period from 1945 to 2000. The data series of biomass from 1945 to 1995 is provided by Marshall *et al.* (2000), and that from 1995 to 2000 by ICES (2001a).

Systems theory

The biomass in the Barents Sea is related to a complex food-chain system. In this investigation the Barents Sea is modelled by the simplified general-system architecture

$$S(t) = \{B_B(t), \{S_n(t), S_o(t), S_f(t), S_{ca}(t), S_{he}(t), S_{co}(t), S_v(t)\}\} \quad (1)$$

where $S_n(t)$ is the lunar-nodal system, $S_o(t)$ the ocean system, $S_f(t)$ the food-chain system, $S_{ca}(t)$ the capelin-biomass system, $S_{he}(t)$ the herring-biomass system, $S_{co}(t)$ the cod-biomass system, $S_v(t)$ an unknown source, and $B_B(t)$ is the mutual binding between the Barents Sea system elements. According to Equation (1) the Barents Sea system is expected to be time varying, structurally unstable, and mutually state-dependent. In a mutually related system, a stationary dominant energy source will influence the others.

The lunar-nodal cycle

The lunar-nodal cycle represents the moving cross-point between the Moon plane-cycle and the ecliptic plane to the Sun. This cross-point describes a lunar-nodal cycle of 18.6134 years. The corresponding cycle of changing inclination of the Moon's orbit to the Earth's equatorial plane is described by the model

$$u_n(t) = 23°27' + 5°09' \sin(\omega_0 t + 1.0\pi) \quad (2)$$

where $\omega_0 = 2\pi/T_0 = 2\pi/18.6134$ (rad/year) is the lunar-nodal angle frequency and t (year) is the time. The cycle amplitude has a maximum in November 1987 and a minimum in March 1996. The lunar-nodal cycle introduces a 18.6-year gravity-force cycle from the Moon. This cycle produces the 18.6-year lunar-nodal tide in the Atlantic Ocean and the 18.6-year nutation of the Earth axis.

Biomass state dynamics

The system-state dynamics of stock numbers may be represented by the state differential equation

$$\dot{X}(t) = A(t)X(t) + B(t)U(t) + V(t) \quad (3)$$

where X(t) represents a $[n \times 1]$ state vector of the year-class stock numbers, A(t) a $[n \times n]$ system-growth matrix, U(t) a $[n \times 1]$ vector from a known source of

catch, B(t) a $[n \times n]$ binding matrix from the U(t) vectors, V(t) a $[n \times 1]$ disturbance vector from an unknown source $S_v(t)$, and n is the maximum age numbers in the biomass. The disturbance V(t) is expected to have a non-correlated red spectrum. The system-growth matrix A(t) has the elements

$$A(t) = \begin{bmatrix} R(t)Ma(t) \\ S(t) \end{bmatrix} \tag{4}$$

where R(t) is the recruitment-rate function, Ma(t) a $[1 \times n]$ maturing vector, and S(t) is a $[(n-1) \times n]$ survival matrix.

Biomass eigen-frequency

From the state-dynamic model (Equations (3) and (4)), we may formulate the recursive-recruitment model

$$\begin{aligned} x_0(t) &= R(t)Ma(t)x_s(t) + \nu(t) \\ x_0(t) &= R(t)Ma(t)S_n(t)x_0(t-\tau) + \nu(t) \\ x_0(t) &= K(t)x_0(t-\tau) + \nu(t) \end{aligned} \tag{5}$$

where $x_0(t)$ is the recruited-stock numbers, $x_s(t)$ a year-class of spawning-stock numbers, R(t) the recruitment rate, Ma(t) the spawning rate, $S_n(t)$ the survival rate from recruitment to the spawning biomass, and τ is the delay-time from recruitment to a maximum spawning-year class.

According to the general-system model (Equation (1)) there is a binding from the lunar-nodal system $S_n(t)$ to the ocean systems $S_o(t)$ and to the biomass food chain in the Barents Sea. An analysis of the recruitment rate of Northeast Arctic cod and Barents Sea capelin has identified an exponential relationship between the recruitment rate R(t) and the stationary Kola temperature cycles of 6.2 and 18.6 years (Yndestad, 1996a, b, 1999a, b; Yndestad and Stene, 2002). This relation may be expressed by the simplified model

$$K(t) = K\exp(k_1 U(6,t) + k_2 U(18,t)) \tag{6}$$

where K is the recruitment number per spawning biomass, k_1 and k_2 the binding to the Kola temperature cycles, U(6,t) the 6.2-year Kola temperature cycle, and U(18,t) is the 18.6 year Kola temperature cycle. The time-variant recruitment property (Equations (5) and (6)) introduces a:

1. maximum biomass-growth period when U(6,t) and U(18,t) are in a positive state;
2. mean biomass growth when U(6,t) or U(18,t) is in a negative state;
3. minimum biomass growth when U(6,t) and U(18,t) are in a negative state.

The code of long-term biomass cycles

Long-term growth is represented by growth in a set of biomass life cycles. We have a:

1. long-term biomass growth when U(6,t) and U(18,t) are positive in a set of life cycles;
2. short biomass growth when U(6,t) or U(18,t) is negative in a set of life cycles;
3. biomass collapse when U(6,t) and U(18,t) are negative in a set of life cycles.

Frequency modulation

A Fourier transformation of Equation (5) has the frequency transfer-function

$$\frac{x_0(j\omega)}{\nu(j\omega)} = \frac{1}{1 - Ke^{-j\omega\tau}} \tag{7}$$

when $K(t) = K$. This function system is asymptotically stable when $K < 1$. Equation (7) has a singularity for when $K = 1$, $\omega\tau = 2\pi n$, and $n = 0, 1, 2, 3, \ldots, N$. A singularity at an angle-frequency cycle ω_e means that the recruitment $x_0(t)$ will have a frequency cycle $x_0(j\omega_e)$ where the amplitude is amplified to infinity. A singularity in the frequency function will introduce a stochastic resonance in the biomass. In this paper a resonance frequency is called an eigen-frequency. The biomass eigen-frequency cycle is observed at the maximum biomass year class (Yndestad and Stene, 2000). When $K(t) = K\exp(j\omega_0 t)$ the transfer-function has singularities for $K = 1$ and $(\omega\tau + \omega_0 t) = 2\pi n$. This transfer-function has singularities at $\tau = 0$, $\omega 3\tau = \omega_0 t$, and $\omega\tau = \omega_0 3t$. Consequently an interaction between the recruitment feedback (Equations (5) and (7)) and the stationary forced cycle (Equation (6)) is expected to introduce a 3. harmonic and a 3. sub-harmonic cycle in the biomass time-series. When $\omega_0 = 2\pi/T_0 = 2\pi/18.6$ (rad/year), there will be singularities in cycles of $T_0 = 18.6$, $T_0/3 = 6.2$, and $3T_0 = 55.8$ years.

Cycle identification

The gravity from the stationary 18.6-year lunar-nodal cycle is expected to have an influence on all the elements of the Barents Sea system (Equations (2) and (3)). We may then present the hypothesis that time-series from the Barents Sea have a set of stationary cycles represented by the state model

$$x(t) = \sum_k U(k,t) + \nu(t) \tag{8}$$

$$U(k,t) = u(k,t)\sin(k\omega_0 t + \varphi(k,t))$$

where x(t) is the measured time-series, U(k,t) a dominant stationary cycle, k a cycle period, and $\nu(t)$ is a disturbance from an unknown source. The temporary stationary cycle U(k,t) has an amplitude u(k,t), an angle frequency $\omega_k = 2\pi/k$, (rad/year), and a time-variant phase angle $\varphi(k,t)$.

The time-series are analyzed by a wavelet transformation to identify a dominant cycle period U(k,t) and the time-variant phase angle φ(k,t). The set of dominant cycle periods are identified by a four-step investigation. The first step is to compute the wavelet spectrum by the transformation

$$W(a,b) = \frac{1}{\sqrt{a}} \int_R x(t) \Psi\left(\frac{t-b}{a}\right) dt \qquad (9)$$

where x(t) is the analyzed time-series and Ψ( ) is the wavelet-impulse function, W(a,b) a set of wavelet cycles, b the translation in time and a is the time-scaling parameter in the wavelet transformation. The computed wavelets W(a,b) represent a correlation between x(t) and the impulse functions Ψ( ) over the whole time-series x(t). The Coiflet3 wavelet transformation was chosen after many trials on tested data. By this wavelet transformation it is possible to identify single long-period cycles in short time-series. Errors in long-period estimates are reduced by the "sym" property in Matlab (Daubehies, 1992; Matlab, 1997).

The computed wavelet transformation has a set of wavelets W(1,…,m,b). Dominant wavelet cycles in W(1,…,m,b) have a maximum amplitude as the result of the best correlation to cycles in the time-series x(t). The most dominant cycle W(k,b) in the wavelet set W(1,…,m,b) is identified by a maximum cycle amplitude. The source of a dominant wavelet cycle W(k,b) is identified by computing the cross-correlation coefficient r(k) between a dominant wavelet cycle W(k,b) and a known stationary cycle U(k,t). The phase delay between time-series is identified by the phase difference $\varphi_d(k,t) = \varphi_i(k,t) - \varphi_j(k,t)$.

Results

The Barents Sea system (Equation (1)) has a mutual interaction B(t) between the Earth-nutation system $S_n(t)$, the ocean system $S_o(t)$, the food-chain system $S_f(t)$, and the fish-biomass systems $S_f(t)$. According to the general-systems theory a dominant 18.6-year gravity-force cycle from lunar-nodal cycle $S_n(t)$, will influence all the others. In this investigation long-term cycles of the Kola Section temperature in the Barents Sea, Norwegian spring herring, Northeast Arctic cod and Barents Sea capelin are analyzed.

Kola Section temperature

The oceanographic system $S_o(t)$ is a complex time-variant dynamic process influenced by sea currents and atmospheric conditions. To reduce complexity, the Kola Section data are chosen as a climate indicator to represent the temperature in the Barents Sea.

The Kola Section time-series is an indicator of Atlantic inflow to the Barents Sea. A wavelet transform (Equation (9)) of the Kola temperature series $x_K(nT)$ has a wavelet set $W_K(1:80,nT)$. In this wavelet set the dominant cycles $W_K(6,nT)$, $W_K(18,nT)$, $W_K(55,nT)$, and $W_K(74,nT)$, are identified and they have a cycle time of 6, 18, 55, and 74 years, respectively (Figure 1). The 6-year wavelet $W_K(6,nT)$ has a maximum at the years 1907, 1915, 1921, 1930, 1937, 1944, 1951, 1961, 1975, 1983, and 1991, the 18-year wavelet $W_K(18,nT)$ has a maximum at the years 1909, 1922, 1935, 1955, 1973, and 1991, the 55-year wavelet $W_K(55,nT)$ has a maximum in 1945 and 2000. The correlation coefficient between the data series $x_K(nT)$ and

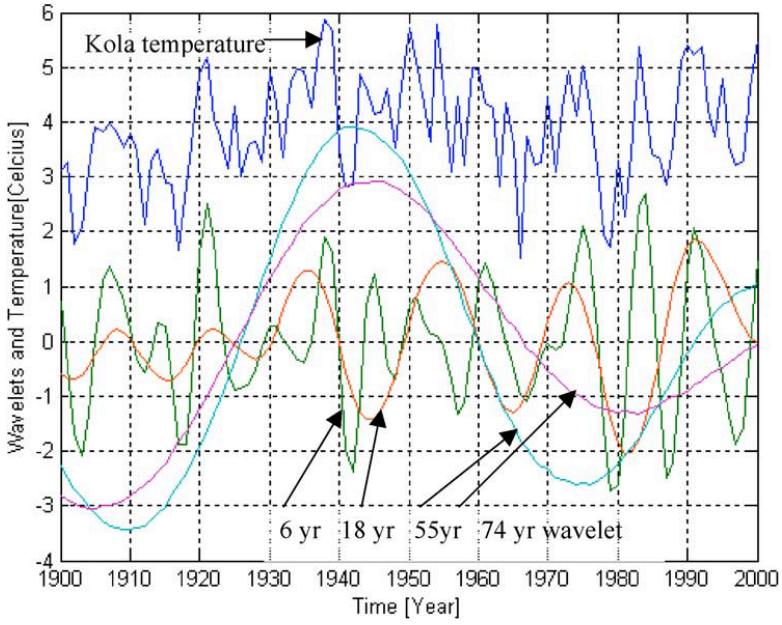

Figure 1. The time-series of Kola Section temperature series and the dominant 6-, 18-, 55-, and 74-year wavelet cycles.

the estimated, dominant wavelet cycles is $r_{uw} = 0.73$. The identified, dominant wavelet cycles are correlated to the lunar-nodal cycles

$$\begin{aligned}
&U_K(74,nT) = u_K(74,nT)\sin(\omega_n nT/4 + 0.29\pi)\\
&\quad \text{when } n = 1900,\ldots,2000\\
&U_K(55,nT) = u_K(55,nT)\sin(\omega_n nT/3 + 0.90\pi)\\
&\quad \text{when } n = 1900,\ldots,2000\\
&U_K(18,nT) = u_K(18,nT)\sin(\omega_n nT + \varphi_K(18,nT))\\
&\quad \text{when } n = 1900,\ldots,2000\\
&U_K(06,nT) = u_K(6,nT)\sin(3\omega_n nT + \varphi_K(6,nT))\\
&\quad \text{when } n = 1900,\ldots,2000
\end{aligned} \tag{10}$$

The 74-year cycle $W_K(74,nT)$ has a trend shift in 1925 and 1960, minimum values in 1905 and 1980, and a maximum in 1945. The cross-correlation coefficient between the wavelet cycles $W_K(74,nT)$ and $W_K(55,nT)$, and the lunar-nodal cycles $U_K(74,nT)$ and $U_K(55,nT)$, are $r_{uw}(74) = 0.95$ and $r_{uw}(55) = 0.89$. The 74-year cycle introduces a phase reversal on the 18- and 6-year cycles. The phase angle $\varphi_K(18,nT) = 0.90\pi$ (rad) in the period $n = 1930,\ldots,2000$ and $\varphi_K(18,nT) = 1.90\pi$ in the period $n = 1900,\ldots,1930$. There was a phase reversal when the 74-year cycle shifted from a negative to a positive state. The correlation coefficient $r_K(18) = 0.90$ when the phase angle $\varphi_K(18,nT)$ is shifted in this period. The 6-year cycle has a correlation coefficient $r_K(6) = 0.4$ when $\varphi_K(6,nT) = -0.09\pi$ (rad) in the period $n = 1930,\ldots,1970$ and the 74-year cycle is in a positive state. The phase angle has a phase reversal to $\varphi_K(6,nT) = -1.09\pi$ (rad) in the period $n = 1970,\ldots,2000$ when the 74-year cycle is in a negative state.

The phase relation between the dominant Kola temperature cycles is expected to have a major influence on the biomass growth in the Barents Sea (Equations (4)–(7)). The identified 6- and 18-year wavelet cycles are positive at the same time in the years 1907, 1921, 1937, 1951, 1975, and 1991. According to the code of long-term growth we may expect a

- Maximum biomass-growth period from $1920,\ldots,1937$
- Medium biomass-growth period from $1900,\ldots,1920$ and $1945,\ldots,1975$
- Minimum recruitment or biomass collapse in 1905, 1942, 1966, and 1979

(11)

Norwegian spring-spawning herring

The Norwegian spring-spawning herring system $S_h(t)$ may be modelled by the simplified general system $S(t) = \{B_B(t),\{S_n(t),S_o(t),S_f(t),S_{ca}(t),S_{he}(t),S_{co}(t),S_v(t)\}\}$ (Equation (1)) where $B_B(t)$ represents a mutual binding between each system element. In this simplified system the capelin system $S_{ca}(t)$, the herring system $S_{he}(t)$, and the cod system $S_{co}(t)$ are mutually related as food and predators. If the nodal system $S_n(t)$ influences the food chain, it will influence the biomass long-term growth.

The spawning-biomass time-series of Norwegian spring-spawning herring has a mean weight-of-age vector

$$\begin{aligned}
Xs_{he}(age) = [\ &0 \quad 0.5 \quad 14.0 \quad 94.8 \quad 37.4\\
&569.9 \quad 561.2 \quad 428.7 \quad 332.9 \quad 281.0]\ 1000\ \text{tons}
\end{aligned}$$

Maximum spawning biomass is 569 900 tons at the age of 6 years. The herring biomass then has an eigen-frequency of about $X_{he}(j\omega_e) = 2\pi/T_{he} = 2\pi/6.2$ (rad/year). The herring biomass eigen-frequency cycle of $T_{he} = 6.2$ years and the interacting dominant Kola temperature cycles of $T_0/3 = 6.2$, $T_0 = 18.6$ and $3T_0 = 55.8$ years are expected to introduce dominant, harmonic biomass cycles of $T_{her} = 6.2$, $3T_{her} = 18.6$, and $6T_{her} = 55.8$ years (Equation (7)).

Herring recruitment rate

The herring recruitment-rate time-series is computed by $R_{he}(nT) = x_0(nT)/x_S(nT)$ from 1907 to 1999 where $x_0(nT)$ is the recruited numbers (in millions) of herring and $x_S(nT)$ is the spawning biomass (tons) (Figure 2). A wavelet transform (Equation (9)) of the recruitment-rate time-series $R_{he}(nT)$ has the wavelet set $W_{he}(1{:}80,nT)$. In this wavelet set the dominant cycles are $Wr_{he}(6,nT)$, $Wr_{he}(18,nT)$, and $Wr_{he}(55,nT)$, which have a cycle time of 6, 18, and 55 years (Figure 1). The 6-year wavelet $Wr_{he}(6,nT)$ has a maximum value at the years 1913, 1918, 1924, 1930, 1937, 1944, 1950, 1957, 1963, 1983, and 1993; the 18-year wavelet $Wr_{he}(18,nT)$ has a maximum value at the years 1920, 1938, 1973, and 1992, and the 55-year wavelet $Wr_{he}(55,nT)$ has a maximum value at the years 1927 and 1982. The cross-correlation coefficient between the herring spawning-biomass recruitment rate $R_{he}(nT)$ and the dominant wavelet cycles $Wr_{he}(nT) = [Wr_{he}(6,nT) + Wr_{he}(18,nT) + Wr_{he}(55,nT)]$ is $r_{xw} = 0.60$. The estimated recruitment wavelet cycles $Wr_{he}(6,nT)$ and $Wr_{he}(18,nT)$ have a maximum at about the same years as the Kola temperature cycle $W_K(6,nT)$ and $W_K(18,nT)$ in the period $n = 1910,\ldots,1950$ and from $n = 1970,\ldots,2000$. This mean that the recruitment cycles of herring have the same cycle time and phase as the Kola Section temperature cycles.

The identified recruitment-rate wavelet cycles confirm the code of long-term growth (Equations (7) and (11)). There was a set of three 6-year cycles in the period from 1920 to 1937 when the 6- and 18-year Kola temperature cycles were positive at the same time. The same situation happened in the period 1972–1991. From 1937 to 1950 there was a period of about $2 \times 6.2 = 12.4$ years to the next optimum recruitment in 1950. The next optimal recruitment came in 1972. The recruitment came after a period of $4 \times 6.2 = 24$ years. The estimated 55-year

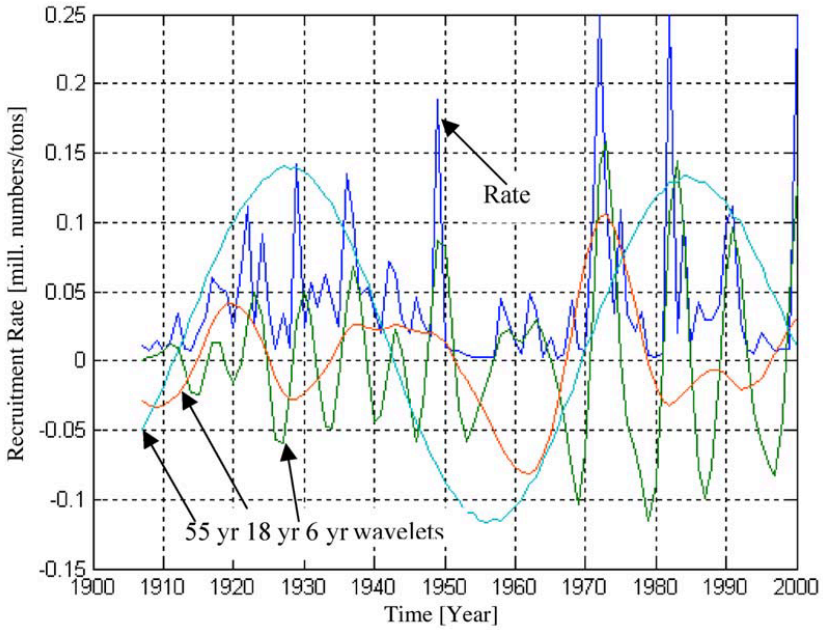

Figure 2. Herring recruitment rate and the dominant wavelet cycles of 6, 18, and 55 years.

cycle $Wr_{he}(55,nT)$ has information about the mean dynamic trend of the recruitment rate. The 55-year wavelet cycle has a maximum in 1937 and 1982.

Herring stock number

Figure 3 shows the stock-number time-series of Norwegian spring-spawning herring from 1906 to 2000 and the identified dominant wavelet cycles of 6, 18, and 55 years. The 6-year wavelet cycle $Wn_h(6,nT)$ has a maximum value at the years 1919, 1925, 1932, 1938, 1945, 1951, 1959, 1984, 1992, and 2000, the 18-year wavelet $Wn_h(18,nT)$ has a maximum value at the years 1922, 1938, 1964, and 1994, and the 55-year cycle $Wn_h(55,nT)$ has a maximum value in 1935 and 1995. The identified dominant wavelet cycles of stock numbers have a delay of about 1 year compared to the recruitment-rate wavelet cycles. The data series is influenced by a collapse in the period 1965−1990 which was caused by overfishing. The cross-correlation coefficient between the herring spawning-biomass recruitment rate R(nT) and the dominant wavelet cycles $Wn_{he}(nT) = [Wn_{he}(6,nT) + Wn_{he}(18,nT) + Wn_{he}(55,nT)]$ is $r_{Rw} = 0.81$. The wavelet cycles of stock numbers are closely related to the recruitment-rate wavelet cycles since stock numbers are dominated by 1-year recruitment. The estimated wavelet cycles show that the stock numbers have modulated cycles of about $T_{he} = 6.2$, $3T_{he} = 18.6$, and $6T_{he} = 55.8$ years which are harmonic cycles of the biomass eigen-frequency cycle time of $\tau_{he} = 6.2$ years.

The stock number increased in the growth period from 1920 to 1937 when the 6.2- and 18.6-year Kola cycle were positive at the same time. The stock numbers were reduced to a medium level in the period from 1945 to 1970 when the 6.2- and 18.6-year Kola temperature cycle were not positive at the same time. In 1965 the 6.2- and 18.6-year cycle were negative at the same time and there was a collapse in the stock numbers. The 55-year wavelet cycle $Wn_{he}(55,nT)$ describes the position of the mean number of herring. This cycle has a maximum in 1937 and 1995.

This analysis shows that the stock-number reduction started about 1937 when there was no longer a match between the optimum Kola temperature cycles and the biomass eigen-frequency cycle. When the biomass collapsed in 1965 there was a minimum condition of new recruitment (Equation (11)). The biomass collapse must then be a combination of climate change and overfishing.

Herring biomass

Figure 4 shows the biomass time-series $xb_{he}(nT)$ of Norwegian spring-spawning herring from 1906 to 2000 and the identified, dominant biomass-wavelet cycles of 6, 18, and 55 years. The 6-year wavelet cycle $Wb_{he}(6,nT)$ has a maximum in 1910, 1929, 1927, 1924, 1945, 1955, 1964, and 1998, the 18-year wavelet $Wb_{he}(18,nT)$ has a maximum in 1910, 1918, 1952, and 1995, and the 55-year cycle $Wb_{he}(55,nT)$ in 1940 and 2000. In this data series the biomass had a collapse in the period 1965−1990 which was caused by overfishing. The cross-correlation coefficient between the herring spawning-biomass time-series $xb_{he}(nT)$ and the dominant wavelet cycles sum $Wb_{he}(nT) = [Wb_{he}(6,nT) + Wb_{he}(18,nT) + Wb_{he}(55,nT)]$, is $r_{xw} = 0.81$. The estimated wavelet cycles show the biomass has modulated cycles of about $T_{he} = 6.2$, $3T_{he} = 18.6$, and $6T_{he} = 55.8$ years which are harmonic cycles of the biomass-resonance cycle time of $\tau_{he} = 6.2$ years.

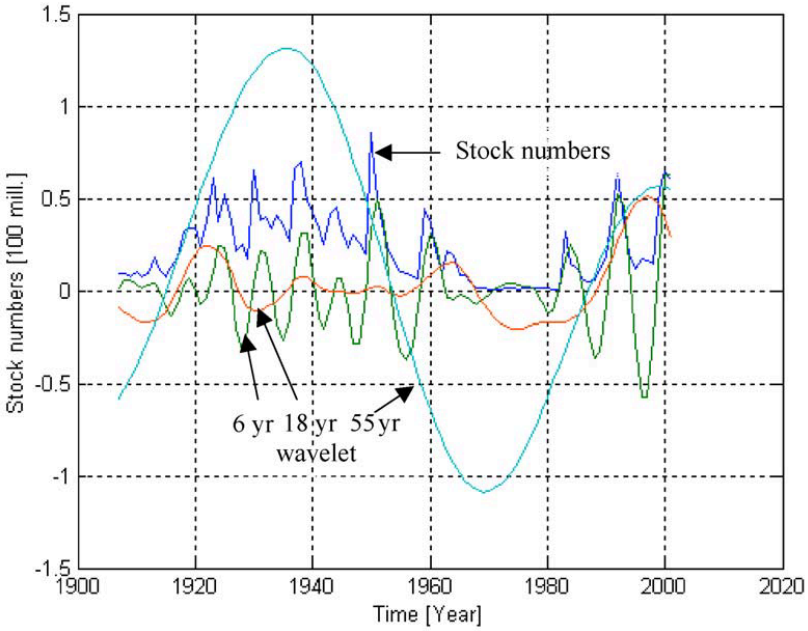

Figure 3. Stock numbers (100 million) of Norwegian spring-spawning herring and the dominant wavelet cycles of 6, 18, and 55 years.

The 6- and 18-year Kola Section temperature cycles were positive at the same time in 1921, 1930, and 1937. In this period there was an optimum recruitment of three life cycles. Each life cycle had a cycle time of about 6 years and the biomass grew over the long-term from about 5−25 million tons (Figure 4). In 1942 the 6- and 18-year Kola cycles were negative at the same time. This introduced a collapse situation and the biomass growth had a turning point. In 1945 only the 6-year Kola cycle temperature was positive and the biomass was slightly reduced. After a period of 2×6.2 years the 6- and 18-year Kola cycles were again positive at the same time. The optimal condition kept the level of the large biomass for about 5 years.

From 1950 there were four optimal life cycles in a period of about $4 \times 6.2 = 24.8$ years before there was a new optimum Kola temperature-cycle condition in 1975. In this period there was no optimum growth condition over a set of biomass life cycles and the biomass was reduced to about

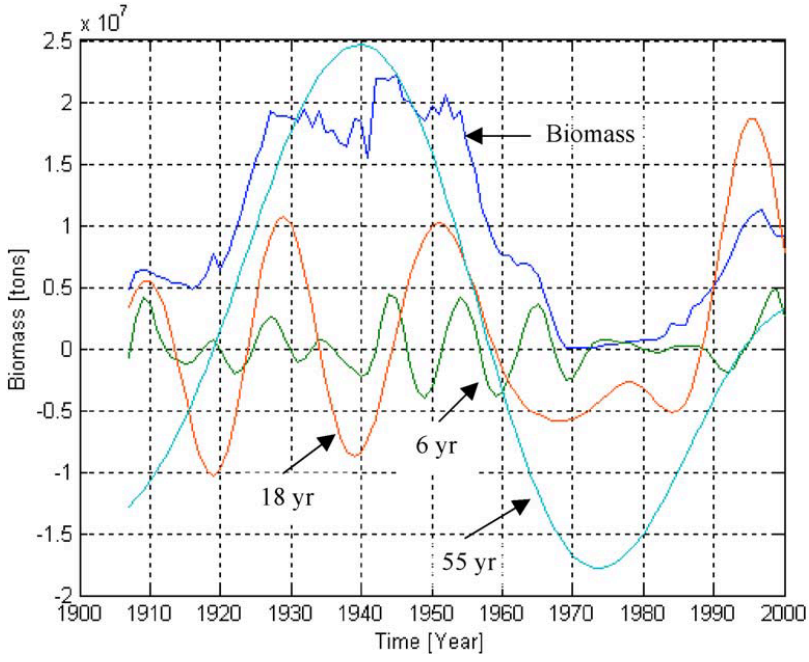

Figure 4. The biomass of Norwegian spring-spawning herring and the 6-, 18-, and 55-year wavelets.

seven million tons in 1960. In 1965 the 6- and 18-year Kola temperature cycles were negative at the same time and there was a total collapse in the biomass. It has been a common belief that the biomass collapse in 1965 was caused by overfishing. This analysis shows that the biomass reduction started about 25 years earlier.

The 6- and 18-year Kola temperature cycles were positive again in 1975 and 1991. A positive 6-year Kola cycle introduced a small growth in 1972 and 1982 (Figures 1–3) and when both temperature cycles were positive in 1991, the biomass again increased to about 10 million tons.

Northeast Arctic cod

The Northeast Arctic cod system $S_{co}(t)$ is part of the simplified Barents Sea system $S(t)=\{B_B(t),\{S_n(t), S_o(t),S_f(t),S_{ca}(t),S_{he}(t),S_{co}(t),S_v(t)\}\}$ (Equation (1)) where $B_B(t)$ represents binding between each system element. In this simplified system there is a mutual relation between all systems. If there is one stationary energy source, it will influence the cod system.

The spawning-biomass time-series of Northeast Arctic cod has a mean weight-of-age vector

$$Xs_{co}(age)=[\ 0\quad 201\quad 6078\quad 20341\quad 65388\quad 103012\quad 93124\quad 63528\quad 41586\quad 13932]\ \text{tons}$$

from age 1 until age 10 years. The maximum biomass year class is 103 012 tons at the age of 6 years. Then the cod biomass has an eigen-frequency at about $X_{co}(j\omega_e) = 2\pi/T_{co} = 2\pi/6.2$ (rad/year). This means that the biomass of Northeast Arctic cod has a resonance close to the $\tau_{co} = 6.2$ years which is the same cycle time as the biomass eigen-frequency cycle time τ_{he} of Norwegian spring-spawning herring and the Kola temperature cycle of $T_K/3 = 6.2$ years. The cod-biomass cycle time $\tau_{he} = 6.2$ years and the interacting dominant Kola temperature cycles of $T_K/3 = 6.2$, $T_K = 18.6$ and $3T_K = 55.8$ years are expected by the approach taken here to introduce dominant cycles of $T_{co}=6.2$, $3T_{co}=18.6$, and $6T_{co}=55.8$ years (Equation (7)).

Cod biomass

A wavelet transform (Equation (9)) of the time-series $x_{co}(nT)$ of Northeast Arctic cod has identified a set of wavelets $Wb_{co}(1{:}50,nT)$ (Figure 5). The computed wavelet set has dominant wavelets of 6 and 18 years. The 6-year wavelet $Wb_{co}(6,nT)$ has a maximum value at about the years 1903, 1912, 1923, 1926, 1936, 1945, 1955, 1961, 1968, 1975, 1986, and 1993, and the 18-year wavelet $Wb_{co}(18,nT)$ has a maximum value at the years 1906, 1925, 1941, 1952, 1973, and 1995. The cross-correlation coefficient between the biomass time-series $x_{co}(nT)$ and the identified dominant wavelet cycles sum $Wb_{co}(nT)=[Wb_{co}(6,nT)+Wb_{co}(18,nT)+Wb_{co}(55,nT)]$ is $r_{xw}=0.87$. The dominant wavelet cycles have the same cycle time as the dominant Kola Section temperature cycles, but lag by about $\tau_{co} = 6.2$ years. This delay is the time from recruitment to a maximum year class of about 6 years. The estimated 55-year wavelet is influenced by low fishing activity from 1940 to 1945 and in 1983 there was a collapse in the biomass.

The identified dominant biomass cycles confirm the code theory of long-term growth (Equations (7) and (11)). The biomass of Northeast Arctic cod had a growth period from 1920 to 1945 when the 6- and 18-year Kola Section cycles were positive at the same time in 1921, 1930, and 1937. After a delay of about 6 years (τ_{co} years) the cod biomass was maximum in 1928, 1940, and 1946. The biomass had a reduction from 1945 to 1980. Again the 6- and 18-year Kola cycles were positive at the same time only in the years 1962, 1973, and 1975. In these years the biomass had a small growth in 1960 and a strong growth in 1968 and 1975. These estimates demonstrate that the biomass of Northeast Arctic cod grows when the 6-, 18-, and 55-year Kola Section temperature cycles are positive. This analysis shows that the long-term biomass cycles of Northeast Arctic cod have the same character as the long-term cycles of Norwegian spring-spawning herring.

Cod catch

It is a common belief that there is a close relationship between catch and stock numbers and so the same dominant cycles in each parameter are expected (Figure 6). The wavelet set $Wc_{co}(1:80,nT)$ has been computed from the time-series $xc_{co}(nT)$ of cod in Lofoten (Godø, 2000) in the period 1864–1978 and does have the same dominant wavelets of 6, 18 and 55 years as estimated in the biomass time-series. The 6-year wavelet cycle $Wc_{co}(6,nT)$ has a maximum value in the years 1880, 1886, 1896, 1905, 1915, 1921, 1927, 1939, 1946, 1952, 1961, and 1972, the 18-year wavelet cycle $Wc_{co}(18,nT)$ has a maximum value at the years 1880, 1892, 1910, 1928, 1946, and 1970, and the 55-year wavelet $Wc_{co}(55,nT)$ has maximum values in the years 1885 and 1938. The cross-correlation coefficient between the time-series of catch and the estimated dominant wavelet cycles $Wc_{co}(nT) = [Wc_{co}(6,nT) + Wc_{co}(18,nT) + Wc_{co}(55,nT)]$ is $r_{xw} = 0.82$. The dominant wavelet cycles of catch numbers have the same cycle time as in the biomass time-series. The different cycle-phase is explained by the difference between the stock-number distribution and the biomass distribution.

The dominant 6- and 18-year wavelets of the Lofoten catch have the same pattern as the dominant biomass-wavelet cycles. The growth period was from 1920 to 1940, while the decline was from 1940 to 1960. In these data the long-term reduction of biomasses occurs earlier because of less fishing effort in the period 1940–1945. The catch grew from 1877 to 1895 when the 6- and 18-year cycles were positive at the

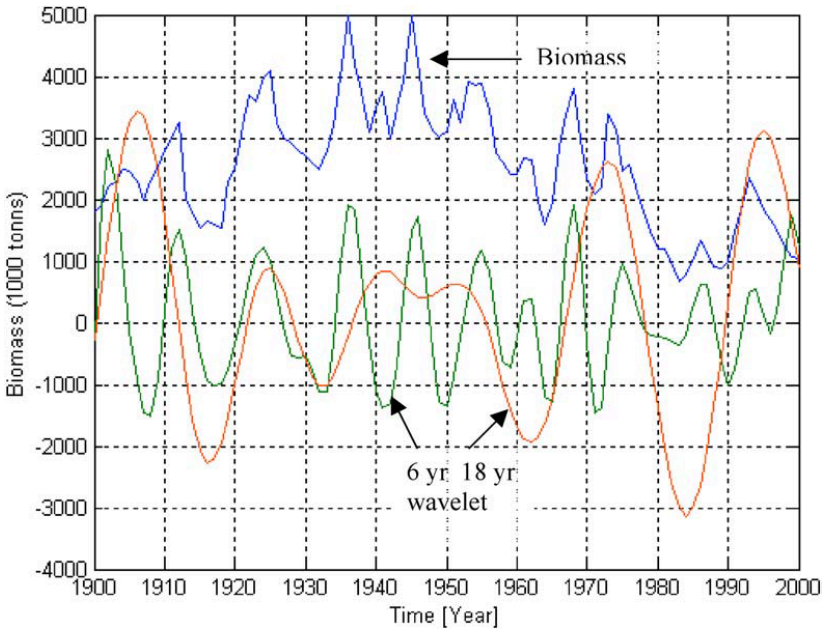

Figure 5. The time-series of the Northeast Arctic cod biomass and computed wavelets of 6 and 18 years.

same time and was reduced in the period 1900−1920 when only in 1908 were the wavelet cycles positive at the same time. The 55-year wavelet indicates that the biomass has a natural long-term fluctuation of about 55 years.

Barents Sea capelin

The Barents Sea capelin stock is of vital importance in the Arctic food web. It is the main plankton feeder in the area and serves as an important forage fish for other fish stocks, seals, whales, and sea birds. The capelin is therefore influenced by its abiotic environment and by the abundance of food, predators, and fisheries.

The Barents Sea capelin-system biomass $S_c(t)$ is thus influenced by a set of external systems in the Barents Sea. The recruitment dynamics of Barents Sea capelin are dependent on a complex set of conditions such as the life-cycle time, the eigen-frequency, the predator life cycles, catch-to-landings, the sea temperature, and food supply. If

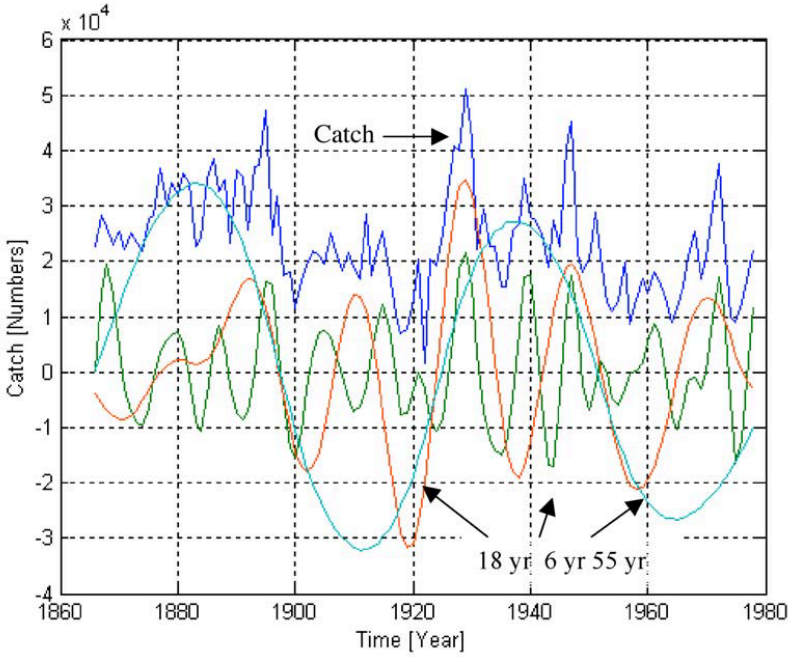

Figure 6. The catch numbers of Northeast Arctic cod at Lofoten and the computed wavelets of 6, 18, and 55 years.

one of these external systems has a dominant property it will influence the long-term capelin dynamics.

The spawning-biomass time-series of Barents Sea capelin has a mean weight-at-age vector $Xs_{ca}(age) = [0.0\ 0.0\ 29.3\ 12.8\ 0.3]$ in 1000 tons. Maximum spawning biomass is 29 300 tons at the age of 3 years. This means that the 3-year-old capelin is the most dominant year class in the spawning stock. A frequency analysis of the capelin stock numbers has identified an eigen-frequency cycle time $\tau_{ca} = 3.1$ years, which introduces large fluctuations in the biomass (Yndestad and Stene, 2001).

The interacting Kola Section temperature in the Barents Sea has dominant stationary cycles of $T_0 = 18.6$ years and $T_0/3 = 6.2$ years. The eigen-frequency cycle at $\tau_{ca} = 3.1$ years and the interacting dominant Kola temperature cycles should introduce dominant cycles of $T_{ca} = 3.1$, $2T_{ca} = 6.2$, $3T_{ca} = 9.3$, and $6T_{ca} = 18.6$ years (Equation (7)). A biomass eigen-frequency period of about $6.2/2 = 3.1$ years implies that the biomass will have a different dynamic property compared to the herring biomass and the cod biomass.

A wavelet transform of the Barents Sea capelin time-series $x_{ca}(nT)$ from 1946 to 2000 has a set of wavelets $Wb_{ca}(1:30,nT)$. In this wavelet set there are dominant wavelet cycles of 6 and 18 years. The 6-year wavelet cycle $W_{ca}(6,nT)$ has a maximum value around the years 1951, 1960, 1969, 1975, 1983, and 1991 and the 18-year wavelet cycle $W_{ca}(18,nT)$ has a maximum value at about the years 1951, 1975, and 1994. The cross-correlation coefficient between the biomass time-series $x_{ca}(nT)$ and the dominant wavelet sum $W_{ca}(nT) = [W_{ca}(6,nT) + W_{ca}(18,nT)]$ is $r_{xw} = 0.72$.

The 18-year cycle $W_{ca}(18,nT)$ has a maximum around the years 1952, 1975, and 1994. This is a growth delay of about $\tau_{ca} = 3.1$ years compared to the 18-year cycle of the recruitment rate and the 18-year Kola Section wavelet cycle $W_K(18,nT)$. Potential errors in these cycle estimates are the short-time series and the collapses of the biomass in 1985 and 1995. The computed wavelet cycles show an 18-year cycle and a higher-frequency cycle shifting between a period of about 6 and 9 years. The 18-year cycle follows the 18-year Kola temperature cycle, which had maximum values at about the years 1955, 1972, and 1991. When the 18-year cycle is in a negative state the biomass growth is dependent on the relationship between the 6-year Kola temperature cycle and the $6.2/2 = 3.1$ year biomass eigen-frequency cycle. Figure 7 shows that this introduces a 9-year cycle time when the 18-year Kola cycle is negative and a 6-year cycle time when the 18-year Kola cycle is positive. These estimated wavelet cycles confirm that the biomass has modulated cycles of about $2T_{ca} = 6.2$, $3T_{ca} = 9.3$, and $6T_{ca} = 18.6$ years which are sub-harmonic cycles of the biomass eigen-frequency cycle time of $\tau_{ca} = 3.1$ years.

The recruitment rate R(nT) has a maximum around the years 1976, 1981−1982, 1989−1990, and 1995−1997 which are close to the maximum of the Kola temperature cycles. The recruitment rate R(nT) had a maximum when the 6.2-year cycle or the 18.6-year temperature cycle had a maximum (Yndestad and Stene, 2001). This change in the recruitment cycle introduces dominant biomass cycles of about $2T_{ca} = 6.2$ years when the 18.6-year temperature cycle had a positive state and a cycle of $3T_{ca} = 9.3$ years when the 18.6-year cycle was in a negative state.

The Barents Sea capelin has a short eigen-frequency cycle time of about $\tau_{ca} = 3.1$ years. The biomass then has maximum growth each time the 6.2-year Kola cycle is positive. The capelin biomass has a growth time of about three years and a cycle time of about six years. The short eigen-frequency cycle time influences how the biomass-cycle phase is able to adjust to the 6.2- and 18.6-year Kola temperature cycle. The biomass had a maximum growth in period 1951, 1960, 1970, 1975, and 1991 when the 6.2- and 18.6-year Kola temperature cycles were positive at the same time. The biomass had a minimum level in 1950, 1965, 1978, and 1995 when the 6.2-year Kola cycle had a minimum. In 1987 and 1995 the biomass changed from a minimum to a collapse.

When the 6.2- and 18.6-year temperature cycles have a negative state, it takes about $3\tau_{ca} = 9.3$ years for the adjustment to an optimum condition. In this period the recruitment system (Equation (5)) is shifted from a positive-feedback system to that of negative-feedback. The result is a collapse in the biomass as happened in 1955, 1963, and 1986. The collapse in 1995 was most likely caused by overfishing in the 1980s (Yndestad and Stene, 2001). The short eigen-frequency cycle time of $\tau_{ca} = 3.1$ years made it possible to adapt the next biomass cycle to the next 6.2-year temperature cycle in 1960 and 1991.

This analysis shows that the biomass of Barents Sea capelin has a long-term growth when the 6- and 18-year Kola Section temperature cycle has a positive state and a pronounced decline when both temperature cycles have a negative state. When the 18-year Kola cycle turns to a negative state the biomass loses the synchronic phase relation between the biomass eigen-frequency cycle and the Kola temperature cycles. After a cycle time of $3\tau_{ca}$ years there is a new adaptation and a new growth period. In a long time-series this adaptation is shown as a cycle phase reversal and the cycle time is increased from six to nine years.

Discussion

The dominant biomass dynamics in the Barents Sea are a result of different environmentally random, mutual interactions between the ocean system, the food chain, catch, and a multi-species system (Equation (1)). A frequency analysis of the long-term time-series from this system is expected to be represented by a non-deterministic and non-correlated red spectrum. The approach taken in this paper produces a different result.

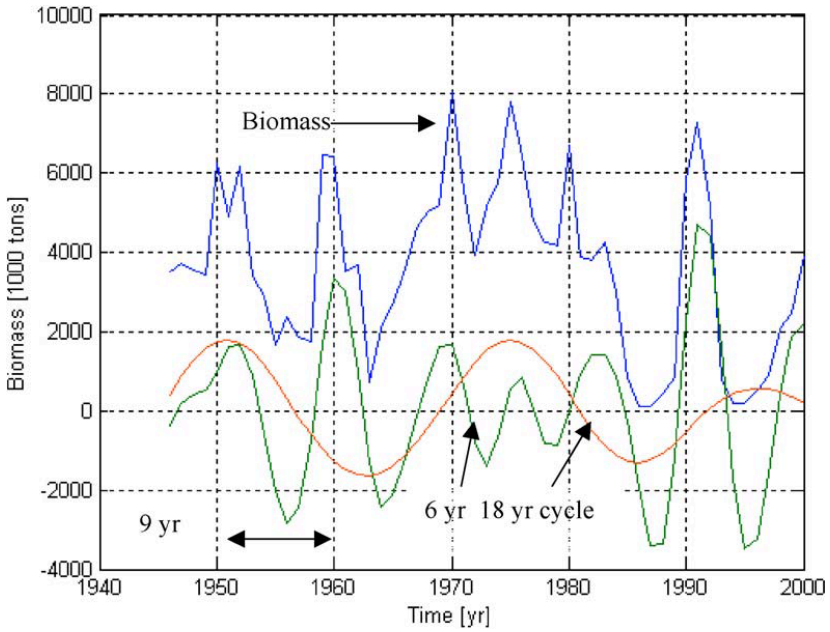

Figure 7. The Barents Sea capelin biomass and the dominant-wavelet cycles of 6 and 18 years.

The code of biomass dynamics

In this investigation, fluctuations in Kola Section temperatures and the stocks of the Barents Sea capelin, the Norwegian spring-spawning herring and Northeast Arctic cod are analyzed by a wavelet transformation to identify the source of dominant biomass fluctuations. The results show a common source of long-term biomass cycles.

The forced oscillator

The Kola Section temperature has dominant temperature cycles of about 6.2, 18.6, and 55 years which are related to the 18.6-year lunar-nodal tide. The 18.6-year temperature cycle is expected to be a deterministic cycle controlled by gravity from the Moon. This cycle behaves like a forced, oscillating temperature cycle, which will influence the biomass dynamics in the food chain.

Eigen-frequency biomass cycle

The biomass of herring, cod and capelin has an eigen-frequency biomass cycle which is adapted to the 6.2-year temperature cycle in the Barents Sea.

The long-term biomass growth

The long-term biomass growth is related to a set of optimal recruitment periods when the 6- and 18-year Kola Section temperature cycles are positive at the same time. In this period the 6-year eigen-frequency of recruitment has an optimal growth in a period of three to four life cycles.

Long-term biomass reduction

The long-term biomass reduction is related to a period when the 6- and 18-year Kola Section temperature cycles are not positive at the same time. The growth and reduction of biomass is therefore not related to the absolute temperature value, but rather to the phase relation between the dominant eigen-frequency cycle and the Kola temperature cycles in the Barents Sea.

The biomass collapse

The biomass collapse is related to a period when the 6- and 18-year Kola Section temperature cycles are negative at the same time. In this period there are poor conditions of recruitment and growth over a period of two to four life cycles.

The three causes of fluctuation

There are three causes of fluctuation in the biomasses. The 6-year cycle in herring and cod is caused by the biomass eigen-frequency, which is a feedback property where optimal recruitment is adapted to the 6.2-year Kola temperature cycle. The 18-year biomass cycle is related to a period of about nine years when there was good recruitment. The long-term 55-year cycle is caused by a chain of optimal life cycle recruitment.

The biomass fluctuations in the Barents Sea may be explained by a deterministic model. According to this model the optimum biomass life-cycle time is linked with the Kola temperature cycles of 18.6 and $18.6/3 = 6.2$ years. Biomass growth, reduction, and collapse are associated with the phase relation between these cycles.

The Norwegian spring-spawning herring

The Norwegian spring-spawning herring stock has been characterized by large fluctuations. Norwegian historical records document good herring periods from 1500 to 1570, 1600 to 1650, 1690 to 1774 and from 1808 to 1874 (Vollan,

1971). These records show biomass fluctuations of about 50−80 years. The findings in this paper support the theory that long-term biomass fluctuations in the Barents Sea have a cycle of 55−74 years. The changes from 50 to 80 years may be explained by a time-variant phase in the biomass cycle, which is controlled by the 74-year temperature cycle.

There is a common belief that the collapse in 1965 was caused by overfishing. The results here show that the biomass reduction started 30 years earlier as a climate-driven process. In the long-term period of less recruitment from 1940 to 1965, overfishing increased the speed of biomass reduction. The biomass collapsed in 1965 when the 6- and 18-year temperature cycles were negative at the same time. The new biomass-growth period came from 1992 when the 6.2-, 18.6-, and 55.8-year Kola Section temperature cycles were again in a positive state.

The Northeast Arctic cod

The wavelet-cycle analysis shows that the Northeast Arctic cod has the same growth and reduction cycles as the Norwegian spring-spawning herring. The dominant cycles of 6.2-, 18.6-, and 55.8-years support cycles of 18.6 years in the biomass identified in earlier studies (Wyatt *et al.*, 1994; Yndestad, 1999b). The adopted 6.2-year biomass eigen-frequency cycle and the 55-year cycle in Lofoten catch, indicates very long-term cycles.

The estimated relationship between biomass cycles and temperature cycles supports the "matching" theory of Hjort (1914) at a macro level. In that paper he analyzed the length distribution of Northeast Arctic cod and explained fluctuations in the biomass as caused by a match between the spawning time and food for the larvae.

The Barents Sea capelin

The Barents Sea capelin stock has an eigen-frequency cycle of about $6.2/2 = 3.1$ years. In the time-series from 1945 to 2000 the biomass has an increased growth rate when the 6.2- and 18.6-year Kola Section temperature cycles are in a positive state. The biomass was reduced from six to two million tons in 1955 and in 1964 when the 6.2- or 18.6-year Kola Section temperature cycles were in a negative state. In 1987 there was a new collapse in the biomass. This collapse was partly caused by the lower temperatures when the 6.2- and 18.6-year cycles were in a negative state, and partly by overfishing. The biomass collapse in 1993 is explained by the overfishing in the 1980s, which caused a limited age distribution in the capelin stock (Yndestad and Stene, 2001).

Some aspects of the materials and methods

The analytical approach that has been taken has some potential sources of errors. For example, there may be errors in the data samples, which cannot be controlled. In this investigation long trends in the data are analyzed and so changes in the methods of estimating data may then influence the long-term cycles. A potential source of a long-term error in long-term fluctuations is between linked-up time-series. The herring time-series has a link-point in 1946, the cod time-series in 1946, the Lofoten catch in 1958, and capelin from 1995. This may have influenced the phase of the estimated dominant cycles. However, the computed wavelets represent a low-pass filtered data series so that single random data errors are unlikely to be a major problem in their analysis.

The time-series are analyzed by a wavelet transformation to identify the dominant cycle periods and phase relations. The Coiflet3 wavelet transformation (Matlab Toolbox, 1997) was chosen after many trials on tested data. The cycle identification has two fundamental problems. One problem is that of identifying periodic cycles when the phase has a reversal in the time-series. The phase-reversal property of the stationary cycles excludes traditional spectral analysis methods. The problem is solved by first identifying the dominant cycles and correlating the cycles to known reference cycles. A second problem is that of identifying the long-period cycles of 55 and 74 years. This problem is solved by the same method. First, identify the dominant long-wavelet periods and then correlate the periods to a known cycle reference.

The results show a good correlation between the time-series and the dominant wavelet cycles, and there is another good correlation between the dominant wavelet cycles and the lunar-nodal cycles of $18.6/3 = 6.2$, 18.6, and $3 \times 18.6 = 55.8$ years. The close relationship between the lunar-nodal tide cycles and the biomass eigen-frequency is a strong indication of a long-term adopted property. The Kola Section temperature data have dominant stationary cycles that are of the greatest importance in forecasting future biomass cycles in this area.

The 18.6-year Kola Section temperature cycle has a stationary frequency but not always a stationary phase. The phase reversal of the lunar-nodal cycles explains why this cycle has been difficult for others to identify (Ottersen *et al.*, 2000). A closer analysis of the Kola Section temperature series and ice extent in the Barents Sea, has shown that the phase of the 18.6-year temperature cycle has shifted 180° in the period from about 1890 until 1925 when a 74-year cycle was in a negative state (unpublished). In this analysis a 55- and a 74-year temperature cycle in the Barents Sea has been found. The relationship between the two cycles is still unclear. The wavelet analysis of the Kola temperature series indicates that the 55-year temperature cycle is the sum of the 6.2- and 18.6-year cycles where the phase relation between them is slowly changing in a period of $3 \times 18.6 = 55.8$ years. The 55.8-year cycle may be explained as the envelope of the two cycles. An analysis of the Arctic ice extent indicates that the 74-year cycle has its source in the Arctic Ocean. The fact that the 74-year Kola cycle has the energy to control the phase of the 18-year Kola cycle, explains why the herring biomass has a fluctuation between 50 and 80 years.

Implications of the results

This analysis shows that the long-term growth of the stocks of herring, cod, and capelin are influenced by a matching between the biomass eigen-frequency and the stationary temperature cycles of 6.2 and 18.6 years in the Barents Sea. The close relationship to the 18.6-year lunar-nodal cycle indicates that the stationary cycles are stationary lunar-nodal tides controlled by gravity from the Moon. These results suggest that we are able to explain the cause of the long-term biomass dynamics in the Barents Sea. The deterministic property of the 18.6-year lunar-nodal tide provides a new way of long-term forecasting over period of 50–80 years or more.

Acknowledgements

I would like to thank Vladimir Ozhigin at PINRO institute in Murmansk for access to the Kola Section temperature data series, Reidar Toresen at the Institute of Marine Research in Bergen for access to the data series of Norwegian spring-spawning herring and Olav Rune Godø at the Institute of Marine Research in Bergen for access to the data series on the Northeast Arctic cod.

References

Bochkov, Y. A. 1982. Water temperature in the 0–200 m layer in the Kola-meridian in the Barents Sea, 1900–1981. Sb. Nauchn. Trud. PINRO, Murmansk, 46: 113–122 (in Russian).

Daubehies, I. 1992. Ten lectures of wavelet. SIAM Journal on Mathematical Analysis, 24(2): 499–519.

Gjøsæter, H. 1997. Studies of the Barents Sea capelin, with emphasis on growth. Dr scient thesis, Department of Fisheries and Marine Biology, University of Bergen, Norway. Paper III, IV and V.

Godø, O. R. 2000. Fluctuation in stock properties of arcto-norwegian cod related to long-term environmental changes. IIASA. Interim report IR-00-023. 6 April 2000. Austria. http://www.iiasa.ac.at/cgi-bin/pubsrch/IR00023.

Hamre, J. 2000. Capelin and herring as key species for the yield of Northeast Arctic cod. Results from multispecies model runs. SAP Symposium 4–6 December 2000. Bergen, Norway.

Helland-Hansen, B., and Nansen, F. 1909. The Norwegian Sea. Report on Norwegian fishery and marine-investigations, Volume II (2), Kristiania.

Hjort, J. 1914. Fluctuations in the great fisheries of Northern Europe. Conseil Permanent International pour L'Exploration de la Mer, Rapports, II(2):20.

Hylen, A. 2002. Fluctuations in abundance of Northeast Arctic cod during the 20th century. ICES Marine Science Symposia, 534–550.

ICES 2001a. Northern pelagic and blue whiting fisheries working group. ICES CM 2001/ACFM: 17. 18–27 April 2001. Reykjavik.

ICES 2001b. Report of the Arctic fisheries working group. ICES CM 2001/ACFM: 19. 24 April–3 May 2001. Bergen, Norway.

Izhevskii, G. K. 1961. Oceanological Principles as Related to the Fishery Productivity of the Seas, 95 pp. Pishcepromizdat, Moscow (Translated 1966: Israel Program for Science Transactions. Jerusalem).

Izhevskii, G. K. 1964. Forecasting of oceanological conditions and the reproduction of commercial fish. All-Union Science Research Institute of Marine Fisheries and Oceanography. Israel Program for Science Transactions. 22 pp.

Loder, J. W., and Garret, C. 1978. The 18.6-year cycle of the sea surface temperature in the shallow seas due to tidal mixing. Journal of Geophysical Research, 83: 1967–1970.

Maksimov, I. V., and Smirnov, N. P. 1964. Long-range forecasting of secular changes of the general ice formation of the Barents Sea by the harmonic component method. Murmansk Polar Science Research Institute, Sea Fisheries, 4: 75–87.

Maksimov, I. V., and Smirnov, N. P. 1965. A contribution to the study of causes of long-period variations in the activity of the Gulf Stream. Oceanology, 5: 15–24.

Maksimov, I. V., and Smirnov, N. P. 1967. A long-term circumpolar tide and its significance for the circulation of ocean and atmosphere. Oceanology, 7: 173–178 (English edition).

Maksimov, I. V., and Sleptsov-Shevlevich, B. A. 1970. Long-term changes in the tide-generation force of the moon and the iciness of the Arctic Seas. Proceedings of the N. M. Knipovich Polar Scientific-Research and Planning Institute of Marine Fisheries and Oceanography (PINRO), 27: 22–40.

Marshall, T. C., Yaragina, N. A., Ådlandsvik, B., and Dolgov, A. V. 2000. Reconstruction of the stock-recruit relationship for Northeast Arctic cod using a bioenergetic index of reproductive potential. Canadian Journal of Fisheries and Aquatic Sciences, 57: 2433–2442.

Matlab Toolbox 1997. Users Guide. The Math Works Inc., Natick.

Nakken, O. 1994. Causes of trends and fluctuations in the Arcto-Norwegian cod stock. ICES Marine Science Symposium, 212–228.

Ottersen, G., Ådlandsvik, B., and Loeng, H. 2000. Predicting the temperature of the Barents Sea. Fisheries Oceanography, 9(2): 121–135.

Ottestad, P. 1942. On periodical variations on the yield on the Great Sea Fisheries and the possibility of establishing yield prognoses. Fiskeridirektoratets Skrifter, VII(5).

Pettersson, O. 1905. On the probable occurrence in the Atlantic Current of variations periodical, and otherwise, and their bearing on metrological and biological phenomena, Rapp. P.-v. R'eun. Cons. perm. int. l'Explor. Mer, 42: 221–240.

Pettersson, O. 1914. Climatic variations in historic and prehistoric time: Svenska Hydrogr. Biol. Kommissiones Skrifter, No. 5. 26 pp.

Pettersson, O. 1915. Long-periodical variations of the tide-generating force: Conseil Permanente International pour l'Exploration de la Mer (Copenhagen), Pub. Circ. No. 65, pp. 2–23.

Pettersson, O. 1930. The tidal force. A study in geophysics. Geografiska Annaler, 18: 261–322.

Royer, T. C. 1993. High-latitude oceanic variability associated with the 18.6-yr nodal tide. Journal of Geophysical Research, 98(C3): 4639–4644.

Toresen, R., and Østvedt, O. J. 2000. Variation in abundance of Norwegian spring herring (*Cluea harangus*, Clupeidae) through the 20th century and the influence on climatic fluctuation. Fish and Fisheries, 2000(1): 231–256.

Vollan, O. 1971. Sildefisket gjennom tusen år. Det Norske Samlaget, Oslo.

Wyatt, T., Currie, R. G., and Saborido-Ray, F. 1994. Deterministic signals in Norwegian cod records. ICES Marine Science Symposium, 198: 49–55.

Yndestad, H. 1996a. Stationary temperature cycles in the Barents Sea. The cause of causes. The 84th International ICES Annual Science Conference. Hydrography Committee. 27 September–4 October 1996. Reykjavik, Iceland.

Yndestad, H. 1996b. Systems dynamics of North Arctic cod. The 84th International ICES Annual Science Conference. Hydrography Committee. 27 September–4 October 1996. Reykjavik, Iceland.

Yndestad, H. 1999a. Earth nutation influence on the temperature regime in the Barents Sea. ICES Journal of Marine Science, 56: 381–387.

Yndestad, H. 1999b. Earth nutation influence on system dynamics of Northeast Arctic cod. ICES Journal of Marine Science, 56: 562–657.

Yndestad, H. 2002. The code of Norwegian spring spawning herring long-term cycles. ICES Annual Science Conference. October 2002. Copenhagen.

Yndestad, H., and Stene, A. 2001. System dynamics of Barents Sea capelin. ICES Annual Science Conference. 26–29 September 2001, Oslo.

Paper VI

Available online at www.sciencedirect.com
SCIENCE DIRECT®
Journal of Marine Systems 44 (2004) 107–124
JOURNAL OF MARINE SYSTEMS
www.elsevier.com/locate/jmarsys

The cause of Barents Sea biomass dynamics

Harald Yndestad*

Aalesund University College, N-6025 Aalesund, Norway

Received 8 October 2002; accepted 15 August 2003

Abstract

The fluctuations of the biomasses in the Barents Sea have been poorly understood and caused problems in biomass management. Better long-term forecasting is thus crucial for an economical and sustainable utilization of the biomass.

The present paper presents a wavelet analysis of the Kola temperature series and the biomass time series of Barents Sea Shrimp (*Pandalus borealis*), Barents Sea capelin (*Mallotus villosus*), Norwegian spring spawning herring (*Clupea harengus*), Northeast Arctic cod (*Gadus morhua*), and Northeast Arctic haddock (*Melanogrammus aeglefinus*). The wavelet shows a close relation between the 18.6-year lunar nodal tide and dominant temperature cycles in the Kola temperature series. It also shows that all biomass time series are correlated to dominant cycles of 18.6/3 = 6.2, 18.6 and 3∗18.6 = 55.8 years in the Kola section. This indicates that fluctuations of the temperature and the biomass in the Barents Sea are a deterministic process caused by the lunar nodal cycle.

The close relation to the stationary 18.6-year lunar tide opens new possibilities for better forecasting and long-term management. The deterministic relation between biomass growth and the Kola cycles opens a possibility of more optimal management in short-term periods of 6 years, medium-term management of 18 years and long-term management of 55–75 years. The stationary biomass cycles can be represented by a simple phase-clock which indicates the current state of the biomass. This method represents a new possibility of long-term biomass forecasting.

Keywords: 18.6-year lunar tide; Biomass dynamics; Barents Sea; Forecasting; Wavelet analysis

1. Introduction

The Barents Sea has some of the most productive biomasses in the world. During centuries, these biomasses have been of vital importance for settlement and economic growth in the western part of Norway. Some years, the biomass influx is abundant and some years the influx may be insufficient in relation to the demand. People dependent on fishing have always known that the biomass stock has a short time and long time fluctuation. These fluctuations have been explained by migrations, climate change, predators, introduction of new fishing equipment and more. When the marine research started at the beginning of the last century, the main task was to uncover how nature influenced the stock biomass and the impact of fluctuation on people living by fishing (Rollefsen et al., 1949). Better forecasting in a time span of 5–10 years will be crucial for better planning of an economical and sustainable biomass in the Barents Sea.

A long-term biomass management is based on the theory that if we are able to forecast the biomass

* Tel.: +47-70-16-12-00; fax: +47-70-16-13-00.
E-mail address: Harald.Yndestad@hials.no (H. Yndestad).

0924-7963/$ - see front matter © 2003 Elsevier B.V. All rights reserved.
doi:10.1016/j.jmarsys.2003.08.004

dynamics, then we may control the biomass. To forecast a future biomass, the biomass dynamics has to be deterministic and we need a scientific framework to describe expected biomass fluctuations. System dynamics in nature may be modeled as a holistic approach or as autonomous dynamic systems. The Aristotle (384–322 BC) 'principle of motion and change' represents a holistic approach on systems dynamics. He argued that the causes of movements in nature were a result of a history of chain of movements, that may be traced backwards to the motion of the Sun, the Moon and the stars. In modern science, we may call this approach a domino theory or Earth system science.

Isaac Newton (1642–1727) introduced the mathematical framework of system dynamics by the differential equation $dx/dt = Ax(t)$. From this simple equation, the future state $x(t)$ may be computed when the parameter A and the initial condition $x(0)$ are known. In biomass modeling, $x(t)$ represents the biomass state vector, and the system matrix A represents parameters of recruitment rates, maturing rates, growth rates and mortality rates. Introducing a quota vector $u(t)$, we have the biomass management model $dx/dt = Ax(t) + u(t)$. The biomass is managed by the control law $u(t) = Fx(t)$, where F is the catch rate. By this simple model, we may predict how a quota $u(t)$ may influence the biomass state $x(t)$ in the future. A management model opens a possibility of computing an optimum quota $u(t)$, a sustainable biomass $x(t)$, and biological reference points related to the catch rate F. According to this approach, we may forecast the biomass dynamics as an autonomous system, but at the same time, we have little room for a holistic understanding of long-term biomass dynamics.

In the Barents Sea, there is a predator and prey relation between spices in the biomass. A mutual relation between species introduces a time variant growth model. To overcome this problem, we have to introduce the augmented time variant model $dx/dt = A(t)x(t) + u(t)$ where all interacting species are represented. A time variant dynamic system implies that the new biomass state $x(t)$ and the parameters $A(t)$ have no stationary mean value. No stationary mean growth matrix implies that forecasting is dependent on the initial value $x(0)$, there is no stationary optimum quota $u(t)$, no stable biomass $x(t)$, and no stationary biological reference points of F. Each species in the Barents Sea is still dependent on a food chain outside the model, which is dependent on the ocean dynamic and the climate dynamics. In other words, the more this model is augmented, the more the model is moving into the holistic approach from Aristotle.

The biomass fluctuations in the Barents Sea may be more or less influenced by the autonomous biomass dynamics, interactions between the species, fishing activity, and a more complex dynamic chain that may be traced back to the movement of the Earth and the Moon. In this investigation, the Kola section temperature series, the biomass of Northeast Arctic shrimp (*Pandalus borealis*), Barents Sea capelin (*Mallotus villosus*), Norwegian Spring spawning herring (*Clupea harengus*), Northeast Arctic cod (*Gadus morhua*), and Northeast Arctic haddock (*Melanogrammus aeglefinus*) are analysed. The time series are analysed by a wavelet transformation to identify the cycle time and phase of the dominant fluctuations. The analysis has identified a close relation to the 18.6-year lunar cycle in all time series.

The identified dominant cycles of about 18.6, 18.6/3 = 6.2, and 3∗18.6 = 55.8 years in the Kola time series indicated that Atlantic inflow to the Barents Sea is influenced by long-term tides. When the same cycles are identified in the analysed biomasses, it indicates that cycles of Atlantic inflow influence the food chain and biomass growth in the Barents Sea. Since the fluctuations are related to deterministic periods of 6.2, 18.6 and 55.8 years, the cycle vectors may be visualized by a phase-clock. In biomass forecasting, this phase-clock is an indicator of when we may expect changes in the biomass fluctuations.

2. Materials and methods

2.1. Materials

Russian scientists at the PINRO institute in Murmansk have provided monthly temperature values from the upper 200 m in the Kola section along the 33°30′E meridian from 70°30′N to 72°30′N in the Barents Sea (Bochkov, 1982). The data series from 1900 until 2000 has quarterly values from the period 1906–1920 and monthly values from 1921, partly measured and partly interpolated. In this presentation, the annual mean temperature is analysed.

Northeast Arctic shrimp (*P. borealis* Krøyer 1838) is located in the in the Barents Sea and near Spitsbergen at the ICES areas I and IIa in deep-water from 20 to 900 m. The data time series covers the areas East Finnmark, Tiddly Bank, Thor Iversen Bank, Bear Island Trench and Hopen from 1982 until 2001 (ICES, 2002b).

The time series of Barents Sea capelin (*M. villosus*) covers the time from 1945 to 2000. The data series of biomass from 1945 to 1995 is provided from Marshall et al. (2000), and the biomass data from 1995 to 2000 is provided by ICES (2002a). The recruitment rate is computed from 1-year recruitment (October) and spawning numbers provided from official ICES data (ICES, 2002a).

The time series of Norwegian spring spawning herring (*C. harengus*) covers the time from 1907 to 2001. The data are provided from ICES (2002b). The time series of Northeast Arctic haddock (*M. aeglefinus*) covers the period from 1950 to 2001 and they are provided from ICES (2002a).

The total time series of Northeast Arctic cod (*G. morhua*) covers the period from 1866 to 2001. The time series of from 1866 to 1900 is provided by Godø (2000). The data are interpolated from catch numbers to biomass by the scaling of 3.5 (tons/1000 numbers). The period from 1900 to 1945 is based on published estimates from Hylen (2002) and the period from 1946 to 2000 is provided by ICES (2002b).

2.2. Systems theory

The Barents Sea is a complex dynamic system of sea currents, and fluctuations in temperature, nutrients, phytoplankton, zooplankton, and fish biomasses. The system may be represented by the simplified general system model

$$S(t) = \{B(t), \{S_n(t), S_o(t), S_f(t), S_b(t), S_v(t)\}\} \quad (1)$$

where $S_n(t)$ is the lunar nodal system, $S_o(t)$ is the ocean system, $S_f(t)$ is the food chain system, $S_b(t)$ is a biomass system, $S_v(t)$ is an unknown source and $B(t)$ is the mutual binding between the Barents Sea system elements. According to the general system model, the Barents Sea is expected to be a time varying, structurally unstable, and a mutually dependent system.

The system dynamics of a biomass system $S_b(t)$ is dependent on the eigen dynamics in each system and the mutual binding $B(t)$ between the systems. If there is a stationary dominant energy cycle in one element, the cycle is expected to influence the others. In this case, the lunar nodal system $S_n(t)$ is expected to have some influence on the ocean system $S_o(t)$ and the ocean system is expected to influence the food chain to fish $S_f(t)$. The food chain $S_f(t)$ is expected to influence the biomass $S_b(t)$ of shrimp, capelin, cod, herring, and haddock in the Barents Sea. This influence may be more or less detectable dependent on the binding $B(t)$ and the disturbance $S_v(t)$.

2.2.1. The lunar nodal cycle

The Earth is influenced by planetary cycles in the time span from hours to thousands of years. A planetary cycle of special interest is the 18.6-year lunar nodal cycle. This cycle time is close to a needed planning range and it is close to life cycle of species in the Barents Sea. In this analysis, the lunar nodal system $S_n(t)$ represents gravity energy from the 18.6-year lunar nodal cycle, caused by a mutual interaction between the Earth, the Moon, and the Sun. The Moon's orbital plane changes $\pm 5°09'$ from the ecliptic plane in a cycle 18.6134 years. The maximum angle to the equatorial is $(23°27' + 5°09') = 28°36'$ and 9.3 years later, the angle is $(23°27' - 5°09') = 18°18'$. The lunar node is the cross point between the Moon plane cycle and the ecliptic plane. This cross point describes a lunar nodal cycle of 18.6134 years. The gravity energy from the Moon introduces an 18.6-year lunar nodal tide in the Atlantic Ocean and the energy introduces an 18.6-year wobbling of the Earth axis (Pugh, 1996). The orbital angle to the Moon is described by the model

$$u_0(t) = U_0 + u_0 \sin(\psi_0(t)) = U_0 + u_0 \sin(\omega_0 t + \varphi_0) \quad (2)$$

where the eccentricity $U_0 = 23°27'$. The lunar nodal cycle amplitude $u_0 = 5°09'$ (deg) and $\omega_0 = 2\pi/T_0 = 2\pi/18.6134$ (rad/year) is the lunar nodal angle frequency and t (year) is the time from $t = 1900$. The cycle amplitude of $u_0(t)$ has a maximum in November 1987 and a minimum in March 1996 (Pugh, 1996) when the phase-angle is about $\varphi_0 = 1.0\pi$ (rad).

Changes in the energy force on the Earth introduce a 18.6-year lunar nodal tide, the 18.6-year nutation of the Earth axis, and a Polar motion.

2.2.2. The ocean system

An 18.6-year lunar nodal cycle introduces an 18.6-year lunar nodal tide in the Atlantic Ocean. This lunar nodal tide may be described by the model

$$u_{\mathrm{nt}}(t) = u_{\mathrm{nt}}\sin(\Phi_{\mathrm{nt}}(t)) = u_{\mathrm{nt}}\sin(\omega_0 t + \varphi_{\mathrm{nt}}) \tag{3}$$

where the amplitude $u_{\mathrm{nt}}=3$ (cm), the nodal angle frequency $\omega_0=2\pi/T_0=2\pi/18.6134$ (rad/year) is the lunar nodal angle frequency, t (year) is the time from $t=1900$, and a phase at about $\varphi_{\mathrm{nt}}=0.5\pi$ (rad) when the tide had a maximum in January 8, 1974 (Pugh, 1996; Keeling and Whorf, 1997). This tide cycle $u_{\mathrm{nt}}(t)$ has a phase delay of about $\pi/2$ (rad) or 18.6/4 years compared to the Moon high cycle $u_0(t)$ (Eq. (2)).

The 18.6-year lunar nodal cycle is a forced energy cycle on the Earth and on-linear ocean system $S_{\mathrm{o}}(t)$. The cycle energy is then distributed as a set of harmonic and sub-harmonic cycles of tides, flow and temperature states in the ocean system. These harmonic cycles are expected to influence the Atlantic tides (Keeling and Whorf, 1997) and the Atlantic inflow to the Barents Sea. The harmonic cycles may be modelled by

$$u(t) = \sum_{n,m} u_{n,m}\sin(n\omega_{\mathrm{nt}}t/m + \varphi_{n,m}) \tag{4}$$

where $u(t)$ here is called the *lunar nodal spectrum*, $u_{n,m}$ is a cycle amplitude, m the sub-harmonic index, n the harmonic index and $\varphi_{n,m}$ the phase delay. Each harmonic cycle may then introduce a new set of harmonic cycles.

2.2.3. The biomass system

A biomass system $S_{\mathrm{b}}(t)$ has an autonomous eigen frequency that behaves like a resonance in physics. This eigen frequency is related to the maximum spawning year class (Yndestad and Stene, 2002; Yndestad, 2002). According to the general systems theory (Eq. (1)), there is a relation between all system elements. This may be modulated as a chain of events from the lunar nodal cycle $S_{\mathrm{n}}(t)$, to the ocean system $S_{\mathrm{o}}(t)$, and from the ocean system $S_{\mathrm{o}}(t)$ to biomass system $S_{\mathrm{b}}(t)$. The chain of events may be modulated by the frequency transfer function

$$x_i(j\omega) = H_i(j\omega)[u(j\omega) + v(j\omega)] \tag{5}$$

where $u(j\omega)$ represents a correlated lunar nodal spectrum, $v(j\omega)$ is non-correlated disturbance from an unknown source, $x_{\mathrm{i}}(j\omega)$ represents the frequency response in the system element $S_{\mathrm{i}}(t)$, and $H_{\mathrm{i}}(j\omega)$ represents the frequency transform function between the lunar nodal cycle and the i-te system element. In a chain of events, the mean result of a non-correlated disturbance $v(j\omega)$ is expected to have a reduced influence on $x_{\mathrm{i}}(j\omega)$. A sum of correlated stationary cycles $u(j\omega)$ is expected to amplify the influence on the element $x_{\mathrm{i}}(j\omega)$ since they have the same frequency and phase.

2.3. System identification

A stationary cycle will introduce cycles of a time variant amplitude and phase in a system element when the elements have a time variant binding $B(t)$ (Eq. (1)). In a long time series, this will introduce a time variant amplitude and phase in the estimated cycles. This property makes it difficult to identify stationary cycles by straightforward statistical methods. A second problem is that in these short time series, it is difficult to identify low frequent cycles and to separate the high frequent cycles from noise. Wavelet transformation is an appropriate method to analyse the time variant data series. A continuous wavelet spectrum is computed by the wavelet transform

$$W(a,b) = \frac{1}{\sqrt{a}}\int_R x(t)\Psi\left(\frac{t-b}{a}\right)\mathrm{d}t \tag{6}$$

where $x(t)$ is the analysed time series, $\Psi(\ )$ is a wavelet impulse function, $W(a,b)$ is the computed wavelet cycles, b is a translation in time and a is a time scaling parameter in the wavelet filter function. The computed wavelets $W(a,b)$ represent a set of filtered time series between the time series $x(t)$ and the impulse functions $\Psi(\ )$. In the following analysis, a Coiflet3 wavelet transform was chosen from many trials on tested data (Matlab Toobox, 1997; Daubehies, 1992). This wavelet represents a linear phase filter which is able to separate additive cycles from a time series. Computed low frequent wavelets

will have an error at the beginning and at the end of the time series. To reduce this effect, there is introduced symmetric time series by the 'sym' property in the wavelet transform (Matlab Toobox, 1997). The Kola data series is scaled by data=(data − mean(data))/sqrt(variance) to reduce the same type of error.

2.3.1. Cycle period identification

The time series $x(t)$ may be represented by a sum of dominant wavelets that has most of the energy in the time series $x(t)$. Then we have

$$x(t) = [W(k1,t) + W(k2,t) + .. + W(kn,t)] + v(t) = W(t) + v(t) \quad (7)$$

where $W(k,t)$ represents a dominant wavelet cycle and $v(t)$ is error. A wavelet cycle $W(k,t)$ represents a moving correlation to an impulse period k. A dominant cycle period thus represents the best correlation to a cycle period k and a minimum error in Eq. (7). The wavelet cycle time k is tested by computing the correlation coefficient $r(k)$ between the dominant wavelet cycle $W(k,t)$ and a potential known cycle $u(k,t)$. The correlation value of quality is computed by $q(k)=r(k)*\text{sqrt}[(n-2)/(1-r(k)*r(k))]$ where n is the number of samples. The signal to noise relation between the dominant wavelets and the error (Eq. (7)) is computed by $S/N=\text{var}(W(t))/\text{var}(x(t)-W(t)$ where k represents the dominant wavelets.

2.4. The phase-clock

Dominant stationary cycles $W(t)$ in the time series $x(t)$ (Eq. (7)), are deterministic cycles dependent on the cycle amplitude $|W(k,t)|$ and the cycle time k. A stationary cycle is represented by the model

$$W(k,t) = a(k,t)\sin(\Phi_k(t)) \quad (8)$$

where $W(k,t)$ is the cycle amplitude and $\Phi_k(t)=\omega_k t+\varphi_k$ is the rotating angle cycle. The angle frequency $\omega_k=2\pi/k$ (rad/year) and the phase delay is φ_k.

A stationary cycle may be visualized as a vector or a phase-clock. (Fig. 1) where $a(k,t)$ represents the vector amplitude and the phase-angle $\Phi_k(t)=\omega_k t+\varphi_k$. When the time t is changing from $t=2000$, 2001, 2002... the angle $\Phi_k(t)$ is turning in the direction from

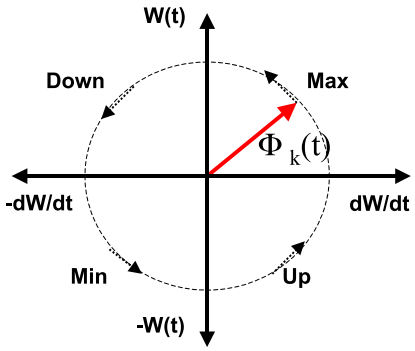

Fig. 1. The phase-clock.

0 to 2π and the vector is turning in an anti-clockwise direction. In biomass forecasting, the future biomass state is unknown, but the phase of the biomass fluctuation may be known. This opens a possibility of introducing a biomass forecast indicator based on a simple phase-clock.

3. Results

According to General System theory (Eq. (1)), there is a mutual relation between the system elements where the dominant energy source will influence the others. In this case, the lunar nodal system $S_n(t)$ is expected to influence the ocean system $S_o(t)$, the ocean system is expected to influence the food chain to fish $S_f(t)$, and the food chain to fish is expected to influence the biomass $S_b(t)$.

3.1. The Barents Sea temperature

The Barents Sea has an inflow of warm North Arctic water. This inflow meets a stream of cold Arctic water from the North and cool mixed water goes back to East Greenland. These streams may vary in intensity and slightly in position and cause biological changes in the Barents Sea. In this investigation, the Kola section temperature series $x_K(nT)$ represents an indicator of Atlantic inflow to the Barents Sea (Fig. 2).

A wavelet transform $W_{ko}(a,nT)$ of the Kola time series $x_{ko}(nT)$ has identified dominant wavelet cycles of 6, 18, 55, and 74 years. The 6-year wavelet $W_{ko}(6,nT)$ identifies temperature maximum values

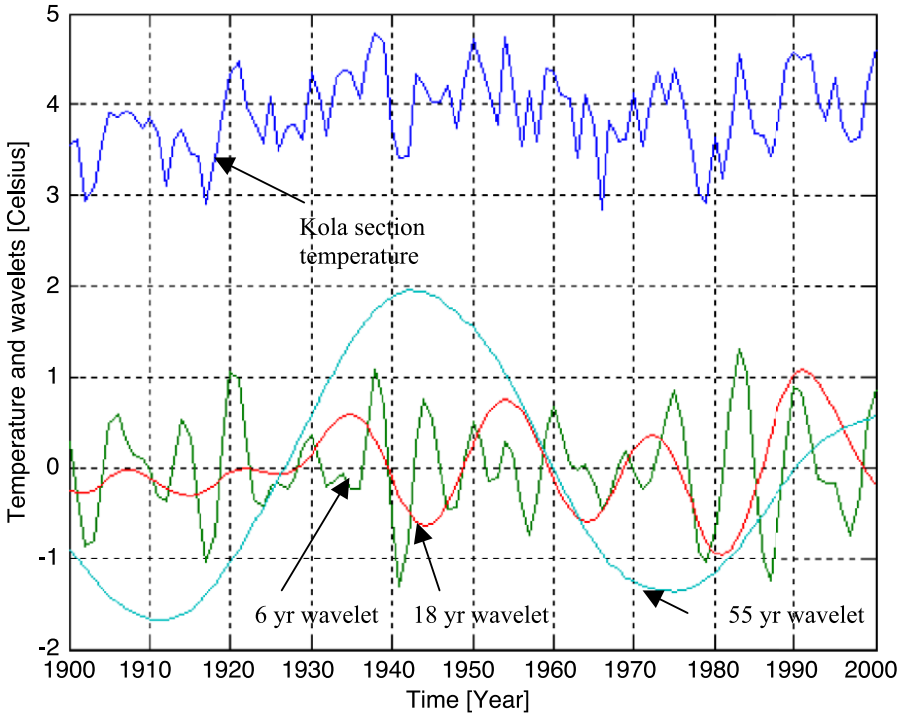

Fig. 2. Time series of Kola section data series and the 6-, 18-, and 55-year wavelet cycles.

for the years [1907 1915 1921 1930 1937 1944 1951 1961 1975 1983 1991], the 18-year wavelet $W_{ko}(18,nT)$ has maximum values in [1909 1922 1935 1955 1973 1991], the 55-year wavelet $W_{ko}(55,nT)$ has maximum values in 1945, and the 74-year wavelet $W_{ko}(74,nT)$ in 1945. A stationary model of the dominant cycles is

$$\begin{aligned} W_{ko}(06,nT) &= a_{ko}(6,nT)\sin(3\omega_0 nT - 0.09\pi) \\ W_{ko}(18,nT) &= a_{ko}(18,nT)\sin(\omega_0 nT + 0.55\pi) \\ W_{ko}(55,nT) &= a_{ko}(55,nT)\sin(\omega_0 nT/3 + 0.90\pi) \end{aligned} \tag{9}$$

where $\omega_0 = 2\pi/18.6134$ (rad/year), $T = 1$ year, $n = 1900...2001$, $a_{ko}(55,nT)$, $a_{ko}(18,nT)$, and $a_{ko}(06,nT)$ are time variant amplitudes. The angle $3\omega_0 nT = 0.92\pi$, $\omega_0 nT = 0.31\pi$, and $\omega_0 nT/3 = 0.85\pi$, when $n = 2001$. The estimated correlation coefficients r between the identified dominant wavelet cycles $W_{ko}(06,nT)$, $W_{ko}(18,nT)$, $W_{ko}(55,nT)$ and the estimated stationary cycles in Eq. (9) are estimated to $r_6 = 0.37$, $r_{18} = 0.88$, $r_{55} = 0.88$, and $r_{74} = 0.95$. The correlation value of quality is estimated to $q_6 = 3.9$, $q_{18} = 18.3$, $q_{55} = 30.1$ and the number of freedom $n - 2 = 98$. This gives a better than 95% confidence in a t-distribution. The signal to noise relation between the wavelets $W_{ko}(nT) = [0.4W_{ko}(06,nT) + 0.4W_{ko}(18,nT) + 0.1W_{ko}(55,nT)]$ and the estimate difference $(x_{ko}(nT) - W_{ko}(nT))$ are estimated to $S/N_{ko} = 3.2$. This confirms that the estimated nodal spectrum represents most of the fluctuations in the time series. The estimated phase-angle of the 18-year cycle is estimated to

$$\begin{aligned} \Phi_{ko}(18,nT) &= \omega_0 nT + 0.55\pi \\ &= \Phi_{nt}(18,nT) + 0.05\pi \end{aligned} \tag{10}$$

Eqs. (3) and (10) show that estimated 18-year Kola temperature cycle has the same cycle time and phase as the 18.6-year lunar nodal tide.

3.1.1. The Barents Sea temperature phase-clock

Fig. 3 shows the phase state of the dominant wavelet cycles $W_{ko}(06,nT)$, $W_{ko}(18,nT)$, and $W_{ko}(55,nT)$ at the year 2001. The 55-year cycle

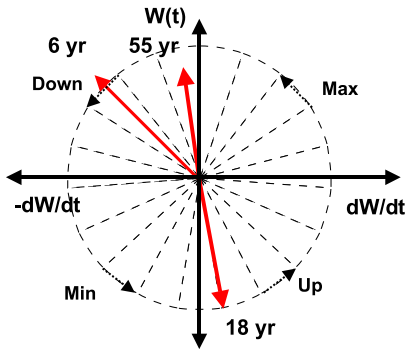

Fig. 3. The Kola section temperature phase state in the year 2001.

$W_{ko}(55,nT)$ has a maximum value, the 18-year cycle $W_{ko}(18,nT)$ has a minimum value, and the 6-year cycle $W_{ko}(06,nT)$ has passed a maximum value. This is the same maximum state as 55 years earlier in 1945.

A wavelet time series analysis of the Kola section temperature, the biomass of Northeast Arctic cod, the biomass of Barents Sea capelin, and the biomass of Norwegian Spring spawning herring show that long-term biomass growth is dependent on the phase-relation between the 6- and the 18-year temperature cycles. The biomass has a long-term growth when the two cycles are positive at the same time. There is a long-term biomass reduction when only one cycle is positive at the same time, and there is a biomass collapse when both cycles are negative at the same time (Yndestad, 2002). A phase-diagram of the cycle states may then represent a "Temperature phase-clock" where the cycle vectors indicate the climate state and the forecasting in cycles of 6, 18, and 55 years.

This climate clock indicates that the mean sea temperature is expected to be reduced in the next period of about 25 years. At the same time, the 18-year cycle is expected to increase the temperature the next 9 years and the 6-year cycle will decrease the temperature in the next 2 years. According to the code of long-term biomass dynamics, the 18- and the 6-year cycle are expected to be negative at the same time at about 2003. This may cause a temporary strong biomass reduction in the biomass food chain (Yndestad, 2002).

3.2. Barents Sea shrimp

Northeast Arctic shrimp (*P. borealis*) are located in the Barents Sea and near Spitsbergen and represent an important economic resource. The biomass fluctuations in local populations may change 2–105% from one year to the next (ICES, 2002a). The fluctuations are a result of the biomass growth property and environment disturbance. The growth properties of shrimp biomass have been studied for years, and it is known that water temperature has influence on the biomass recruitment, growth and mortality (Rassmussen, 1953; Teigsmark, 1980; Andersen, 1991). Other important sources of fluctuation are catching and consumption from Northeast Arctic cod and other predators.

The time series of spawning biomass of Barents Sea shrimp from 1982 until 2002 has a mean weight of age $x_{sh}(\text{age})$=[0 0 0 8 14 25 22 19 17 14] 1000 tons at the age of 1 to 10 years. Maximum spawning year class is estimated to be 25,000 tons at 6 years. The Barents Sea shrimp then have an eigen frequency at about $X_{sh}(j\omega_e)=2\pi/T_e=2\pi/6.2$ (rad/year) (Yndestad and Stene, 2002). This is the same frequency as the 6.2-year Kola temperature cycle. The biomass is then expected to follow the 6.2-year temperature cycle.

The data series $x_{sh}(nT)$ of shrimp biomass from Norwegian surveys in the Barents Sea is presented in Fig. 4. The time series cover the areas East Finnmark, Tiddly Bank, Thor Iversen Bank, Bear Island Trench and Hopen. A wavelet analysis of the shrimp biomass time series $x_{sh}(nT)$ has identified the dominant cycles of 6 and 18 years. The data series $x_{sh}(nT)$ and the identified dominant wavelet cycles $W_{sh}(6,nT)$ and $W_{sh}(18,nT)$ are shown in Fig. 4. The cross correlation coefficient between the biomass data series $x_{sh}(nT)$ and $W_{sh}(6,nT)$, $W_{sh}(18,nT)$, and $W_{sh}(nT)$=[$W_{sh}(6,nT)+W_{sh}(18,nT)$] are estimated to $r(6)=0.45$, $r(18)=0.95$, and $r_{sh}=0.85$. The correlation value of quality is estimated to $q_{ch}=8.3$, and the number of freedom $n-2=27$. This gives a better than 95% confidence in a t-distribution. The signal to noise relation between the estimated wavelets $W_{sh}(nT)$ and the estimate difference error ($x_{sh}(nT)-W_{sh}(nT)$) are estimated to $S/N_{sh}=3.5$.

The dominant wavelet cycles $W_{sh}(06,nT)$ and $W_{sh}(18,nT)$ indicate that the dominant fluctuations of the shrimp biomass are related to the biomass eigen frequency of 6.2 years and the 18.6 years Kola temperature cycle. A stationary representation

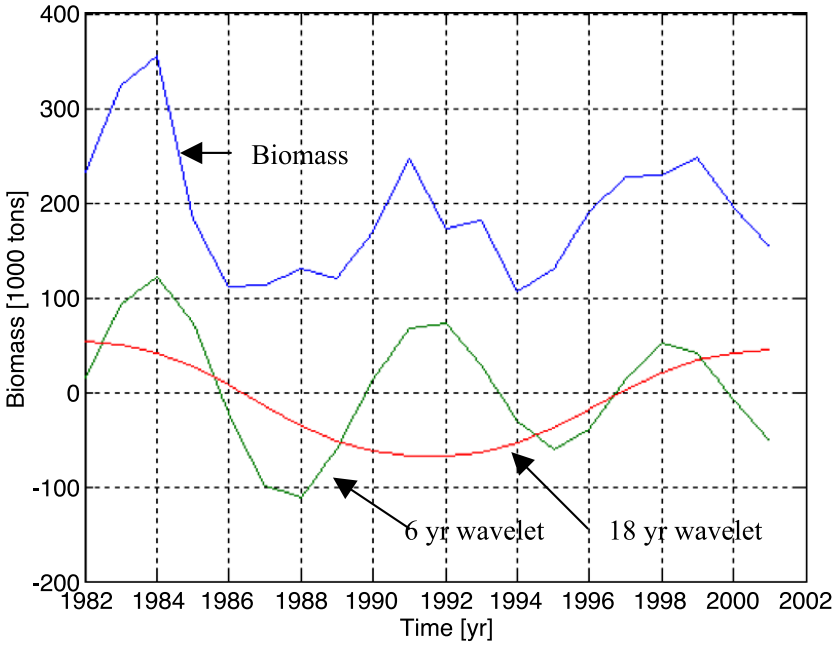

Fig. 4. The shrimp biomass from the Norwegian surveys, 6- and 18-year wavelet cycles.

of the dominant wavelet cycles is described by the model

$$W_{\mathrm{sh}}(06,nT) = 70.000\sin(3\omega_0 nT - 1.09\pi)$$

$$W_{\mathrm{sh}}(18,nT) = 30.000\sin(\omega_0 nT + 1.55\pi) \qquad (11)$$

at the years $n = 1982\ldots2001$ and sampling periods of $T = 1$ year. The cycle phase-angle of the 6- and 18-year cycle is estimated to

$$\Phi_{\mathrm{sh}}(06,nT) = 3\omega_0 nT - 1.09\pi = \Phi_{\mathrm{ko}}(06,nT) - 1.0\pi$$

$$\Phi_{\mathrm{sh}}(18,nT) = \omega_0 nT + 1.55\pi = \Phi_{\mathrm{ko}}(18,nT) - 1.0\pi \qquad (12)$$

The dominant biomass cycle has a phase delay of 1.0π (rad/year) compared to the Kola temperature cycles. This inverse relation between the shrimp biomass and the Kola temperature is explained by the additional larvae from eggs which will survive in reduced temperature.

3.2.1. The shrimp biomass phase-clock

Fig. 5 shows the state of the shrimp phase-clock at the year 2001. The 55-year cycle indicates that we may expect a long-term biomass growth the next 25 years. The 18- and the 6-year cycle have about the same state as in 1982. In a more short-term biomass growth, the 18-year cycle is expected to introduce a biomass reduction. The next 9 years, the 6-year cycle is expected to indicate a biomass growth over the first 3 years.

3.3. The Barents Sea capelin

The capelin (*M. villosus)* has a northerly circumpolar distribution. In the Atlantic, the capelin is

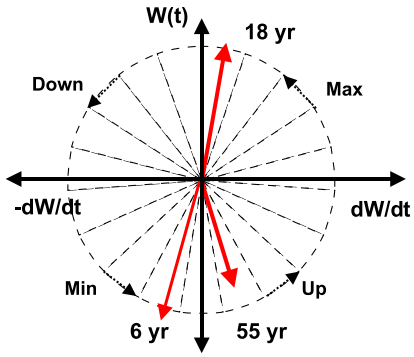

Fig. 5. The shrimp biomass phase-clock state in the year 2001.

located in the Barents Sea (ICES areas I and IIa), Iceland, Greenland, Labrador and Newfoundland. The capelin stock in the Barents Sea is the largest in the world and has maintained annual fishery catches up to 3 million tons. The capelin stock is of vital importance in the Arctic food web. It is the main plankton feeder in the area and serves as an important forage fish for other fish stocks, seals, whales and sea birds. The capelin is therefore influenced by its abiotic environment and by the abundance of food, predators, and fisheries (Gjøsæter, 1997).

The time series from 1989 until 2001 of the spawning biomass of Barents Sea capelin has a mean weight of age $x_{ca}(\text{age})=[0\ 2\ 357\ 89\ 2]$ 1000 tons at the age of 1 to 5 years. Maximum spawning biomass is estimated to be 357,000 tons at 3 years (ICES, 2002a). The Barents Sea capelin then has an eigen frequency at about $X_{ca}(j\omega_e)=2\pi/T_e=2\pi/3.1$ (rad/year), which is close to the half of the 6.2-year Kola temperature cycle. This short cycle will introduce a more unstable phase in the biomass cycles and the capelin is therefore able to adapt to the growth of random fluctuations in food and predators (Yndestad and Stene, 2002).

The time series of Barents Sea capelin from 1945 until 2001 has fluctuations from about 20 to 8000 thousand tons (Fig. 6). A wavelet analysis of the time series has identified dominant wavelets cycles $W_{ca}(06,nT)$ and $W_{ca}(18,nT)$ which have cycle times of 6 and 18 years. The cross correlation coefficient between the biomass data series $x_{ca}(nT)$ and $W_{ca}(nT)=[W_{ca}(06,nT)+W_{ca}(18,nT)]$ is estimated to $r_{ca}=0.73$. The correlation value of quality is estimated to $q_{ca}=8.0$, and the number of freedom $n-2=55$. This gives a better than 95% confidence in a t-distribution. The signal to noise relation between the estimated wavelets $W_{ca}(nT)$ and the estimate difference error $(x_{ca}(nT)-W_{ca}(nT))$ is estimated to $S/N_{ca}=1.8$.

This means that the capelin biomass has harmonic dominant cycles related to the Kola temperature cycles of 6 and 18 years. The 6-year cycle is shifted to a 9-year cycle when the 18-year Kola temperature cycle has a negative state and this shift influences the phase of the 18-year cycle (Figs. 2 and 6). This important shift to a 9-year cycle is explained by a mismatch between the short biomass eigen frequency of 3.1 year and the Kola cycles influence on the recruitment rate (Yndestad and Stene, 2002). A sta-

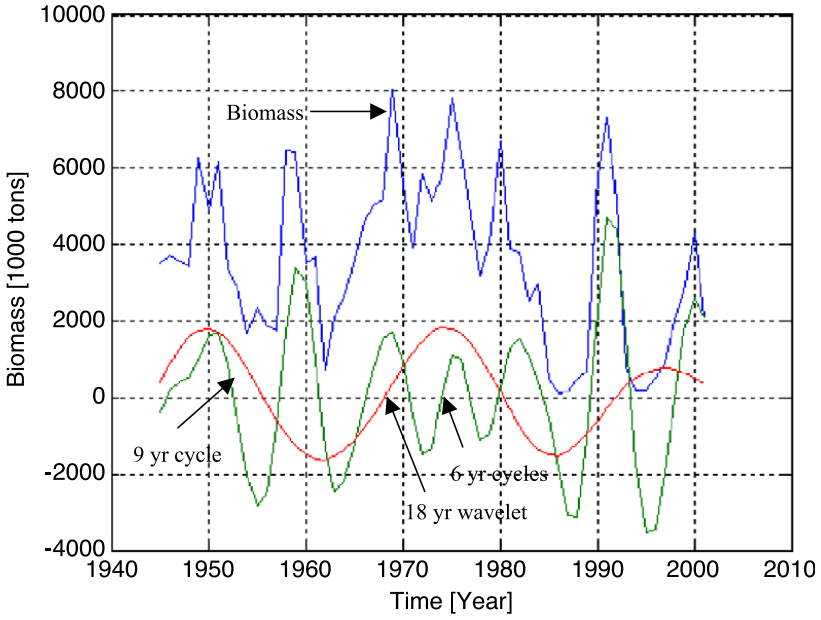

Fig. 6. The time series of Barents Sea capelin biomass from 1945 to 2001, a 18-year dominant wavelet cycle, and a dominant wavelet cycle where the cycle time changes between 6 and 9 years.

tionary representation of the dominant wavelet cycles is described by the model

$$W_{ca}(06,nT) = a_{ca}(06,nT)\sin(3\omega_0 nT - 0.09\pi)$$

$$W_{ca}(09,nT) = a_{ca}(09,nT)\sin(\omega_0 nT/2 - 0.09\pi)$$

$$W_{ca}(24,nT) = a_{ca}(24,nT)\sin(3\omega_0 nT/4 + 0.22\pi) \quad (13)$$

where $n = 1982\ldots2001$, $T = 1$ year, $W_{ca}(06,nT)$ is active when the 18-year Kola temperature is positive, and $W_{ca}(06,nT)$ is active when the 18-year Kola temperature is negative. The 24-year cycle $W_{ca}(24,nT)$ is the mean cycle of $18.6 + 6.2 = 24.8$ year. The cycle phase-angle of the 6- and 18-year cycle is estimated to

$$\Phi_{ca}(09,nT) = \omega_0 nT/2 - 1.09\pi$$

$$\Phi_{ca}(24,nT) = 3\omega_0 nT/4 + 0.22\pi \quad (14)$$

The capelin stock has an eigen frequency cycle of only 3 years. This explains the close phase-relation between the 6-year Kola cycle and the dominant biomass cycles of 6 and 9 years. The 24-year cycle has a phase delay of 0.22π (rad). This is about 3 years compared to the 18-year Kola temperature cycle. This delay is explained as a mean delay time of about 3-year growth delay in the total biomass.

3.3.1. The capelin biomass phase-clock

Fig. 7 shows the state of the Barents Sea capelin phase state at the year 2001. The 24-year cycle

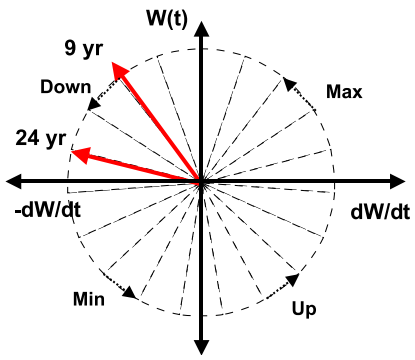

Fig. 7. The state of the Barents Sea capelin biomass phase-clock in the year 2001.

$Ws(24,nT)$ is still in a positive sector and the 9-year cycle has passed the maximum state. The climate clock indicates the same situation as in 1945. The 18-year Kola cycle is at a minimum state and the 6-year Kola cycle has passed a maximum state (Fig. 3). This will influence long-term recruitment.

In the long-term, the biomass is expected to be influenced by the relation between the 18- and the 6-year cycle during a period of 55 years in the Kola temperature cycle. The 24-year capelin biomass cycle indicates a biomass reduction the next 6 years. In a short-time range, the 9-year cycle is expected to reduce the biomass cycle the next 3–4 years, and then there is expected to be a new growth in the biomass when the 9- and the 24-year cycle turn in a positive direction.

3.4. The Norwegian spring spawning herring

The time series of Norwegian spring spawning herring (*C. harengus*) had a growth period from 5 million tons in 1920 to about 20 million tons in 1930. In the period 1950 to 1960, the biomass was reduced to 7 million tons, and in the period 1965 to 1985, there was a collapse caused by overfishing.

The spawning biomass time series of Norwegian Spring Spawning herring has a mean weight of age $x_{he}(age)$=[0 0.5 14.0 94.8 37.4 569.9 561.2 428.7 332.9 281.0] thousand tons (ICES, 2002a). The mean maximum spawning biomass is 569.9 thousand tons at the age of 6 years and indicates a herring biomass eigen frequency of about $X_{he}(j\omega_e) = 2\pi/T_{he} = 2\pi/6.2$ (rad/year). This is the same cycle time as the 6.2-year Kola temperature cycle.

The wavelet analysis of the herring biomass time from 1907 to 2001 has identified the dominant wavelets cycles $W_{he}(06,nT)$, $W_{he}(18,nT)$ and $W_{he}(55,nT)$ or a cycle time of 6, 18 and 55 years (Fig. 8). The cross correlation coefficient between the biomass time series $x_{he}(nT)$ and the wavelets sum $W_{he}(nT) = [W_{he}(06,nT) + W_{he}(18,nT) + 0.4\ W_{he}(55,nT)]$ is estimated to $r_{he} = 0.92$. The correlation value of quality is estimated to $q_{he} = 23.0$, and the number of freedom $n - 2 = 93$. This gives a better than 95% confidence in a t-distribution. The signal to noise relation between the estimated wavelets $W_{ca}(nT)$ and the estimate error difference $(x_{ca}(nT) - W_{he}(nT))$ are estimated to $S/N_{sh} = 3.0$. This analysis shows the

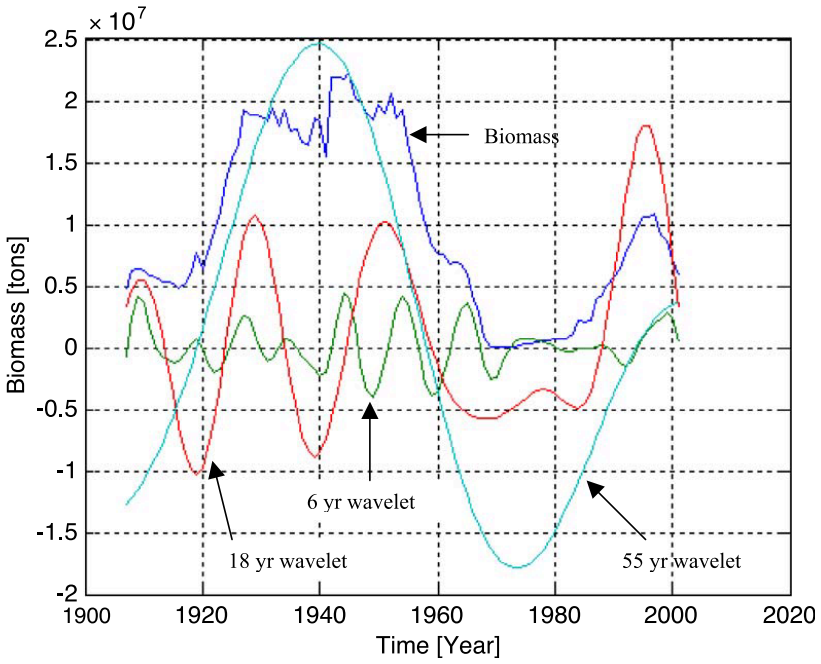

Fig. 8. Biomass of Norwegian spring spawning herring and 6-, 18- and 55-year wavelets.

biomass of Norwegian spring spawning herring is influenced by the Kola section temperature cycles of 6, 18 and 55 years. The data series and the dominant wavelet cycles are shown in Fig. 8. A stationary representation of the dominant wavelet cycles is described by the model

$$W_{\mathrm{he}}(06,nT) = a_{\mathrm{he}}(06,nT)\sin(3\omega_0 nT - 0.09\pi)$$

$$W_{\mathrm{he}}(18,nT) = a_{\mathrm{he}}(18,nT)\sin(\omega_0 nT + 1.05\pi)$$

$$W_{\mathrm{he}}(55,nT) = a_{\mathrm{he}}(55,nT)\sin(\omega_0 nT/3 + 0.90\pi) \quad (15)$$

where the year $n = 1906\ldots2001$ and sampling periods of $T = 1$ year. The cycle phase-angle of the 6- and 18-year cycle is estimated to

$$\Phi_{\mathrm{he}}(06,nT) = 3\omega_0 nT - 0.09\pi = \Phi_{\mathrm{ko}}(06,nT) + 0.0\pi$$

$$\Phi_{\mathrm{he}}(18,nT) = \omega_0 nT + 1.05\pi = \Phi_{\mathrm{ko}}(18,nT) - 0.5\pi$$

$$\Phi_{\mathrm{he}}(55,nT) = \omega_0 nT/3 + 0.90\pi = \Phi_{\mathrm{ko}}(55,nT) + 0.0\pi \quad (16)$$

The estimated 6-year cycle has the same frequency and phase as the 6-year Kola temperature cycle. This close phase-relation is explained by a biomass eigen frequency cycle of about 6 years. Maximum recruitment will then follow the temperature cycle. The 18-year cycle has a delay of $\pi/2$ (rad) compared to the 18-year Kola temperature cycle. This confirms that the 18-year Kola cycle controls the long-term biomass growth (Yndestad, 2002). The estimated 55-year biomass cycle has the same frequency and phase as the 55-year Kola temperature cycle. This indicates that both cycles represent a mean of the 6- and the 18-year cycles.

3.4.1. The herring biomass phase state

Fig. 9 shows the phase state of Norwegian spring spawning herring biomass phase-clock in the year 2001. This corresponds to the same state as in 1945. The 55-year cycle state shows that we may expect a mean long-term biomass reduction the next 25 years. This indicated that the biomass has reached a maximum state. In 1945, the herring biomass was about 20 million tons, and in 1997, the biomass was about 10 million tons. The difference in the maximum biomass in 1945 and 2001 may be explained by the 1970 collapse in the biomass and the short period

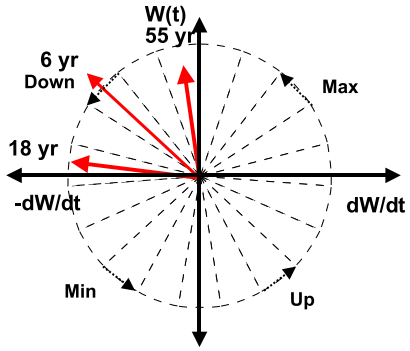

Fig. 9. The state of Norwegian spring spawning herring biomass phase-clock in the year 2001.

of biomass growth from the 1980s when the 55-year Kola cycle started to turn in a positive direction. In a short-term of 6 years, the biomass is expected to be reduced the next 3 years when the 6-year cycle is turning in a negative direction. The medium-term cycle of 18 years is expected to introduce a new growth period of 9 years when the 18-year Kola cycle goes into a positive state.

3.5. The northeast arctic cod

Northeast Arctic cod (*G. morhua*) is the largest stock of *G. morhua* cod in the world. The fishery of this stock is located along the northern coast of Norway and in the Barents Sea. For centuries, this stock of cod has been the most important economic biomass for Norwegian fisheries and of vital importance for settlement and economic growth in the western part of Norway. The biomass of Northeast Arctic cod has always fluctuated. In the wavelet analysis, we will identify the source of dominant cycles in the time series.

The time series $x_{co}(nT)$ of Northeast Arctic cod spawning biomass has a mean weight of age $x_{co}(\text{age})$= [0 201 6078 20341 65,388 103,012 93,124 63,528 41,586 13,932] tons from age 1 until 10 (ICES, 2002b). In this estimate, the maximum biomass is 103,012 tons at the age of 6 years. From this age distribution, we may conclude that the cod biomass has an eigen frequency at about $X_{co}(j\omega_e)=2\pi/T_{co}=2\pi/6.2$ (rad/year).

Fig. 10 shows the time series $x_{co}(nT)$ of Northeast Arctic cod from 1866 until 2001 (Godø, 2000; ICES, 2002b). The wavelet analysis of the cod biomass time from 1866 to 2000 has identified the dominant wavelets cycles $W_{co}(06,nT)$, $W_{co}(18,nT)$ and $W_{co}(55,nT)$ or a cycle time of 6, 18 and 55–75 years (Fig. 10). The 55-year cycle is a dominant cycle, but is influenced by short connected time series and the biomass collapse in the 1980s. The cross correlation coefficient be-

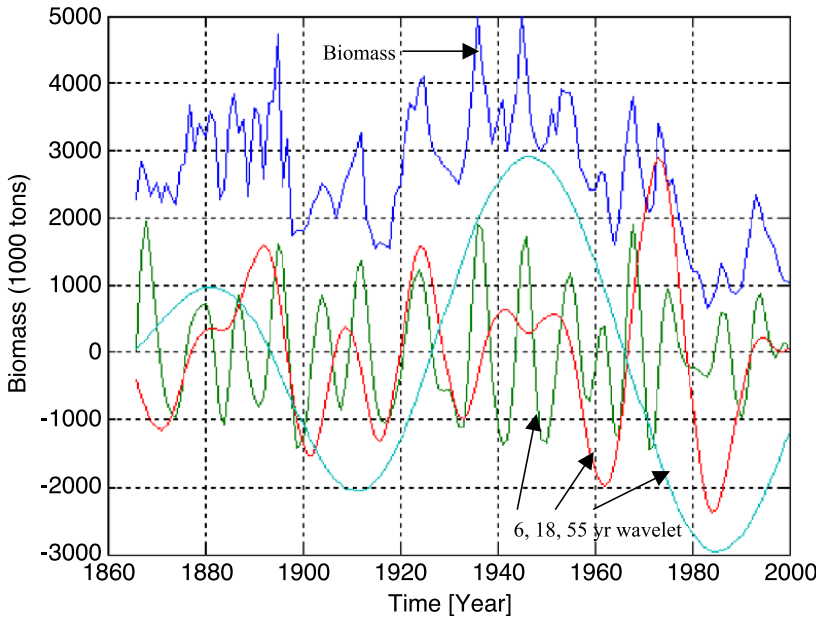

Fig. 10. Time series of Northeast Arctic cod and dominant wavelet cycles of 6, 18, and 55 years.

tween the biomass time series $x_{co}(nT)$ and the wavelets sum $[W_{co}(06,nT)+W_{co}(18,nT)+W_{co}(55,nT)]$ is estimated to $r_{co}=0.85$. The correlation value of quality is estimated to $q_{he}=18.6$, and the number of freedom $n-2=133$. This gives a better than 95% confidence in a t-distribution. The signal to noise relation between the estimated wavelets $W_{co}(nT)=[0.7W_{co}(06,nT)+0.5W_{co}(18,nT)+0.3W_{co}(55,nT)]$ and the estimate difference $(x_{co}(nT)-W_{co}(nT))$ is estimated to $S/N_{co}=3.8$.

The dominant wavelet cycle indicates that most fluctuations of the Northeast Arctic cod biomasses are related to the 6.2-year biomass eigen frequency and the Kola temperature cycle of 6.2, 18.6 and 55.8 years. In this estimate, the 55-year wavelet estimate is influenced by the collapse in 1980 (Yndestad, 2002). A stationary representation of the dominant wavelet cycles is described by the model

$$W_{co}(6,nT) = a(6,nT)\sin(3\omega_0 nT - 1.09\pi)$$

$$W_{co}(18,nT) = a(18,nT)\sin(\omega_0 nT + 0.22\pi)$$

$$W_{co}(55,nT) = a(55,nT)\sin(\omega_0 nT + 0.72\pi) \qquad (17)$$

in the years $n=1866...2001$ and sampling periods of $T=1$ year. The cycle phase-angle of the 6 and 18-year cycle is estimated to

$$\Phi_{co}(06,nT) = 3\omega_0 nT - 1.09\pi = \Phi_{ko}(06,nT) + 1.0\pi$$

$$\Phi_{co}(18,nT) = \omega_0 nT + 0.22\pi = \Phi_{ko}(18,nT) - 0.33\pi$$

$$\Phi_{co}(55,nT) = \omega_0 nT/3 + 0.72\pi = \Phi_{ko}(55,nT) + 0.18\pi \qquad (18)$$

This shows that the cod biomass has dominant cycles which are closely related to the Kola temperature cycle. The 6-year cycle $W_{co}(06,nT)$ has a delay of π (rad) or 3 years compared to the 6-year Kola temperature cycle $W_{ko}(06,nT)$. This represents a delay of 3 years which is the delay for the time when the Kola cycle introduces maximum recruitment to the first 3-year class in the biomass. The 18-year cycle $W_{co}(18,nT)$ has a delay of 0.33π (rad) or 3 years compared to the 18-year Kola temperature cycle. The $W_{co}(55,nT)$ cycle delay of 0.18π (rad) or about 6 years is the delay to maximum biomass in the eigen frequency cycle.

3.5.1. The cod biomass phase-clock

Fig. 11 shows the state of Northeast Arctic cod biomass phase-clock at the years 2001. The phase-clock has about the same state as in 1945. The 55-year Kola cycle is expected to introduce a long-term mean biomass reduction in a period of about 25 years. In short-term forecasting, the 6-year cycle in expected to introduce a biomass reduction the next 3 years. At this state, there is a critical period that may introduce a collapse in the biomass. In 6 years, the 18-year cycle will turn in a positive direction and introduce a positive state the next 9 years.

3.6. The northeast arctic haddock

Northeast Arctic haddock (*M. aeglefinus*) is a bottom fish found at a depth of 130–1.000 ft. Its most important spawning grounds are off Mid Norway, Southwest Iceland and the Faroe Islands. Little is known about the migratory patterns of haddock. The young haddock is located in the Barents Sea while the larger haddock tend to migrate south. Some spawning migration occurs along the coast of Northern Norway, whereafter it migrates back to the Barents Sea. Most haddock fishing is coastal, but in the North, fishing also takes place in the eastern reaches of the Norwegian Economic Zone.

The spawning biomass time series of Northeast Arctic haddock has a mean age weight vector x_{ha}

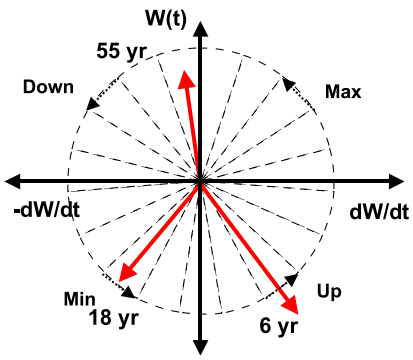

Fig. 11. The state of Northeast Arctic cod biomass phase-clock in the year 2001.

(age)=[0 0 1 7 14 16 12 6 1.5] million tons (ICES, 2002b). The maximum biomass is 16 million tons at the age of 6 years, and identifies a haddock biomass eigen frequency of about $X_{ha}(j\omega_e)=2\pi/T_{ha}=2\pi/6.2$ (rad/year). This is close to the same cycle time as the 6.2-year Kola section temperature cycle.

The time series of Northeast Arctic haddock has the same fluctuations as the Northeast Arctic cod. In the period 1950 to 1975, the biomass was reduced from about 4 million to about 2 million tons, and in first part of the 1990s, there was a temporary increase in of the biomass. A wavelet analysis of the time series has identified dominant wavelets cycles $W_{ha}(06,nT)$ and $W_{ha}(18,nT)$ or cycle time of 6 and 18 years.

The wavelet analysis of the haddock biomass time from 1950 to 2001 has identified the dominant wavelets cycles $W_{ha}(06,nT)$, $W_{ha}(18,nT)$ or a cycle time of 6 and 18 years (Fig. 12). The cross correlation coefficient between the biomass time series $x_{co}(nT)$ and the wavelets sum $[W_{ha}(06,nT)+W_{ha}(18,nT)]$ is estimated to $r_{ha}=0.80$. The correlation value of quality is estimated to $q_{ha}=9.4$, and the number of freedom $n-2=49$. This gives a better than 95% confidence in a t-distribution. The signal to noise relation between the estimated wavelets $W_{ha}(nT)=[W_{ha}(06,nT)+0.5W_{ha}(18,nT)+0.5W_{ha}(55,nT)]$ and the estimate difference is estimated to $S/N_{ha}=6.5$. The data series and the dominant wavelet cycles are shown in Fig. 12. A stationary representation of the dominant wavelet cycles is described by the model

$$W_{ha}(06,nT) = a(06,nT)\sin(3\omega_0 nT - 1.09\pi)$$

$$W_{ha}(18,nT) = a(18,nT)\sin(\omega_0 nT + 0.22\pi) \qquad (19)$$

at the years $n=1950...2001$ and sampling periods of $T=1$ year. The cycle phase-angle of the 6- and 18-year cycle is estimated to

$$\Phi_{ha}(06,nT) = 3\omega_0 nT - 1.09\pi = \Phi_{ko}(06,nT) - 1.0\pi$$

$$\Phi_{ha}(18,nT) = \omega_0 nT + 0.22\pi = \Phi_{ko}(18,nT) - 0.33\pi \qquad (20)$$

The 18-year cycle $W_{ha}(18,nT)$ and the 6-year cycle $W_{ha}(06,nT)$ have a delay of about 3 years compared to the Kola temperature cycles. The same delay is estimated in the cod biomass.

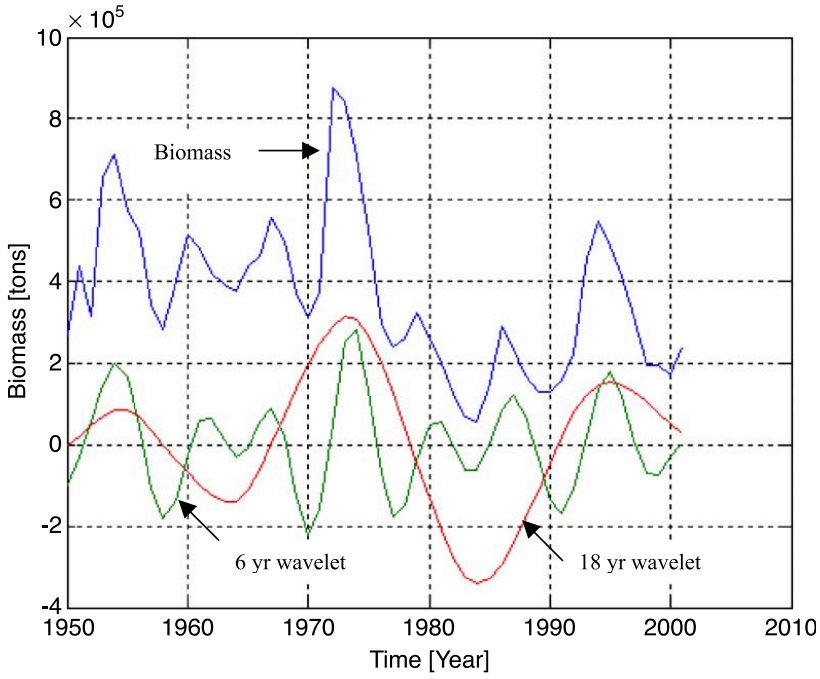

Fig. 12. Time series of Northeast Arctic haddock and dominant wavelet cycles of 6 and 18 years from 1950 to 2001.

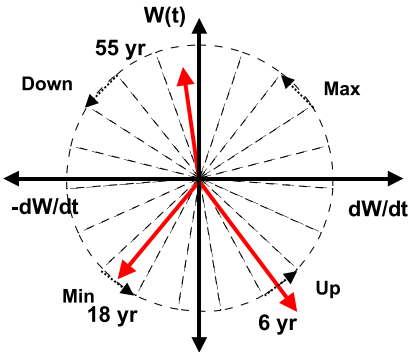

Fig. 13. The state of the Northeast Arctic haddock biomass phase-clock in the year 2001.

3.6.1. The haddock biomass phase-clock

Fig. 13 shows the state of Northeast Arctic haddock biomass phase-clock in 2001. The phase-clock has about the same state as Northeast Arctic cod. The time series is too short to estimate a 55-year cycle, but the 55-year Kola cycle is expected to introduce the same long-term biomass reduction as in the cod biomass. In a short-term forecasting, the 6-year cycle is expected to introduce a biomass growth over the next 2 years, but at the same time, the 18-year cycle will introduce a biomass reduction the next 6 years. In 2005–2006, both cycles are expected to be at a minimum state at the same time. In this state, there is a critical period that may introduce a collapse in the biomass. From 2005–2006, the 18-year cycle is expected to turn in a positive direction and the biomass is expected to grow the next 9 years.

4. Discussion

The biomass dynamics in the Barents Sea is a result of many mutual interactions between the ocean system, the food chain, catch, and a multi-species system (Eq. (1)). A long-term biomass management is based on the theory that if we are able to forecast the biomass dynamics, then we may control the biomass. In this investigation, there is a dominant lunar nodal spectrum identified in all analysed time series. Since the lunar nodal spectrum has a stationary cycle time, it opens a new possibility for a long-term forecasting.

The Newton approach of forecasting by difference equations represents a ballistic view of the reality. By this simple approach, it is difficult to separate natural biomass fluctuations from estimate errors. This problem introduces a short forecast period and it may lead to an instability in biomass management (Yndestad, 2001). The holistic Aristotle approach of forecasting represents a rotary or cycle view of the reality. This analysis indicates that there is a chain of reactions from the lunar nodal cycle to the biomass dynamics in the Barents Sea. This process may be understood as a chain of oscillators where gravity from the Moon is the forced oscillator and where energy is distributed on the Earth. The Earth energy is distributed in the chain of coupled oscillators in ocean tides, the food chain, and the biomasses in the Barents Sea. The stationary cycles in oscillating systems may be represented as vectors or a phase-clock. By this method, we may forecast when the biomass fluctuations are expected to change directions.

4.1. The Kola section temperature

The Kola section temperature series is an indicator of Atlantic inflow to the Barents Sea. It is generally believed that inflow of Atlantic water to the Barents Sea is driven by atmospheric conditions (Loeng et al., 1997). The identified dominant lunar nodal spectrum indicates that Atlantic inflow is influenced by the lunar nodal tide. Long period tides have been identified in the Atlantic Ocean and in the Barents Sea (Pettersson, 1914, 1915, 1930). Maksimov and Smirnov (1965) have analysed the surface temperature in the North Atlantic and found estimated temperature cycles close to the 18.6-year nutation cycle. The 18.6-year nodal tide has a pole-ward velocity component (Maksimov and Smirnov, 1967) and an amplitude that is approximately 7% of the lunar diurnal component. This will influence the surface layer ocean and air temperature at high latitudes (Royer, 1993; Keeling and Whorf, 1997). Maksimov and Smirnov have suggested there is a long period tide in the Barents Sea (Maksimov and Smirnov, 1964, 1967; Maksimov and Sleptsov-Shevlevich, 1970; Yndestad, 1999a). A wavelet analysis of Polar motion, Barents Sea ice extent, the NAO winter index indicates the Earth nutation introduces a nodal spectrum of about $18.6/15 = 1.2$, $18.6/3 = 6.2$, 18.6 and $4*18.6 = 74.5$ years in the Polar motion. The same spectrum is identified in Barents Sea ice extent and in the NAO winter index (Yndestad, 2003). This anal-

ysis indicates that the 6.2-, 18.6- and 74.5-year cycles are caused by a push–pull effect between the Atlantic Ocean and the Arctic Ocean where circulating water in the Arctic Ocean is influenced by Polar motion. A possible source of the 55.8-year cycle is an additive relation between the 6.2- and the 18.6-year cycle.

4.2. The food chain dynamics

Fluctuations in Atlantic inflow to the Barents Sea influence fluctuations in the sea temperature, the ice extent, the air temperature, the light conditions, the nutrients, the phytoplankton biomass, and the zooplankton biomass. *Calanus finmarchicus* is a major component in fuelling the recruitment and growth of capelin, herring and cod in the Barents Sea. Investigations show that there is strong correlation between Atlantic inflow and the growth of the *C. finmarchicus* zooplankton (Sundby, 2000). Total zooplankton density, dominated by the copepod (*C. finmarchicus*) is almost three times higher in the Atlantic water, than in melt water (Hassel et al., 1991; Melle and Skjoldal, 1998). This probably explains the high growth during warm periods. The density of plankton in the largest size fraction is significantly higher in colder Arctic water than in the eastern areas of the Barents Sea (Melle and Skjoldal, 1998). An analysis of zooplankton time from 1987 to 2001 shows there is a close relation between the Kola temperature cycles of 6.2 and 18.6 years, fluctuations in the zooplankton time series and the capelin recruitment rate (Yndestad and Stene, 2002).

4.3. The biomass dynamics

The estimated relation between biomass cycles and temperature cycles support the matching theory from Johan Hjort on a macro-level. Hjort (1914) analysed the length distribution of Northeast Arctic cod and explained fluctuations in the biomass as caused by a match or mismatch between the spawning time and food for the larvae.

The biomass dynamics of Northeast Arctic shrimp, Norwegian Spring spawning herring, Northeast Arctic cod, and Northeast Arctic haddock have an eigen frequency cycle of abort 6.2 years. The Barents Sea capelin has an eigen frequency cycle of about 6.2/2 years. If we look at the biomasses as a set of resonators, there will be an optimal recruitment when there is a match between the 6.2-year Kola temperature cycle and the 6-year biomass resonator cycle time. A more close analysis of long-term herring fluctuations shows that there is a long-term growth when the 6.2- and the 18.6-year cycles are positive at the same time, a biomass reduction when they are not, and a biomass collapse when both cycles are negative (Yndestad, 2002). This property explains estimated long-term fluctuations in the biomass of capelin, cod and herring in the Barents Sea (Izhevskii, 1961, 1964; Ottestad, 1942; Wyatt et al., 1994; Yndestad, 1999b; Malkov, 1991, 2002).

4.4. Methods and materials

The analysis has some potential sources of errors. There may be errors in the data samples which cannot be controlled. In this investigation, long trends in the data are analysed. Changes in methods of estimating data may then influence the long-term cycles. There is a potential source of a long-term error in long-term fluctuations between connected time series. The herring time series has a connection in 1946, the cod time series in 1900 and 1946. This may have influenced the phase of the estimated dominant cycles. The computed wavelets represent a low-pass filtered data series. Single random data errors are not therefore supposed to be a major problem in the wavelet analysis.

The time series is analysed by a wavelet transformation to identify dominant cycle periods and phase relations. The Coiflet3 wavelet transformation (Matlab Toobox, 1997) is chosen from many trials on tested data. This wavelet transformation is useful to identify cycles in the time series. The cycle identification has two fundamental problems. One problem is identifying periodic cycles when the phase has a reversal in the time series. The phase reversal property of the stationary cycles excludes traditional spectrum estimate methods. The problem is solved by first identifying the dominant cycles and correlates the cycles to known reference cycles. The second problem is identifying the long period cycles of 55 and 74 years. This problem is solved by the same method. First, identify the dominant long wavelet periods, then correlate the periods to a known cycle reference.

The results have identified good correlation between the time series and the dominant wavelet cycles, and there is good correlation between the dominant wavelet cycles and the lunar nodal spectrum. There is good correlation between the time series and the estimated dominant wavelet cycles, and there is a good signal to noise relation between the estimated wavelets and the noise difference. The close relation between the lunar nodal tide cycles and the biomass eigen frequency in all biomasses supports the indication of a long-term adopted property. The 18.6-year Kola section temperature cycle has a stationary frequency but not always a stationary phase. This property may influence the Kola temperature phase-clock. A closer analysis of the Kola section temperature series and Barents Sea ice extent has identified that the phase of the 18.6-year temperature cycle has shifted 180° in the period from about 1890 until 1925 when a 74-year was in a negative state (to be published). The phase reversal of the lunar nodal cycles explains why this cycle has been difficult to identify by others (Ottersen et al., 2000).

4.4.1. The implications

The results show a close relation between the stationary 18.6-year lunar nodal tide, dominant temperature cycles in the Barents Sea, and dominant cycles in the biomass of Barents Sea shrimp, Barents Sea capelin, Norwegian Spring spawning herring, Northeast Arctic cod, and Northeast Arctic haddock. This opens a new perspective to describe time variant climate dynamics and biomass dynamics in the Barents Sea. The deterministic property of the cycles opens a new set of possibilities for better forecasting and long-term management. The deterministic relation between biomass growth and the Kola cycles opens a possibility of more optimal management in short-term periods of 6 years, medium-term management of 18 years and long-term management of 55–75 years. The phase-clock is a simple indicator of the current state of the biomass. This will help fisheries and the industry to make better plans for the future.

Acknowledgements

I would like to thank Vladimir Ozhigin at PINRO institute in Murmansk and Svein Sundby at Institute of Marine Research (IMR) in Bergen for access to the Kola section temperature data series, Olav Rune Godø at IMR in Bergen for access to the data series on Northeast Arctic cod and Tara Marshall at IMR in Bergen for access to the Barents Sea capelin data series.

References

Andersen, P.J., 1991. Age, growth and mortality of the nothern Shrimps *Pandalus borealis* Krøyer in Pavlof Bay, Alaska. Fishery Bulletin, vol. 89. US Dept. of Commerce, National Oceanic and Fishery. Washington D.C., pp. 541–553.

Bochkov, Y.A., 1982. Water temperature in the 0–200 m layer in the Kola–Meridian in the Barents Sea, 1900–1981Sb. Nauchn. Trud., vol. 46. PINRO, Murmansk, pp. 113–122 (in Russian).

Daubehies, I., 1992. Ten lectures of wavelet. SIAM Journal on Mathematical Analysis 24 (2), 499–519. Mar. 1993.

Gjøsæter, H., 1997. Studies of the Barents Sea capelin, with emphasis on Growth. Dr scient thesis, Department of Fisheries and Marine Biology, University og Bergen, Norway, Paper III, IV and V.

Godø, O.R., 2000. Fluctuation in Stock Properties of Arco-Norwegian Cod Related to Long-term Environmental Changes. IIASA. Interim Report IR-00-023. April 6, 2000 Austria. http://www.iiasa.ac.at/cgi-bin/pubsrch?IR00023.

Hassel, A., Skjoldal, H.R., Gjøsæter, H., Omli, L., 1991. Impact of grazing from capelin (*Mallotus villosus*) on zooplankton: a case study in the northern Barents Sea in August 1985. Polar Research 10 (2), 371–388.

Hjort, J., 1914. Fluctuations in the Great Fisheries of Northern Europe Andr. Fred. Høst and Files, Copenhagen April.

Hylen, A., 2002. Fluctuations in abundance of Northeast Arctic cod during the 20th century. ICES Marine Science Symposia, 543–550.

ICES, 2002a. Northern Pelagic and Blue Whiting Fisheries Working Group. ICES CM 2002/ACFM:19. Vigo Spain. 29 Aril–8 May. 2002.

ICES, 2002b. Report of the Arctic Fisheries Working Group. ICES CM 2002/ACFM:18. ICES Headquarters 16–25 April 2002.

Izhevskii, G.K., 1961. Oceanological Principles as Related to the Fishery Productivity of the Seas Pishcepromizdat, Moscow [Translated 1966: Israel Program for Science Transactions. Jerusalem]. 95 pp.

Izhevskii, G.K., 1964. Forecasting of oceanological conditions and the reproduction of commercial fish. All Union Science Research Institute of Marine Fisheries and Oceanography. Israel Program for Science Transactions, Jerusalem. 22 pp.

Keeling, C.D., Whorf, T.P., 1997. Possible forcing global temperature by oceanic tides. Proceedings, National Academy of Science of the United States 94, 8321–8328 (August).

Loeng, H., Ozhigin, V., Ådlandsvik, B., 1997. Water fluxes through the Barents Sea. ICES Journal of Marine Science 54, 310–317.

Maksimov, I.V., Smirnov, N.P., 1964. Long range forecasting of secular changes of the general ice formation of the Barents

Sea by the harmonic component method. Murmansk Polar Sci. Res. Inst., Sea Fisheries 4, 75–87.

Maksimov, I.V., Smirnov, N.P., 1965. A contribution to the study of causes of long-period variations in the activity of the Gulf Stream. Oceanology 5, 15–24.

Maksimov, I.V., Smirnov, N.P., 1967. A long-term circumpolar tide and its significance for the circulation of ocean and atmosphere. Oceanology 7, 173–178 (English edition).

Maksimov, I.V., Sleptsov-Shevlevich, B.A., 1970. Long-term changes in the tide-generation force of the moon and the iciness of the Arctic Seas. Procedings of the N.M. Knipovich Polar Scientific-Research and Planning Institute of Marine Fisheries and Oceanography (PINRO) 27, 22–40.

Malkov, A.S., 1991/L. Movement of the earth pole and population dynamics of some commercial fish species from the northern Atlantic. The 79th international ICES Annual Science Symposium. ICES, Copenhagen, p. 77.

Malkov, A.S., 2002. Movements of the Earth pole and population dynamics of Norwegian Spring spawning herring and Arctic cod. The 90'th International ICES Annual Science Symposium, Copenhagen, Denmark, 1 Oct-5. CM 2002/O:09.

Marshall, T.C., Yaragina, N.A., Ådlandsvik, B., Dolgov, A.V., 2000. Reconstruction the stock–recruit relationship for Northeast Arcric cod using a bioenergetic index of reproductive potential. Canadian Journal of Fisheries and Aquatic Sciences 57, 2433–2442.

Matlab Toobox, 1997. Users Guide. The Math Works, 24 Prime Park Way, Natick, USA.

Melle, W., Skjoldal, H.R., 1998. Distribution, life cycle and reproduction of *Calanus finmarchicus*, *C, hyperboreus* and *C. Glacialis* in the Barents Sea. Dr scient thesis, Department of Fisheries and Marine Biology, University og Bergen, Norway, Paper III. 33 pp.

Ottersen, G., Ådlandsvik, B., Loeng, H., 2000. Predicting the temperature of the Barents Sea. Fisheries Oceanography 9 (2), 121–135.

Ottestad, P., 1942. On periodical variations on the yield on the great sea fisheries and the possibility of establishing yield prognoses. Fiskeridirektoratets Skrifter VII (5) (Bergen, Norway).

Pettersson, O., 1914. Climatic variations in historic (*sic*) and prehistoric time. Svenska Hydrogr. Biol. Kommissiones Skrifter 5, 26.

Pettersson, O., 1915. Long periodical (*sic*) variations of the tide-generating force: Conseil Permanente International pour l'Exploration de la Mer (Copenhagen). Pub. Circ. 65, 2–23.

Pettersson, O., 1930. The tidal force. A study in geophysics. Geografiska Annaler 18, 261–322.

Pugh, D.T., 1996. Tides, Surges and Mean Sea-Level. Wiley, New York.

Rassmussen, B., 1953. On the geographical variation in growth and sexual development of deep sea prawn (*Pandalus borealis* Kr.). Fiskeridir. Skr. Havundersøkelser. 10 (3), 1–160 (160 p. Bergen. Norway).

Rollefsen, G., Strøm, J., et al. 1949. NORSK FISKERI OG FANGST HÅNDBOK. BIND 1. Alb. Cammermeyers Forlag. Oslo. Norway (in Norwegian).

Royer, T.C., 1993. High-latitude oceanic variability associated with the 18.6-Yr nodal tide. Journal of Geophysical Research 98 (C3), 4639–4644 (March 15).

Sundby, S., 2000. Recruitment of Atlantic cod stocks in relation to temperature and advection of copepod populations. *Sarsia* 85, 277–298.

Teigsmark, G., 1980. Populasjoner av dyphavsreke (*Pandalus borealis* Krøyer i Barentshavet, Universitetet i Bergen. Norway.

Wyatt, T., Currie, R.G., Saborido-Ray, F., 1994. Deterministic signals in Norwegian cod records. ICES Marine Science Symposium 198, 49–55.

Yndestad, H., 1999a. Earth nutation influence on the temperature regime in the Barents Sea. ICES Journal of Marine Science 56, 381–387.

Yndestad, H., 1999b. Earth nutation influence on system dynamics of Northeast arctic cod. ICES Journal of Marine Science 56, 562–657.

Yndestad, H., 2001. Earth nutation influence on Northeast Arctic management. ICES Journal of Marine Science 58, 799–805.

Yndestad, H., 2002. . The 2002 ICES Annual Science Conference. Copenhagen. "The Code of Long-term Fluctuations of Norwegian Spring spawning herring". CM 2002/Q:02.

Yndestad, H., 2003. A lunar nodal spectrum in Arctic time series. ICES Annual Science Conference. Sept 2003. Tallinn. ICES CM 2003/T. ICES. Copenhagen.

Yndestad, H., Stene, A., 2002. System dynamics of Barents Sea Capelin. ICES Journal of Marine Science 59, 1155–1166.

Paper VII

The Lunar Nodal Cycle influence on the Arctic Climate

Harald Yndestad

Abstract

The Arctic Ocean is a substantial energy sink for the Earth's Northern Hemisphere. Fluctuations in its energy budget will have a major influence on the Arctic climate. This paper presents an analysis of the time series for the polar position, the extent of Arctic ice, the sea level at Hammerfest, the Kola section sea temperature, the Røst air winter temperature and the NAO winter index as a way to identify a source of dominant cycles. The investigation uses a wavelet transform to identify the time and phase of dominant cycles in these Arctic time series. The system dynamics is identified by studying of the phase-relation between the dominant cycles in all time series.

The investigation has identified a harmonic spectrum from the 18.6-year lunar nodal cycle in the Arctic time series. The cycles in this harmonic spectrum have a stationary cycle time, but not a stationary amplitude and phase. A sub-harmonic cycle of about 74 years may introduce a phase-reversal of the 18.6-year cycle. The signal- to noise-ratio between the lunar nodal spectrum and other sources changes from 1.6 to 3.2. A lunar nodal cycle in all time series indicates that there is a forced Arctic oscillating system controlled by the pull of gravity from the moon. This Arctic oscillation system influences long-term fluctuations in the extent of Arctic ice. The lunar nodal spectrum of Arctic ice extent influences the NAO winter index, the weather and the climate.

Key words: Arctic oscillation, climate oscillation, NAO winter index, polar motion, 18.6 - year lunar nodal cycle; wavelet analysis

Harald Yndestad: Aalesund University College, 6025 Aalesund, Norway.
Tel: +47 70 16 12 00; fax: +47 70 16 13 00; e-mail: harald.yndestad@hials.no

Introduction

The Greek word for bear is arctos, a word that has lent its name to the stellar constellation of the Great Bear. The Arctic region takes its name from this constellation, thus linking the region with the compass direction that points to the cold north. Small fluctuations in this northern pole may explain the Arctic climate oscillation.

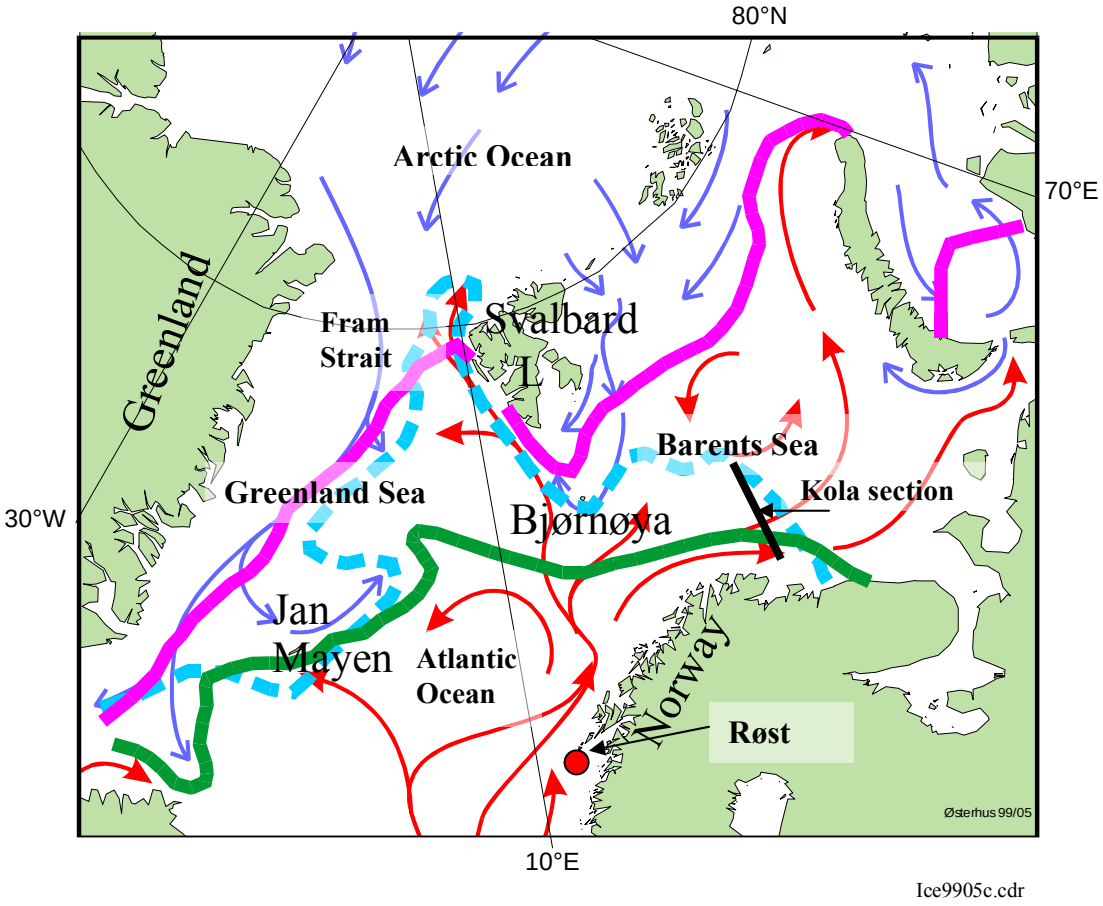

Figure 1 The study area with some ice edge observations and outlined ocean current pattern (Vinje, 2001).

The Arctic is the area north of the Arctic Circle (66°32'N), which includes the area of the midnight sun. The cold Arctic Ocean acts as an energy sink. The sun is never high on the sky, and most of its energy is reflected back to space by snow and ice in the summer. Cooled water accumulates in circulating layers. The Arctic Ocean has four layers; the Arctic Surface Water, the Atlantic Water, the Deep Water and Bottom Water, all of which have different densities and circulation patterns. Atlantic water from the Norwegian Sea enters the Eurasian Basin through the Fram Strait and underneath the surface layer. At a level of about 200-900 m it follows the continental slope eastward and north till it meets the Transpolar Drift and returns to the Greenland Sea. The Atlantic water residence time is about 25 years (Aagaard and Greisman, 1975; Wallace and Moore, 1985). The circulating pattern in the Arctic Ocean is most likely influenced by the circulating polar movement. Deep Water down to 2600 m from

the Norwegian Sea is exchanged between the Greenland Sea and the Eurasian Basin (Nansen Basin and Amundsen Basin). Deep Water residence time in the Eurasian Basin is estimated to be about 75 years (Bonisch and Schlosser, 1995). In this presentation a 75-year residence time is the same cycle period is identified in the polar motion, Barents Sea ice extent and Greenland ice extent. In the Amundsen Basin, Bottom Water (depth > 2600 m) residence time is estimated to be 290 -year +/- 30 years (Bonisch and Schlosser, 1995). A 290-year residence time is a fourth sub-harmonic of the 75-year cycle in the upper Deep Water.

Inflow to the Arctic Ocean passes from the North Atlantic through the Barents Sea and the eastern Fram Strait, with a minor inflow from the Bering Strait. The outflow is concentrated at the Canadian Archipelago and along East Greenland. Large-scale circulation processes in the Arctic Ocean's deep Canadian Basin, Markov Basin and Eurasian Basin all have a strong influence on the southward water transmission (Carmack et al., 1997; Gregor et al., 1998; Rudels et al., 1998). Cold Arctic water from the Eurasian Basin passes the western Fram Strait and moves into the Greenland Sea. From the Greenland Sea the cold water continues south with the East Greenland Current and the Labrador Current. East of Newfoundland the cold current meets the warm Atlantic drift from the south, and some of the water returns to the northern part of the Atlantic Ocean. Some Atlantic drift flows into the Barents Sea, and some returns to the Eurasian Basin through the Fram Strait (Anderson et al. 1994; Bonisch and Schlosser, 1995).

Izhevskii (1961, 1964) introduced a system view of interacting processes between the hydrosphere, the atmosphere and the biosphere. He argued that the heat in the ocean is an non-homogenous flow from a warm equator to the cold pole. This flow of heat in the ocean influences atmospheric processes. Atmospheric processes are reflected in the North Atlantic Oscillation (NAO) and the NAO has an influence on weather and climate in the Atlantic region. A strong positive NAO winter index will lead to stronger winds and warmer air in the winter. A positive trend since 1960 has increased winter temperatures in the northeastern Atlantic and the North Sea. This trend shift has led to speculations about more fundamental climate change.

The North Atlantic Oscillation may be caused by a more fundamental oscillation system. The Swedish oceanographer Dr. Otto Pettersson [1848-1941] postulated that the orbit of the moon and the earth have an influence on long period tides, climate cycles, and fluctuations of marine biomasses (Pettersson, 1905, 1914, 1915, 1930). Long-period tides have been identified in the Atlantic Ocean and in the Barents Sea. Maksimov and Smirnov (1965) and Currie (1981, 1984, 1987) have analyzed surface temperatures in the North Atlantic and estimated temperature cycles that are close to the 18.6-year lunar nodal cycle. Loder and Garret (1978) and Royer (1989, 1993) have estimated an 18.6-year temperature cycle on the east and west coast of North America. The 18.6-year nodal tide has a poleward velocity component (Maksimov and Smirnov, 1967) and an amplitude that is approximately 7% of the lunar diurnal component (Neuman and Pierson, 1966). This will influence the surface layer ocean and air temperature at high latitudes (Royer, 1993; Keeling and Whorf, 1997). Maksimov and Smirnov have suggested there is a long-period tide in the Barents Sea (Maksimov and Smirnov, 1964, 1967; Maksimov and Sleptsov-Shevlevich, 1970). Atlantic inflow to the Barents Sea is reflected in the Kola section temperature series (Bochkov, 1982). Harmonic lunar nodal cycles of 18.6/3=6.2, 18.6 and 3*18.6=55.8 years have been identified in this time series (Yndestad, 1999a; Yndestad, 2003).

There seems to be a chain of events linking the 18.6-year lunar nodal cycle and the same period cycles in the Barents Sea. This paper presents a wavelet spectrum analysis of the time series from the polar position, the Barents Sea ice extent, the sea level at Hammerfest, the

Kola section sea temperature, the Greenland Sea ice extent, the Røst winter air temperature and the NAO winter index. The time series are analyzed with a wavelet transformation to identify dominant cycle periods and phase in each time series. The analysis has identified an 18.6-year nodal spectrum in all time series. The identified spectrum is explained by an oscillating climate disturbance caused by a gravity oscillation from the moon. The gravity force from the 18.6-year lunar nodal cycle influences the polar position and circulating water in the Arctic Ocean. A stationary polar position cycle forces the Arctic Ocean and introduces an Arctic oscillation that interacts with the Atlantic Ocean, the Arctic ice extent and Arctic atmospheric conditions. The force from the lunar nodal spectrum is transformed into a spectrum of oscillating water circulation where some harmonic cycles are preserved by resonance. A continuous supply of movement energy is distributed throughout circulating water in the Atlantic Ocean. In this circulating process, the Arctic Ocean influences the Atlantic Ocean inflow to the Barents Sea, as well as fluctuations in the water temperature, the Arctic ice extent, the air temperature and the North Atlantic Oscillation.

Materials and methods

The polar position data series (x-direction and y-direction) are based on the official data from the International Earth Rotation Service (IERS) and covers the years from 1846 until 2002. The time series can be found at: <http://hpiers.obspm.fr/eoppc/eop/eopc01/>. The time series contains 10 samples per year from 1846 to 1900, and 20 samples per year from 1900 to 2002, with the celestial pole offset represented in arc degrees. This time series was used to analyze the Chandler wave. The 6-, 18- and 74-year cycles are all identified by the annual mean value of this time series.

The area of Greenland Sea ice extent that is referred to in this paper covers the Greenland Sea, the Iceland Sea and the Norwegian Sea bounded by 30°W, 10°E and 80°N. The data are based on April values from 1864 until 1998 (Vinje, 2001). The area of Barents Sea ice extent covers the Norwegian Sea, the Barents Sea and the Kara Sea bounded by 10°E, 80°N and 70°E. The data are based on April values from 1864 until 1998 (Vinje, 2001).

Russian scientists at the PINRO institute in Murmansk have provided monthly temperature values from the upper 200 m in the Kola section along the 33°30'E medial from 70°30'N to 72°30'N in the Barents Sea (Bochkov, 1982). The data series from 1900 until 2001 contains quarterly values from the period 1906-1920 and monthly values from 1921, some of which are measured and some of which are interpolated. This paper analyzes the annual mean temperature.

The Røst air temperature data series have been provided by the Norwegian Meteorological Institute in Oslo. The time series has monthly values. For the purposes of this analysis, the winter air temperature at Røst has been computed as the mean winter temperature between December and March. The total time series covers Røst (67°35’N, 12°E) from 1880 to 1969, Skomvær (67°30’N, 12°E) from 1970 to 1978, and Røst from 1979 to 1997.

The North Atlantic Oscillation (NAO) is defined as the normalized pressure difference between a station on the Azores and one on Iceland. The NAO index analysis is based on the official data from Climate Research Unit and covers the years 1822 until 2001. The data series can be found at: <http://www.cru.uea.ac.uk/cru/data/nao.htm>. In this analysis the NAO winter index is computed as the mean temperature from December to March.

Systems theory

The investigated climate system is represented by the simplified general system architecture:

$$S(t) = \{B(t), \{S_{Sun}(t), S_{Moon}(t), S_{Earth}(t), S_{Oce}(t), S_{Atm}(t), S_v(t)\}\} \quad (1)$$

where $S_{Sun}(t)$ represents the sun system, $S_{Moon}(t)$ the moon system, $S_{Earth}(t)$ the earth geo system, $S_{Oce}(t)$ the oceanographic system, $S_{Atm}(t)$ atmospheric system, $S_v(t)$ represents an unknown source, and B(t) represents a time variant mutual binding between the systems. In a system which all sub-systems are mutually related, a dominant energy source will influence the others.

Gravity effects between the sun, the earth and the moon result in a set of long orbital cycles that influence climate on the earth (Imbrie and Imbrie, 1980; Satterley, 1996). The earth's average orbital motion around the sun defines the ecliptic. At the same time the earth's spin axis rotates around the pole of the equatorial plane. The earth's nutation is a predictable cycle of the earth's spin around its axis on a time scale less than 300 years. The four dominant periods of nutation are cycles of 18.6134 years, 9.3 years, 182.6 days (half a year), and 13.7 days (half a month). The most dominant of the four cycles is the nutation cycle of 18.6134 years. The polar position changes in the x- and y-direction of the pole of ecliptic. The pole position changes from about 0.1 to 0.3 arc degrees, which represents a displacement of about 5 to 15 meters. This investigation examines the potential influence of the 18.6-year lunar nodal cycle on time series.

The lunar node is the cross-point between the moon plane cycle and the ecliptic plane to the sun. This cross-point describes a lunar nodal cycle of 18.6134 years. The corresponding cycle of the changing inclination of the moon's orbit with respect to the earth's equatorial plane is described by the model:

$$u_0(t) = 23^\circ 27' + 5^\circ 09' \sin(\omega_0 t + \varphi_0) \quad (2)$$

where $\omega_0 = 2\pi/T_0 = 2\pi/18.6134$ (rad/year) is the lunar nodal angle frequency, $\varphi_0 = 0.90\pi$ is the lunar nodal cycle phase and t (year) is the time. The cycle amplitude has a maximum in November 1987 and a minimum in March 1996 (Pugh, 1996). The gravity energy from the moon introduces a horizontal and vertical 18.6-year lunar nodal tide in the Atlantic Ocean and the 18.6-year nutation of the earth's axis.

Energy from a forced stationary cycle is expected to be distributed in a harmonic spectrum on a nonlinear system (Moon, 1987). A similar effect is expected from an oscillating gravity force on a nonlinear earth system. This spectrum has a set of harmonic and sub-harmonic cycles. A lunar nodal spectrum may be represented by the model:

$$u(t) = \sum_{n,m} u_{n,m}(t) \sin(n\omega_0 t / m + \varphi_{n,m}(t)) \quad (3)$$

where u(t) is the lunar nodal spectrum, $u_{n,m}(t)$ is the cycle amplitude, and $\varphi_{n,m}(t)$ is the cycle phase. Some of these cycles may be amplified by resonance in the earth's circulating geo system, the ocean system and the atmospheric system.

Cycle identification

The present analysis is based on the hypothesis that the time series have a set of stationary cycles represented by a state that can be modeled:

$$x(t) = \sum_k U(k,t) + v(t) \qquad (4)$$
$$U(k,t) = u(k,t)\sin(k\omega_0 t + \varphi(k,t))$$

where x(t) is the measured time series, U(k,t) is a dominant stationary cycle, k is a cycle period, and v(t) is a disturbance from an unknown source. The temporary stationary cycle U(k,t) has an amplitude u(k,t), an angle frequency $\omega_k=2\pi/k$, (rad/year) and a time variant phase angle φ(k,t). The phase delay between the time series is identified by a phase difference $\varphi_i(k,nT)-\varphi_j(k,nT)$. The stationary cycle U(k,t) may have a phase-reversal that changes the phase angle φ(k,t) π rad in the analyzed time series. A phase-reversal may be explained by an amplitude modulation U(t)=K[1+mU(a,t)]U(a,t) where U(a,t) and U(b,t) represent two stationary cycles. An amplitude modulation will introduce a phase-reversal when mU(a,t) > 1 (Carlson, 1968).

The time series have been analyzed by a wavelet transformation to identify a dominant cycle period U(k,t) and the time variant phase angle φ(k,t). The dominant cycle periods have been identified by a three step investigation. The first step was to compute the wavelet spectrum by the transformation:

$$W(a,b) = \frac{1}{\sqrt{a}}\int_R x(t)\Psi(\frac{t-b}{a})dt \qquad (5)$$

where x(t) is the analyzed time series and Ψ( ) is the wavelet impulse function, W(a,b) is a set of wavelet cycles, b is the translation in time and a is the time scaling parameter in the wavelet transformation. The computed wavelets W(a,b) represent a correlation between x(t) and the impulse functions Ψ( ) over the whole time series x(t). The Coiflet3 wavelet transformation was chosen from many trials on tested data. Using this wavelet transformation it is possible to identify single, long-period cycles in short time series. Errors at the beginning and at the end of a time series are reduced by the 'sym' property in Matlab (Matlab, 1997; Daubechies, 1992).

The time series x(t) may be represented by a sum of dominant wavelets that contains most of the energy in the time series x(t). Then we have:

$$x(t) = [\mathrm{W(k1,t)} + \mathrm{W(k2,t)} + ... + \mathrm{W(kn,t)}] + \mathrm{v(t)} = \mathrm{W(t)} + \mathrm{v(t)} \qquad (6)$$

where W(k,t) represents a dominant wavelet cycle and v(t) is disturbance from an unknown source. A wavelet cycle W(k,t) represents a moving correlation with an impulse period k. A dominant cycle period thus represents the best correlation with a cycle period k. The wavelet cycle time k is tested by computing the cross-correlation coefficient R(k) between the

dominant wavelet cycle W(k,t) and a potential known cycle u(k,t). The correlation value of quality is computed by Q(k)=R(k)*sqrt[(n-2)/(1-R(k)*R(k))] where n is the number of samples. The signal-to-noise ratio between the dominant wavelets and an unknown source (Equation 6) is computed by S/N=var(W(t))/var(v(t)) where v(t)=(x(t)-W(t)) is the disturbance from an unknown source.

Results

Polar position

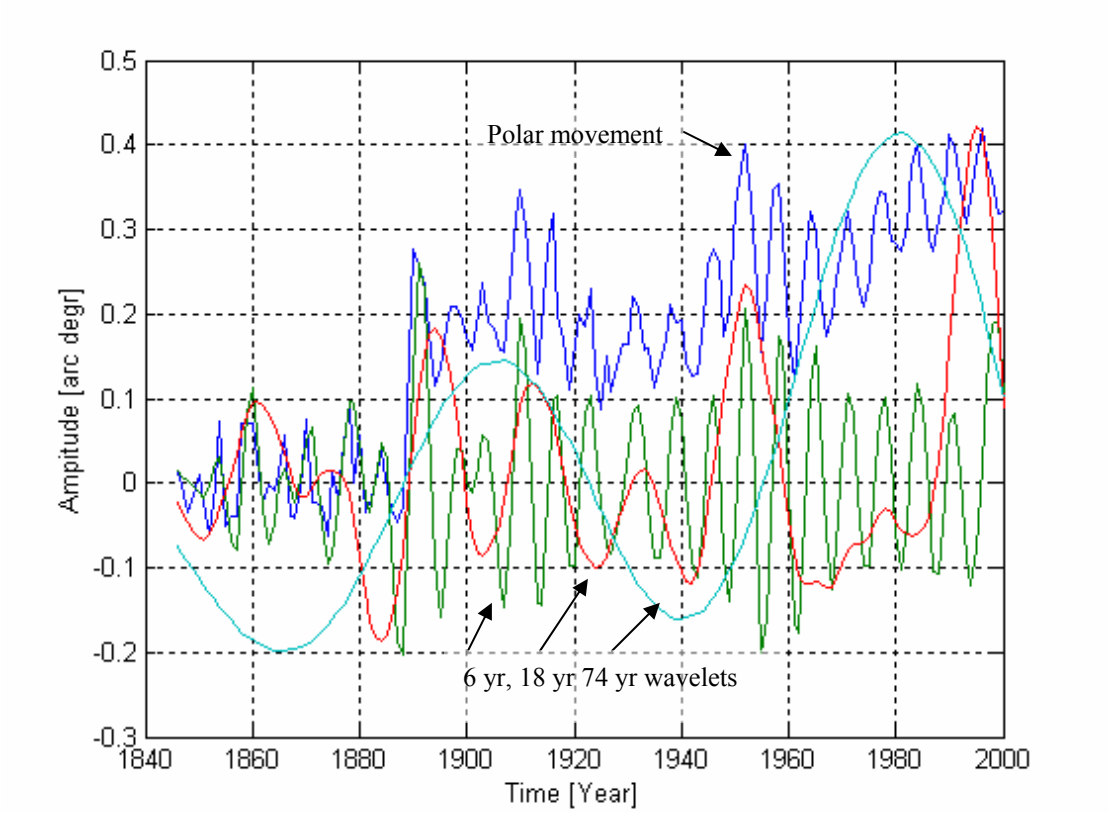

Figure 2 Polar position in the y-direction and estimated dominant wavelet cycles of 74, 18 and 6 years.

The pole position changes from about 0.1 to 0.3 arc degrees, which represents a displacement of about 5 to 15 meters. A wavelet analysis of the polar position time series from 1846 to 2002 has identified dominant wavelet cycles of about 1.2, 6, 18 and 74 years in the wavelet spectrum $W_P(1:100,nT)$. The time series and the estimated dominant wavelet cycles of 6, 18 and 74 years are shown on Figure 2. The identified dominant cycles are close to the stationary cycles:

$$
\begin{aligned}
&U_P(74,nT)=u_P(74,nT)\sin(\omega_0 nT/4+1.29\pi) \quad \text{when } n=1846\ldots2000\\
&U_P(18,nT)=u_P(18,nT)\sin(\omega_0 nT+0.90\pi) \quad \text{when } n=1870\ldots1960\\
&U_P(06,nT)=u_P(06,nT)\sin(3\omega_0 nT-1.09\pi) \quad \text{when } n=1846\ldots2000\\
&U_P(1.2,nT)=u_P(1.2,nT)\sin(3*5\omega_0 nT-1.09\pi) \quad \text{when } n=1991\ldots1997
\end{aligned}
\tag{7}
$$

These cycles represent a lunar nodal spectrum. The cross-correlation coefficients between the dominant wavelets and the stationary cycles are $R_P(74)=0.86$, $R_P(18)=0.70$, and $R_P(6)=0.44$ in when n=1846…2000. The correlation values of quality are computed as Q(74)=20.5, Q(18)=5.2, Q(6)=6.0. The degrees of freedom are 153, 78 and 153. The cross-correlation coefficient between the polar position and the dominant wavelets are estimated to be $R_{x,w}$ = 0.85. The signal-to-noise ratio is estimated to be S/N=2.6. This close correlation indicates that the gravity force from the lunar nodal cycle has a major influence on polar movement.

The cycle phase-relation between the 18.6-year lunar nodal cycle is $\varphi_L(18,nT)-\varphi_P(18,nT)=(0.90\pi-0.90\pi)=0.0\pi$ (rad) in the period from about n=1870…1960. At about 1960, the 18-year cycle had a π rad phase-reversal. A phase difference of about 0.0π (rad) demonstrates that the 18-year polar movement cycle $W_P(18,nT)$ is correlated in both frequency and phase to the 18.6-year lunar nodal cycle. The cycle has a phase-reversal of π (rad) when the 74-year cycle has a minimum at about 1870 and 1950. The phase-reversal shows that the phase is controlled by the 74-year cycle. The close relationship identifies the lunar nodal cycle as the energy source that influences the 18.6-year cycle of polar movement. The polar y-position state has increased step by step in the period from 1846 to 2000. This indicates there may be longer sub-harmonic cycles in the polar position. A wavelet analysis of polar position in the x-direction has a stationary cycle of about 6.2 to 6.5 years. A dominant long-term cycle has a maximum at about the years 1890, 1930, 1950 and 1980 and a minimum at about 1910, 1935 and 1960. This indicates a relation to the 74-year cycle in the y-direction.

A wavelet analysis of the polar position in the y-direction and the x-direction show a stationary cycle of about 6.2 to 6.5 years that is connected to the 1.2-year Chandler Wave. In this time series there is no 18-year cycle. A longer-period dominant cycle has a maximum at about the years 1890, 1925, 1950 and 1990, and minimum at about 1910, 1935 and 1965. This indicates that this cycle is related to turning points of the 74-year cycle in the y-direction.

The 1.2-year wavelet cycle $W_P(1.2,nT)$ is a fifth harmonic cycle of the 6.2-year cycle. The correlation to $U_P(1.2,nT)$ is $R_P(1.2)=0.96$ when nT=1991.50, 1991.55…1997.50. This indicates that the 1.2-year Chandler Wave cycle may be a harmonic cycle in the lunar nodal spectrum. The cycle difference between the estimated wavelet cycle W(1.2,nT) and the stationary cycle U(1.2,nT) shows a small phase delay when the 6.2-year cycle is shifted between negative and positive values. This delay may have been caused by a force delay or a synchronization of resonance between the 1.2-year cycle and the 6.2-year cycle.

Barents Sea ice extent

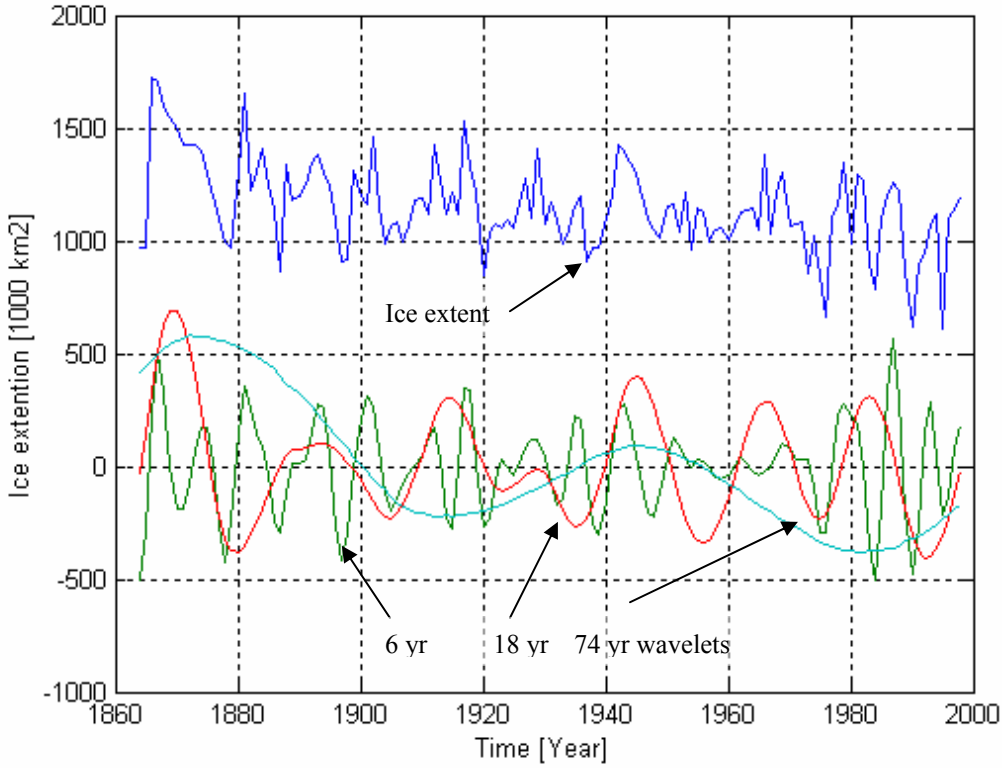

Figure 3 Barents Sea ice extent and dominant wavelets of 6, 18 and 74 years during the period 1864 to 1998.

The Barents Sea is a mixture of cold Arctic water from the Arctic Ocean and an inflow of warmer Atlantic water. The Barents Sea ice extent time series is a climate indicator in this area (Figure 3). The indicator covers a large area of the Barents Sea and the Kara Sea. The computed set of wavelets $W_B(1{:}80,nT)$ from the Barents Sea ice extent show the dominant wavelets $W_B(6,nT)$, $W_B(18,nT)$ and $W_B(74,nT)$, which represent dominant cycles of about 6, 18, and 74 years. Figure 3 shows the Barents Sea ice extent data series and the dominant wavelet cycles. The identified stationary dominant cycles are:

$$\begin{aligned} U_B(74,nT) &= u_B(74,nT)\sin(\omega_n nT/4+0.25\pi) \quad \text{when } n=1864\ldots1998 \\ U_B(18,nT) &= u_B(18,nT)\sin(\omega_n nT+0.50\pi) \quad \text{when } n=1930\ldots1998 \\ U_B(6,nT) &= u_B(6,nT)\sin(3\omega_n nT+\varphi_B(6,nT)) \quad \text{when } n=1864\ldots1998 \end{aligned} \tag{8}$$

$W_B(74,nT)$ shows a trend shift in the years 1890, 1930 and 1965, a minimum in 1910 and 1980, and a maximum in 1945. The cross-correlation coefficients between the dominant wavelet cycles and the lunar nodal cycles are $R_P(74)=0.73$ and $R_P(18)=0.74$. The correlation values of quality are computed to be $Q(74)=12.2$ and $Q(18)=8.0$, with 133 degrees of freedom.

The cycle has a phase-reversal in periods when the 74-year cycle $W_B(74,nT)$ has a maximum, a minimum and a zero value. The 74-year cycle introduces a phase-reversal in the 18-year and the 6-year cycles. The phase angle $\varphi_B(18,nT)=1.50\pi$ (rad) in the period n=1895…1930 when $W_B(74,nT)$ has a negative period and $\varphi_B(18,nT)=0.50\pi$ (rad) from n=1930…1998 when $W_B(74,nT)$ has shifted to a positive period. The variable $\varphi_K(18,nT)$ is reversed π (rad) in the

time periods n= 1895…1930. The 6-year cycle has a phase-reversal when the 74-year cycle is reaches a minimum state or a maximum state at about 1870, 1815, 1945 and 1980. The cycle phase $\varphi_B(6,nT)=-0.09\pi$ (rad) in the period n=1980…1998 has a cross-correlation of $R_P(6)=0.64$, an estimated quality value of Q(6)=3.5 and 17 degrees of freedom. The signal-to-noise ratio is estimated to be $S/N_B=2.0$. The cycle phase differences between the polar position and Barents Sea ice extent are:

$$\varphi_P(74,nT)-\varphi_B(74,nT)= (1.29\pi-0.25\pi)=1.04\pi \text{ (rad) when n=1884…1998}$$
$$\varphi_P(18,nT)-\varphi_B(18,nT)= (0.90\pi-0.50\pi)=0.40\pi \text{ (rad) when n=1930…1998} \quad (9)$$
$$\varphi_P(06,nT)-\varphi_B(06,nT)=(-1.09\pi--0.09\pi)= 1.0\pi \text{ (rad) when n=1980…1998}$$

The dominant cycle 74 years have a phase delay of about π (rad) compared to the same polar position cycle. The 18-year ice extent cycle is more closely related to the 18 year Kola cycle. The polar position is then expected to be the source of the long-term 74 year oscillation in ice extent. At the same time the 6-years and the 18-year lunar nodal tide is expected to be the source of the 6-year and the 18-year oscillation.

The Kola section temperature

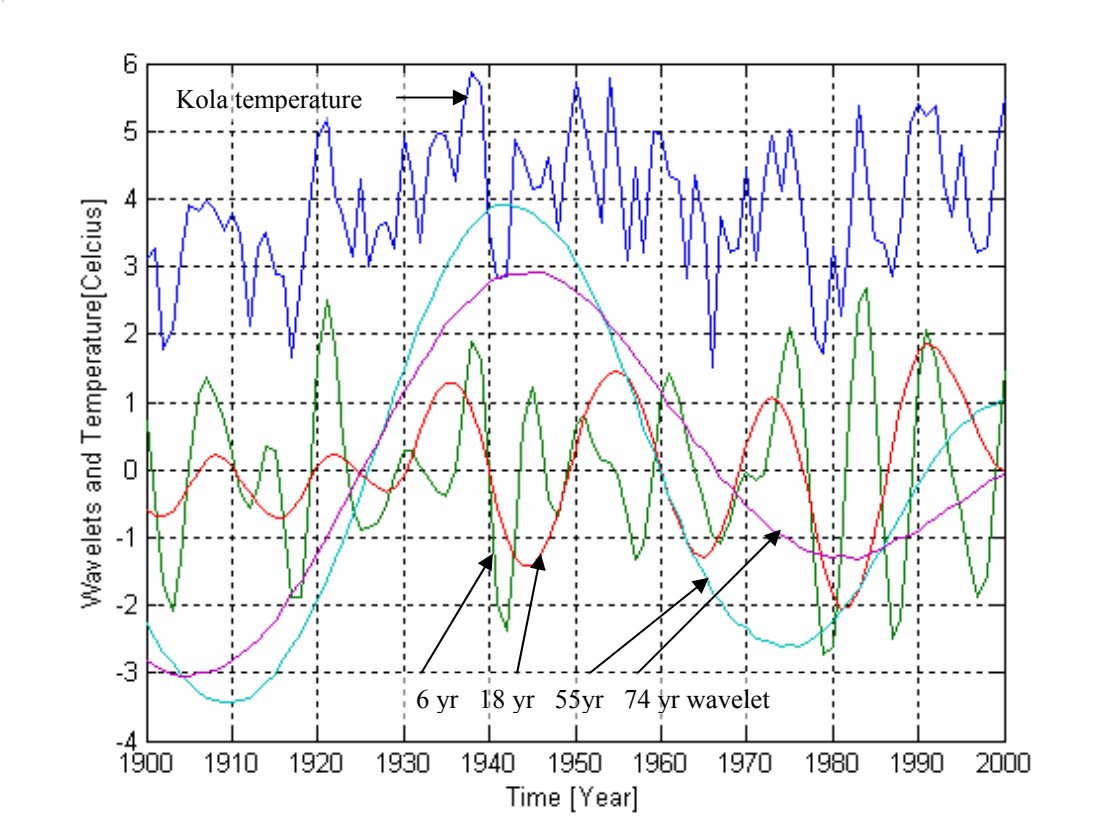

Figure 4 Kola data series and dominant wavelets of 6, 18, 55 and 74 -year.

The Kola section time series is an indicator of the Atlantic inflow to the Barents Sea. The computed set of wavelets $W_K(1:80,nT)$ for the Kola temperature data series has the dominant wavelets $W_K(6,nT)$, $W_K(18,nT)$, $W_K(55,nT)$ and $W_K(74,nT)$. Figure 4 shows the time series

from the time where n=1900…2000 and the identified dominant wavelets cycles of 6, 18, 55 and 74 years. A stationary representation of the dominant cycles is:

$$\begin{aligned} &U_K(74,nT)=u_K(74,nT)\sin(\omega_n nT/4+0.29\pi) \text{ when } n=1900\ldots2000 \\ &U_K(55,nT)=u_K(55,nT)\sin(\omega_n nT/3+0.90\pi) \text{ when } n=1900\ldots2000 \\ &U_K(18,nT)=u_K(18,nT)\sin(\omega_n nT+0.55\pi) \text{ when } n=1930\ldots2000 \\ &U_K(06,nT)=u_K(06,nT)\sin(3\omega_n nT+\varphi_K(06,nT)) \text{ when } n=1900\ldots2000 \end{aligned} \quad (10)$$

The 74-year cycle has a trend shift in 1925 and 1960, minimum values in 1905 and 1980, and a maximum in 1945. The cross-correlation coefficients for to the long periods are $R_K(74)=0.95$ and $R_K(55)=0.89$ and value of quality is estimated to $Q_K(55)=30.1$. There are n-2=98 degrees of freedom. This gives a better than 95% confidence in a t-distribution.

The 74-year cycle introduces a phase-reversal in the 18-year and the 6-year cycle. The phase-angle is $\varphi_K(18,nT)=0.55\pi$ (rad) in the period n=1930…2000 and $\varphi_K(18,nT)=1.55\pi$ in the period n=1900…1930. There was a phase-reversal when the 74-year cycle shifted from a negative to a positive state. The cross-correlation coefficient and the quality are $R_K(18)=0.90$ and $Q(18)=18.3$ when the phase of $\varphi_K(18,nT)$ is shifted in this period. The 6-year cycle has a cross-correlation coefficient of $R_K(6)=0.4$ when $\varphi_K(6,nT)=-0.09\pi$ (rad) in the period n=1930…1970 when the 74-year cycle is in a positive state. The phase angle has a phase-reversal of $\varphi_K(6,nT)=-1.09\pi$ (rad) in the period n=1970…2000 when the 74-year cycle is in a negative state. In this period the cross-correlation coefficient is estimated to be $R_K(6)=0.37$ and $Q_K(6)=3.9$. The signal-to-noise ratio between the wavelet sum $W_K(nT) = [0.4W_K(06,nT) + 0.4W_K(18,nT) + 0.1W_K(55,nT)]$ and the unknown source $v(nT)=(x_K(nT)-W_K(nT))$ is estimated to be $S/N_K=3.2$. This confirms that the estimated nodal spectrum represents most of the fluctuations in the time series.

The phase-delay between the polar position cycles and the estimated 18.6-year Kola temperature cycles are:

$$\begin{aligned} &\varphi_P(74,nT)-\varphi_K(74,nT)=(1.29\pi-0.29\pi) = 1.00\pi \text{ (rad)} \\ &\varphi_P(18,nT)-\varphi_K(18,nT)=(0.90\pi-0.55\pi) = 0.35\pi \text{ (rad)} \\ &\varphi_P(06,nT)-\varphi_K(06,nT)=(-1.09\pi--0.09\pi) = 1.0\pi \text{ (rad)} \end{aligned} \quad (11)$$

The 6-year and the 18-year cycles have a delay of about one year between the cycle of ice extent and the Kola section temperature. This confirms that there is less ice when there is more Atlantic inflow. The phase difference between the estimated 74-year ice extent cycle and the Kola cycle is estimated to be about -0.04π (rad). The 74-year Kola cycle and the 74-year cycle of ice extent have the same phase. This surprising estimate suggests that the two cycles are controlled by different sources.

The Tide at Hammerfest

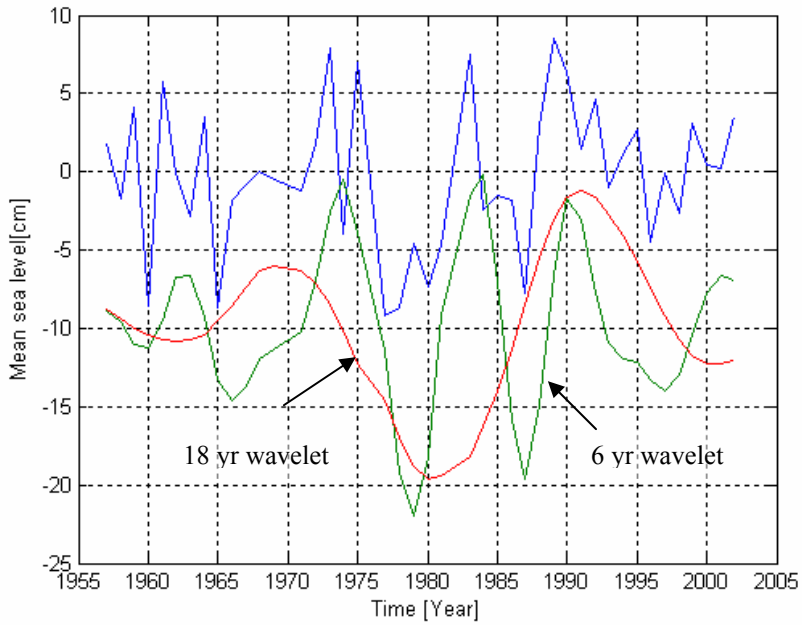

Figure 5 The annual mean sea level at Hammerfest and dominant wavelets of 6 and 18 years.

Figure 5 shows the time series of the annual mean sea level at Hammerfest in the period when n=1957…2002 and with the identified dominant wavelets cycles of 6 and 18 years. A stationary representation of the dominant cycles is:

$$U_H(18,nT)=u_H(18,nT)\sin(\omega_n nT+0.55\pi) \text{ when } n=1957\ldots2002 \quad (12)$$
$$U_H(06,nT)=u_H(6,nT)\sin(3\omega_n nT-0.09\pi) \text{ when } n=1980\ldots1992$$

The cross-correlation coefficient and the correlation quality are estimated to be $R_H(18)=0.73$ and $Q(18)=6.9$ with 41 degrees of freedom. The 6-year cycle has the phase angle $\varphi_H(6,nT)=-0.09\pi$ in the period n=1957…1956 and $\varphi_H(6,nT)=-1.09\pi$ from 1980…1992. In the period 1957 to 1977 there was a phase-reversal of π (rad) when the 18-year cycle had a minimum. The cross-correlation coefficient and the correlation quality in the total period are estimated for the 6-year cycle as $R_H(6)=0.37$ and $Q(2)=2.5$ with 41 degrees of freedom. The low correlation is related to the phase-reversal in the 6–year cycle. In this period, the cross-correlation coefficient is estimated to be $R_H=0.61$ and $Q=6.4$. The signal-to-noise ratio between the wavelets is $W_H(nT)=[W_H(06,nT)+0.9W_H(18,nT)]$ and the estimate difference $(x_K(nT)-W_K(nT))$ is estimated to $S/N_K=1.6$. The small S/N-ratio is caused by the phase-reversal of the 6-year cycle.

The phase delays between the polar position cycles and the estimated sea level cycles at Hammerfest are:

$$\varphi_P(18,nT)-\varphi_H(18,nT)=(0.90\pi-0.55\pi) = 0.35\pi \quad (13)$$
$$\varphi_P(06,nT)-\varphi_H(06,nT)=(-1.09\pi--1.09\pi) = 0.0\pi$$

The phase-relation between the 18-year cycles in the Hammerfest sea level and the Kola section sea temperature is $\varphi_H(18,nT)-\varphi_K(18,nT)=(0.55\pi-0.55\pi) = 0.0\pi$. This close relation shows that the long-term temperature fluctuation in the Kola section is influenced by the 18.6-year lunar nodal tide.

The Greenland Sea ice extent

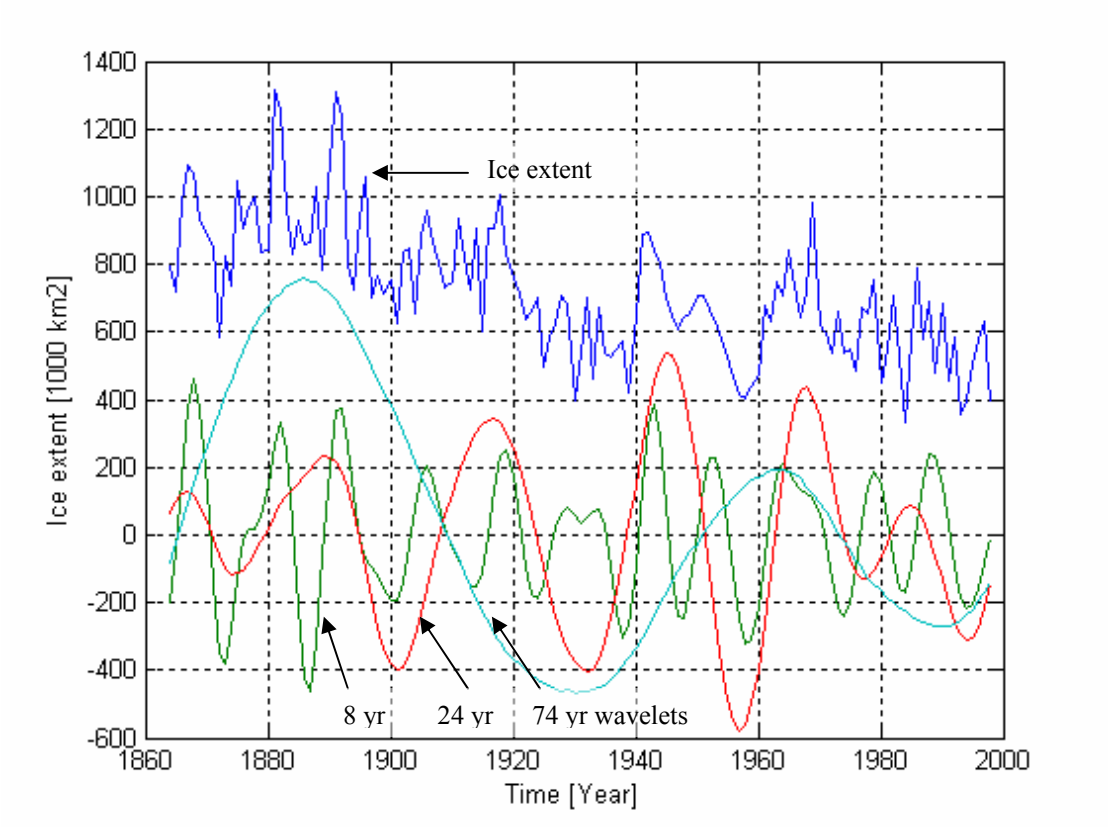

Figure 6 Wavelet cycles 1 to 80 of Greenland Sea ice extent.

The Greenland Sea ice extent covers an important area between West Greenland and Svalbard and serves as a climate indicator of the Arctic Ocean outflow to the Greenland Sea. The computed set of wavelets $W_G(1:100,nT)$ of the Greenland Sea ice extent shows dominant cycles at the wavelet cycles $W_G(6,nT)$, $W_G(24,nT)$ and $W_G(74,nT)$, representing cycle periods of 6, 24, and 74 years. The Greenland Sea ice extent data series and the dominant wavelet cycles are shown on Figure 6. The stationary representation of the dominant cycles is:

$$\begin{aligned} U_G(74,nT)&=u_G(74,nT)\sin(\omega_n nT/4+1.78\pi) \text{ when } n=1864\ldots1900 \\ U_G(24,nT)&=u_G(24,nT)\sin(3\omega_n nT/4+1.70\pi) \text{ when } n=1910\ldots1980 \\ U_G(08,nT)&=u_G(8,nT)\sin(9\omega_n nT/4+0.38\pi) \text{ when } n=1950\ldots1990 \end{aligned} \qquad (14)$$

All estimated cycles are related to the 18.6-year lunar nodal spectrum. A cycle period of 18.6*4=74.5 years is the fourth sub-harmonic cycle of the 18.6-year lunar nodal cycle and 74.5/3=24.8 years is a third harmonic cycle of the 74-year cycle. The cycle period of 24.8/3=8.5 years is a third sub-harmonic cycle of the 24-year cycle. The dominant 74-year wavelet cycle has a trend shift in the years 1870, 1910, 1945 and 1975, a minimum in 1930

and 1990, a maximum in the 1890 and 1960, and a cross-correlation coefficient of $R_G(74)=0.50$, a correlation value $Q(74)=5.89$ and 133 degrees of freedom. The 74-year cycle introduces a phase-reversal in the 24-year and the 8-year cycle in the time series. The estimated 24-year cycle W(24,nT) has the cross-correlation coefficient $R_G(24)=0.77$ with respect to the stationary cycle U(24,nT) in the 74-year cycle period n=1910…1980. The phase is $\varphi_G(24,nT)=0.70\pi$ (rad) when n=1864…1910 and $\varphi_G(24,nT)=1.70\pi$ (rad) in the period n=1910…1980. In this estimate the correlation quality value is $Q(24)=14.1$. The estimated 8-year cycle $W_G(8,nT)$ shows a phase shift in 1910, 1950 and 1980 when the 74-year cycle shifted between a positive and a negative state. In the period n=1950…1990 the phase angle is about $\varphi_G(8,nT)=0.38\pi$ (rad). In this period the cross-correlation coefficient is $R_G(8)=0.54$, and the quality value is estimated to be $Q(8)=4.01$ with 40 degrees of freedom. The signal-to-noise ratio between the wavelet sum $W_G(nT)=[100W_K(8,nT)+ 60W_K(24,nT)+60W_K(74,nT)]$ and the unknown source $v(nT)=(x_K(nT)-W_K(nT))$ are calculated to be $S/N_K=3.2$. This confirms that the estimated nodal spectrum from the 74-years cycle represents most of the fluctuations in the time series.

The phase delay between the estimated 74-year polar position cycle and the Greenland ice extent is $\varphi_P(74,nT)–\varphi_G(74,nT)=(1.29\pi-1.78\pi)=0.49\pi$ (rad). This estimate shows a delay of about 18.5 years between the 74-year cycle in the Polar position and the 74-year cycle outflow of cold arctic water from the Arctic Ocean to the Greenland Sea.

The Røst winter temperature

The winter air temperature at Røst is influenced by cold polar arctic winds from Greenland, via the surface of the North Atlantic Ocean, to the coast of northern Norway. The winter air temperature at Røst is measured on a small island in the Norwegian Sea on the Norwegian coastline.

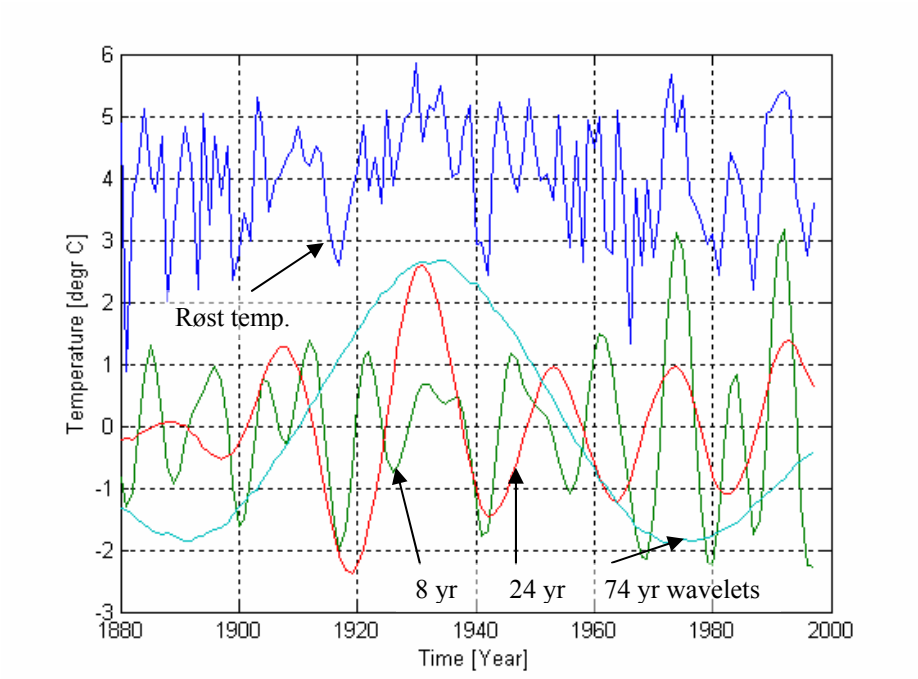

Figure 7 Winter air temperature data (+4) at Røst and dominant wavelets of 74, 24 and 8 years.

The computed set of wavelets $W_R(1{:}80,nT)$ from the Røst winter temperature has dominant wavelets at the wavelet cycles $W_R(8,nT)$, $W_R(24,nT)$ and $W_B(74,nT)$, which represent cycles of 8, 24, and 74 years. Figure 7 shows the temperature time series and the estimated dominant wavelets. The winter air temperature at Røst is scaled by +4 to separate the data series from the estimated wavelets. The stationary representation of the dominant cycles is:

$$\begin{aligned} U_R(74,nT)&=u_R(74,nT)\sin(\omega_n nT/4+0.51\pi) \text{ when } n=1880\ldots1997 \\ U_R(24,nT)&=u_R(24,nT)\sin(3\omega_n nT/4-0.701\pi) \text{ when } n=1880\ldots1910 \\ U_R(08,nT)&=u_R(08,nT)\sin(9\omega_n nT/4-0.382\pi) \text{ when } n=1880\ldots1930 \end{aligned} \quad (15)$$

The 74-year cycle has a trend shift at about the year 1910 and 1950, a minimum in 1900 and 1965, a maximum at about the year 1938, a cross-correlation coefficient of $R_R(74)=0.92$, a correlation value of $Q(74)=24$, with 116 degrees of freedom. This 74-year cycle controls a phase-reversal in the 24-year and the 8-year cycle. The cross-correlation coefficient is $R_R(24)=0.88$ with a quality value of $Q(24)=11.8$ in the period $n=1880\ldots1910$ when the 74-year cycle had a positive state. In this period there are 35 degrees of freedom. The cycle has a π (rad) phase-reversal to $\varphi_R(24,nT)=-1.70\pi$ (rad) when the 74-year cycle had a negative state from $n=1910\ldots1950$. The 8-year cycle has a phase of $\varphi_R(8,nT)=-0.382\pi$ (rad) in the period $n=1880\ldots1930$. In this period the cross-correlation coefficient is $R_R(8)=0.37$, the correlation quality value is $Q(8)=3.3$, with 68 degrees of freedom. The cycle phase was delayed about $\pi/2$ (rad) when the 74-year period had a maximum in 1950. The phase delay was π (rad) when the 74-year cycle had a minimum level in 1970. The signal-to-noise ratio between the dominant wavelet sum $W_R(nT)=[W_R(8,nT)+0.5W_R(24,nT)+0.2W_K(74,nT)]$ and the unknown source $v(nT)=(x_K(nT)-W_K(nT))$ is calculated to be $S/N_K=1.8$. This confirms that the estimated nodal spectrum from the 74-year cycle represents most of the fluctuations in the time series.

The phase-delay in the dominant Røst winter air temperature is estimated by:

$$\begin{aligned} \varphi_P(74,nT)-\varphi_R(74,nT)&=(1.29\pi-0.51\pi)=0.78\pi \text{ (rad)} \\ \varphi_G(24,nT)-\varphi_R(24,nT)&=(1.70\pi-0.70\pi)=1.0\pi \text{ (rad)} \end{aligned} \quad (16)$$

The 24-year cycle has a phase delay of 1.0π (rad) and this shows that there is a close correlation between more ice in the Greenland Sea and colder winter temperatures at Røst. The winter temperature time series at Røst has the same dominant cycles as has been estimated for the Greenland ice extent time series. The phase delay between the 74-year NAO and Røst temperature cycles is $(1.01\pi-0.51\pi)=0.5\pi$. This means the 74-year cycle at Røst is moving from its maximum value when the NAO 74-year cycle is headed in a negative direction.

The NAO winter index

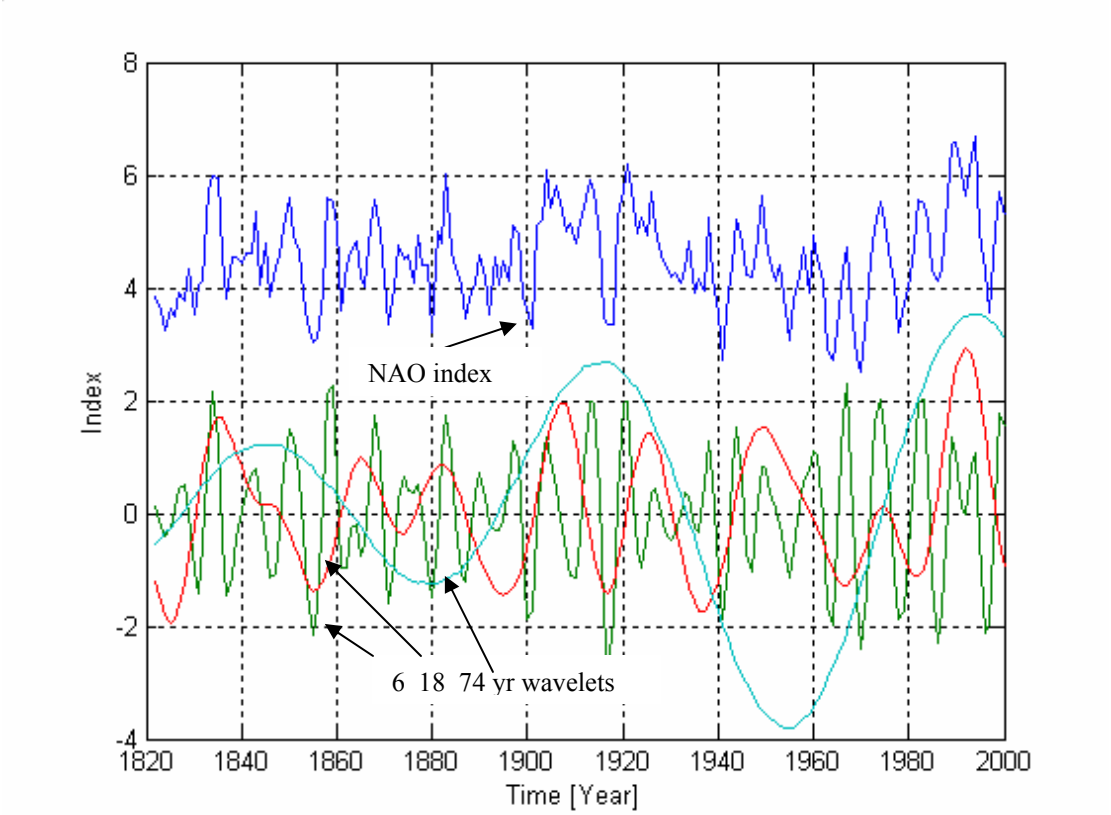

Figure 8 Time series of NAO winter index (+4) and the dominant wavelet cycles of 6, 18 and 74 years.

The NAO winter index time series has the same dominant cycles in the wavelet spectrum $W_N(1:80,nT)$. This investigation has identified dominant wavelet cycles of about 6, 18, 30-34, and 74 years. Figure 8 shows the time series for the NAO winter index and the estimated dominant wavelet cycles of 6, 18, and 74 years. The NAO winter index data series in Figure 8 is scaled by +4 to separate the original data from the computed wavelets. The stationary representation of the dominant cycles is:

$$\begin{aligned} U_N(74,nT)&=u_N(74,nT)\sin(\omega_n nT/4+1.01\pi) \text{ when } n=1880\ldots1997 \\ U_N(18,nT)&= u_N(74,nT)\sin(\omega_n nT+0.48\pi) \text{ when } n=1950\ldots2000 \\ U_N(06,nT)&=u_N(06,nT)\sin(3\omega_n nT-0.29\pi) \text{ when } n=1822\ldots2000 \end{aligned} \qquad (17)$$

The 74-year cycle has a trend shift in 1825, 1860, 1895, 1935 and 1970, a minimum in 1880 and 1955, a maximum in the years 1845, 1918 and 1995, and a cross-correlation coefficient of $R_N(74)=0.90$, a correlation quality of $Q(74)=2.4$, and 177 degrees of freedom.

The 18-year NAO-index cycle is at a maximum the same years that the 18-year cycle of Barents Sea ice extent is at a minimum. This confirms that there is a warmer winter when there is a reduction in the Arctic ice cover. The 18-year cycle has a π (rad) phase-reversal at about the years 1840, 1890 and 1950. In this period the phase-reversal is related to turning points from the 74-year cycle. The 18-year phase angle is $\varphi_N(18,nT)=0.48\pi$ (rad) in the period $n=1845\ldots1890$, $\varphi_N(18,nT)=1.48\pi$ (rad) in the period $n=1890...1950$ and $\varphi_N(18,nT)=0.48\pi$

(rad) in the period n=1950…2000. The cross-correlation coefficient for the stationary cycle period $U_N(18,nT)$ is $R_N(18)=0.58$ in the total period n=1822…2000 when the phase $\varphi_N(18,nT)$ is shifted. In this estimate we have a correlation quality of Q(18)=9.6, and 177 degrees of freedom. The cross-correlation coefficient is $R_N(6)=0.2$ when the phase angle is $\varphi_N(6,nT)=-0.29\pi$ (rad) in the total period n=1822…2000. This estimate has a correlation quality of Q(6)=2.4, and 177 degrees of freedom. The small correlation is related to the phase control from the 74-year cycle.

The signal-to-noise ratio between the dominant wavelets $W_N(nT) = [W_R(8,nT) + 0.5W_R(24,nT) + 0.5W_K(74,nT)]$ and the unknown source $v(nT)=(x_K(nT)-W_K(nT))$ is calculated as $S/N_K=3.0$. This confirms that the estimated nodal spectrum represents most of the fluctuations in the time series. The phase-relation with respect to other cycles is:

$$\varphi_P(74,nT)-\varphi_N(74,nT)=(1.29\pi-1.01\pi)=0.28\pi \text{ (rad)} \quad (18)$$
$$\varphi_P(18,nT)-\varphi_N(18,nT)=(0.90\pi-0.48\pi)=0.42\pi \text{ (rad)}$$

The mean phase delay between the 74-year cycle of the Barents Sea and Greenland Sea ice extent is $(\varphi_B(74,nT)+\varphi_G(74,nT))/2=(0.25\pi+1.78\pi)/2=1.01\pi$. The phase angle of the 74-years $\varphi_N(74,nT)=1.01\pi$. This estimate shows that the 74-year cycle in the NAO winter index follows the mean long-term fluctuations of Arctic ice extent.

In 1865 the mean Barents Sea ice extent was about 1,250,000 km2 and the fluctuations were about 500,000 km2. In 1997 the mean level was decreased to about 750,000 km2 and the fluctuations were still about 500,000 km2. The mean area of fluctuation has increased from about 40% to 67% of the total ice extent. The fluctuation has increased by about 27%. In the same period the fluctuation in the NAO winter index increased from about 2 to 2.5. This represents an increased fluctuation of about 25%. This ratio indicates that relatively more fluctuation in the extent of Arctic ice introduces relatively more disturbance in the NAO winter index. The same ration may be a possible explanation of the increased amplitude fluctuation in the NAO winter index during the last 50 years. This means that if the Arctic ice extent continues to be reduced, the amplitude of the NAO index will increase, resulting in an increase in extreme climate fluctuations.

Arctic climate cycles

Climate Indicator	***Nodal spectrum*** ω_0 **(rad/yr)**	***Cycle phase*** φ **(rad)**	***Phase delay to polar*** $\Delta\varphi$ **(rad)**	***Nodal cycle correlation*** **R**	***Signal to noise ratio*** **S/N**
Lunar nodal cycle	ω_0	0.90π	0.00π		
Polar position	$\omega_0/4$ ω_0 $3\omega_0$ $15\omega_0$	1.29π $1.00/0.00\pi$ -1.09π -1.09π		0.86 0.70 0.44 0.96	2.6
Arctic Ocean	$\omega_0/4$ $3\omega_0/4$ $9\omega_0/4$				
Barents ice ext.	$\omega_0/4$ $\omega_0/$ $3\omega_0$	0.25π $1.50/0.50\pi$ $-1.09/-0.09\pi$	1.04π 0.50π 1.00π	0.73 0.74 0.64	2.0
Kola section temp.	$\omega_0/4$ $\omega_0/3$ ω_0 $3\omega_0$	0.29π 0.90π $1.55/0.55\pi$ $-1.09/0.09\pi$	1.00π 0.45π 0.00π	0.95 0.89 0.90 0.37	3.2
Hammerfest sea level	ω_0 $3\omega_0$	0.55π $-1.09\pi/-0.09\pi$	0.45π 1.0π	0.73 0.37	1.6
Greenland ice ext.	$\omega_0/4$ $3\omega_0/4$ $9\omega_0/4$	1.78π $0.70/1.70\pi$ $1.38/0.38\pi$	-0.49π	0.50 0.77 0.54	3.2
Røst winter temp.	$\omega_0/4$ $3\omega_0/4$ $9\omega_0/4$	0.51π $-1.70/-0.70\pi$ $-1.38/-0.38\pi$	0.78π	0.92 0.88 0.37	1.8
NAO winter index	$\omega_0/4$ ω_0 $3\omega_0$	1.01π $1.48/0.48\pi$ $-1.29/-0.29\pi$	0.28π -0.48π 0.2π	0.90 0.48 0.2	3.0

Table 1 Identified Arctic climate cycles.

Table 1 shows the lunar nodal spectrum as identified in all analyzed Arctic climate indicators. In this table the angle frequency is $\omega_0=2\pi/T_0=2\pi/18.6134$ (rad/yr). This indicates there is a stationary Arctic oscillating system controlled by the deterministic 18.6-year lunar nodal cycle.

The time series of the Polar position, the Barents Sea ice extent, the Kola section temperature, the Hammerfest sea level and the NAO winter index all have a dominant harmonic spectrum that is derived from the T_0=18.6-year cycle. The Greenland ice extent and the Røst winter air temperatures have a harmonic spectrum from the sub-harmonic cycle of $4T_0=4*18.6=74.4$ years. Table 1 shows that the identified cycles have a good correlation to nodal reference cycles and a good signal-to-noise ratio between the identified cycles and influences from

other sources. These estimates show that the cycles from the lunar nodal spectrum have a major influence on the dominant fluctuations in the time series.

Discussion

The sea level at Hammerfest

The identified 18-year cycle in the sea level at Hammerfest has a phase delay of about $\varphi_H(18,nT)=0.55\pi$ (rad). Maksimov and Smirnov (1965, 1967) estimated a maximum lunar nodal tide at about the year 1950 in the Atlantic Ocean and in the Kola section. This represents the phase delay of $\varphi_H(18,nT)=0.45\pi$ (rad), which represents a phase distance of less than a year. Keeling and Worf (1997) have estimated strong 18-year tidal waves in 1974 and 1987 from lunar cycle events. From these estimates a 93-year tide and a group of 9-year and 6-year tide events were calculated. This group of events had their maximums in 1965, 1974 and 1983. The same maximum periods are identified in the Hammerfest sea level time series. This means that the long-term tide shows a lunar-nodal spectrum. The group event between a 9-year cycle and a 6-year cycle has been identified as a phase-reversal of the 6-year cycle in this wavelet cycle analysis.

The polar position

The wavelet analysis of the polar position time series in the y-direction has identified a lunar nodal spectrum of about 4*18.6=74.5, 18.6, 18.6/3=6.2 and 6.2/5=1.2 years. The 18-year cycle has the same cycle time as the earth's nutation. The earth's nutation is a 9 arc degree wobble of the spinning earth's axis in a period of 18.6 years (Pugh, 1996). This wobbling is caused by a gravity interaction between the earth, the sun and the moon. The 18-year cycle has the same phase as the lunar nodal cycle. This phase indicates that the 18-year polar movement is caused by a gravity force from the moon and the earth's nutation. The phase-reversal in 1960 indicates that the 18-year cycle is influenced by the more powerful 74-year harmonic cycle.

The position of the pole has a stepwise displacement in the y-direction in the years 1890 and 1960. The step came at about the same year as the 74-year Barents Sea ice cycle had shifted toward a negative value and the 74-year Greenland ice extent turned from its maximum to a negative direction. This connection leads to the hypothesis that a long-term stepwise displacement in the y-direction will lead to inflow of more Atlantic water to the Arctic Ocean and a long-term reduction in the extent of the Arctic ice cover.

Chandler[1846-1913] discovered that the polar position has a wobble with a period of about 1.2 years or 435 days. The present analysis indicates that this cycle may be a forced oscillator controlled by the 6.2-year polar movement cycle. The estimated 1.2-year polar position cycle has a cross-correlation coefficient of $R_P(1.2)=0.96$ to the harmonic cycle of 18.6/3*5=6.2/5=1.2 years or 443 days. The 1.2-year cycle has a phase delay after 6 periods. This phase delay introduces a mean Chandler wave period of about 6.2 to 6.5 years. The cause of the Chandler wobble is unclear. The stationary property of this cycle and the close relationship to a 6.2-year cycle indicate that this is a forced harmonic cycle controlled by a gravity force from the 18.6-year lunar nodal cycle.

The Arctic oscillation system

The Arctic Ocean oscillation

The wavelet analysis of the polar position has identified a harmonic lunar nodal cycle in the y-direction of about 4*18.6=74.5 years. This residence time represents a third harmonic cycle of the 74-year cycle or 74.5/3=24.5 years. The same cycle is estimated in the time series of the Barents Sea ice extent, the Greenland Sea ice extent and the winter temperature at Røst. The close relationship between these cycles may be explained by the circulating polar position that controls the residence time of circulating water in the Arctic Ocean. The circulating layers in the Arctic Ocean have residence times which are reflected in the time series of Greenland Sea ice extent. This may be explained by a "wine glass" theory.

The wine glass theory is based on the idea that the rotating Arctic Ocean behaves like liquid in a rotating wine glass. According to this theory, the Deep Water oscillation has a resonance of about 74 years. This resonance is related to water volume and density. A forced polar position cycle of about 74.5 years will then control a 74-year cycle of Deep Water circulation in the Arctic Ocean. Energy from the forced 74-year Deep Water oscillation is distributed as a harmonic spectrum. In this spectrum there is a new 4*74.5≈290-year resonance in the Bottom Water where the water has the most density, and with a 74.5/3=25-year resonance in the Atlantic Water where the water is less dense.

The mean area of the Barents Sea ice extent has decreased by about 30% in the total time series. At the same time the polar position in the y-direction has increased from about 0.08 to 0.35 arc degrees. This long-term motion in the pole indicates that the long-term reduction in the Barents Sea ice extent may be caused by a longer period polar movement. A long-term displacement of the pole in the y-position is expected to influence the gradient of Arctic inflow, the Arctic temperature, and the Arctic Ocean ice extent.

The Barents Sea oscillation

It is generally believed that the inflow of Atlantic water to the Barents Sea is driven by atmospheric conditions (Loeng et al., 1997). The lunar nodal spectrum in the polar position and Barents Sea ice extent indicates there is a more fundamental cause of a long-term Atlantic inflow. This investigation shows that there is a close relationship in cycle times and phases between the lunar nodal spectrum in the polar position, the Barents Sea ice extent, the Kola section temperature and Hammerfest sea level. This shows that the long-term inflow of Atlantic water is controlled by long-term tides. The long-term tides influences the biomasses in the Barents Sea (Wyatt et al., 1994; Yndestad, 1999b, Malkov, 2002) At the same time a close relationship has been identified between the 18-year fluctuations in the NAO winter index and the Barents Sea ice extent. This explains the close link between the Barents Sea temperature and atmospheric conditions.

The 74-year Kola temperature cycle and the 74-year cycle of Barents Sea ice extent share the same cycle period and phase. This surprising estimate shows that the 74-year cycles of the ice extent and Kola temperatures are controlled by different sources. A potential source of the 74-year Kola cycle is the Greenland Sea. There is a mutual interaction of Deep Water between the Eurasian Basin, the Greenland Sea and the Norwegian Sea. The North Atlantic Norwegian Basin receives about a 0.95 Sv flux from the Greenland Sea and a 0.37 Sv flux from the Eurasian Basin, with the Deep Water residence time estimated to be 31 years (Bonisch and Schlosser, 1995), or about 74.5/2 years. The Arctic flow has a phase delay of $\pi/2$ rad (18.6 years) from the polar movement to the Greenland Sea. A phase delay of $\pi/2$ rad (18.6 years)

from the Greenland Sea to the Kola section may have a total phase delay of π rad between Barents Sea ice extent and the Kola section temperatures.

The Greenland Sea

The Greenland Sea ice extent has dominant cycles of 74 and 24 years. These are the same cycle periods as the residence time for Deep Water and Atlantic water in the Arctic Ocean. The close correlation confirms that the Greenland ice extent is dominated by the Arctic outflow. The reported salinity plume (Dickson et al., 1988, 2000) in the Atlantic circulation had a trend shift in 1960. This was the same year the 74-year cycle had a maximum value and the 24-year cycle had a trend shift.

The winter temperature at Røst is influenced by cold winds from the East. This fact is reflected in the estimated air temperature at Røst. The Røst winter air temperature time series has dominant cycles of 74 and 24 years. Both cycles are closely correlated with the 74-year and 24-year cycles of the Greenland ice extent.

The NAO winter index

The NAO winter index is an important climate indicator. This investigation shows that the NAO winter index is dominated by the 18.6-year lunar nodal spectrum. The 18-year cycle is closely correlated in both cycle period and phase to the 18-year cycle of the Barents Sea ice extent. This indicates that the 18-year cycle in the NAO winter index is influenced by the 18.6-year tide and the Barents Sea ice extent. The 74-year cycle introduces a phase-reversal of the dominant cycles of 18 and 6 years. A phase-reversal of stationary cycles explains why the 18-year cycle has been difficult to estimate using traditional spectral estimate methods. The 18-year cycle has, however, been found in a number of other climate indicators. The 18.6-year cycle has been identified in tree rings, weather records, wine harvest, and fish catch (Currie, 1981; 1984, 1987, Currie et al., 1993).

The identified 74-year cycle in the NAO winter index represents a long-term climate change indicator. The 74-year cycle has a phase which is the mean of the 74-year cycle phase for the extent of ice in both the Barents Sea ice extent and the Greenland Sea. The Arctic ice extent is then expected to be the source behind this important 74-year climate indicator. Schlesinger and Ramankutty (1994) have analyzed the long-term temperatures from the Northern Hemisphere continental regions bounding the Northern Atlantic Ocean. In the North Atlantic region they found a dominant temperature cycle of about 76 years. The 76-year cycle has a maximum in 1945. This is the same year the identified 74.5-year cycle of Barents Sea ice extent is at a minimum.

The Nile flood in Egypt is an indicator of rainfall in Africa. Records from the periods 3150 BC to 2400 BC and 622 AD to 1470 AD show a peak with periods of 18.4, 53 and 77 years. Greenland ice cores show periodic cycles of 20, 78, and 181 years and temperature records from central England from 1700 to 1950 show periodicities at cycles of 23 and 76 years (Borroughs, 1992; Currie, 1995). This indicates that this 74-76 year cycle represents a long-term stationary oscillation.

The 74-year NAO cycle explains the climate shift in 1960 and a possible new shift in the 1990s. From 2000 we may expect the 18-year NAO winter index cycle to turn in a positive direction over the next 10 years and the 74-year cycle will be turning in a negative direction the next 30 years. These cycle estimates indicate we may expect a temporary period of colder climate in the Northern Hemisphere. The long-term relationship between a step in the polar motion and the Arctic ice extent reduction suggest that in the long run we may expect a warmer climate.

Materials and methods

This analysis has some potential sources of errors. There may be errors in the data samples which cannot be controlled. In this investigation, long trends in the data are analyzed. Single data errors or white noise should then not pose a problem. Different methods of estimating are a potential source of long-term fluctuations if time series are connected.

All time series represent a time variant stochastic process. The problem with time series analysis is to identify periodic cycles when the cycles have a time variant phase. This time variant phase property excludes traditional spectrum estimate methods. The cycles have been identified by separating the dominant cycles in the time series using a wavelet transform. The Coiflet3 wavelet transformation (Matlab, 1997) has been chosen from many trials on tested data. The cycle time has been identified by a cross-correlation to a known reference cycle and the cycle influence has been identified by computing the signal-to-noise ratio. The results show a good correlation with the lunar nodal spectrum. The estimated signal-to-noise ratio shows that the lunar nodal spectrum has dominant influence on all time series. The most important support for this observation is the coherence between the identified cycles in the Polar position, the Barents Sea ice extent, the Kola temperature and the sea level at Hammerfest.

Conclusion

This investigation has identified a harmonic spectrum from the 18.6-year lunar nodal cycle in a number of Arctic time series. The identified cycles have a stationary cycle time but not stationary amplitude and phase. A sub-harmonic cycle of about 74 years may introduce a phase-reversal of the harmonic cycles. The high signal-to-noise ratio shows that the lunar nodal spectrum has a major influence on the Arctic oscillation system. This Arctic oscillation system influences long-term fluctuations in the extent of Arctic ice. The lunar nodal spectrum of Arctic ice extent influences the NAO-winter index, the weather and the climate.

Acknowledgments. I would like to thank Vladimir Ozhigin at PINRO institute in Murmansk for access to the Kola section temperature data series, Torgny Vinje at the Norwegian Polar Institute in Oslo who provided the ice extent data series, and Gudmund Anders Dalsbø at Norwegian Meteorological Institute in Oslo who provided the Røst data series.

References

Aagaard, K. and P. Gresman. 1975. Towards new mass and heat budgets for the Arctic Ocean. Journal of Geophysics Research. 80: 3821-3827.

Anderson, L.G.; Björk, G.; Holby, O. Jones, E. P.; Kattner, G.; Kolterman, K. B.; Liljeblad, B.; Lindegren, R.; Rudels, B.; Swift, J. 1994. Water masses and circulation in the Eurasian Basin: Results from the Oden 91 expedition. Journal of Geophysical Research.99:3273-3283.

Bochkov, Yu. A. 1982. Water temperature in the 0-200 m layer in the Kola-Meridian in the Barents Sea, 1900-1981. Sb. Nauchn. Trud. PINRO, Murmansk, 46: 113-122 (in Russian).

Bonisch, G and Schlosser, P. 1995. Deep water formation and exchange rates in the Greenland/Norwegian Seas and the Eurasian Basin of the Arctic Ocean derived from tracer balances. Prog. Oceanography. 35:29-52.

Borroughs, William James. 1992. Weather cycles real or imaginary? Cambridge University Press.

Carmack E. C. K. Aagaard, J.H. Swift, R.W. MacDonald, F.A. McLaughlin, E. P. Jones, R. G. Perking, J. N. Smith, K. M. Ellis and L. R. Lillius 1997. Changes in the temperature and tracer distributions with the Arctic Ocean: results from the 1994 Arctic Ocean section. Deep Sea Research.44:1487-1502.

Carlson, A. Bruce. 1968. Communication systems. An Introduction to Signal and Noise in Electrical Communication. McGraw-Hill. London. ISBN 0-07-009957-X.

Currie, R. G. 1981. Evidence for 18.6 year (*sic*) signal in temperature and drought conditions in North America since A. D. 1800: Journal of Geophysical Research.86:11,055-11,064.

Currie, R. G.1984. Evidence for 18.6 year (*sic*) lunar nodal (*sic*) drought in western North America during the past millennium: Journal of Geophysical Research.89:1295-1308.

Currie, R. G. 1987. Examples and implications of 18.6- and 11--year terms in world weather records, Chap. 22, p. 378-403 *in* M.R. Rampino, J.E. Sanders, W.S. Newman,and L.K. Konigsson, *eds*. Climate: History, periodicity, and predictability: International Symposium held at Barnard College, Columbia University, New York, New York, 21-23 May 1984 (R. W. Fairbridge Festschrift): New York, NY, Van Nostrand Reinhold Publishing Corp., 588 p.

Currie, R. G. 1995. Variance Contribution of M_n and S_c Signals to Niele River Data over a 30-8 Year Bandwith. Journal of Coastal Research Special Issue No. 17: Holocene Cycles: Climate, Sea Levels and Sedimentation, pp 29-38.

Currie, R. W., T. Wyatt, and D.P. O'Brien. 1993. Deterministic signals in European fish catches, wine harvests, sea level, and further experiments: International Journal of Climatology. 8:255-281.

Daubechies I. 1992. Ten lectures of wavelet. SIAM Journal on Mathematical Analysis. 24:499-519.

Dickson R.R., J. Meincke, S.A. Malmberg and A.J. Lee. 1988. Progress in Oceanography.20:103-151.

Dickson R R, T. J. Osborn, J.W. Hurrel, J. Meincke, J. Blindheim, B. Adlandsvik, T. Vinje, G. Alekseev, W. Maslowski. 2000. The Arctic Ocean Response to the North Atlantic Oscillation. Journal of Climate. 13:, No. 15, 1 August 2000.

Gregor, D. J., Harald Loeng and Barrie Len. 1998. The Influence of Physical and Chemical Processes on Containtment Transport into and within the Arctic. AMAP Assessment Report: Arctic Pollution Issues. pp 25-117. AMAP Secretariat. Oslo.

Izhevskii, G. K., 1961. Oceanological Principles as Related to the Fishery Productivity of the Seas. Moscow: Pishcepromizdat. [Translated 1966: Israel Program for Science Transactions. Jerusalem]. 95 pp.

Izhevskii, G. K., 1964. Forecasting of oceanological conditions and the reproduction of commercial fish. All Union Science Research Institute of Marine Fisheries & Oceanography. Israel Program for Science Transactions, 22 pp.

Imbrie John, Imbrie John Z. 1980. Modeling the Climate response to Orbital Variations. Science. 207, 29 February 1980.

Keeling, Charles D. and T. P. Whorf. 1997. Possible forcing global temperature by oceanic tides. Proceedings, National Academy of Sciences of the United States. 94:8321-8328.

Loder J. W. and C. Garret. 1978. The 18.6 year cycle of the sea surface temperature in the shallow seas due to tidal mixing. Journal of Geophysical Research. 83: 1967-1970.

Loeng Harald, V. Ozhigin and B. Ådlandsvik. 1997. Water fluxes through the Barents Sea. ICES Journal of Marine Science. 54: 310-317.

Maksimov, I. V. and N.P. Smirnov. 1964. Long range forecasting of secular changes of the general ice formation of the Barents Sea by the harmonic component method. Murmansk Polar Sci. Res. Inst., Sea Fisheries. 4: 75-87.

Maksimov, I. V. and N.P. Smirnov. 1965. A contribution to the study of causes of long-period variations in the activity of the Gulf Stream. Oceanology. 5:15-24.

Maksimov, I. V. and N.P. Smirnov. 1967. A long-term circumpolar tide and its significance for the circulation of ocean and atmosphere. Oceanology 7: 173-178 (English edition).

Maksimov, I. V. and B.A. Sleptsov-Shevlevich. 1970. Long-term changes in the tide-generation force of the moon and the iciness of the Arctic Seas. Proceedings of the N. M. Knipovich Polar Scientific-Research and Planning Institute of Marine Fisheries and Oceanography (PINRO). 27: 22-40.

Malkov A.S. 2002. Movements of the Earth pole and population dynamics of Norwegian Spring spawning herring and Arctic cod. The 90th International ICES Annual Science Symposium. Copenhagen. Denmark, 1 Oct-5. CM 2002/O:09.

Matlab. 1997. Matlab. Wavelet Toolbox. Users Guide. The Math Works Inc.

Moon, F. C. 1987. Chaotic Vibrations. John Wiley & Sons, New York. 300 pp.

Neuman G. and Pierson W. J., 1966. Principles of Physical Oceanography, Prentice-Hall, Englewood Cliffs, N. J. 545 pp.

Petterson, Otto, 1905. On the probable occurrence in the Atlantic current of variations periodical, and otherwise, and their bearing on metrological and biological phenomena. Rapp. P.-v. R´eun. Cons. Perm. Int. l´Explor. Mer. 42: 221-240.

Pettersson, Otto, 1914, Climatic variations in historic (*sic*) and prehistoric time: Svenska Hydrogr. Biol. Kommissiones Skrifter, No. 5, 26 p.

Pettersson, Otto, 1915, Long periodical (*sic*) variations of the tide-generating force: Conseil Permanente International pour l'Exploration de la Mer (Copenhagen), Pub. Circ. No. 65, p. 2-23.

Pettersson, Otto, 1930, The tidal force. A study in geophysics: Geografiska Annaler.18:261-322.

Pugh, D T. 1996. Tides, Surges and Mean Sea-Level. John Wiley & Sons. New York.

Royer Thomas C. 1989. Upper ocean temperature variability in the northeast Pacific: Is it an indicator of global warming?, Journal of Geophysical Research., 94:175-183.

Royer Thomas C. 1993. High-Latitude Oceanic variability associated with the 18.6-year nodal tide. Journal of Geophysical Research. 98:4639-4644.

Rudels, Bert, H.J. Friedrech and D. Quadfasel. 1998. The Arctic Circumpolar Boundary Current. Deep-Sea Research II 46:1023-1062.

Satterley, A. K. 1996. The Milankovitch Theory. Earth-Science Reviews. 40:181-207.

Schlesinger, M. E. and N. Ramankutty.1994. An oscillation in the global climate system of period 65-70 years. Nature. 367:723-726.

Vinje, Torgny. 2001. Anomalies and trends of sea ice extent and atmospheric circulation in the Nordic Seas during the period 1864-1998. Journal of Climate. 14:255-267.

Wallace, D.W.R. and R.M. Moore. 1985. Vertical profiles of CC13F (F-11) and CC12F2(F-12) in the central Arctic Ocean basin. Journal of Geophysics Research. 90:1155-1166.

Wyatt T, R.G. Currie and F. Saborido-Rey. 1994. Deterministic signals in Norwegian cod records. ICES Annual Science Symposium. 198:49-55.

Yndestad, H. 1999a. Earth nutation influence on the temperature in the Barents Sea. ICES Journal of Marine Science. 56: 381-387.

Yndestad, H. 1999b. Earth nutation influence on system dynamics of Northeast Arctic cod. ICES Journal of Marine Science, 56: 652-657.

Yndestad H: 2003. A lunar nodal spectrum in Arctic time series. ICES Annual Science Conference. Sept 2003. Tallinn. ICES CM 2003/T. ICES. Copenhagen.